HIGHWAY RESEARCH RECORD

Number 34

Bridge Design, Analysis, and Costs

7 Reports

Presented at the
42nd ANNUAL MEETING
January 7-11, 1963

HIGHWAY RESEARCH BOARD
of the
Division of Engineering and Industrial Research
National Academy of Sciences—
National Research Council
Washington, D. C.
1963

Department of Design

T.E. Shelburne, Chairman
Director of Research
Virginia Department of Highways, Charlottesville

COMMITTEE ON BRIDGES

J.N. Clary, Chairman
Bridge Engineer
Virginia Department of Highways, Richmond

W.C. Anderson, Chief, Research and Development Engineer, The Union Metal Manufacturing Company, Canton, Ohio
Raymond Archibald, Kalispell, Montana
W.E. Baumann, Engineer of Bridge and Traffic Structures, Illinois Division of Highways, Springfield
J.M. Biggs, Associate Professor of Structural Engineering, Massachusetts Institute of Technology, Cambridge
Vernon J. Burns, Assistant Deputy Chief Engineer (Bridge), New York Department of Public Works, Albany
E.M. Cummings, Manager of Sales, Bethlehem Steel Company, Bethlehem, Pa.
Frederick H. Dill, Assistant to Vice President - Engineering, United States Steel Corporation, Pittsburgh, Pennsylvania
E.S. Elcock, Bridge Engineer, Kansas State Highway Commission, Topeka
Arthur L. Elliott, Bridge Engineer - Planning, California Division of Highways, Sacramento
Eric L. Erickson, Chief, Bridge Division, Office of Engineering, U.S. Bureau of Public Roads, Washington, D. C.
R.S. Fountain, Bridge Engineer, Portland Cement Association, Chicago, Illinois
F.M. Fuller, Assistant Vice President, Raymond International, Inc., New York, N.Y.
H. deR. Gibbons, The Union Metal Manufacturing Company, Canton, Ohio
T.R. Higgins, Director of Engineering and Research, American Institute of Steel Construction, New York, N.Y.
Rudolph Hofer, Jr., Highway Products and Structural Section, Sales Development Division, Aluminum Company of America, New Kensington, Pennsylvania
John J. Hogan, Consulting Structural Engineer, Portland Cement Association, New York, N.Y.
C.L. Hulsbos, Department of Civil Engineering, Fritz Laboratory, Lehigh University, Bethlehem, Pennsylvania
J.J. Kozak, Supervising Bridge Engineer, California Division of Highways, Sacremento
W.T. Lankford, Applied Research Laboratory, United States Steel Corporation, Monroeville, Pennsylvania
C.A. Marmelstein, Bridge Engineer, Georgia State Highway Department, Atlanta
William H. Munse, Jr., Department of Civil Engineering, University of Illinois, Urbana
LeRoy T. Oehler, Physical Research Engineer, Michigan State Highway Department, Lansing
D.H. Overman, Columbus, Ohio
Adrian Pauw, Professor of Civil Engineering, University of Missouri, Columbia
M.N. Quade, Consulting Engineer, Parsons, Brinckerhoff, Quade and Douglas, New York, N.Y.
William H. Rabe, Columbus, Ohio
W.T. Robertson, Bridge Design Engineer, Washington Department of Highways, Olympia
Charles F. Scheffey, Department of Civil Engineering, University of California, Berkeley
C.P. Siess, Department of Civil Engineering, University of Illinois, Urbana

Charles B. Trueblood, Armco Drainage and Metal Products, Inc., Middletown, Ohio
Ivan M. Viest, Structural Engineer, Bethlehem Steel Corporation, Bethlehem, Pa.
George S. Vincent, U.S. Bureau of Public Roads, Washington, D.C.

Department of Materials and Construction

John H. Swanberg, Chairman
Chief Engineer
Minnesota Department of Highways, St. Paul

W.F. Abercrombie, State Highway Materials Engineer, State Highway Department of Georgia, Atlanta
Harold Allen, Chief, Office of Research, U.S. Bureau of Public Roads, Washington, D.C.
J.F. Barbee
E.E. Bauer, University of Illinois, Urbana
E.W. Bauman, Managing Director, National Slag Association, Washington, D.C.
D.L. Bloem, Director of Engineering, National Ready Mixed Concrete Association, Washington, D.C.
F.C. Brownridge, Special Assignments Engineer, Department of Highways, Toronto, Ontario, Canada
Jack H. Dillard, Highway Research Engineer, Virginia Department of Highways, University Station, Charlottesville
A.W. Eatman, Materials and Tests Engineer, Texas Highway Department, Camp Hubbard, Austin
Bruce E. Foster, Inorganic Bilding Materials Section, National Bureau of Standards, Washington, D.C.
William H. Goetz, Joint Highway Research Project, Purdue University, Lafayette, Indiana
John M. Griffith, Director of Research & Development, The Asphalt Institute, University of Maryland, College Park
LaMotte Grover, Welding Engineer, Air Reduction Company, Inc., New York, N.Y.
H.W. Humphres, Assistant Construction Engineer, Washington Department of Highways, Olympia
F.N. Hveem, Materials and Research Engineer, California Division of Highways, Sacramento
Frank H. Jackson, Chevy Chase, Maryland
Emmett H. Karrer, Professor of Highway Engineering, Ohio State University, Columbus
Fred W. Kimble, Flexible Pavements Engineer, Ohio Department of Highways, Columbus
H.L. Lehmann, Chief Engineer of Research and Testing, Louisiana Department of Highways, Baton Rouge
R.R. Litehiser, Engineer of Tests, Ohio Department of Highways, Columbus
Bryant Mather, Engineer, Concrete Division, Waterways Experiment Station, Jackson, Mississippi
J.F. McLaughlin, School of Civil Engineering, Purdue University, Lafayette, Indiana
Harry H. McLean, Director, Materials Laboratory, New York State Department of Public Works, Albany
Richard C. Mielenz, Director of Research, The Master Builders Company, Cleveland, Ohio
C.E. Minor, Materials and Research Engineer, Washington Department of Highways, Olympia
K.K. Moore, Supervising Paint Engineer, Texas Highway Department, Austin
Howard Newlon, Jr., Highway Research Engineer, Virginia Council of Highway Investigation and Research, Charlottesville
R.L. Peyton, Assistant State Highway Engineer, State Highway Commission of Kansas, Topeka

Lloyd F. Rader, Department of Civil Engineering, University of Wisconsin, Madison
Gordon K. Ray, Manager, Paving Bureau, Portland Cement Association, Chicago, Illinois
Thomas W. Reichard, Building Technology Division, National Bureau of Standards, Washington, D.C.
E.O. Rhodes, Pittsburgh, Pennsylvania
C.H. Scholer, Department of Applied Mechanics, Kansas State University, Manhattan
K.R. Scurr, Bridge Consultant, South Dakota Department of Highways, Pierre
M.G. Spangler, Iowa State University Ames
Egons Tons, Assistant Director, Joint Highway Research Project, Massachusetts Institute of Technology, Cambridge
J.F. Tribble, Research and Development Engineer, Alabama State Highway Department, Montgomery
J. York Welborn, U.S. Bureau of Public Roads, Washington, D.C.
Kurt F. Wendt, Dean of Engineering, University of Wisconsin, Madison
George Werner, U.S. Bureau of Public Roads, Washington, D.C.
K.B. Woods, Head, School of Civil Engineering and Director, Joint Highway Research Project, Purdue University, Lafayette, Indiana
Warren J. Worth, Engineer of Highways, Board of Wayne County Road Commissioners, Detroit, Michigan

CONSTRUCTION DIVISION

R. L. Peyton, Chairman
Assistant State Highway Engineer
State Highway Commission of Kansas, Topeka

R. W. Humphres, Vice Chairman
Assistant Construction Engineer
Washington Department of Highways, Olympia

COMMITTEE ON CONSTRUCTION PRACTICES—STRUCTURES

K.R. Scurr, Chairman
Bridge Consultant
South Dakota Department of Highways, Pierre

Randle B. Alexander, American Concrete Pipe Association, Austin, Texas
Leo F. Beckett, Assistant to Chief Engineer, Missouri State Highway Commission, Jefferson City
H.B. Britton, Senior Structural Specifications Writer, New York State Department of Public Works, Albany
W.E. Crum, Bridge Design and Plans Engineer, South Carolina State Highway Department, Columbia
L.C. Dillard, Bridge Construction Engineer, North Carolina State Highway Commission, Raleigh
Eric L. Erickson, Chief, Bridge Division, Office of Engineering, U.S. Bureau of Public Roads, Washington, D.C.
Albert L. Grubb, Chief, Bureau of Bridges, Maryland State Roads Commission, Baltimore
John G. Hendrickson, Jr., Director of Engineering Research, American Concrete Pipe Association, Chicago, Illinois
John J. Hogan, Consulting Structural Engineer, Portland Cement Association, New York, N.Y.

I.O. Jahlstrom, Bridge Engineer, Operations, California Division of Highways, Sacramento
Fred Kellam, Regional Bridge Engineer, U.S. Bureau of Public Roads, Chicago, Illinois
Norman L. Scott, Executive Secretary, Prestressed Concrete Institute, Chicago, Illinois
M.G. Spangler, Iowa State University, Ames
H.L. White, Chief Sales Engineer, Armco Drainage & Metal Products, Inc., Middletown, Ohio

Contents

Apparatus and Instrumentation for Creep and Shrinkage Studies

BERNARD L. MEYERS and ADRIAN PAUW, University of Missouri

With the rapid development of concrete technology during the past two decades, longer concrete bridge spans have become feasible as a result of increased permissible working stresses, by developing structural continuity through composite construction and by prestressing. As a result of these technological changes, new problems have arisen which previously were of only minor consequence. Among the more important are the volume changes resulting from creep and shrinkage of concrete.

In September 1959, the University of Missouri Engineering Experiment Station initiated a cooperative research project with the Missouri State Highway Commission and the Bureau of Public Roads to investigate the basic nature of creep and shrinkage and the effects of these volume changes on deflection and strength of reinforced concrete bridges. Eventually, it is hoped that from analysis and test results, design criteria can be developed which will enable the engineer to predict such deflections and thereby control them within reasonable limits.

SELECTION OF SPECIMENS

• THE initial stage of the experimental program was designed to obtain information concerning the effect of variation of the concrete constituents, the intensity and duration of load, the environment, and the geometry of the specimens. The variables selected for consideration were (a) size, (b) shape, (c) length, (d) stress intensity, (e) curing conditions, (f) water-cement ratio, (g) type of aggregate, (h) mix proportions (gradation, consistency, admixtures), (i) time of load application, (j) environmental conditions (temperature, humidity), and (k) reinforcement (normal, prestressed).

To study all these variables in a reasonable period of time, specimens which could be cast quickly and would be adaptable to instrumentation were needed. Other important considerations were concerned with the placement of reinforcement. It was felt that the effect of reinforcing should be studied using the same specimen as that used for the other variables. Rectangular prisms were selected because they seemed to fit these requirements better than standard 6-×12-in. cylinders[1]. Such prisms can be conveniently cast in large quantities on specially constructed casting beds. Other advantages of the prismatic specimen are: instrumentation can be readily affixed to the flat surfaces, specimens need not be capped, and they can be easily stored.

Figure 1 shows a 40-specimen casting bed. The forms consist of slotted steel plate sides into which the desired number of spacer plates are placed. The concrete is cast and finished using a vibrating screed. The bed can make reinforced specimens by using different forms (Fig. 2).

Paper sponsored by Committee on Bridges.

[1] Cylinder-Prism Strength and Elastic Modulus Correlation Study, letter report submitted to the Missouri State Highway Commission and the Bureau of Public Roads.

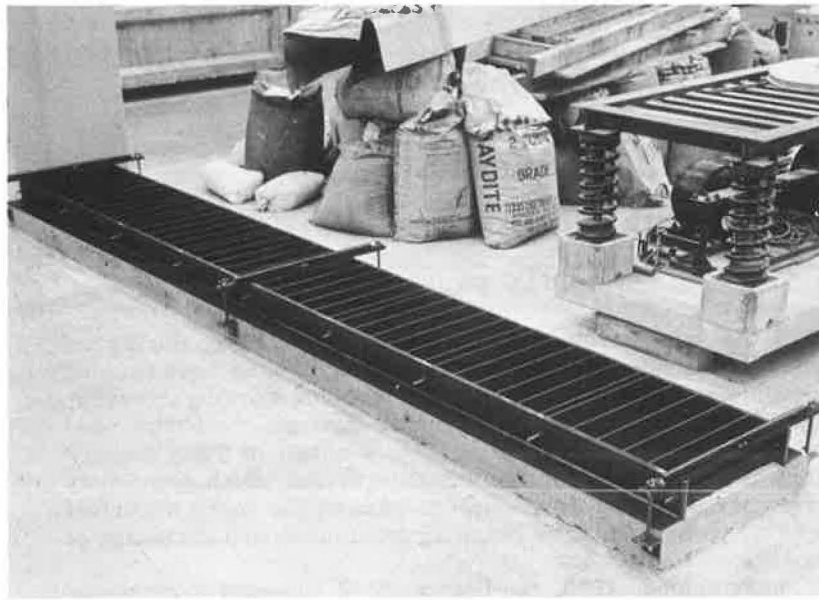

Figure 1. Casting bed.

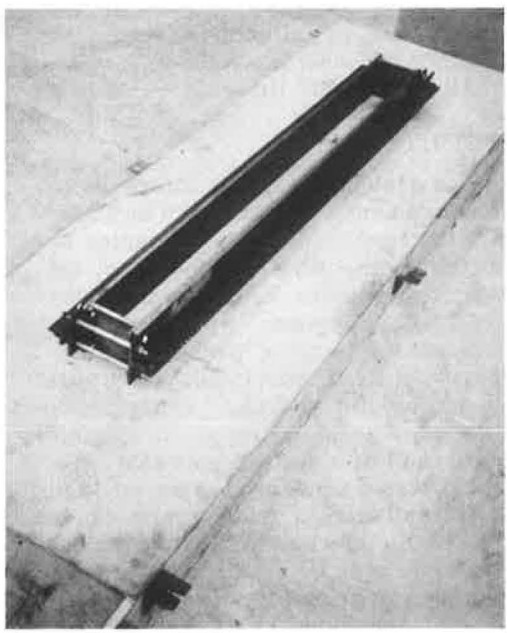

Figure 2. Form for reinforced specimen.

To determine the statistical reliability of the prism specimen, modulus of elasticity and strength tests were carried out using nine sets of prisms and standard 6- × 12-in. companion cylinders. The decision to use the prism for all experimental work on this project was based on an analysis of the data obtained in these tests.

LOADING REQUIREMENTS

Because creep and shrinkage of concrete are time-dependent variables, it was necessary to develop loading systems that would apply and maintain a constant load over a long period of time. These systems must be similar to a testing machine during the application of load, because data must be obtained to determine the elastic properties of the specimen while it is being placed under load. The loading systems should also permit the application of a concentric load, because volume changes are measured in terms of strain in both the longitudinal and the lateral directions.

In addition to the above requirements, the system should permit loading or unloading of any number of individual specimen groups without disturbing the other specimens under load. Finally, because it is desirable to perform the tests in a controlled temperature and humidity environment, the loading system should be as compact as possible.

LOADING SYSTEMS

A hydraulic loading system and a spring loading system were developed to accomplish these objectives. In the hydraulic system, the load is applied by oil pressure, and in the spring system, the load is applied by large nested springs. Each system will be considered separately and described in detail.

The Hydraulic Loading System

The hydraulic system permits a large number of specimens to be loaded quickly. The basic system consists of a motor, an oil-injection pump, an accumulator, a pressure-control system, pressure cells and associated plumbing, and loading frames. A schematic diagram of the system is shown in Figure 3.

A loading rack can accommodate a stack of three 16-in. long specimens or a single specimen up to 60 in. in length. The load is applied at the lower end of the rack by the floating circular plate of the pressure cell. A fully loaded frame consisting of six racks is shown in Figure 4. Castings machined to finished dimensions are used for the body of the pressure cells as shown in Figure 5. Oil is pumped under pressure through flexible hosing to each pressure cell and the loading pressure is transmitted to the floating plate through a rubber piston cup. The reaction is provided by high-strength steel tension rods and cold-rolled flat steel plates.

A fuel-injection pump, driven intermittently by a small $\frac{1}{4}$-hp gear-head motor (Fig. 6), is used to pump oil under pressure to the pressure cells. A $2\frac{1}{2}$- gal hydraulic accumulator is used to maintain constant pressure between pumping cycles. The pumping system is regulated to increase the pressure when leakage causes a 10-psi drop in the load. The regulator is shown in Figure 7.

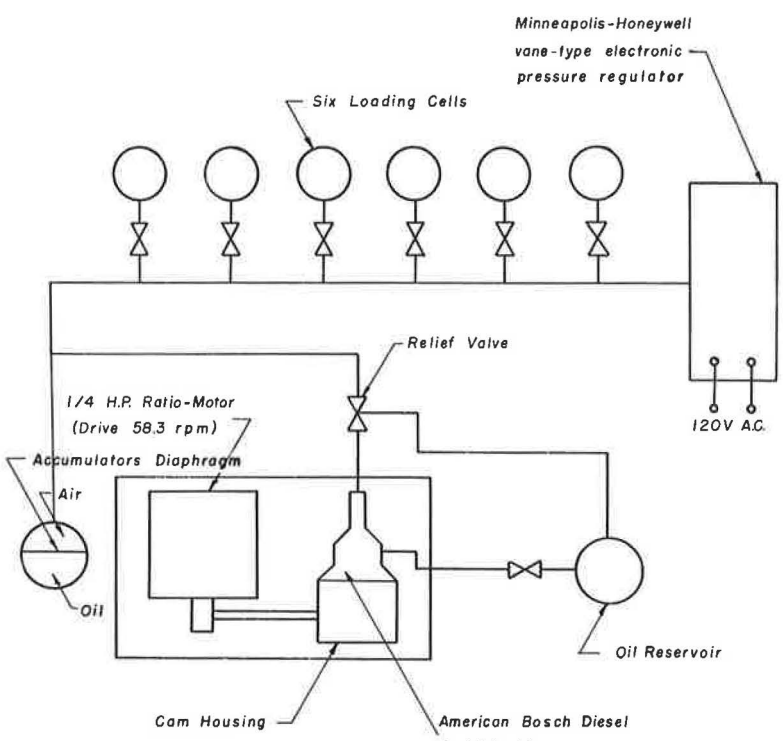

Figure 3. Hydraulic loading system.

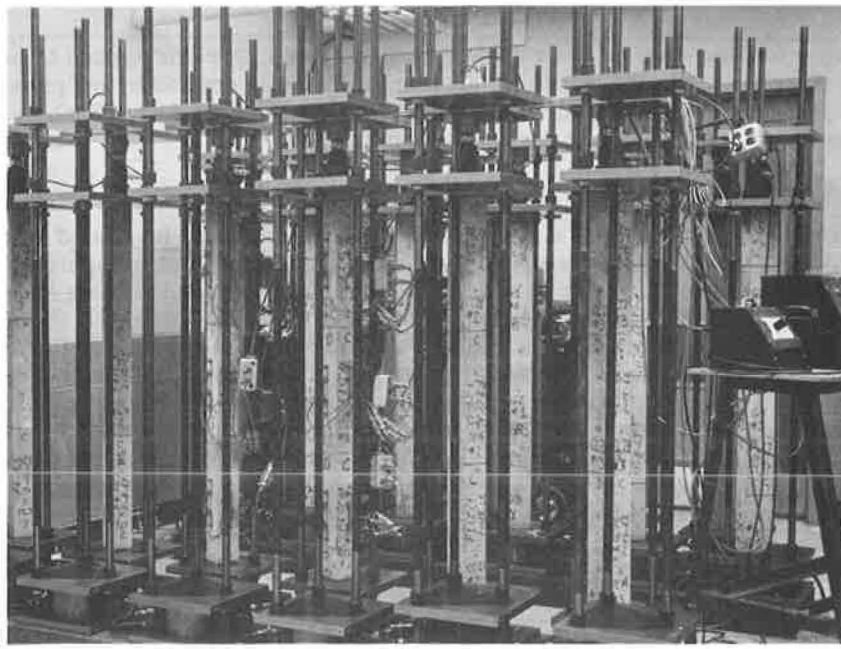

Figure 4. Loading frame.

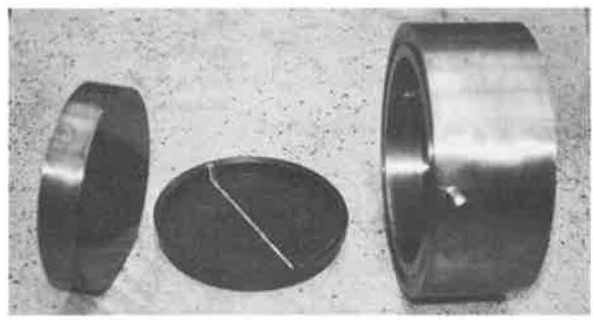

Figure 5. Pressure cell.

It is usually impractical to load a complete frame in a single operation. Therefore, a series of shut-off valves have been provided to permit cutting individual racks off the main pressure line while loading or unloading the other racks.

The system is equipped with a number of safety features designed to prevent overloads or pressure losses in case of specimen failure. A safety plate is provided above the floating plate of the pressure cell and immediately below the lower specimen. Three high-strength nuts, set with enough clearance above the safety plate, allow for normal volume changes. In case of a specimen failure, the load is transferred to these nuts. Thus, other loaded specimens are unaffected by the failure. A second safety feature is a pressure-relief valve to shut off the system should the control mechanism break down and the pressure become dangerously high. In over a year of continuous operation, neither of the safety devices was needed.

In loading, the specimens are centered in the rack using scribe lines on the upper and lower plates. The load-measuring device, which is placed on a floating plate

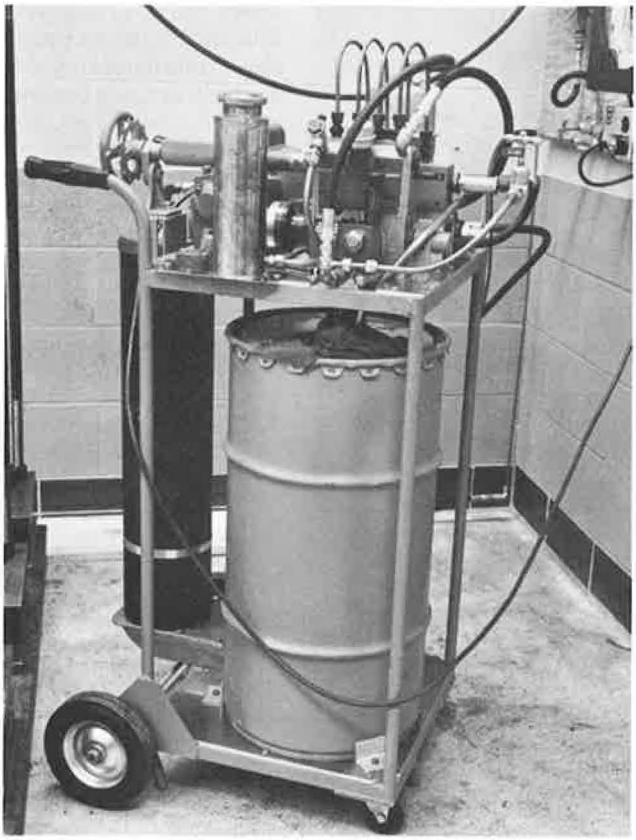

Figure 6. Pumping system.

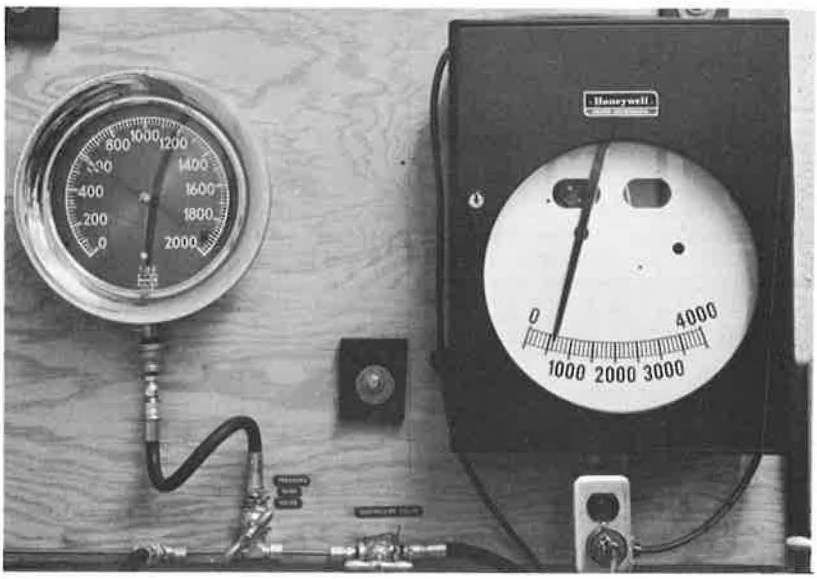

Figure 7. Control system.

Figure 8. Dead-weight gage tester.

above the specimens, contains a ball seat. Therefore, when properly centered, the upper plate applies a uniform load to the surface of the specimen. As the load is applied, a number of strain readings are taken. If the strain-reading increments are unequal, indicating eccentricity, the specimens are re-centered and the procedure is repeated. The final load is applied in 50-psi increments using a dead-weight gage tester (Fig. 8). Because the specimens have been preloaded at least twice, the stress-strain curve is almost a straight line.

The Spring Loading System

The spring system was designed to load specimens in the field. The nested springs used were tested and calibrated. In calibrating the springs, load was applied with a mechanical testing machine and deflection of the springs was recorded using a 4-in. dial gage.

The load is applied to the specimen by placing a hydraulic jack between the two steel plates at the upper end of the rack (Fig. 9). The load is measured with a load cell placed between the floating plate above the specimen and the plate below the jack. The preloading procedure is also used in this system. When the final load has been applied, high-strength nuts are tightened down on the plate above the load cell and the hydraulic jack is removed (Fig. 10). A safety plate similar to the one used with the pressure cells is used above the springs.

The loading systems described are similar to the one recommended in an ASTM publication (4). A comparison of the two systems is shown in Figure 11.

INSTRUMENTATION REQUIREMENTS

The volume changes caused by creep and shrinkage are measured in terms of lateral and longitudinal strain. The requirements suggested by ASTM for measuring such strains are summarized.

> Suitable apparatus shall be provided for measurement of longitudinal strain in the specimen to the nearest 10 micro-in. The apparatus may be embedded, attached, or portable.... The gages may be instrumented so that the average strain on all gage lines may be read directly.... The prime requirement of the strain measuring device is that it shall be capable of measuring strains for at least one year without change in calibration. Systems in which the varying strains are compared with a constant-length standard bar are considered most reliable, but unbonded electrical strain gages are satisfactory.

In addition to measuring the strains, it is also desirable to monitor the load, especially for specimens in the spring-loaded frames. A special load-measuring device, employing strain gages mounted on a prestressed sleeve, was developed for this purpose.

THE CLIP-ON STRAIN METERS

The clip-on strain meter (Fig. 12) is essentially a two-link mechanism joined by thin flexure elements which simulate hinges. Thus, the action of the instrument may be considered to be that of a three-hinged arch. The center hinge (the reduced section) is the strain-sensing element. The effective gage length is determined by the center-to-center distance of the gage points on which the instrument is mounted. The relative movement of these points rotates the center hinge by an amount proportional to the strain in the specimen. The bending strains induced by the rotation are measured by SR-4 strain gages attached to the upper and lower faces of the center hinge.

Because most of the measured strains are compressive and might cause buckling of the strain-sensing element, a pretensioning screw was incorporated into the instrument. After the meter is attached to the specimen, a screw is tightened to pretension the instrument and subject it to a tensile force throughout the test.

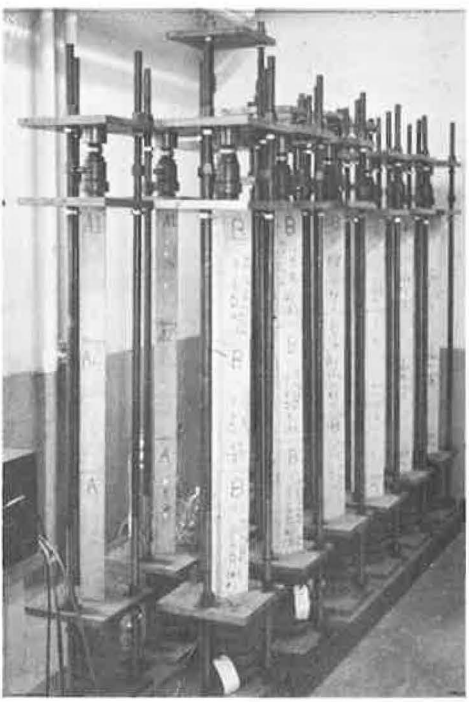

Figure 10. Spring-loaded frame.

Figure 9. Hydraulic jack used in spring-loading system.

The meter is constructed of 24S-T aluminum and requires the use of only two machines — a milling machine and a drill press. The SR-4 gages are cemented to the strain-sensing element and a laminated fiberglass terminal board with three copper eyelets is provided to make electrical connection between the strain gage lead wires and the main lead wires.

The strain meter is attached to the specimen by means of steel connecting posts which serve as the gage points (Fig. 13). The posts are cemented to the specimen using a strong adhesive and are positioned with a special mounting jig. The meter is pushed down firmly on the connecting posts after the adhesive has hardened. Clamp nuts are then threaded onto the posts and run down against the ends of the strain meter. The clamp nuts are tapered slightly to fit into beveled holes in the meter thereby preventing rotation of the ends of the strain meter.

Some of the major advantages of the instrument are derived from the fact that the SR-4 gages are attached to both faces of the strain-sensing element. Rotation of this element produces tension on one face and compression on the other. This design feature automatically compensates for changes in gage resistance due to tem-

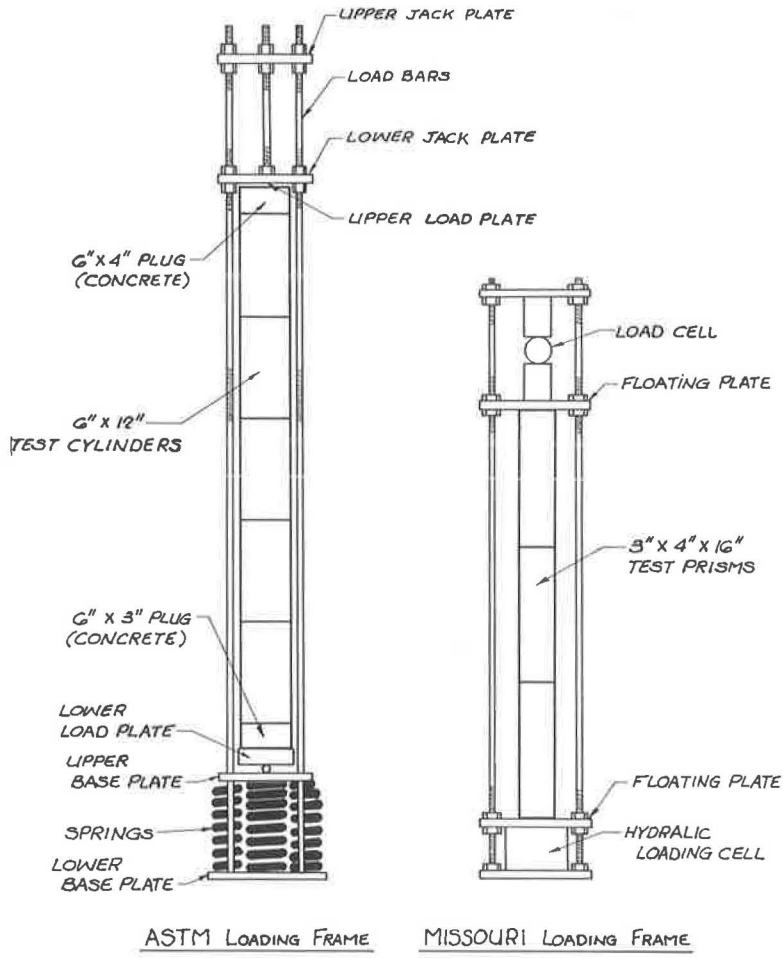

Figure 11. ASTM loading frame and Missouri loading frame.

perature variations, and because both gages are active, the sensitivity of the instrument is doubled.

An additional advantage is obtained by wiring the two clip-on strain meters in a bridge circuit on opposite faces of the specimen. In this way, the readings of the two meters are automatically averaged, eliminating the bending strain component.

The strain meter is calibrated with the instrument shown in Figure 14. The motion of the tapered floating gage block relative to the fixed block is measured by means of a dial gage. The calibration is performed by recording 20 strain-meter readings at 100 micro-in. displacement increments as measured by the dial gage. The strain-meter output is linear to an accuracy of ±2% within a range of 200 micro-in. per in.

THE LONGITUDINAL EXTENSOMETER

Because of the large number of variables studied in this program, it became necessary to develop a strain-measuring device to supplement the clip-on strain meter. It was felt that the reliability of the clip-on meter should be incorporated into a portable instrument.

In the instrument shown in Figure 15, one end of a clip-on strain meter is attached to a fixed-end block and the other to a floating-end block. The gage points attached to the specimen consist of small ball bearings swedged into small aluminum discs. Dur-

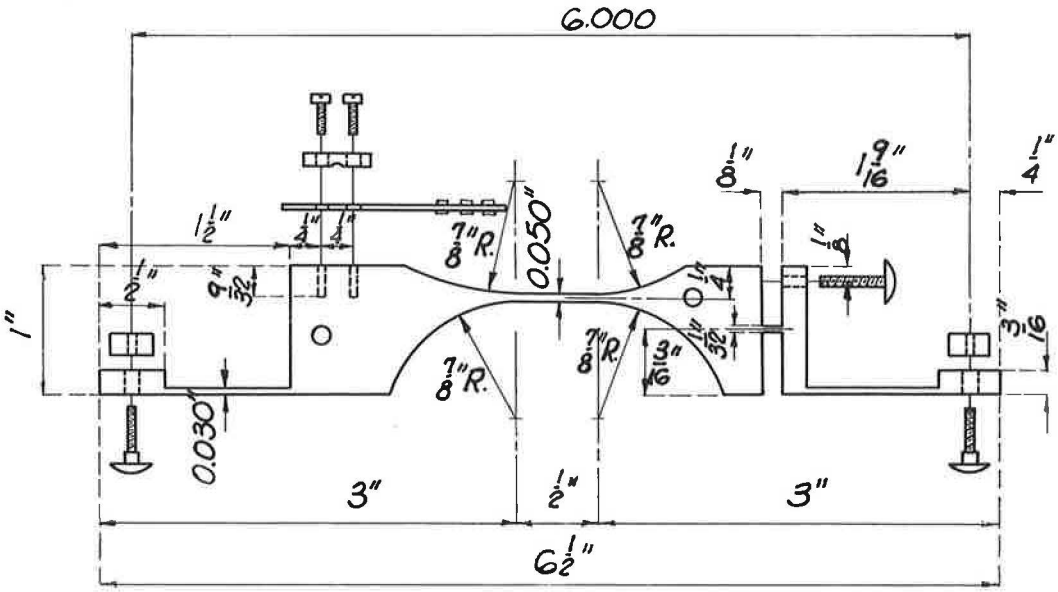

Figure 12. Clip-on strain meter.

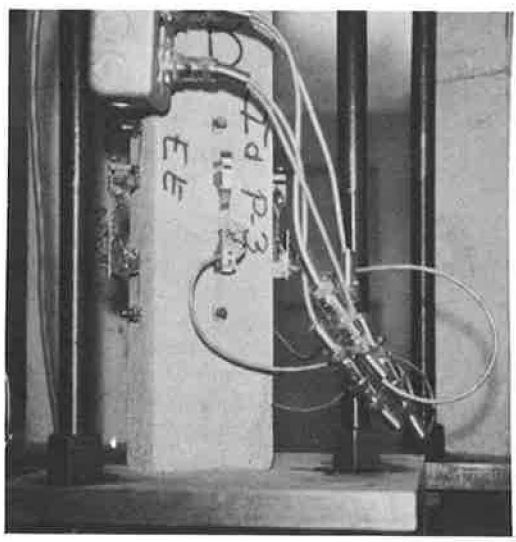

Figure 13. Clip-on strain meter attached to specimen.

ing the use of the instrument, these balls fit into holes drilled into tapered studs threaded into the end blocks. The apparatus used to swedge the steel balls into the aluminum discs is shown in Figure 16. The swedging action creates excellent anchorage by causing the aluminum in the discs to flow around the steel ball.

The end blocks and base of the extensometer are made of the same material as the clip-on strain meter and the entire instrument is enclosed in a plastic case to provide a protective covering and thermal insulation.

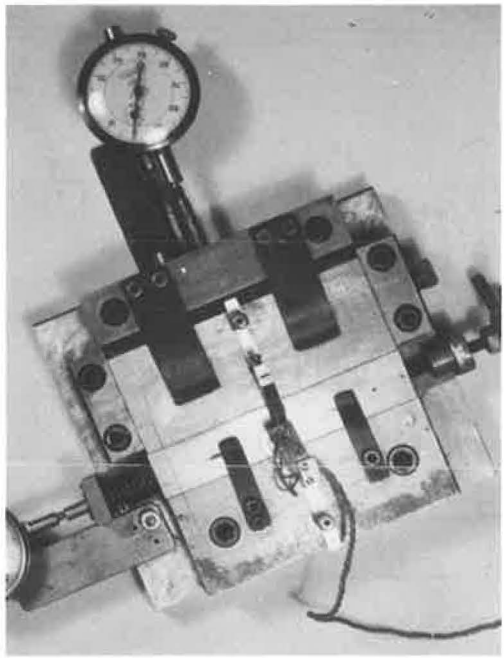

Figure 14. Calibration device for clip-on strain meter.

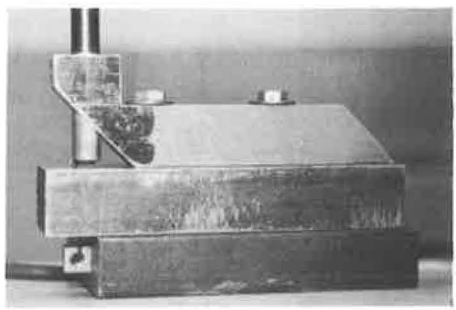

Figure 16. Swedging jig used to make gage joints.

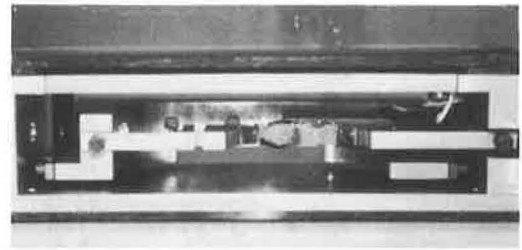

Figure 15. Longitudinal extensometer.

The advantages of the instrument are its economy, its flexibility, and its ease of calibration. The only calibration required is that of the clip-on strain meter encased in the instrument. Before and after each set of measurements, the zero stability of the instrument is checked on a standardized gage bar. In this way, any change in zero can be recorded and incorporated into the reduced data.

With the longitudinal extensometer, the strain measurements on opposite faces of the specimen cannot be automatically averaged. Therefore, the strains measured on each face of the specimen must be recorded and labeled so that average strains can be calculated.

THE LATERAL EXTENSOMETER

To determine the volume changes due to creep and shrinkage, it is necessary to measure both the longitudinal and the lateral strains. The lateral extensometer shown in Figure 17 was designed to measure lateral strains using the tapered studs shown at the left of the instrument. These studs are similar to those used on the longitudinal extensometer. The instrument is attached to the specimen by applying pressure to the hand grip to increase the distance between the studs, permitting them to slide over the spherical gage points on the specimen. The strain-sensing element consists of two SR-4 strain gages cemented on each side of a flexural element at the center of the instrument. The strain gages are connected in a full bridge circuit.

Aluminum is also used for the lateral extensometer to reduce its weight. Advantages of the instrument are that it is removable and the same gage points used for the longitudinal extensometer can be used.

A special jig was devised to insure uniform longitudinal and lateral gage point spacing. This jig (Fig. 18) has two fixed points, an adjustable point and a grinding tool with a fixed stop at the desired lateral gage length. The gage points are applied in the following manner: points are cemented on two adjacent sides of the specimen; the mounting jig is placed on the specimen with the fixed points over the gage points already in place; the adjustable point is tightened down; and the specimen is ground to the desired depth. The grinding tool is then replaced by a special centering tool to hold the

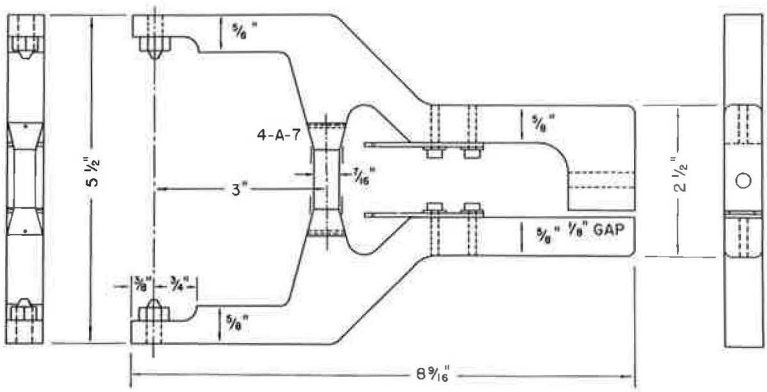

Figure 17. Lateral extensometer.

disc at the exact gage length until the cement has hardened. The procedure is repeated at the lower end, thereby creating the gage length required for the longitudinal extensometer.

Figure 19 shows the calibration device for the lateral extensometer. The extensometer is placed over the two gage points at the right end of the calibration device. The distance between these points is varied by means of a thumb screw at the left end of the device. These variations are indicated by a 0.0001-in. dial gage. Dial gage readings must be divided by the lever ratio of the calibration device. The extensometer has an accuracy equivalent to that of the read-out equipment.

THE MECHANICAL COMPRESSOMETER

In the early stages of the project, the instruments described were used in the following manner. In a test series consisting of three specimens, clip-on strain meters were mounted on one, and spherical gage points were mounted on the other two. Using this type of instrumentation, the elastic properties of the concrete were obtained using the clip-on strain meters. Early in the load period, an independent check of the creep and shrinkage strain rate was also obtained by using the clip-on strain meters as well as the longitudinal extensometer. When the data indicated a satisfactory check, the clip-on meters were removed for use on other specimens.

It seemed desirable also to obtain an independent check of the elastic properties measured by the clip-on strain meters

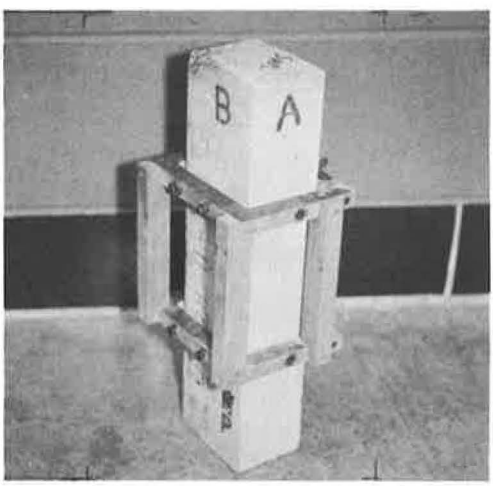

Figure 18. Apparatus used to mount gage points.

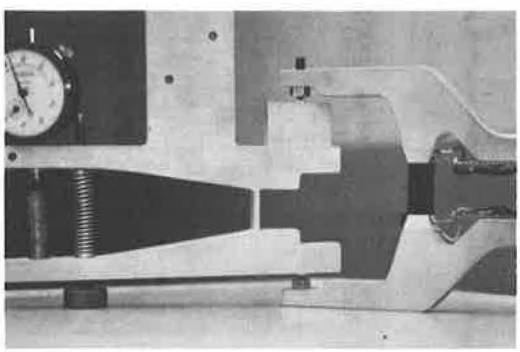

Figure 19. Calibration device for lateral extensometer.

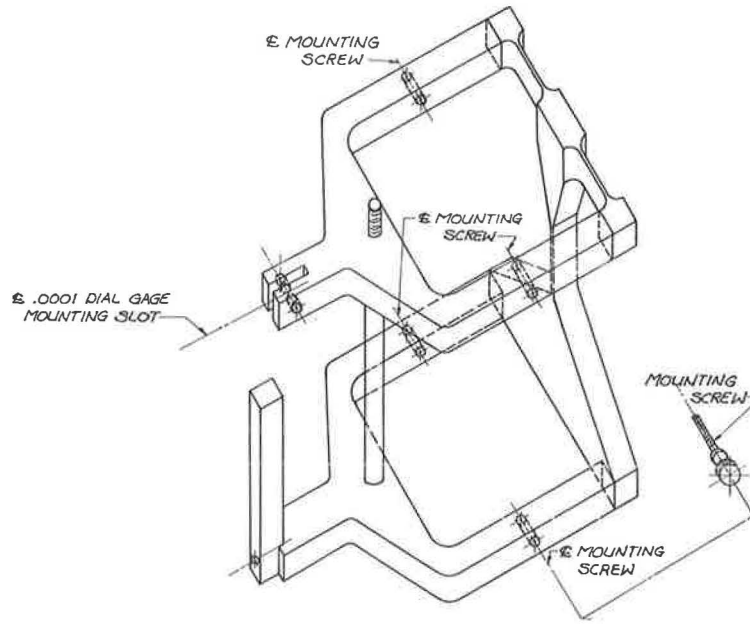

Figure 20. Mechanical compressometer.

during the initial loading. A mechanical compressometer (Fig. 20) for direct mounting on the spherical gage points was developed for this purpose. The instrument is designed so it can be removed after the initial loading period.

The compressometer is constructed with a pivot on one side of the specimen to increase the mechanical advantage. By simulating the pivot with a bi-axial flexure hinge, it was possible to construct an automatically-averaging instrument with no moving parts.

The longitudinal extensometer, the lateral extensometer, and the mechanical compressometer all use the same gage points. The system provides a check of all longitudinal strain measurements, both elastic and creep, through duplication of specimen and the use of clip-on strain meters, the longitudinal extensometer, and the mechanical compressometer. The system is flexible, complete and easy to operate.

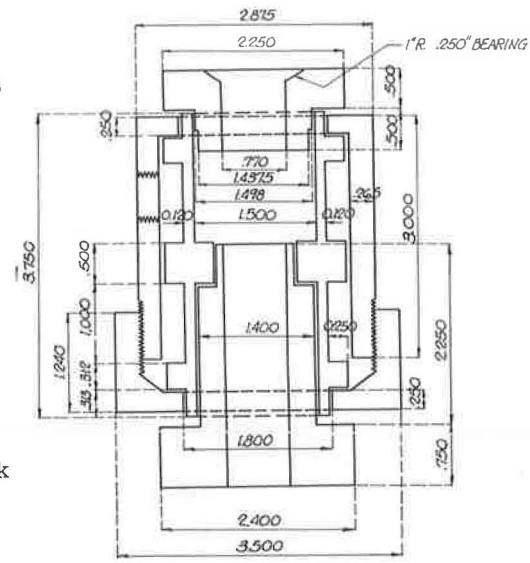

Figure 21. Load cell.

THE LOAD CELL

Figure 21 shows the special load-measuring instrument developed for use on this project. This device performs two important functions: the ball seat at the top insures a uniform load distribution to the specimen, and the instrument can be used to monitor the load transmitted to the specimen.

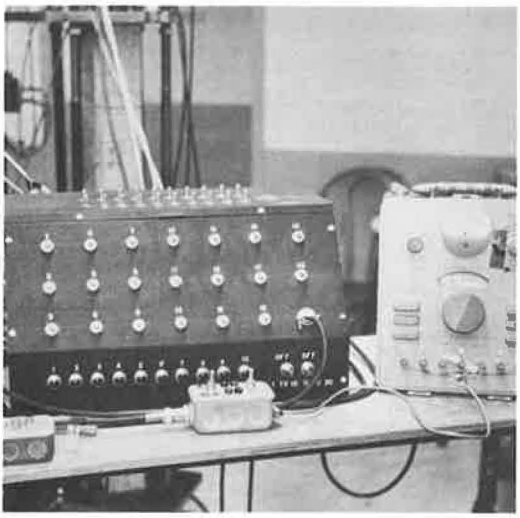

Figure 22. Read-out equipment.

The transducer consists of four SR-4 strain gages attached to a strain-sensing sleeve. The gages are connected in a bridge circuit with two gages mounted above and two mounted below the center of the sleeve. The sleeve is prestressed so that it is subjected to a tensile force throughout the test. The load is applied to the center of the sleeve by a plunger located directly below the ball and is transmitted to the case which serves as the reaction. Thus, the external load increases the strain in the top half of the sleeve and decreases the strain in the bottom half. Hence, all four of the gages are subjected to a change in strain. By mounting the gage pairs in opposite quadrants of the sleeve, the average axial-strain component is measured.

The load cells are calibrated in a hydraulic testing machine. Before used, all load cells are placed under a sustained load until all measurable creep has been eliminated. The load cells used in this test series have a capacity of 35,000 lb with an accuracy of ±100 lb.

THE READ-OUT EQUIPMENT

All of the electrical instruments described in this paper have one important common feature: the strain-sensing elements are bridge circuits using SR-4 strain gages. This makes it possible to read all the instruments with a single strain indicator. The strain indicator is connected to a 20-channel switch-and-balance unit (Fig. 22). The switch-and-balance unit is provided with 20 plug-type receptacles to connect the various instruments required for measuring the load and strain for a given series of specimens. With the four switch-and-balance units presently available connected in series, the output from 80 channels can be read with a single strain indicator.

INSTRUMENT RELIABILITY

Each instrument was calibrated and tested before it was used in the tests. Calibration data for the lateral extensometer, and for a typical clip-on strain meter and load cell are given in Table 1. Calibration curves, plotted using these data, are shown in Figures 23, 24, and 25. The mechanical compressometer does not require calibration, because the multiplication ratio for the dial readings can be determined by measuring the lever arms. Each instrument is re-calibrated every few months as a check on instrument stability. In most cases, there has been no appreciable change in the calibration.

Figure 26 shows a comparison of typical load-deflection curves using data obtained with the mechanical compressometer and the clip-on strain meters. The calculated moduli of elasticity seem to be in excellent agreement.

Figure 27 shows the average creep and shrinkage measured by four clip-on strain meters during the first 14 days under load and the average creep and shrinkage measured on a specimen in the same series using the longitudinal extensometer. The curves indicate sufficient agreement to warrant removal of the clip-on strain meters at the end of 14 days.

Data obtained with the lateral extensometer indicate that lateral creep and shrinkage strains are extremely small, the order of magnitude of the strains being about the same as the accuracy of the read-out equipment. This result may be due to the fact that lateral shrinkage and dilation due to creep tend to compensate each other.

TABLE 1

CALIBRATION DATA

Clip-on Electrical Strain Meter No. 601		Lateral Extensometer	
Δ, in. x 10^{-4}	K-Box Rdg.	Δ, in. x 10^{-4}	K-Box Rdg
0	0	0	0
4	50	117	350
8	100	235	700
12	150	353	1040
16	200	471	1390
20	250	588	1740
24	295		
26	320		

Load Cell No. 3504

Load, kips	K-Box Rdg.	Load, kips	K-Box Rdg.
0	0	16	1725
1	105	17	1825
2	215	18	1935
3	325	19	2040
4	430	20	2145
5	535	21	2250
6	645	22	2355
7	755	23	2465
8	865	24	2565
9	975	25	2665
10	1085	26	2775
11	1195	27	2875
12	1300	28	2980
13	1405	29	3085
14	1515	30	3185
15	1615		

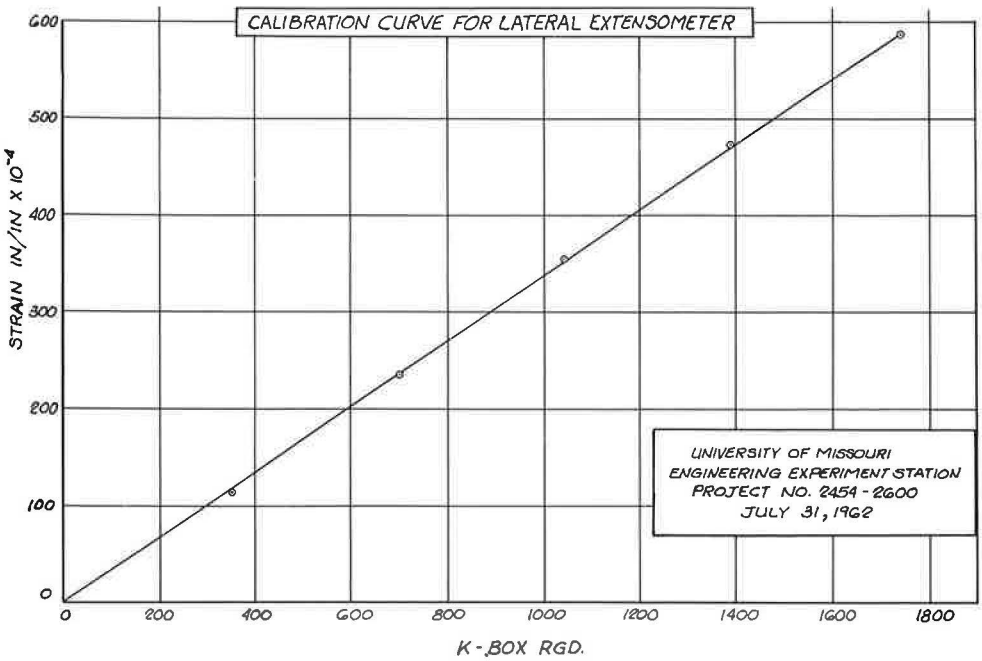

Figure 23. Calibration curve for lateral extensometer.

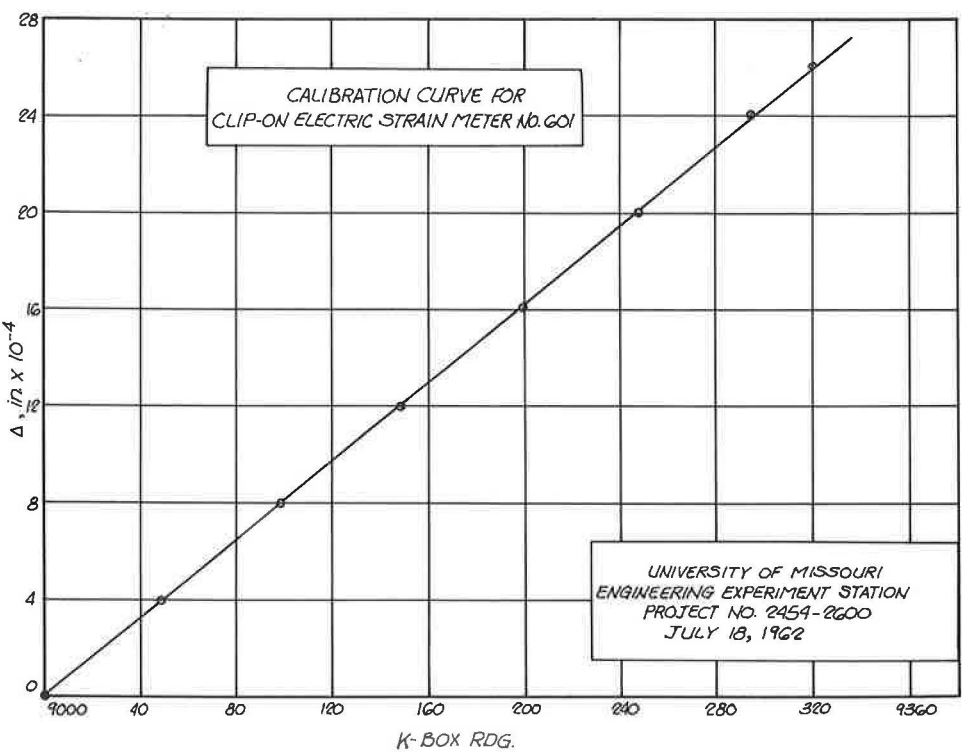

Figure 24. Calibration curve for clip-on electric strain meter.

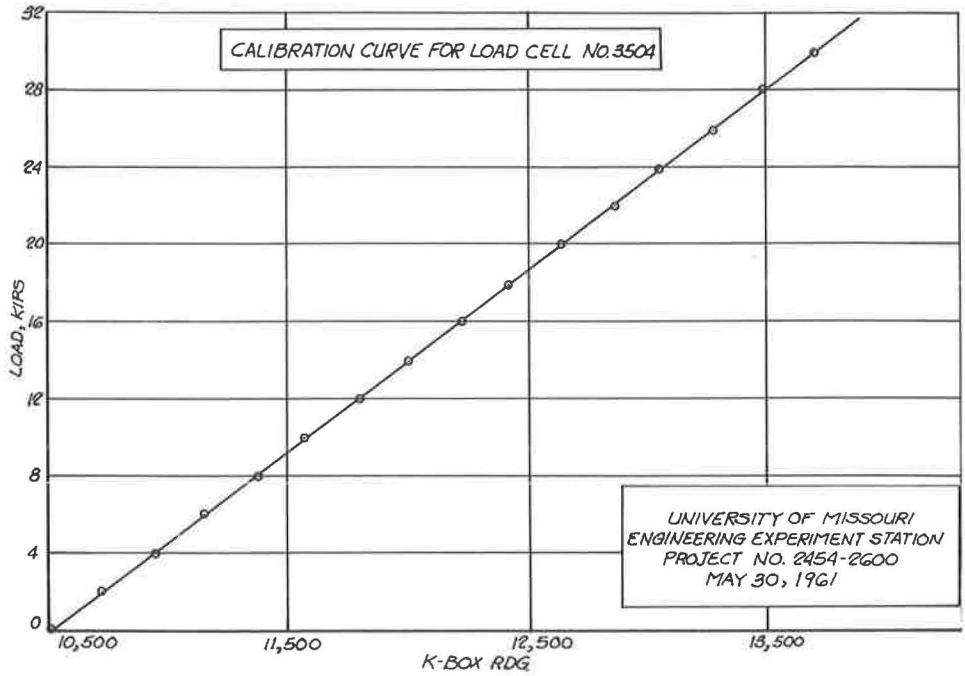

Figure 25. Calibration curve for load cell.

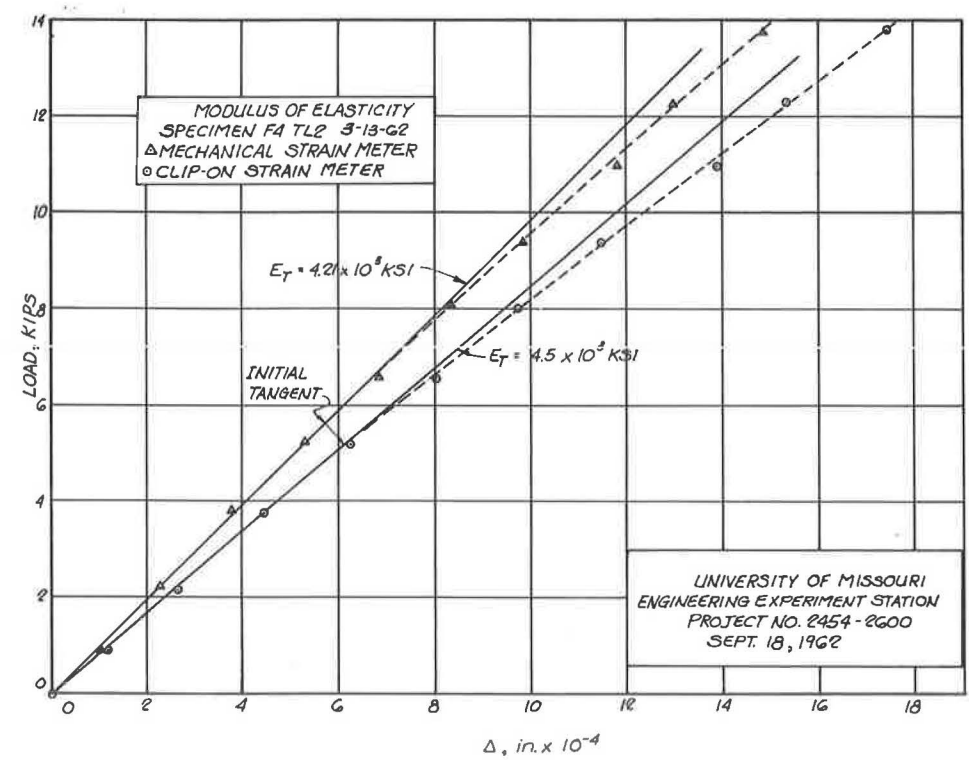

Figure 26. Modulus of elasticity.

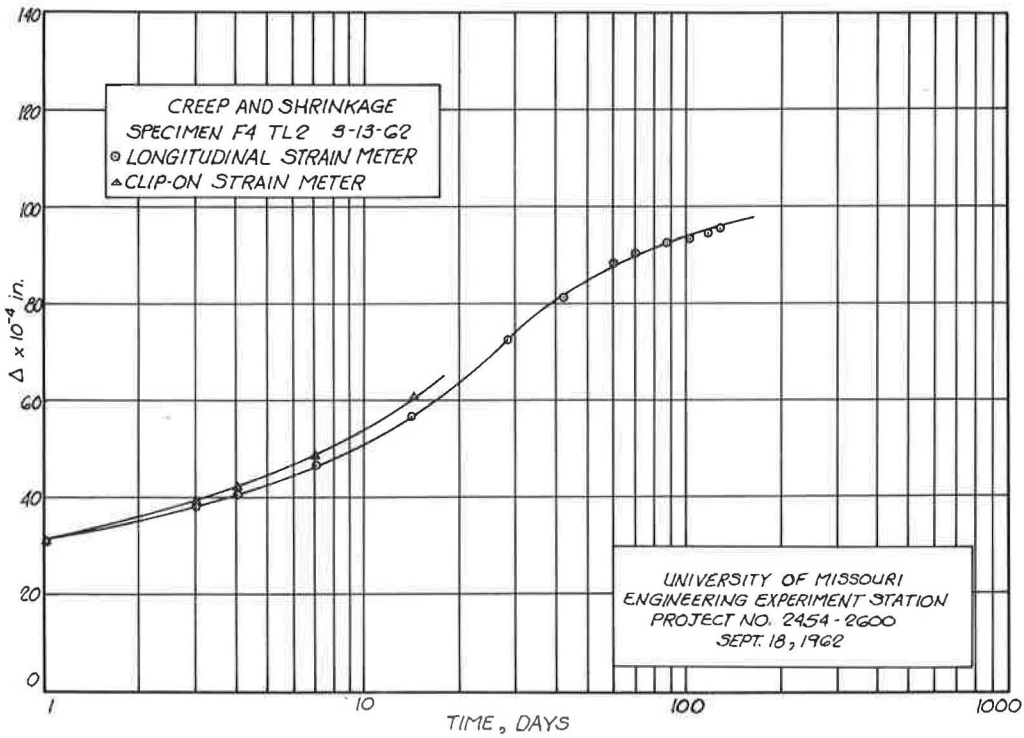

Figure 27. Creep and shrinkage.

CONCLUSIONS AND RECOMMENDATIONS

The loading frames used in this project are similar to the one recommended by ASTM and have performed satisfactorily during the past year's operation.

The design of the pumping-and-control system was based on apparatus originally developed at the University of California. Oil leakage past the piston cups has been much smaller than anticipated and seems to decrease with continued operation as reflected by the frequency of the pumping cycle. This cycle has decreased from several strokes every few minutes to several strokes every few hours. Therefore, it appears that the capacity of the oil-injection system may have been somewhat overdesigned.

The strain- and load-measuring instruments described have produced consistent data. The accuracy of all instruments meets the proposed ASTM requirements.

ACKNOWLEDGMENTS

The instrumentation described herein was developed as a part of the work of the Engineering Experiment Station of the University of Missouri. The program was sponsored jointly by the Missouri State Highway Commission and the Bureau of Public Roads.

Research assistants assigned to the project were James Monsees, Dean Froerer, and Jack Hill. The manuscript was typed by Jonette Rielle. The study was under the direction of Bernard L. Meyers, Project Engineer; Adrian Pauw, Professor of Civil Engineering; and H. D. Comins, Associate Professor of Civil Engineering.

REFERENCES

1. Pauw, A., and Breen, J. E., "Field Testing and Analysis of Two Prestressed Concrete Girders." HRB Bull. 307 (1961).

2. Technical Report No. 1, "Structural and Economic Study of Precast Bridge Units—Instrumentation." Univ. of Missouri, Eng. Experimentation (1957).
3. Pauw, A., and Meyers, B. L., "A Review of Literature Pertaining to Creep and Shrinkage of Concrete." Bull. 56, Univ. of Missouri, Eng. Exp. Sta. (1963).
4. "Tentative Method of Test for Creep of Concrete in Compression." ASTM (August 1, 1962).

Analysis of Continuous Skewed Slab Bridge Decks

ASIM YEGINOBALI, Ohio State University

In recent years, highway engineers have been making frequent use of the continuous skewed slab bridges on modern highways. Despite this fact, an adequate mathematical analysis of such bridges has not been available for the bridge engineer.

A bridge slab can be analyzed by the principles of the theory of plates. However, due to the complexity of the existing boundary conditions in continuous skewed slabs, the application of the high-order differential equations becomes extremely difficult and the use of finite difference equations for the mathematical analysis of such slabs provides a more practical and yet adequate approach. Utilizing such a finite differences method, altogether 32 different bridge slabs, with unstiffened edges, were analyzed. Twenty-three of these were three-span continuous slabs and had different angles of skew, width-center span length and end span-center span ratios. The remaining 9 single-span slabs had also different geometric parameters. The range of these parameters was determined such that the slab group encompassed the most common types that are being built in actual practice. The mathematical analysis of each slab included the simultaneous solutions of groups of finite difference deflection equations, computations of influence coefficients for deflections and moments at critical slab points, together with uniform load deflections and moments. IBM 704 and IBM 709 electronic computers were used in connection with the mathematical analysis, and results are presented in the form of tables, influence surface diagrams for deflections and moments, and contour diagrams for uniform load deflections and moments. Also included in the paper are various diagrams showing the effect of variation of each parameter on the maximum deflection and moment values. To verify the findings of the mathematical analysis and to correlate the results to reinforced concrete structures, 6 continuous-span and 2 single-span laboratory test structures were designed by utilizing various reinforcement patterns and tested under concentrated and uniform loads. Test results are indicated on corresponding deflection, moment diagrams and compared with the theoretical values. Finally, comments are made on the significance of the theoretical and experimental findings of the research.

• THIS PAPER is based on a research project sponsored by the Ohio Department of Highways and the U.S. Bureau of Public Roads and conducted at the Transportation Engineering Center of the Engineering Experiment Station at the Ohio State University. The purpose of this research project was the development of reliable design criteria for continuous skewed slab bridges through mathematical and experimental investigations. Altogether 32 different bridge slabs were analyzed using a finite differences method and 8 reinforced concrete laboratory test structures were designed, constructed and tested to verify the findings of the mathematical analysis and to correlate the re-

Paper sponsored by Committee on Bridges.

sults to reinforced concrete structures. The results of the mathematical analysis were presented in the form of some 300 tables and about 400 influence surface and contour diagrams in the final report of the project. The final report also included detailed information on the design and testing of all the test structures. This paper will summarize the theoretical and experimental phases of the research project and will include typical samples from the tables and diagrams of the final report.

APPLICATION OF THE FINITE DIFFERENCES METHOD

Finite differences methods have been successfully applied to several slab problems by various investigators. Among the most significant work in this field is the application of the elastic-web method to slabs of various shapes by Marcus (1) and the analysis of single-span simply-supported skewed slabs by Jensen (2). A similar method, as illustrated in a previous work (3), was used in this study for the analysis of continuous skewed slabs with unstiffened edges.

The finite differences method utilizes a series of deflection equations rather than the high-order differential equations which usually appear in slab problems. The infinite number of points on the deflecting surface of a slab is reduced to a finite number of points arranged to form a certain network. For each of the network points the following fourth-order differential equation is written in a linear form by making use of the finite differences.

$$\frac{\partial^4 w}{\partial x^4} + 2\frac{\partial^4 w}{\partial x^2 \partial y^2} + \frac{\partial^4 w}{\partial y^4} = \frac{p}{D} \qquad (1)$$

In its linear form the equation contains expressions for the deflection of the slab at the particular network point and for the deflections of the neighboring points on the left-hand side. The right-hand side of the equation contains an expression showing the loading and flexural rigidity of the slab at the particular network point. Similarly, second-order differential equations for the moments are also written in terms of the finite differences. A simultaneous solution of all the deflection equations for all the network points over the slab surface yields the numerical values for the deflections at these points. By substitution of these values of the deflections in the proper moment equations, numerical values of the moments are found. By such a procedure, the difficult and sometimes impossible task of solving high-order differential equations with complicated boundary conditions is simplified to the simultaneous solution of a finite number of linear equations.

The deflection and moment equations pertaining to various positions of the network points in different network systems are listed in the Appendix.

The major portion of the theoretical phase of this research project consisted of application of the finite differences method to 32 different bridge slabs. Of these slabs 23 were continuous-span type with symmetrical end spans and 9 were single-span slabs. All had unstiffened edges. For continuous-span slabs angle of skew, ϕ end span-center span ratio, b_e/b and width-center span ratio, a/b were chosen as the geometric parameters. The numerical values assigned to these parameters were

ϕ: 0^0, 30^0, 45^0 $\quad$ b_e/b: 0.6, 0.8, 1.0 $\quad$ a/b: 0.5, 1.0, 2.0

The geometric parameters and their numerical values for the single-span slabs

ϕ: 0^0, 30^0, 45^0 $\quad$ a/b: 1.0, 2.5, 5.0

Continuous-span slabs were designated as ϕ - b_e/b-a/b and single-span slabs as ϕ - a/b. Thus, individual slabs were defined by the assigned numerical values of these parameters: slab 30^0-0.6-0.5 indicating the continuous-span slab with 30^0 skew, having an end span-center span ratio of 0.6 and width-center span ratio of 0.5 and slab 0^0-1.0 defining a single-span square slab.

Figure 1. Network point numbers (slab 0°-0.8-1.0).

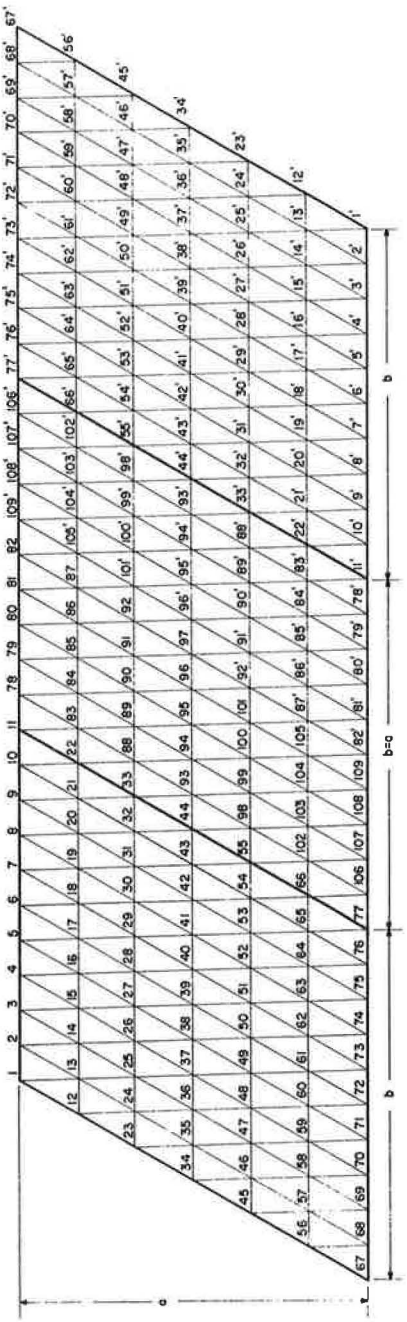

Figure 2. Network point numbers (slab 30°-1.0-1.0).

It was felt that by forming all the possible combinations of these parameters with their numerical values as indicated, the geometric shapes of the majority of the bridge slabs being constructed in actual practice would be encompassed. Due to uniform variations of deflections and moments in the rectangular slab group, 5 rectangular continuous-span slabs were omitted from the program and altogether 32 slabs were considered for the analysis.

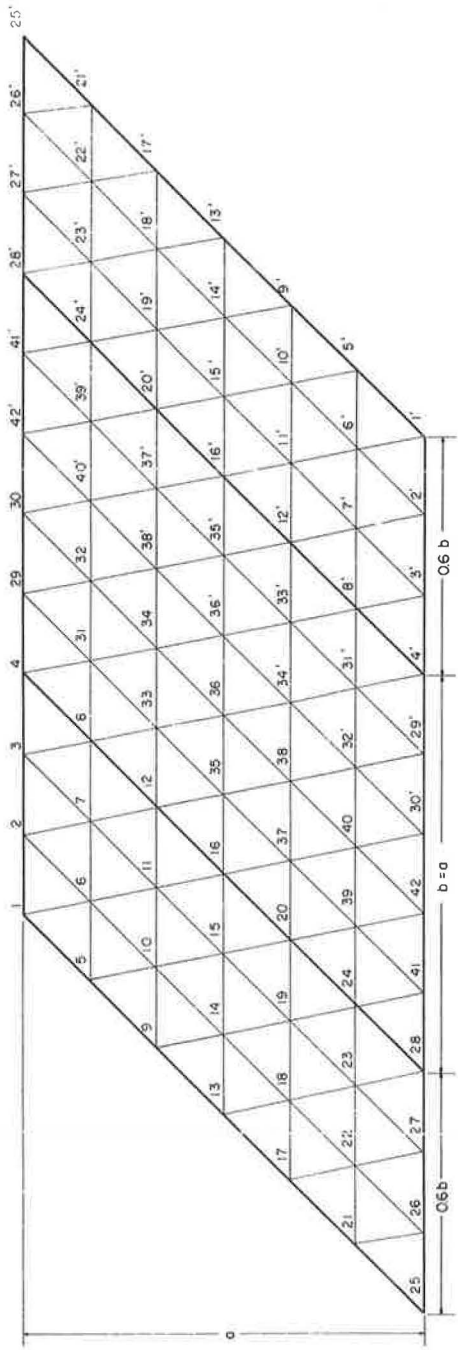

Figure 3. Network point numbers (slab 45°-0.6-1.0).

TABLE 1

NUMBER OF NETWORK POINTS AND DEFLECTION EQUATIONS FOR THE SLAB GROUP

Slab	Total Network Points	No. of Deflection Eqs.	Network Type
ϕ - b_e/b - a/b			
0°-0.6-0.5	115	48	Rectangular
0°-0.6-1.0	115	48	Rectangular
0°-0.6-2.0	115	48	Rectangular
0°-0.8-1.0	135	58	Rectangular
0°-1.0-1.0	155	68	Rectangular
30°-0.6-0.5	161	67	Skew
30°-0.6-1.0	161	67	Skew
30°-0.6-2.0	161	67	Skew
30°-0.8-0.5	189	81	Skew
30°-0.8-1.0	189	81	Skew
30°-0.8-2.0	189	81	Skew
30°-1.0-0.5	217	95	Skew
30°-1.0-1.0	217	95	Skew
30°-1.0-2.0	217	95	Skew
45°-0.6-0.5	84	28	Skew
45°-0.6-1.0	84	28	Skew
45°-0.6-2.0	132	44	Square
45°-0.8$\hat{3}$-0.5	85	33	Skew
45°-0.8$\hat{3}$-1.0	119	46	Square
45°-0.8$\hat{3}$-2.0	221	85	Square
45°-1.0-0.5	117	41	Skew
45°-1.0-1.0	117	41	Skew
45°-1.0-2.0	117	41	Square
ϕ - a/b			
0°-1.0	81	32	Rectangular
0°-2.5	55	17	Rectangular
0°-5.0	105	32	Rectangular
30°-1.0	81	32	Skew
30°-2.5	55	17	Skew
45°-1.0	81	32	Square
45°-2.5	55	17	Square
45°-5.0	105	32	Square

After establishing such a representative group of bridge slabs, the next step was to assign a point network system to each individual slab for finite differences analysis. Figures 1, 2, 3 and 4 show these networks and the numbering systems of the slab points on the surfaces of typical slabs. For the 45° skewed continuous-span group b_e/b ratio of 0.8 is replaced by 5/6 (or 0.83) for better fitting of the particular network systems. In all the slabs, at least the minimum number of network points required for an accurate analysis are maintained.

The slab points are divided into two symmetrical groups about an axis through the middle of the slab. The points to the left of this axis are numbered as 1, 2, etc., and the ones on the right side are numbered as 1′, 2′, etc. Under a symmetrical loading, points having the same number with and without a prime have the same deflection and moment.

Table 1 gives the total number of network points, the number of deflection equations for each slab and the type of network used. The number of deflection equations are

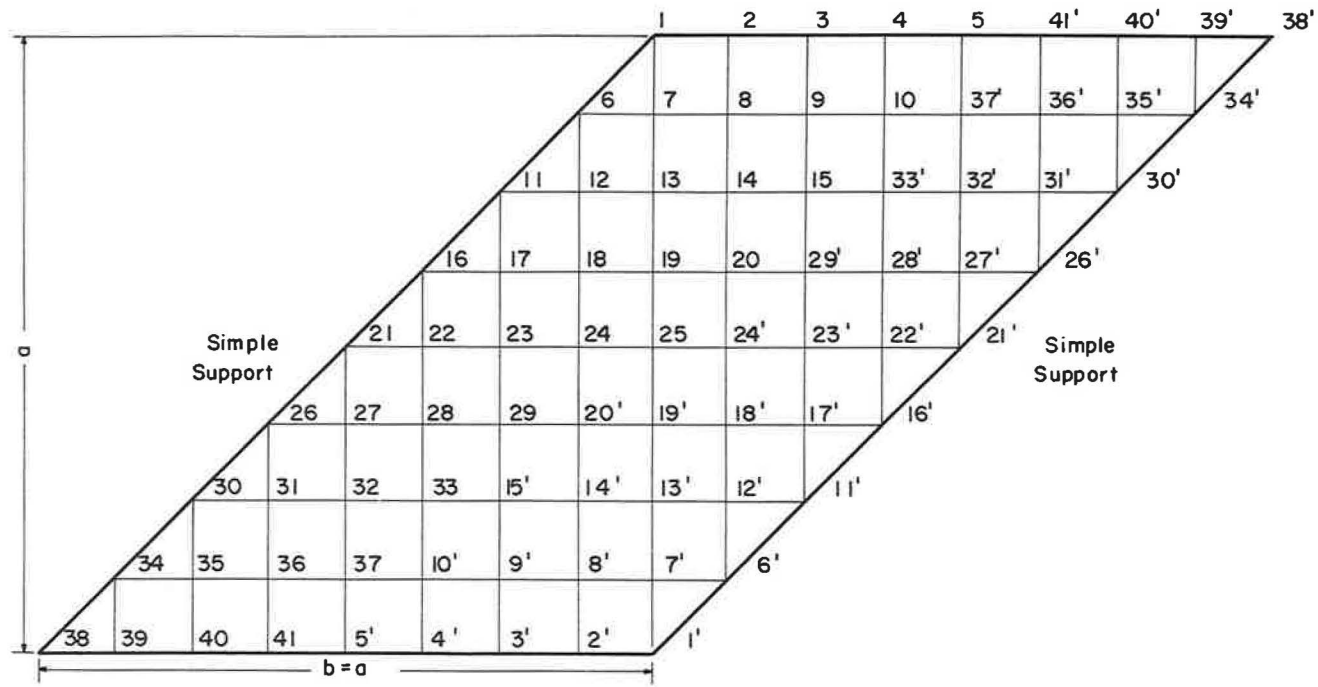

Figure 4. Network point numbers (slab 45°-1.0).

TABLE 2

INFLUENCE COEFFICIENTS FOR POINT 97, SLAB 30°-1.0-1.0

(Deflections as $\frac{Pa^2}{Eh^3}$; moments as P; θ, in degrees)

Load at	w	M_x	M_y	M_{xy}	M_{max}	M_{min}	θ
2	-0.01402	-0.01039	-0.00500	-0.00343	-0.01205	-0.00334	25.9
3	-0.02824	-0.02129	-0.01005	-0.00644	-0.02422	-0.00712	24.4
4	-0.04094	-0.03148	-0.01445	-0.00870	-0.03514	-0.01079	22.8
5	-0.05100	-0.03999	-0.01760	-0.00998	-0.04380	-0.01379	20.9
6	-0.05708	-0.04591	-0.01890	-0.01020	-0.04933	-0.01548	18.5
7	-0.05760	-0.04824	-0.01782	-0.00941	-0.05092	-0.01514	15.9
8	-0.05322	-0.04589	-0.01409	-0.00785	-0.04772	-0.01226	13.1
9	-0.04166	-0.03762	-0.00814	-0.00585	-0.03874	-0.00703	10.8
10	-0.02344	-0.02231	-0.00192	-0.00354	-0.02291	-0.00132	9.6
13	-0.00922	-0.00613	-0.00326	-0.00318	-0.00818	-0.00121	32.9
14	-0.01934	-0.01317	-0.00701	-0.00615	-0.01697	-0.00322	31.7
15	-0.02933	-0.02043	-0.01088	-0.00868	-0.02548	-0.00583	30.4
16	-0.03799	-0.02703	-0.01437	-0.01018	-0.03269	-0.00871	29.1
17	-0.04412	-0.03211	-0.01696	-0.01073	-0.03767	-0.01140	27.4
18	-0.04661	-0.03479	-0.01806	-0.01009	-0.03953	-0.01331	25.2
19	-0.04434	-0.03415	-0.01704	-0.00831	-0.03752	-0.01367	22.1
20	-0.03627	-0.02912	-0.01339	-0.00563	-0.03093	-0.01158	17.8
21	-0.02057	-0.01835	-0.00717	-0.00262	-0.01893	-0.00659	12.5
24	-0.00685	-0.00414	-0.00197	-0.00316	-0.00639	0.00028	35.5
25	-0.01429	-0.00880	-0.00445	-0.00617	-0.01317	-0.00008	35.3
26	-0.02179	-0.01367	-0.00725	-0.00882	-0.01985	-0.00108	35.0
27	-0.02862	-0.01827	-0.01015	-0.01083	-0.02578	-0.00265	34.7
28	-0.03393	-0.02198	-0.01283	-0.01193	-0.03018	-0.00436	34.5
29	-0.03674	-0.02411	-0.01489	-0.01188	-0.03224	-0.00675	34.4
30	-0.03601	-0.02391	-0.01573	-0.01049	-0.03107	-0.00857	34.3
31	-0.03057	-0.02055	-0.01451	-0.00771	-0.02581	-0.00926	34.3
32	-0.01911	-0.01307	-0.00990	-0.00384	-0.01564	-0.00733	33.8
35	-0.00513	-0.00287	-0.00085	-0.00300	-0.00503	0.00130	35.7
36	-0.01070	-0.00608	-0.00211	-0.00596	-0.01038	0.00219	35.8
37	-0.01631	-0.00940	-0.00368	-0.00869	-0.01568	0.00261	35.9
38	-0.02148	-0.01252	-0.00543	-0.01095	-0.02049	0.00254	36.0
39	-0.02559	-0.01506	-0.00718	-0.01251	-0.02424	0.00200	36.3
40	-0.02794	-0.01651	-0.00872	-0.01311	-0.02630	0.00106	36.7
41	-0.02768	-0.01633	-0.00971	-0.01246	-0.02591	-0.00013	37.5
42	-0.02385	-0.01390	-0.00960	-0.01024	-0.02221	-0.00128	39.1
43	-0.01520	-0.00858	-0.00725	-0.00615	-0.01411	-0.00173	41.9
46	-0.00386	-0.00203	-0.00066	-0.00270	-0.00392	0.00183	35.0
47	-0.00803	-0.00428	-0.00040	-0.00543	-0.00810	0.00343	35.2
48	-0.01221	-0.00659	-0.00094	-0.00800	-0.01225	0.00472	35.3
49	-0.01604	-0.00875	-0.00162	-0.01023	-0.01602	0.00565	35.4
50	-0.01905	-0.01048	-0.00232	-0.01188	-0.00190	0.00616	35.5
51	-0.02072	-0.01147	-0.00289	-0.01271	-0.02060	0.00623	35.7
52	-0.02041	-0.01136	-0.00317	-0.01242	-0.02034	0.00581	35.9
53	-0.01744	-0.00973	-0.00295	-0.01064	-0.01751	0.00482	36.2
54	-0.01099	-0.00614	-0.00200	-0.00682	-0.01120	0.00305	36.5
57	-0.00297	-0.00148	0.00040	-0.00239	-0.00312	0.00203	34.3
58	-0.00615	-0.00309	0.00063	-0.00482	-0.00640	0.00394	34.4
59	-0.00932	-0.00474	0.00073	-0.00713	-0.00964	0.00563	34.5
60	-0.01220	-0.00627	0.00071	-0.00915	-0.01257	0.00701	34.6

TABLE 2

INFLUENCE COEFFICIENTS FOR POINT 97, SLAB 30°-1.0-1.0 (Cont'd.)

Load at	w	M_x	M_y	M_{xy}	M_{max}	M_{min}	θ
61	-0.01442	-0.00747	0.00064	-0.01065	-0.01481	0.00798	34.6
62	-0.01556	-0.00812	0.00057	-0.01139	-0.01597	0.00842	34.5
63	-0.01516	-0.00796	0.00057	-0.01107	-0.01556	0.00817	34.5
64	-0.01273	-0.00672	0.00060	-0.00937	-0.01312	0.00700	34.3
65	-0.00783	-0.00415	0.00055	-0.00587	-0.00812	0.00453	34.1
68	-0.00248	-0.00117	0.00063	-0.00219	-0.00264	0.00210	33.8
69	-0.00504	-0.00240	0.00119	-0.00439	-0.00536	0.00414	33.9
70	-0.00754	-0.00363	0.00166	-0.00650	-0.00801	0.00603	33.9
71	-0.00982	-0.00475	0.00204	-0.00835	-0.01037	0.00766	33.9
72	-0.01156	-0.00562	0.00233	-0.00975	-0.01218	0.00888	33.9
73	-0.01242	-0.00607	0.00252	-0.01044	-0.01306	0.00852	33.8
74	-0.01202	-0.00589	0.00256	-0.01014	-0.01264	0.00933	33.7
75	-0.01002	-0.00489	0.00238	-0.00851	-0.01051	0.00800	33.4
76	-0.00604	-0.00294	0.00169	-0.00523	-0.00634	0.00509	33.1
78	0.02468	0.02464	-0.01086	0.00888	0.02673	-0.01296	13.3
79	0.04436	0.04308	-0.02266	0.02247	0.05003	-0.02960	17.2
80	0.05556	0.04878	-0.02878	0.03733	0.06382	-0.04382	21.9
81	0.05764	0.04432	-0.02938	0.04562	0.06611	-0.05117	25.5
82	0.05220	0.03493	-0.02646	0.04541	0.05905	-0.05057	28.0
83	0.02734	0.02835	0.00309	0.00198	0.02850	0.00293	4.5
84	0.05278	0.05915	-0.00050	0.00856	0.06036	-0.00170	8.0
85	0.07026	0.08071	-0.00655	0.02243	0.08614	-0.01197	13.6
86	0.07631	0.07783	-0.00717	0.04144	0.09469	-0.02403	22.1
87	0.07162	0.06213	-0.00621	0.04821	0.08706	-0.03114	27.3
88	0.02870	0.02197	0.01661	0.00080	0.02208	0.01649	8.3
89	0.06015	0.05656	0.03172	0.00066	0.05658	0.03170	1.5
90	0.08732	0.10350	0.03899	0.00379	0.10373	0.03877	3.3
91	0.10289	0.14854	0.03509	0.01778	0.15126	0.03237	8.7
92	0.10076	0.11485	0.03858	0.05342	0.14235	0.01108	27.2
93	0.02454	0.01109	0.01907	0.00779	0.02383	0.00633	-31.4
94	0.05524	0.02993	0.04936	0.01411	0.05677	0.02251	-27.7
95	0.08762	0.06398	0.09188	0.01887	0.10140	0.05446	-26.8
96	0.11602	0.13221	0.14882	0.02618	0.16798	0.11305	-36.2
97	0.13176	0.29445	0.21447	0.05401	0.32167	0.18726	26.7
98	0.01692	0.00961	0.00336	0.01171	0.01861	-0.00563	37.5
99	0.03888	0.02350	0.01117	0.02567	0.04374	-0.00907	38.2
100	0.06312	0.04427	0.02227	0.03978	0.07455	-0.00801	37.3
101	0.08550	0.07472	0.03317	0.05150	0.10948	-0.00158	34.0
102	0.01132	0.00619	-0.00213	0.00935	0.01227	-0.00820	33.0
103	0.02607	0.01528	-0.00427	0.02142	0.02905	-0.01805	32.7
104	0.04291	0.02778	-0.00539	0.03406	0.04907	-0.02669	32.0
105	0.05924	0.04385	-0.00573	0.04426	0.06979	-0.03167	30.4
106	0.00774	0.00357	-0.00358	0.00716	-0.00801	0.00800	31.7
107	0.01778	0.00861	-0.00908	0.01684	-0.01926	0.01879	31.1
108	0.02968	0.01563	-0.01543	0.02805	0.03216	-0.03196	30.5
109	0.04194	0.02466	-0.02151	0.03855	0.04651	-0.04336	29.5

TABLE 3

UNIFORM LOAD DEFLECTIONS AND MOMENTS, SLAB 45^0-0.6-1.0

(All Spans Loaded)

(Deflections as $\frac{pa^4}{Eh^3}$; moments as pa^2; θ, in degrees)

Point	w	M_x	M_y	M_{xy}	M_{max}	M_{min}	θ
1	0	0	0	0.00412	0.00412	-0.00412	45.0
2	-0.00147	0.00311	0	-0.00411	0.00594	-0.00284	-34.6
3	-0.00444	-0.01543	0	-0.00906	-0.01962	0.00419	24.8
4	0	-0.04723	0	0.01256	-0.05036	0.00313	-14.0
5	0	0.00073	-0.00073	0	0.00073	-0000073	0
6	0.00041	0.00458	0.00365	0.00102	0.00524	0.00300	32.7
7	-0.00111	-0.00553	-0.00030	-0.00553	-0.00903	0.00321	32.4
8	0	-0.02252	-0.01169	-0.01265	-0.03086	-0.00334	33.4
9	0	0.00079	-0.00079	0	0.00079	-0.00079	0
10	0.00075	0.00449	0.00401	0.00318	0.00744	0.00106	42.8
11	-0.00037	-0.00348	-0.00253	-0.00290	-0.00594	-0.00006	40.3
12	0	-0.02182	-0.01975	-0.01537	-0.03619	-0.00538	43.1
13	0	0.00193	-0.00193	0	0.00193	-0.00193	0
14	0.00111	0.00554	0.00394	0.00419	0.00901	0.00047	39.6
15	-0.00015	-0.00336	-0.00275	-0.00172	-0.00480	-0.00131	40.0
16	0	-0.02222	-0.02233	-0.01647	-0.03875	-0.00580	-45.1
17	0	0.00432	-0.00432	0	0.00432	-0.00432	0
18	0.00200	0.00797	0.00421	0.00594	0.01232	-0.00014	36.2
19	0.00048	-0.00227	-0.00072	0.00003	-0.00227	-0.00716	- 1.3
20	0	-0.02385	-0.02063	-0.01645	-0.03877	-0.00571	42.2
21	0	0.00415	-0.00415	0	0.00415	-0.00415	0
22	0.00399	0.01296	0.00321	0.00588	0.01573	0.00045	25.2
23	0.00199	0.00050	0.00352	0.00539	0.00761	-0.00359	-37.2
24	0	-0.02407	-0.01293	-0.01368	-0.03327	-0.00373	33.9
25	0	0	0	-0.00496	0.00496	-0.00496	45.0
26	0.00590	0.01107	0	0.00240	0.01156	-0.00050	11.7
27	0.00649	0.01475	0	0.00718	0.01766	-0.00292	22.1
28	0	-0.02397	0	-0.00108	-0.02402	0.00005	2.6
29	0.01914	0.02735	0	0.01596	0.03469	-0.00734	24.7
30	0.02515	0.02895	0	0.00773	0.03089	-0.00193	14.1
31	0.01108	0.00422	0.00916	0.01330	0.02022	-0.00684	-39.7
32	0.02079	0.02580	0.01082	0.01460	0.03472	0.00191	31.4
33	0.00942	0.00411	0.00509	0.00528	0.00991	-0.00070	-42.3
34	0.01724	0.01791	0.01541	0.01599	0.03269	0.00062	42.8
35	0.00921	0.00425	0.00172	0.00284	0.00610	-0.00012	33.0
36	0.01650	0.01737	0.01451	0.01414	0.03015	0.00173	42.1
37	0.00948	0.00299	0.00059	-0.00013	0.00300	0.00059	- 3.1
38	0.01757	0.01934	0.01210	0.01197	0.02822	0.00322	36.6
39	0.00863	-0.00314	0.00160	-0.00419	-0.00558	0.00404	30.3
40	0.01889	0.01872	0.00869	0.00629	0.02175	0.00567	25.7
41	0.00520	-0.01508	0	-0.00903	-0.01930	0.00422	25.1
42	0.01727	0.00911	0	-0.00217	0.00960	-0.00049	-12.7

one-half as many as the number of points on the deflecting slab surface. This is accomplished by resolving all the possible loading systems into symmetrical and antisymmetrical load systems (Appendix).

Most of the computational steps in the application of the finite differences method to the slab group were performed by the electronic computer. These steps included inversion of matrices having sizes as large as 95 by 95 vector multiplication of the inverse matrices with various column vectors and other operations in connection with matrices. Earlier in the project the IBM 704 computer of the Numerical Computation Laboratory and later the IBM 709 computer was used for the computations.

For each of the 32 slabs, deflection and moment influence coefficients have been calculated for critical slab points, and deflections and moments at all the slab points have been found under four different uniform loading systems. The complete results of the mathematical analysis were compiled in some 300 tables. Tables 2 and 3 are typical examples. The first column of Table 2 indicates the position of the moving concentrated load by the numbers of the network points. The second column gives the influence coefficients for the deflection, w. The remaining columns give the influence coefficients for moments M_x, M_y, M_{xy} and the principal moments. The last column indicates the values for angle θ which gives the direction of the maximum moment measured from the x-axis. Positive deflections are measured in a downward direction,

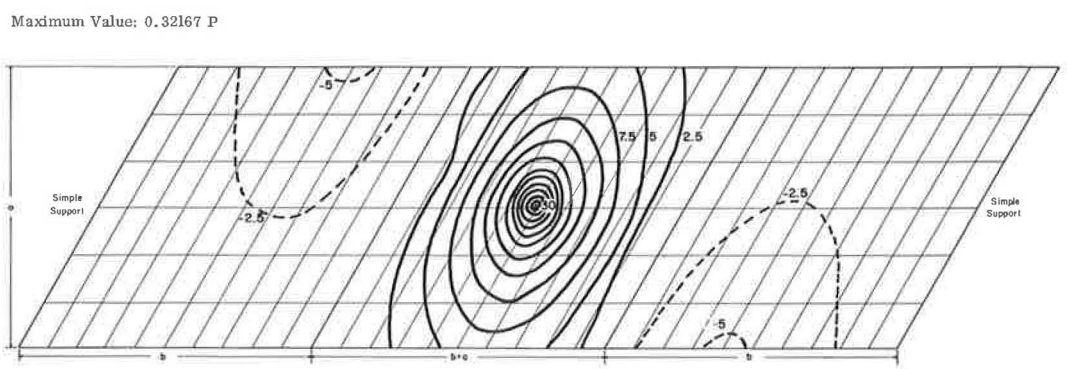

Figure 5. Influence surface for moment (M_{max}) at point 97 (slab 30°-1.0-1.0); contour interval: $2.5 \times 10^{-3} \frac{pa^4}{Eh^3}$.

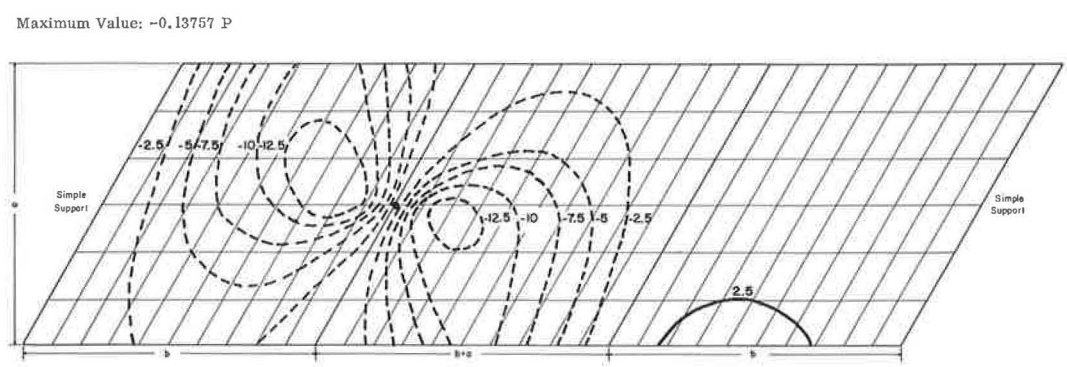

Figure 6. Influence surface for moment (M_{max}) at point 44 (slab 30°-1.0-1.0); contour interval: 2.5×10^{-2} P.

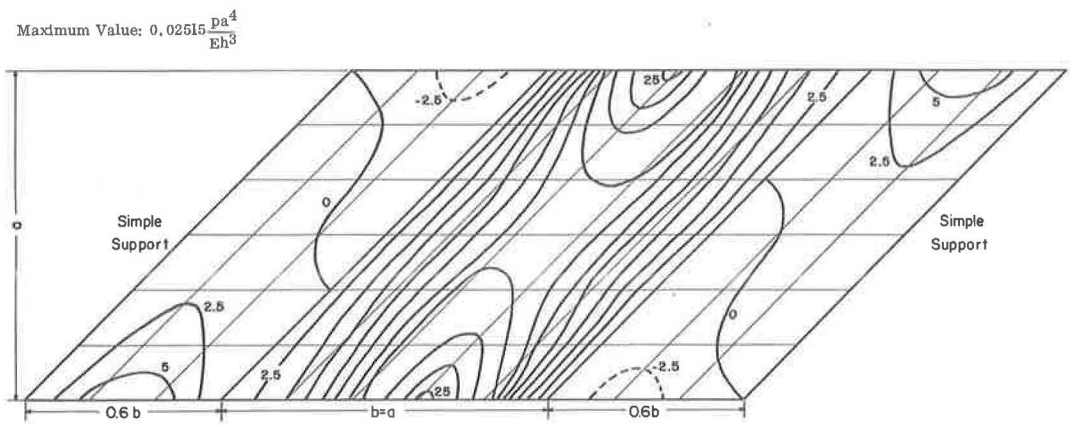

Figure 7. Uniform load deflection contours, all spans loaded; (slab 45°-0.6-1.0); contour interval: $2.5 \times 10^{-3} \frac{pa^4}{Eh^3}$.

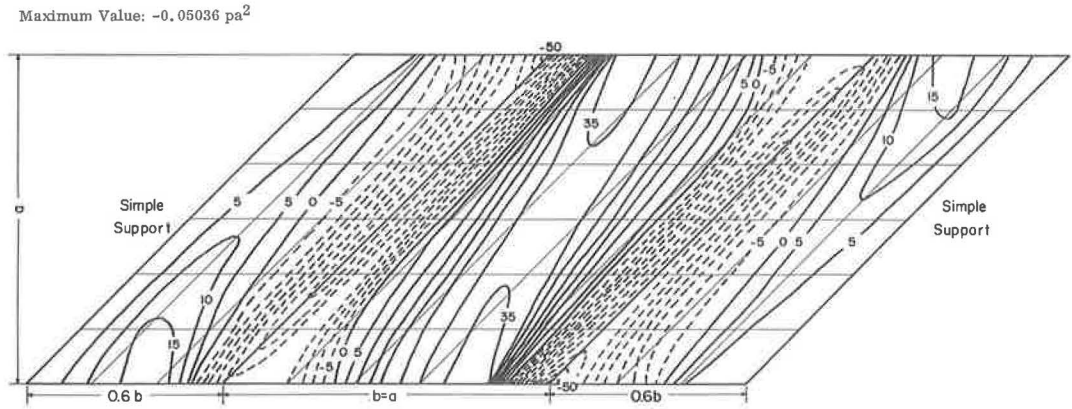

Figure 8. Uniform load moment (M_{max}) contours, all spans loaded; (slab 45°-0.6-1.0) contour interval: $5 \times 10^{-3} pa^2$.

positive moments indicate compression in the top fibers of the slab and the positive values of θ are measured in a clockwise direction. Table 3 is one of the four uniform load tables prepared for slab 45°-0.6-1.0 containing information on deflections and moments at all the slab points when all the spans are uniformly loaded. In the tables, figures smaller than 1×10^{-5} are indicated by a zero. Based on the information in these tables, some 400 influence surface and contour diagrams were prepared for the 32 slabs analyzed. Figures 5 through 8 are samples for this group of diagrams.

EXPERIMENTS ON TEST STRUCTURES

The experimental phase of the research included the design construction and testing of a group of laboratory test structures to correlate the results of the mathematical analysis to reinforced concrete slabs and to provide an experimental basis of comparison for the theoretical analysis obtained through the finite differences method.

Altogether six continuous-span and two single-span slabs were designed and tested. The test structures were 0°-0.6-1.0, 30°-0.6-1.0, 30°-0.8-0.5, 30°-1.0-0.5, 45°-0.6-1.0, 45°-0.83-0.5, 0°-1.0, and 30°-2.5.

The center span lengths of the test structures were 10 ft and the thicknesses of the slabs were either 4 or 6 in.

SR-4 electrical strain gages were used to measure the strains on concrete and on reinforcing bars under various types of loads. Type A-9 electrical strain gages and Type AR-1 rosette gages were mounted on the reinforcing bars. Deflections of the slab were measured by dial indicators. Load cells made of Type A-1 strain gages measured the reactions along the interior and end supports of the slabs. Aluminum alloy (6061-T6) wide-flange beams were placed along each support under the slab. These beams were cut $2\frac{1}{2}$ in. deep to the bottom flange every 6 in. to form a number of segments along the support. Each segment was converted to a load cell by using four strain gages connected in series. These load cells were calibrated by recording increments of strain corresponding to direct load increments.

All the test structures were tested under concentrated and uniform loads. Concentrated loads on the slab surface were simulated by using hydraulic rams with capacities up to 100 kips. In a majority of the cases, the load was transferred to the slab through a $4\frac{1}{2}$- × $4\frac{1}{2}$-in. steel plate 1 in. thick. When the load was applied over a concrete strain gage, a special plate with a groove was used to protect the gage from direct contact. Loads were applied over the slab surface at strategic locations corresponding to the theoretical network points at intensities within the working load range. The intensity of the hydraulic pressure was controlled by an electronic load cell.

Uniformly distributed loading of the slabs was accomplished by exerting air pressure to the slab surface through "air bags" made of polyethylene sheets. The air bags, one for each span, were placed between the slab surface and a steel restraining frame. By controlling the valves' opening to the individual air bags from a common air line, the four different uniform loading systems could be simulated: center span uniformly loaded, two end spans uniformly loaded, all spans uniformly loaded, and adjacent spans uniformly loaded. The intensity of air pressure was measured by a mercury manometer.

The designs of the test structures were based on the mathematical analyses of the corresponding slabs. Altogether four distinct design types were utilized.

In the designs of test structures 0^0-0.6-1.0, 30^0-0.8-0.5, 45^0-0.83-0.5 and 0^0-1.0, the longitudinal and transverse steel bars were placed in the x- and y-directions, respectively.

Test structures 30^0-1.0-0.5, 45^0-0.6-1.0 and 30^0-2.5 were designed with longitudinal steel placed in the x-direction and with transverse steel running in a direction parallel to the supports, making the angle of skew ϕ with the y-axis.

Although it was not used in the actual construction of the test structure, a third type of design was also applied to test structure 45^0-0.6-1.0. The longitudinal and the transverse steel are placed along the general directions of the maximum and the minimum principal moments, respectively.

The fourth type of design, although not practical, was used in the construction of test structure 30^0-0.6-1.0 to provide uniform reinforced-concrete sections throughout the slab for the purpose of comparing the allowable elastic and the ultimate strength loads. The reinforcement patterns were identical for the top and the bottom of the slab, and consisted of closely spaced reinforcing bars running along the x- and y-directions.

A detailed explanation of the four different design procedures is not included in this paper. They were different from the conventional elastic design methods only in the calculation of the effective reinforcing steel areas when the directions of the principal moments and of the reinforcement did not coincide. After the tests with loads in the working range, slabs were tested to failure. Figure 9 shows the reinforcement layout for test structure 30^0-1.0-0.5. This test structure was tested to failure under concentrated loads (Fig. 10). The results of the concentrated- and uniform-load tests on each of the eight test structures were tabulated and the experimental and the theoretical values of the strains, moments and deflections at various points along sections of the slab were compared on diagrams (Figs. 11, 12 and 13). The numbers of the network points along the longitudinal sections are also indicated in these diagrams.

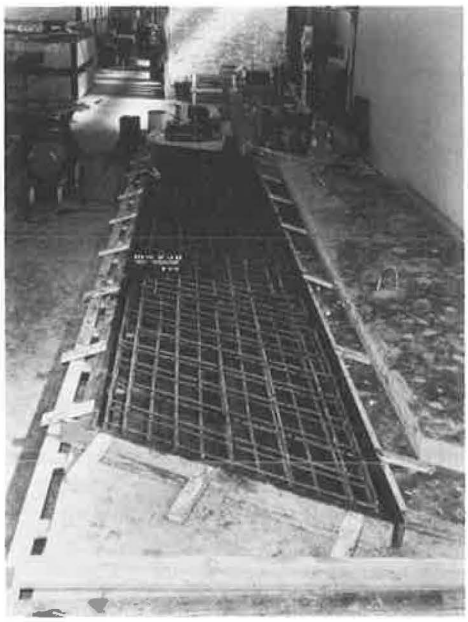

Figure 9. Reinforcement layout (test structure: 30°-1.0-0.5).

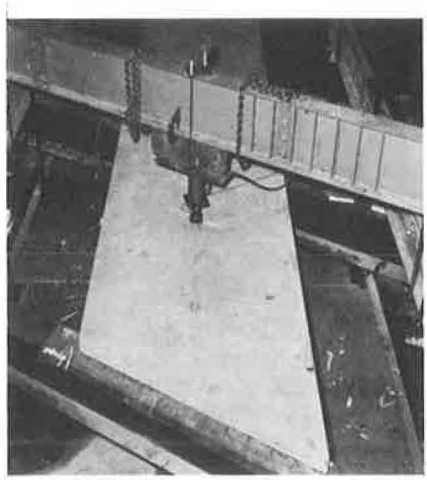

Figure 10. Testing to failure (test structure: 30°-1.0-0.5).

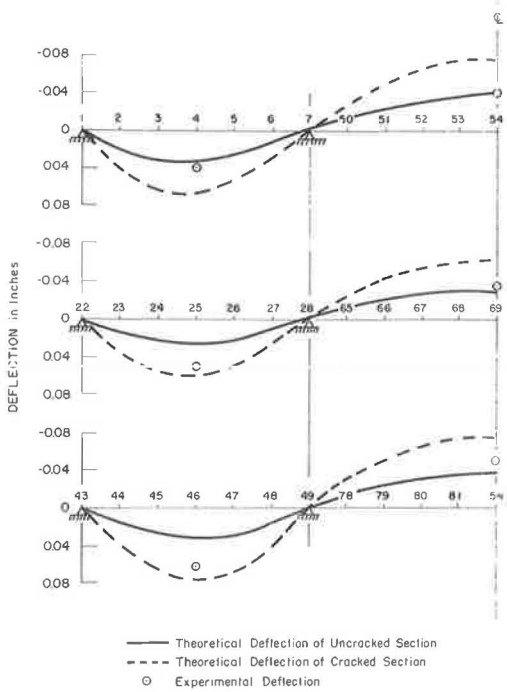

Figure 11. Theoretical and experimental deflections (test structure: 30°-0.6-1.0); two end spans loaded, p = 3 psi.

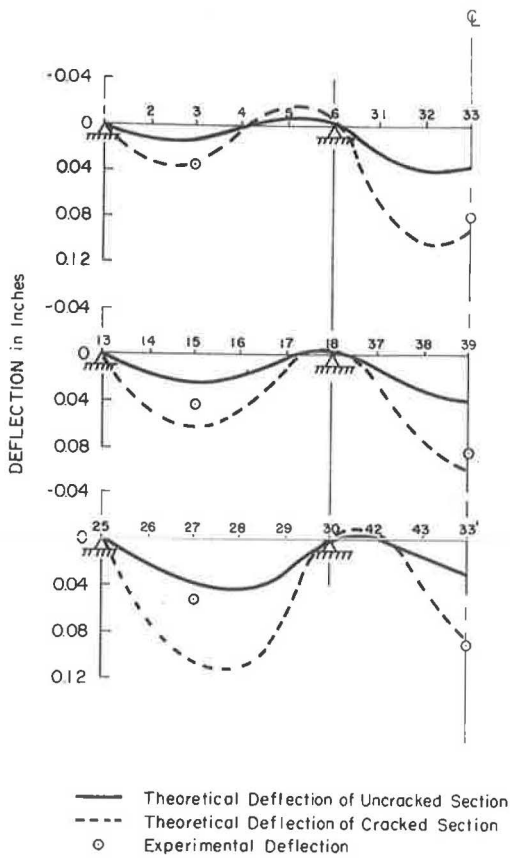

Figure 12. Theoretical and experimental deflections (test structure: 45°-0.83-0.5); all spans loaded, p = 6 psi.

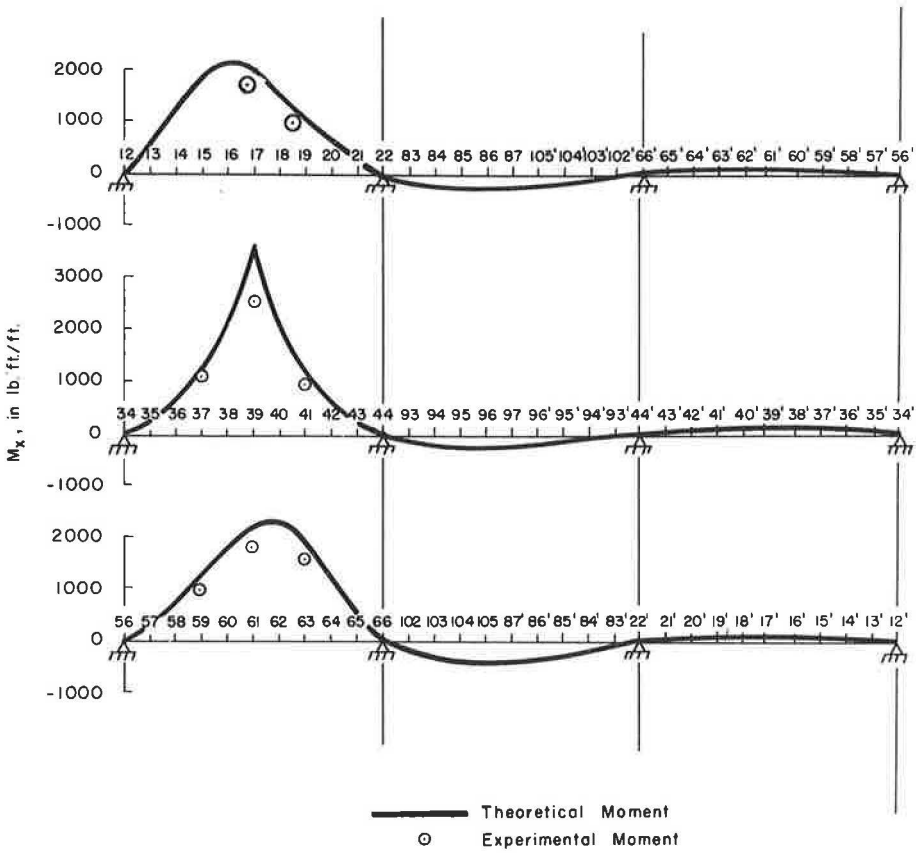

Figure 13. Influence lines for moment (M_x) at point 39 (test structure: 30°-1.0-0.5); P = 8 kips.

SUMMARY AND CONCLUSIONS

The results of the mathematical analyses of the 32 bridge slabs by a finite differences method represent the most significant accomplishment of this research project. Although in the past finite difference methods have been used in connection with the analysis of slabs, this is the first attempt to apply the method to such a large variety of continuous-span and single-span skewed slabs. The finite differences method is not an exact mathematical method. However, when properly applied using reasonably large numbers of network points, it is a sufficiently accurate tool for the analysis of bridge slabs. The finite difference method provides a means of computing the influence coefficients for deflections and moments at various slab points by simple matrix inversion and column vector multiplication operations which can be handled easily by an electronic computer.

The complete results of the mathematical analyses of the slab group were compiled in the form of influence coefficients and uniform load tables for deflections and moments. For better visualization of the mathematical results and to put the data in a more useful form, influence surface and uniform load contour diagrams were prepared for each slab. These diagrams can be used to determine the maximum values of the deflections and moments, their locations on the slab surface under moving concentrated loads, and various systems of uniform loading. If desired, more accurate information can be obtained from the corresponding tables.

The values of the deflection and moments can be interpolated for slabs having geometric parameter values other than the ones used in this study. For instance, critical

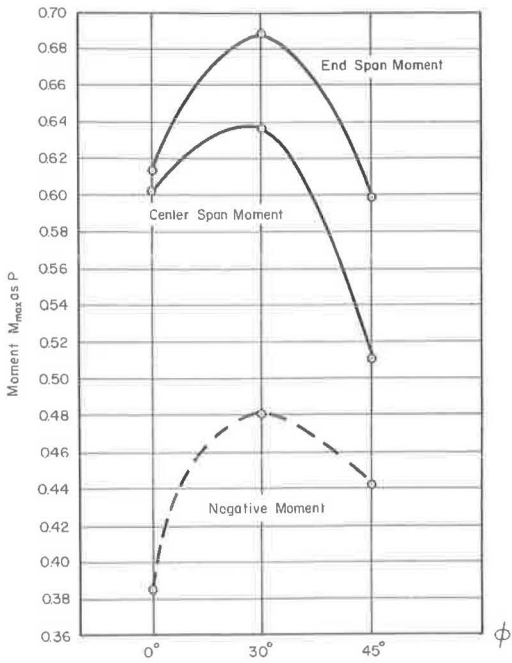

Figure 14. Variation of maximum moments with angle of skew (end span-center span ratio: 0.8; width-center span ratio: 1.0).

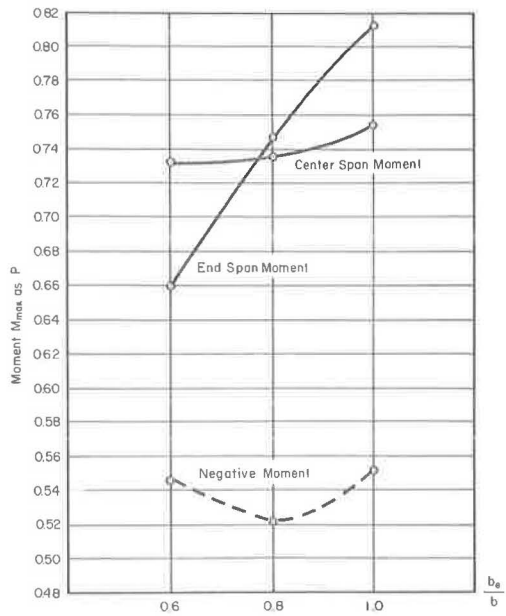

Figure 15. Variation of maximum moments with end span-center span ratio (angle of skew: 0°; width-center span ratio: 0.5).

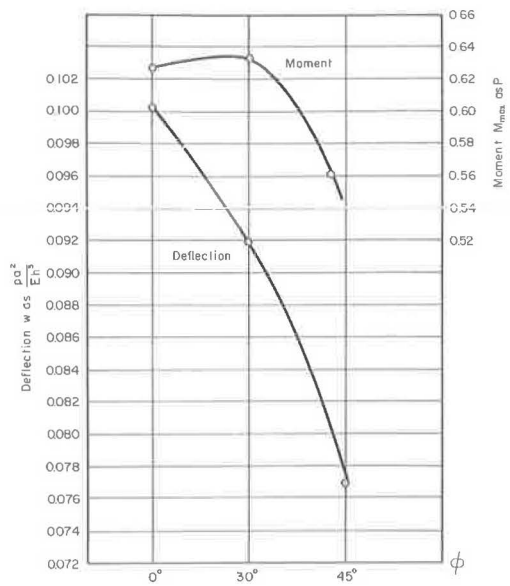

Figure 16. Variation of maximum deflection and moment with angle of skew (single-span slabs; width-span ratio: 2.5).

moments can be found for slab 35^0-0.6-1.0 by using the results obtained for slabs 0^0-0.6-1.0, 30^0-0.6-1.0 and 45^0-0.6-1.0. Similarly, information on slab 30^0-1.0-0.7 can be obtained by referring to the data pertaining to slabs 30^0-1.0-0.5 and 30^0-1.0-1.0 (Figs. 14, 15 and 16). Additional diagrams can be prepared for the influence coefficients and various systems of uniform loading systems by using the information in the tables and varying one of the geometric parameters at a time while keeping the others constant. The curves in these diagrams are fitted through only three points, and in some cases it becomes rather difficult to pinpoint the vertex of the curve. Throughout the research, the span lengths of the slabs are designated as the distances between the supports parallel to the roadway. It should be remembered that to span a crossing of length b, a ϕ^0 skewed slab with a span length $b' = b/\text{Cos}\,\phi$ corresponds to a rectangular slab of span length, b.

The application of the finite differences method to the analysis of slabs under concentrated loads involves the replacement of the term for the uniform load intensity at the right-hand side of a deflection equation by an expression for the concentrated

load using the relationship $P = p\Delta_X\Delta_Y$. In other words, the concentrated load is assumed to be distributed to the slab surface over an area $\Delta_Y\Delta_X$. Although this assumption does not alter the values of the moments at points away from the point of application, it may not indicate the true moments directly under the load depending on the number of network points used. Jensen (2) indicates that a more accurate concept of the distribution of the concentrated load can be developed by using correction factors based on his previous works on single-span slabs and on Westergaard's work on infinitely wide slabs. During the experimental phase of this project, concentrated loads were applied through steel base plates varying in size between 4 by 4 in. and 6 by 6 in. As the influence line diagrams indicate, the experimental and theoretical values of the moments directly under the load are either approximately equal to each other or the theoretical values are higher. Therefore, no corrections were made on the concentrated load distribution area $\Delta_Y\Delta_X$ to further increase the moments under the loads.

Due to the complex nature of the boundary conditions at the simple support corners, the validity of the moment equations used for these points seems questionable. The extremely high values of the twisting moments at the corners should be disregarded whenever they do not seem to fit the moment-change pattern along the end supports and along the free edges.

More research is required for a better understanding of the distribution of reactions along the supports under uniform and concentrated loads. This distribution is almost even in rectangular slabs under uniform loading and can be approximated by assuming the longitudinal strips of the slabs to be uniformly loaded beams. The distribution of the reactions in skewed slabs is uneven, and for uniformly loaded single-span skewed slabs the resultant of the reaction is located near the obtuse simple support corner (Fig. 17).

In Figure 17, $\overline{M}_X$ indicates the total average of the moments M_X at the section of the slab along points 1, 7, 13, 19, 25, 19′, 13′, 7′ and 1′. The total reaction, $pa^2/2$ at the support is located at a distance 0.38a from the obtuse corner. For continuous skewed slabs, this concentration of the reaction at the end and at the interior supports may be found by similar procedures. However, its location will vary according to the uniform loading systems. For the all spans loaded case, for instance, a more uniform distribution of the reactions can be expected along the supports.

The experimental phase of the research consisted of design, construction and testing of 6 continuous-span and 2 single-span reinforced-concrete test structures. Altogether, 4 different design procedures were used according to the directions of transverse and longitudinal reinforcement. Among these, the alternate design method used for test structure 45^0-0.6-1.0 appears to be the most efficient method theoretically. This procedure calls for placing the reinforcing bars in the general directions of the principal moments increasing the load-carrying capacity of the slab almost twice as much as compared with the other design method applied to the same slab. However, placing the main reinforcement in the direction of the maximum principal moment creates the problem of anchoring the bars along the free edges of the slab as well as requiring a large variety of lengths of reinforcing bars. Therefore, this design procedure may not be considered economical from a practical point of view. Design methods

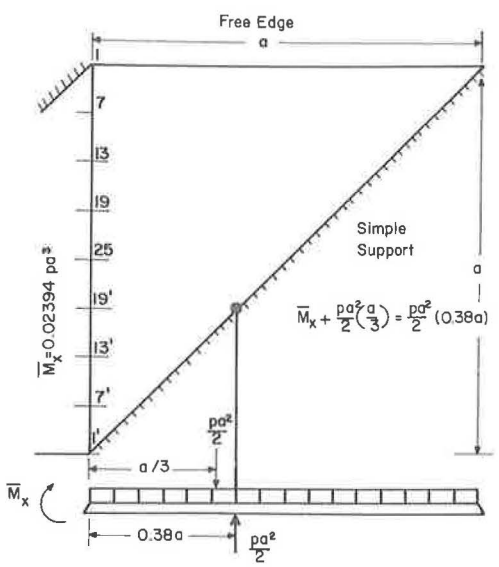

Figure 17. Uniform load reaction (slab 45°-1.0).

involving the placement of the transverse steel in the y-direction or in a direction parallel to the supports while keeping the longitudinal steel in the x-direction seem equally efficient as applied to continuous skewed slabs. For narrow slabs, placing the transverse steel in the y-direction may be a better procedure. However, for very wide slabs this method again necessitates the use of an increased number of bars with uneven lengths, thus, placing the transverse steel parallel to the supports may be preferred.

The experimental deflection values were usually found to be between the two theoretical values based on cracked and uncracked concrete sections confirming that, in the working load range, the concrete is already cracked in the tension side. The agreement between the experimental and the theoretical values of the moments was found to be good considering the numerous possibilities for errors involved in such tests.

The ultimate load tests on the test structures indicate that the ultimate uniform load is about twice as much as the allowable uniform load, whereas the intensity of the ultimate concentrated load is found to be between four to six times its allowable value. Because the slabs were designed in strips of equal width under uniform load, these strips begin to yield as independent uniformly loaded beams. However, under concentrated loads, the yield pattern of the slab is very complex and can be compared to the plastic moment analysis of multi-story, multi-bay steel frames.

The failure of the test structures under the ultimate concentrated load could be termed "shear-compression" failure. As the load intensity increased, tension cracks appeared at the bottom of the slab. However, at the time of failure the usual diagonal tension cracks were accompanied by localized cracks at the top surface. In several instances, tension cracks also appeared over the interior supports. The failure of the slab under the ultimate uniform loading was of the simple flexural type.

The experimental data on the reactions along the supports were inconclusive. Although the values of the total reactions compared well with the total loads on the slab, the distribution of the unit reactions as obtained from the load cells was rather irregular. Reasons for this irregularity may have been (a) the load cells were not sensitive enough to measure the reactions produced during the tests for certain positions and types of loading; (b) a certain amount of yielding of the aluminum beams may have occurred; (c) at certain spots the contact between the slab and the aluminum beams may have been uneven; and (d) a very slight uplift of the slab corners could have produced large errors in reaction readings.

It is believed that the lack of theoretical and experimental data on the distribution of load along the supports does not alter the actual design of the slabs because the intensity of the concentrated load is the primary design criterion in shear consideration.

REFERENCES

1. Marcus, H., "The Elastic Web Theory and Its Use for the Calculation of Flexible Plates." Julius Springer, Berlin (1924).
2. Jensen, V. P., "Analysis of Skew Slabs." Engg. Exp. Sta. Bull. 332, Univ. of Ill. (1941).
3. Yeginobali, Asim, "Continuous Skewed Slabs." Engg. Exp. Sta. Bull. 178, Ohio State Univ. (1959).

Appendix

Three types of network systems have been used in connection with the analysis: the skew, the square, and the rectangular. Figure 18 shows the various possible positions of a typical slab point in a skew network over the surface of a continuous slab with simply-supported ends and free edges. The typical slab point is designed as 10. Points 1 through 9 and 1′ through 9′ indicate the neighboring slab points in their relative positions. This type of network is applicable to most of the skewed slabs. Figure 19 shows different positions of a typical slab point in a square network over a 45^0 skewed continuous slab. Figure 20 shows the same information for a rectangular network over

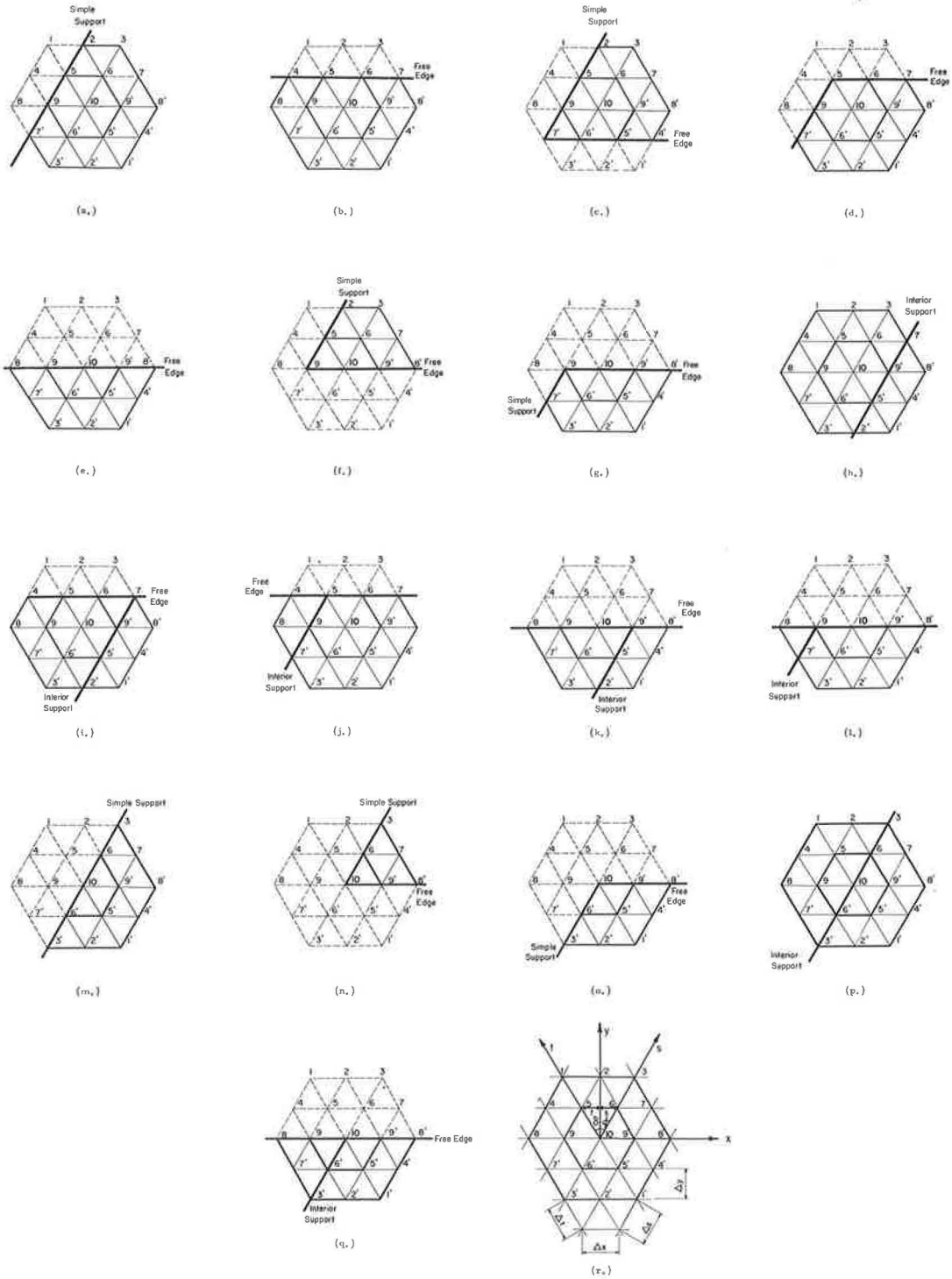

Figure 18. Typical slab point in skew network.

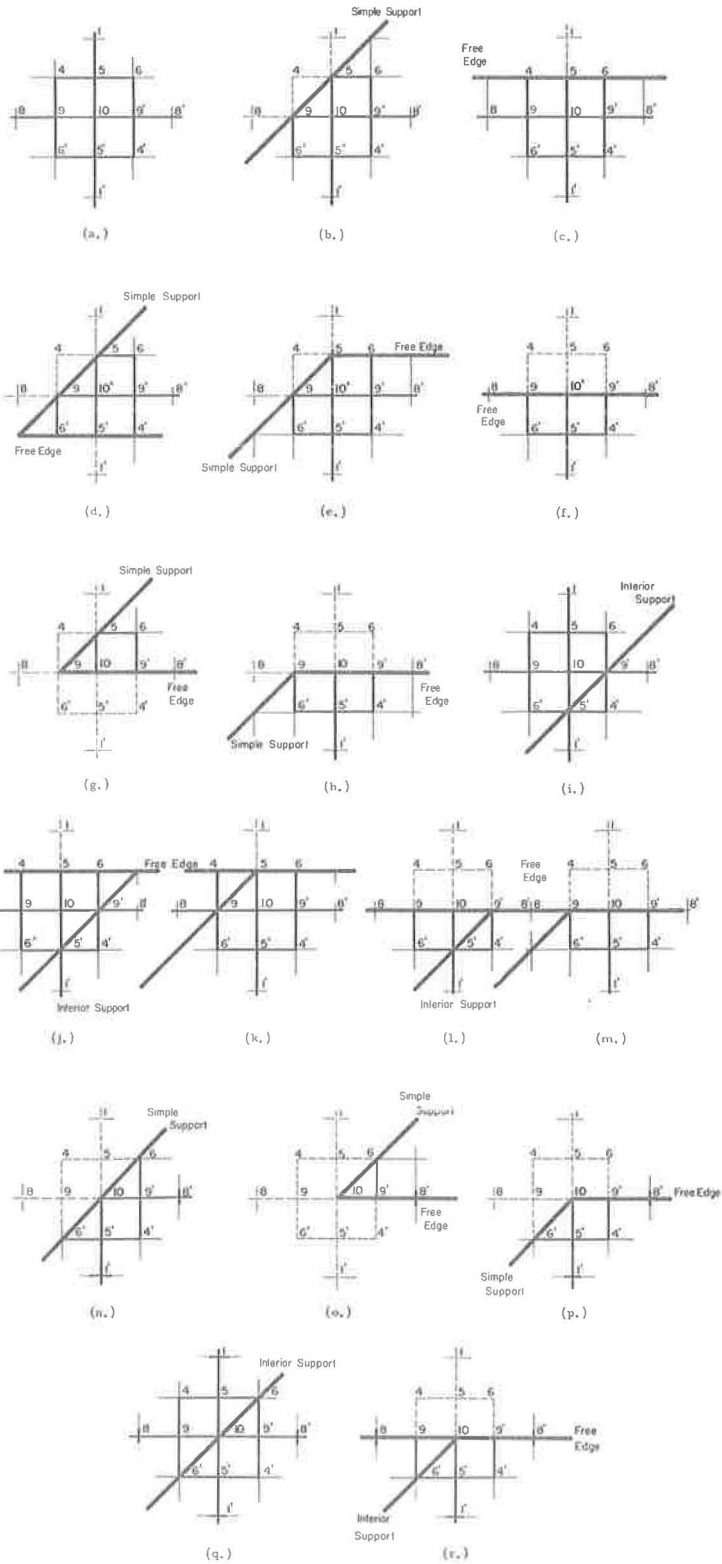

Figure 19. Typical slab point in square network.

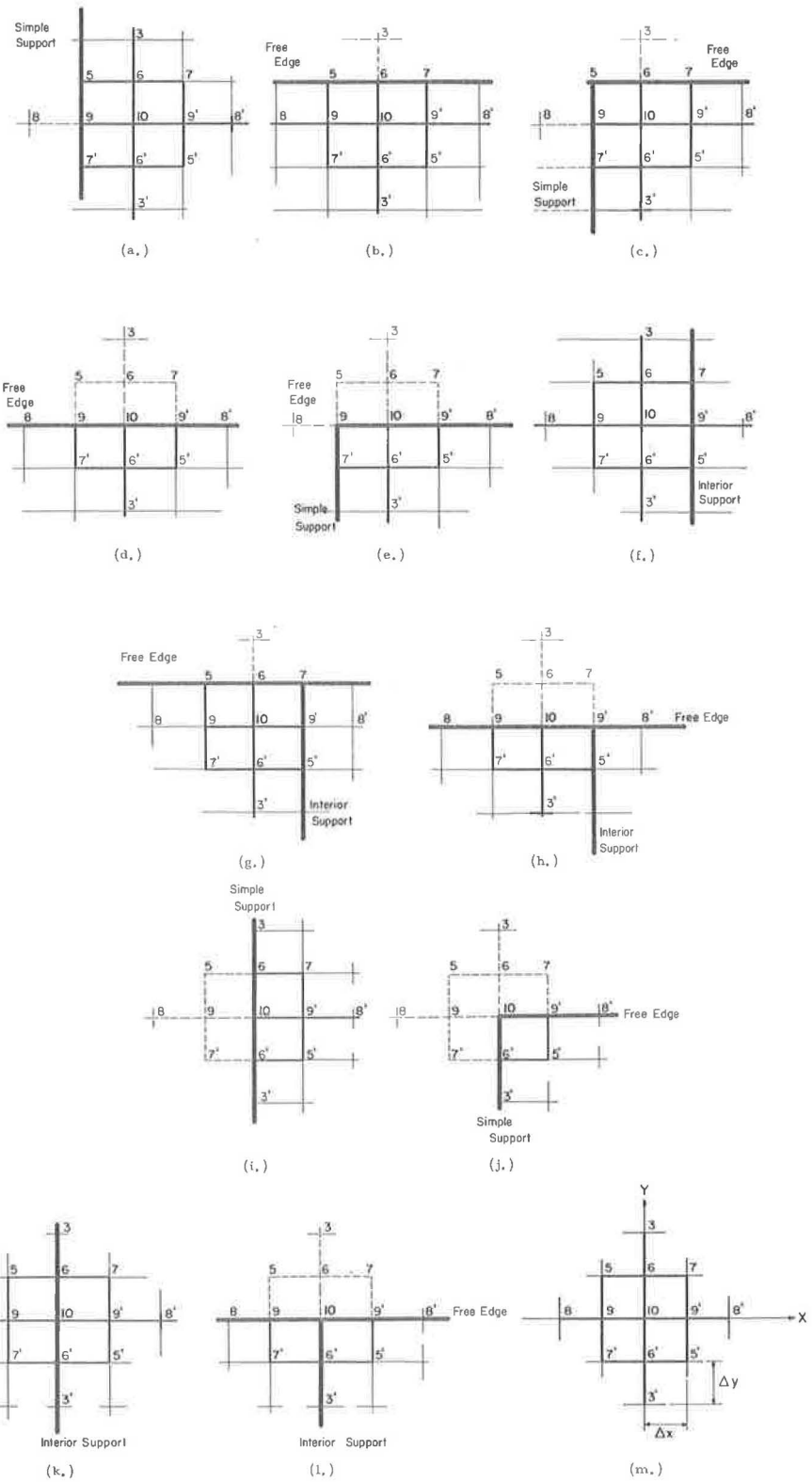

Figure 20. Typical slab point in rectangular network.

a 45^0 skewed continuous slab. Figure 20 shows the same information for a rectangular network over a 0^0 skewed (or rectangular) continuous slab. The position of the typical point 10 in Figure 18r represents a case where the slab point is away from the effects of the boundaries. For such a point, Eq. 1 can be written in finite differences without any modification as Eq. 2 (Fig. 21). For the other positions of point 10, however, Eq. 2 is altered to satisfy the boundary conditions assuming imaginary extensions of the surface of the slab beyond the actual boundaries. The fictitious slab points associated with such cases are joined with dotted network lines (Figs. 18, 19 and 20). Eqs. 2 through 36 in Figure 21 are the deflection equations to be used for various positions of a typical slab point in skew, square and rectangular network systems. Eqs. 37 through 69 are the corresponding expressions for the moments. Derivations of all these equations have been previously reported (3). Referring to Figure 18r, the constants A, B, C, and F in these equations are defined as follows:

$$A = \frac{t}{\Delta_x} \qquad B = \frac{s}{\Delta_x}$$

$$C = \frac{\Delta_y^2}{\Delta_x^2} - AB \qquad F = \frac{\Delta_y^2}{\Delta_x^2}(1 - u)$$

in which

$t = \Delta_y \tan \delta$ and $s = \Delta_y \tan \phi$.

Table 4 gives the applicable deflection and moment equations corresponding to typical slab point positions. The first column indicates the position of point 10 from Figures 18, 19 and 20. The second and third columns give the numbers of the deflection and moment equations from Figure 21 to be used for that particular position of the typical slab point.

Any given loading condition over the slab surface can be resolved into symmetrical and anti-symmetrical load systems requiring the use of only one-half of the slab points in writing the deflection equations (Fig. 22). In Figure 22a the slab is subjected to a concentrated load of P at point 39 which requires the simultaneous solution of N deflection equations for N points on the deflecting slab surface. However, by resolving this load as shown in Figures 22b and 22c, the solution of two sets of only N/2 equations becomes sufficient because of the symmetry. For the loading shown in Figure 22c, deflections of the points on the right half of the slab will have negative deflections. The rest of Figure 22 shows the resolution of the two anti-symmetrical uniform loading systems.

After writing the deflection equations for the points on the left half of a slab, the constants A, B, C, and F are evaluated and from these values the deflection equation coefficients are found. Using the deflection equation coefficients and the deflection equations, two coefficient matrices are written. The first one S is for the condition where the symmetrical points on the left and the right halves of the slab have equal deflections in the positive direction (Fig. 22b). The second coefficient matrix, U is for where deflections of the network points on the right half of the slab are assumed to have negative directions (Fig. 22c). If S^{-1} and U^{-1} denote the inverse matrices corresponding to S and U, then by the law of reciprocal deflections, the elements of the matrices $\frac{S^{-1} + U^{-1}}{2}$, and $\frac{S^{-1} - U^{-1}}{2}$ represent the influence coefficients for deflection at any of the slab points in the left and right halves of the slab, respectively.

Influence coefficients for moments M_x, M_y, M_{xy} are found again by making the use of the reciprocal relationship among the influence coefficients for deflections. From Figure 21, all the moment equations in finite difference form (Eqs. 1-69) can be simplified as

$$M_2 = Aw_1 + Bw_2 + Cw_3 \qquad (70)$$

$$w_{10}(4+2A^2+2B^2+8C+6C^2)-(w_8+w_{8'})(4A+4AC-2BC)$$
$$-(w_6+w_{6'})(4B+4BC-2AC)-(w_9+w_{9'})(4C+4C^2-2AB)+(w_3+w_{3'})A^2$$
$$+(w_1+w_{1'})B^2+(w_8+w_{8'})C^2+2(w_2+w_{2'})AB+2(w_4+w_{4'})BC$$
$$+2(w_7+w_{7'})AC=\frac{p_{10}\Delta_y^4}{D} \qquad (2)$$

$$w_{10}(4+2A^2+B^2+8C+5C^2)-(w_8+w_{8'})(4A+4AC-8C)-w_{6'}(4B+4BC-2AC)$$
$$-w_{9'}(4C+4C^2-2AB)+(w_3+w_{3'})A^2+w_{1'}B^2+w_{8'}C^2+2w_{2'}AB+2w_{4'}BC$$
$$+2w_7AC=\frac{p_{10}\Delta_y^4}{D} \qquad (3)$$

$$w_{10}(4+A^2+B^2+8C+6C^2)-w_8(2A+2AC+2AF-BC-BF)$$
$$-w_6(2B+2BC+2BF-AC-AF)-(w_9+w_{9'})(4C+4C^2-AB)$$
$$-w_{6'}(4A+4AC-2BC)-w_{8'}(4B+4BC-2AC)+w_7(AC+AF)+w_4(BC+BF)$$
$$+(w_8+w_{8'})C^2+2w_{2'}AB+2w_{7'}AC+2w_{4'}BC+w_{3'}A^2+w_{1'}B^2=\frac{p_{10}\Delta_y^4}{D} \qquad (4)$$

$$w_{10}(4+A^2+8C+5C^2)-w_{8'}(2A+2AC+2AF-BF)$$
$$-w_{8'}(2B+2BC+2BF-AC-AF)-w_{9'}(4C+4C^2-AB)-w_8(4A+4AC-BC)$$
$$+w_{4'}(BC+BF)+w_{8'}C^2+2w_7AC+w_3A^2=\frac{p_{10}\Delta_y^4}{D} \qquad (5)$$

$$w_{10}(4+A^2+B^2+8C+5C^2)-w_8(2A+2AC+2AF-BC)-w_{8'}(2B+2BC-AC)$$
$$-w_{9'}(4C+4C^2-AB)-w_{6'}(4A+4AC-8C)+w_7(AC+AF)+2w_{2'}AB+2w_{4'}BC$$
$$+w_{3'}A^2+w_{1'}B^2+w_{9'}C^2=\frac{p_{10}\Delta^4}{D} \qquad (6)$$

$$w_{10}(A^2+B^2+4F+6CF-3F^2)-w_{8'}(2A+2AC+2AF-BC-BF)$$
$$-w_{8'}(2B+2BC+2BF-AC-AF)-(w_8+w_{8'})(2F+4CF-2F^2-AB)$$
$$+w_{7'}(AC+AF)+w_{4'}(BC+BF)+2w_{2'}AB+w_{3'}A^2+w_{1'}B^2$$
$$+(w_8+w_{8'})\left(CF-\frac{F^2}{2}\right)=\frac{p_{10}\Delta_y^4}{2D} \qquad (7)$$

$$w_{10}(A^2+4F+5CF-\frac{5}{2}F^2-BF)-w_8(2A+2AC+2AF-BF)$$
$$-w_{8'}(2F+4CF-2F^2-AB)+w_7(AC+AF)+w_3A^2+w_{8'}\left(CF-\frac{F^2}{2}\right)=\frac{p_{10}\Delta_y^4}{2D} \qquad (8)$$

$$w_{10}(A^2+B^2+4F+5CF+BF-\frac{5}{2}F^2)-w_{8'}(2A+2AC+2AF-BC)$$
$$-w_{8'}(2B+2BC+2BF-AC-AF)-w_{8'}(2F+4CF-2F^2-AB)+w_{4'}(BC+BF)$$
$$+2w_{2'}AB+w_{3'}A^2+w_{1'}B^2+w_{8'}\left(CF-\frac{F^2}{2}\right)=\frac{p_{10}\Delta_y^4}{2D} \qquad (9)$$

$$w_{10}(4+2A^2+2B^2+8C+6C^2)-(w_6+w_{6'})(4A+4AC-2BC)-w_5(4B+4BC-2AC)$$
$$-w_9(4C+4C^2-2AB)+2w_2AB+2w_{7'}AC+(w_4+w_{4'})2BC+(w_3+w_{3'})A^2$$
$$+(w_1+w_{1'})B^2+(w_8+w_{8'})C^2=\frac{p_{10}\Delta_y^4}{D} \qquad (10)$$

$$w_{10}(4+A^2+B^2+8C+6C^2)-w_8(2A+2AC+2AF-BC-BF)$$
$$-w_6(2B+2BC+2BF-AC-AF)-w_9(4C+4C^2-AB)-w_{8'}(4A+4AC-2BC)$$
$$+w_4(BC+BF)+2w_{7'}AC+2w_{4'}BC+w_{3'}A^2+w_{1'}B^2+(w_8+w_{8'})C^2=\frac{p_{10}\Delta_y^4}{D} \qquad (11)$$

$$w_{10}(4+A^2+B^2+8C+6C^2)-w_8(2A+2AC+2AF-BC-BF)-w_{8'}(4C+4C^2-AB)$$
$$-w_{8'}(4A+4AC-2BC)-w_{8'}(4B+4BC-2AC)+w_7(AC+AF)+w_4(BC+BF)$$
$$+2w_{2'}AB+2w_{4'}BC+w_{3'}A^2+w_{1'}B^2+(w_8+w_{8'})C^2=\frac{p_{10}\Delta_y^4}{D} \qquad (12)$$

$$w_{10}(A^2+B^2+4F+6CF-3F^2)-w_{8'}(2A+2AC+2AF-BC-BF)$$
$$-w_8(2F+4CF-2F^2-AB)+w_{7'}(AC+AF)+w_{4'}(BC+BF)+w_{3'}A^2+w_{1'}B^2$$
$$+(w_8+w_{8'})\left(CF-\frac{F^2}{2}\right)=\frac{p_{10}\Delta_y^4}{2D} \qquad (13)$$

$$w_{10}(A^2+B^2+4F+6CF-3F^2)-w_{8'}(2A+2AC+2AF-BC-BF)$$
$$-w_{8'}(2B+2BC+2BF-AC-AF)-w_{9'}(2F+4CF-2F^2-AB)+w_{4'}(BC+BF)$$
$$+2w_{2'}AB+w_{3'}A^2+w_{1'}B^2+(w_8+w_{8'})\left(CF-\frac{F^2}{2}\right)=\frac{p_{10}\Delta_y^4}{2D} \qquad (14)$$

Figure 21. Deflection and moment equations.

$$20w_{10}-8(w_8+w_{8'}+w_9+w_{9'})+2(w_4+w_{4'}+w_6+w_{6'})+w_1+w_{1'}+w_8+w_{8'}=\frac{p_{10}\Delta^4}{D} \quad (15)$$

$$18w_{10}-8(w_{8'}+w_{9'})+2w_{4'}+w_8+w_{8'}+w_{1'}+w_{6'}=\frac{p_{10}\Delta^4}{D} \quad (16)$$

$$19w_{10}-2w_5(3-\mu)+(w_4+w_8)(2-\mu)-8(w_9+w_{9'}+w_{9'})+2(w_{4'}+w_{8'})+w_8+w_{8'}+w_{1'}=\frac{p_{10}\Delta^4}{D} \quad (17)$$

$$17w_{10}-2w_{9'}(3-\mu)+w_{4'}(2-\mu)+w_{6'}(1-\mu)-8w_{9'}+w_{6'}+w_6=\frac{p_{10}\Delta^4}{D} \quad (18)$$

$$18w_{10}-8(w_{6'}+w_9)+2w_{4'}+w_8+w_{6'}+w_{8'}+w_{1'}=\frac{p_{10}\Delta^4}{D} \quad (19)$$

$$w_{10}(8-4\mu-3\mu^2)-(w_9+w_{9'})(4-2\mu-2\mu^2)-2w_{9'}(3-\mu)+(w_{4'}+w_{6'})(2-\mu)+\frac{1}{2}(w_8+w_{8'})(1-\mu^2)+w_{1'}=\frac{p_{10}\Delta^4}{2D} \quad (20)$$

$$\frac{1}{2}w_{10}(11-6\mu-5\mu^2)-w_{9'}(4-2\mu-2\mu^2)+\frac{1}{2}w_{9'}(1-\mu^2)+w_6(1-\mu)=\frac{p_{10}\Delta^4}{2D} \quad (21)$$

$$\frac{1}{2}w_{10}(17-10\mu-5\mu^2)-w_{9'}(4-2\mu-2\mu^2)+\frac{1}{2}w_{9'}(1-\mu^2)-2w_{6'}(3-\mu)+w_{4'}(2-\mu)+w_{6'}+w_{1'}=\frac{p_{10}\Delta^4}{2D} \quad (22)$$

$$20w_{10}-8(w_6+w_9)+2(w_4+w_6)+w_8+w_{6'}+w_1+w_{1'}=\frac{p_{10}\Delta^4}{D} \quad (23)$$

$$19w_{10}-2w_5(3-\mu)+(w_4+w_8)(2-\mu)-8w_9+2(w_{4'}+w_{6'})+w_6+w_{6'}+w_{1'}=\frac{p_{10}\Delta^4}{D} \quad (24)$$

$$19w_{10}+(w_4+w_6)(2-\mu)-8(w_{9'}+w_{9'})+2(w_{4'}+w_{6'})+w_8+w_{8'}+w_{1'}=\frac{p_{10}\Delta^4}{D} \quad (25)$$

$$w_{10}(8-4\mu-3\mu^2)-w_9(4-2\mu-2\mu^2)+\frac{1}{2}(w_9+w_{9'})(1-\mu^2)+(w_{4'}+w_{6'})(2-\mu)+w_{1'}=\frac{p_{10}\Delta^4}{2D} \quad (26)$$

$$w_{10}(8-4\mu-3\mu^2)-w_{9'}(4-2\mu-2\mu^2)+\frac{1}{2}(w_8+w_{8'})(1-\mu^2)-2w_{8'}(3-\mu)+(w_{4'}+w_{6'})(2-\mu)+w_{1'}=\frac{p_{10}\Delta^4}{2D} \quad (27)$$

$$w_{10}(6+8C+6C^2)-(w_6+w_{6'})(4+4C)+2(w_5+w_{5'}+w_7+w_{7'})C-(w_9+w_{9'})(4C+4C^2)+(w_8+w_{8'})C^2+w_{3'}=\frac{p_{10}\Delta_y^4}{D} \quad (28)$$

$$w_{10}(6+8C+5C^2)-(w_6+w_{6'})(4+4C)+2(w_{8'}+w_7)C-w_{9'}(4C+4C^2)+w_{8'}C^2+w_{3'}=\frac{p_{10}\Delta_y^4}{D} \quad (29)$$

$$w_{10}(5+8C+6C^2)-w_6(2+2C+2F)+(w_5+w_7)(C+F)-(w_9+w_{9'})(4C+4C^2)-w_{6'}(4+4C)+2(w_{5'}+w_{7'})C+(w_8+w_{8'})C^2+w_{3'}=\frac{p_{10}\Delta_y^4}{D} \quad (30)$$

$$w_{10}(5+8C+5C^2)-w_8(2+2C+2F)+2w_{5'}C-w_{9'}(4C+4C^2)-w_{6'}(4+4C)+w_7(C+F)+w_{8'}C^2+w_{3'}=\frac{p_{10}\Delta_y^4}{D} \quad (31)$$

$$w_{10}(1+4F+6CF-3F^2)-w_{6'}(2+2C+2F)+(w_{5'}+w_{7'})(C+F)-(w_9+w_{9'})(2F+4CF-2F^2)+w_{3'}+(w_6+w_{6'})\left(CF-\frac{F^2}{2}\right)=\frac{p_{10}\Delta_y^4}{2D} \quad (32)$$

$$w_{10}(1+4F+5CF-\frac{5}{2}F^2)-w_{6'}(2+2C+2F)+w_{5'}(C+F)-w_{9'}(2F+4CF-2F^2)+w_{3'}+w_{8'}\left(CF-\frac{F^2}{2}\right)=\frac{p_{10}\Delta_y^4}{2D} \quad (33)$$

$$w_{10}(6+8C+6C^2)-(w_6+w_{6'})(4+4C)+(w_5+w_{7'})2C-w_8(4C+4C^2)+(w_8+w_{8'})C^2+w_3+w_{3'}=\frac{p_{10}\Delta_y^4}{D} \quad (34)$$

$$w_{10}(5+8C+6C^2)-w_6(2+2C+2F)+w_5(C+F)-w_9(4C+4C^2)-w_{8'}(4+4C)+2w_{7'}C+(w_8+w_{8'})C^2+w_{3'}=\frac{p_{10}\Delta_y^4}{D} \quad (35)$$

$$w_{10}(1+4F+6CF-3F^2)-w_{6'}(2+2C+2F)-w_8(2F+4CF-2F^2)+w_{7'}(C+F)+(w_8+w_{8'})\left(CF-\frac{F^2}{2}\right)+w_{3'}=\frac{p_{10}\Delta_y^4}{2D} \quad (36)$$

Figure 21 (Cont'd.)

$$M_x = -\frac{D}{\Delta_y^2}\left[(F+\mu C)(w_9 - 2w_{10} + w_{9'}) + \mu A(w_8 - 2w_{10} + w_{8'}) + \mu B(w_5 - 2w_{10} + w_{5'})\right]$$

$$M_y = -\frac{D}{\Delta_y^2}\left[(C-F)(w_9 - 2w_{10} + w_{9'}) + A(w_8 - 2w_{10} + w_{8'}) + B(w_5 - 2w_{10} + w_{5'})\right]$$

$$M_{xy} = -\frac{D(1-\mu)}{2\Delta_x \Delta_y}\left[w_5 + w_{5'} - w_8 - w_{8'} + (B-A)(w_9 - 2w_{10} + w_{9'})\right]$$

(37)

$$M_x = -\frac{D}{\Delta_y^2}\left[(F+\mu C)(w_{9'} - 2w_{10}) + \mu A(w_8 - 2w_{10} + w_{8'}) + \mu B(w_5 - 2w_{10} + w_{5'})\right]$$

$$M_y = -\frac{D}{\Delta_y^2}\left[(C-F)(w_{9'} - 2w_{10}) + A(w_8 - 2w_{10} + w_{8'}) + B(w_5 - 2w_{10})\right]$$

$$M_{xy} = -\frac{D(1-\mu)}{2\Delta_x \Delta_y}\left[w_{5'} - w_8 - w_{8'} + (B-A)(w_{9'} - 2w_{10})\right]$$

(38)

$$M_x = -\frac{D(1-\mu^2)}{\Delta_x^2}(w_9 - 2w_{10} + w_{9'})$$

$$M_{xy} = -\frac{D(1-\mu)}{4\Delta_x \Delta_y}\left[2(1+C-F)(w_9 - w_{9'}) + (F-C)(w_8 - w_{8'}) + 2A(w_{5'} - w_{7'}) + 2B(w_4 - w_{4'})\right]$$

(39)

$$M_x = -\frac{D(1-\mu^2)}{\Delta_x^2}(w_{9'} - 2w_{10})$$

$$M_{xy} = -\frac{D(1-\mu)}{4\Delta_x \Delta_y}\left[2w_{9'} + (F-C)(w_{10} - 2w_{9'} + w_{8'}) - 2Aw_7 - 2B(w_{10} + w_5)\right]$$

(40)

$$M_x = -\frac{D(1-\mu^2)}{\Delta_x^2}(w_{9'} - 2w_{10})$$

$$M_{xy} = -\frac{D(1-\mu)}{4\Delta_x \Delta_y}\left[2Aw_{5'} + 2B(w_{4'} - w_8) - 2w_{9'} - (F-C)(w_{8'} - 2w_{9'} + w_{10})\right]$$

(41)

$$M_x = -\frac{D}{\Delta_y^2}\left[(F+\mu C)(w_9 - 2w_{10}) + \mu A(w_8 - 2w_{10} + w_{8'}) + \mu B(w_5 - 2w_{10})\right]$$

$$M_y = -\frac{D}{\Delta_y^2}\left[(C-F)(w_9 - 2w_{10}) + A(w_8 - 2w_{10} + w_{8'}) + B(w_5 - 2w_{10})\right]$$

$$M_{xy} = -\frac{D(1-\mu)}{2\Delta_x \Delta_y}\left[w_5 - w_8 - w_{8'} + (B-A)(w_9 - 2w_{10})\right]$$

(42)

$$M_x = -\frac{D(1-\mu^2)}{\Delta_x^2}(w_9 - 2w_{10})$$

$$M_{xy} = -\frac{D(1-\mu)}{4\Delta_x \Delta_y}\left[2(1+C-F)w_9 + (F-C)(w_8 - w_{8'}) - 2Aw_{7'} + 2B(w_{4'} - w_8)\right]$$

(43)

$$M_x = -\frac{D(1-\mu^2)}{\Delta_x^2}(w_{9'} - 2w_{10})$$

$$M_{xy} = -\frac{D(1-\mu)}{4\Delta_x \Delta_y}\left[2(1+C-F)w_{9'} + (F-C)(w_8 - w_{8'}) + 2Aw_8 + 2B(w_4 - w_{8'})\right]$$

(44)

$$M_x = -\frac{D(1-\mu)}{\Delta_x \Delta_y}(w_{9'} - w_{8'})\sin 2\phi$$

$$M_y = \frac{D(1-\mu)}{\Delta_x \Delta_y}(w_{8'} - w_{8'})\sin 2\phi$$

$$M_{xy} = \frac{D(1-\mu)}{\Delta_x \Delta_y}(w_{8'} - w_{9'})\cos 2\phi$$

(45)

$$M_x = -\frac{D(1-\mu^2)}{\Delta_x^2}(w_9 + w_{9'})$$

$$M_{xy} = -\frac{D(1-\mu)}{4\Delta_x \Delta_y}\left[2(1+C-F)(w_9 - w_{9'}) + (F-C)(w_8 - w_{8'}) + 2A(w_{8'} - w_{7'}) + 2Bw_4\right]$$

(46)

$$M_x = 0$$

$$M_{xy} = -\frac{D(1-\mu)}{4\Delta_x \Delta_y}\left[4\left(1+C-F-\frac{A}{2}\right)w_{9'} + 2(F-C-B)w_{8'} - 2Aw_7\right]$$

(47)

$$M_x = 0$$

$$M_{xy} = -\frac{D(1-\mu)}{4\Delta_x \Delta_y}\left[4\left(1+C-F+\frac{A}{2}\right)w_{9'} - 2(F-C)w_{8'} + 2Aw_{8'} + 2Bw_{4'}\right]$$

(48)

$$M_x = -\frac{D}{\Delta_y^2}\left[(F+\mu C)(w_9 + w_{9'}) + \mu B(w_5 + w_{5'})\right]$$

$$M_y = -\frac{D}{\Delta_y^2}\left[(C-F)(w_9 + w_{9'}) + B(w_5 + w_{5'})\right]$$

$$M_{xy} = -\frac{D(1-\mu)}{2\Delta_x \Delta_y}\left[w_5 + w_{5'} + (B-A)(w_5 + w_{9'})\right]$$

(49)

$$M_x = -\frac{D}{\Delta^2}\left[w_9 - 2w_{10} + w_{9'} + \mu(w_5 - 2w_{10} + w_{5'})\right]$$

$$M_y = -\frac{D}{\Delta^2}\left[w_5 - 2w_{10} + w_{5'} + \mu(w_9 - 2w_{10} + w_{9'})\right]$$

$$M_{xy} = -\frac{D(1-\mu)}{4\Delta^2}(w_4 + w_{4'} - w_8 - w_{8'})$$

(50)

Figure 21 (Cont'd.)

$$M_x = -\frac{D}{\Delta^2}\left[w_9 - 2w_{10} + \mu(w_{9'} - 2w_{10})\right]$$

$$M_y = -\frac{D}{\Delta^2}\left[w_{9'} - 2w_{10} + \mu(w_9 - 2w_{10})\right]$$

$$M_{xy} = -\frac{D(1-\mu)}{4\Delta^2}(w_{4'} - w_{10} - w_8 - w_{9'})$$

(51)

$$M_x = -\frac{D(1-\mu^2)}{\Delta^2}(w_9 - 2w_{10} + w_{9'})$$

$$M_{xy} = -\frac{D(1-\mu)}{4\Delta^2}\left[2(1+\mu)(w_8 - w_{9'}) - 2(w_{9'} - w_{4'}) - \mu(w_8 - w_{8'})\right]$$

(52)

$$M_x = -\frac{D(1-\mu^2)}{\Delta^2}(w_9 - 2w_{10})$$

$$M_{xy} = -\frac{D(1-\mu)}{4\Delta^2}\left[2(1+\mu)w_{9'} - 2(w_8 + w_{10}) - \mu(w_{8'} + w_{10})\right]$$

(53)

$$M_x = -\frac{D(1-\mu)}{\Delta^2}(w_{9'} - 2w_{10})$$

$$M_{xy} = \frac{D(1-\mu)}{4\Delta^2}\left[2(1+\mu)w_{9'} + 2(w_{9'} - w_{4'}) - \mu(w_8 + w_{10})\right]$$

(54)

$$M_x = -\frac{D}{\Delta^2}\left[w_8 - 2w_{10} + \mu(w_8 - 2w_{10})\right]$$

$$M_y = -\frac{D}{\Delta^2}\left[w_8 - 2w_{10} + \mu(w_9 - 2w_{10})\right]$$

$$M_{xy} = -\frac{D(1-\mu)}{4\Delta^2}(w_4 + w_{4'} - w_8 - w_{9'})$$

(55)

$$M_x = -M_y = -\frac{D(1-\mu)}{\Delta^2}(w_{9'} - w_9)$$

$$M_{xy} = 0$$

(56)

$$M_x = 0$$

$$M_{xy} = -\frac{D(1-\mu)}{2\Delta^2}(2w_{9'} - w_9)$$

(57)

$$M_x = 0$$

$$M_{xy} = -\frac{D(1-\mu)}{2\Delta^2}\left[2(1+\mu)w_{9'} + \mu w_9 + w_{4'}\right]$$

(58)

$$M_x = -\frac{D}{\Delta^2}\left[w_9 + w_{9'} + \mu(w_8 + w_{9'})\right]$$

$$M_y = -\frac{D}{\Delta^2}\left[w_8 + w_{9'} + \mu(w_8 + w_9)\right]$$

$$M_{xy} = -\frac{D(1-\mu)}{4\Delta^2}(w_4 + w_{4'})$$

(59)

$$M_x = -\frac{D(1-\mu^2)}{\Delta^2}(w_9 + w_{9'})$$

$$M_{xy} = -\frac{D(1-\mu)}{4\Delta^2}\left[2(1+\mu)(w_9 - w_{9'}) - 2(w_{9'} - w_{4'}) - \mu(w_8 - w_{8'})\right]$$

(60)

$$M_x = -D\left(\frac{w_{9'} - 2w_{10} + w_9}{\Delta_x^2} + \mu\frac{w_8 - 2w_{10} + w_{8'}}{\Delta_y^2}\right)$$

$$M_y = -D\left(\frac{w_8 - 2w_{10} + w_{8'}}{\Delta_y^2} + \mu\frac{w_{9'} - 2w_{10} + w_9}{\Delta_x^2}\right)$$

$$M_{xy} = -D(1-\mu)\frac{w_7 - w_{9'} - w_8 + w_{7'}}{4\Delta_x\Delta_y}$$

(61)

$$M_x = -D\left(\frac{w_{9'} - 2w_{10}}{\Delta_x^2} + \mu\frac{w_8 - 2w_{10} + w_{8'}}{\Delta_y^2}\right)$$

$$M_y = -D\left(\frac{w_8 - 2w_{10} + w_{8'}}{\Delta_y^2} + \mu\frac{w_{9'} - 2w_{10}}{\Delta_x^2}\right)$$

$$M_{xy} = -D(1-\mu)\frac{w_7 - w_{9'}}{4\Delta_x\Delta_y}$$

(62)

$$M_x = -\frac{D(1-\mu^2)}{\Delta_x^2}(w_9 - 2w_{10} + w_{9'})$$

$$M_{xy} = -\frac{D(1-\mu)}{4\Delta_x\Delta_y}\left[2(1+C-F)(w_9 - w_{9'}) + (F-C)(w_9 - w_{9'}) + 2(w_{9'} - w_{7'})\right]$$

(63)

$$M_x = -\frac{D(1-\mu^2)}{\Delta_x^2}(w_{9'} - 2w_{10})$$

$$M_{xy} = \frac{D(1-\mu)}{4\Delta_x\Delta_y}\left[2(1+C-F)w_{9'} + (F-C)(w_{10} + w_{9'}) - 2w_8\right]$$

(64)

Figure 21 (Cont'd.)

$$M_x = -\frac{D(1-\mu^2)}{\Delta_x^2}(w_9 - 2w_{10})$$

$$M_{xy} = -\frac{D(1-\mu)}{4\Delta_x\Delta_y}\left[2(1+C-F)w_9 + (F-C)(w_8 - w_{8'}) - 2w_{7'}\right] \quad (65)$$

$$M_x = 0$$

$$M_{xy} = -\frac{D(1-\mu)}{2\Delta_x\Delta_y}(w_7 - w_{9'}) \quad (66)$$

$$M_x = 0$$

$$M_{xy} = \frac{D(1-\mu)}{4\Delta_x\Delta_y}\left[4(1+C-F)w_{9'} + 2(F-C)w_{8'} - 4w_{5'}\right] \quad (67)$$

$$M_x = -\frac{D}{\Delta_x^2}(w_9 + w_{9'})$$

$$M_y = -\frac{\mu D}{\Delta_x^2}(w_9 + w_{9'})$$

$$M_{xy} = -\frac{D(1-\mu)}{4\Delta_x\Delta_y}(w_5 + w_{5'} - w_7 - w_{7'}) \quad (68)$$

$$M_x = -\frac{D(1-\mu^2)}{\Delta_x^2}(w_9 + w_{9'})$$

$$M_{xy} = -\frac{D(1-\mu)}{4\Delta_x\Delta_y}\left[2(1+C-F)(w_9 - w_{9'}) + (F-C)(w_8 - w_{8'}) + 2(w_{5'} - w_{7'})\right] \quad (69)$$

Figure 21 (Cont'd.)

in which A, B, C, . . . are the coefficients appearing in a particular moment equation and w_1, w_2, w_3, . . . are the deflections of the slab at network points 1, 2, 3, ... M_2 is the moment at point 2 and can be either M_x or M_y, or M_{xy}. The influence coefficients across the slab for moment, M, at point 2 will be the same as the values of deflections across the slab when the slab is loaded with A at point 1, B at point 2, C at point 3, etc. Any loading condition for the slab can be represented by a column vector consisting of the right-hand sides of the deflection equations. For the given loading condition, the column vector will have loads of A, B, C in its rows corresponding to deflection equations for points 1, 2, 3, respectively. Suppose the coefficients A, B, C are obtained from the M_x expression for point 2. If one forms a column vector MX using these coefficients as the loads on the slab, then the two solution matrices can be obtained by the following vector multiplications:

$$\frac{S^{-1}MX + U^{-1}MX}{2} + \frac{S^{-1}MX - U^{-1}MX}{2} \quad (71)$$

TABLE 4

DEFLECTION AND MOMENT EQUATIONS FOR VARIOUS POSITIONS OF A TYPICAL SLAB POINT

Position Fig.	Deflection Eq.	Moment Eq.
(a) Skew Network		
1a	3	38
1b	4	37
1c	5	38
1d	6	38
1e	7	39
1f	8	40
1g	9	41
1h	10	42
1i	11	42
1j	12	38
1k	13	43
1l	14	44
1m	—	45
1n	—	46
1o	—	47
1p	—	48
1q	—	49
1r	2	37
(b) Square Network		
2a	15	50
2b	16	51
2c	17	50
2d	18	51
2e	19	51
2f	20	52
2g	21	53
2h	22	54
2i	23	55
2j	24	55
2k	25	55
2l	26	52
2m	27	52
2n	—	56
2o	—	57
2p	—	58
2q	—	59
2r	—	60
(c) Rectangular Network		
3a	29	62
3b	30	62
3c	31	62
3d	32	63
3e	33	64
3f	34	62
3g	35	62
3h	36	65
3i	—	66
3j	—	67
3k	—	68
3l	—	69
3m	28	61

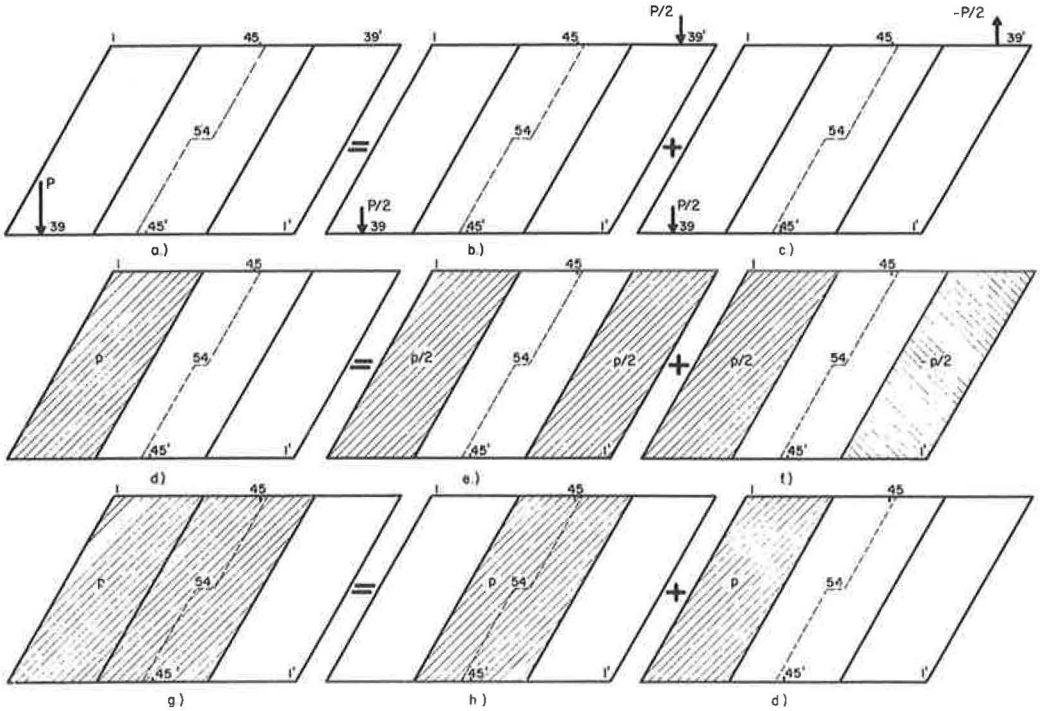

Figure 22. Symmetrical, anti-symmetrical load systems.

The elements of the first solution matrix represents the influence coefficients in the left half of the slab for the moment M_x at point 2, and the second solution matrix contains the influence coefficients in the right half of the slab. Forming column vectors MY and MXY for the moments M_y and M_{xy} at point 2, in a similar way, influence coefficients for those moments are also found.

Finally, combining these three sets of influence coefficients according to the following equations, influence coefficients for the principal moments at point 2 and their direction θ at point 2 can be calculated:

$$M_{\substack{max \\ min}} = \frac{M_x + M_y}{2} \pm \sqrt{\left(\frac{M_x - M_y}{2}\right)^2 + M_{xy}^2} \tag{72}$$

$$\theta = \tfrac{1}{2} \tan^{-1} \frac{2M_{xy}}{M_x - M_y} \tag{73}$$

For the slab points close to the axis of symmetry, the moment equations may also contain the deflections of the points on the right half of the slab, and Eq. 71 is replaced by

$$\frac{S^{-1}MXL + U^{-1}MXL}{2} + \frac{S^{-1}MXR - U^{-1}MXR}{2} \tag{74a}$$

for the influence coefficients in the left half of the slab, and

$$\frac{S^{-1}MXL - U^{-1}MXL}{2} + \frac{S^{-1}MXR + U^{-1}MXR}{2} \tag{74b}$$

for the influence coefficient in the right half of the slab. In these expressions, MXL is the column vector containing the load coefficients for the points to the left of the axis of symmetry and the column vector MXR contains the load coefficients for the points on the right half of the slab. Computations of the influence coefficients for M_y, M_{xy} are carried out in a similar way using column vectors MYL, MYR, MXYL and MXYR.

When a certain moment equation contains the deflection of a singular point such as the midpoint of a center span, which is completely symmetrical, Eqs. 74 become

$$\frac{S^{-1}MXL + U^{-1}MXL}{2} + \frac{S^{-1}MXR - U^{-1}MXR}{2} + S^{-1}MXC \tag{75a}$$

and

$$\frac{S^{-1}MXL - U^{-1}MXL}{2} + \frac{S^{-1}MXR + U^{-1}MXR}{2} + S^{-1}MXC \tag{75b}$$

in which MXC is the column vector containing the coefficient of the singular point deflection in the particular moment equation.

Uniform load deflections are obtained by the multiplication of S^{-1} and U^{-1} matrices by certain A and B column vectors. Column vector A contains unit load expressions on its rows belonging to the points in the center span and column vector B has unit load expressions for the points in the end span. Among these column vectors and the inverse matrices, the following solution matrices are formed:

$$X_1 = S^{-1}A \qquad X_2 = S^{-1}B \qquad X_3 = U^{-1}B \qquad X_4 = X_1 + X_2$$
$$X_5 = \frac{X_2 + X_3}{2} \qquad X_6 = X_2 - X_5 \qquad X_7 = X_1 + X_5 \qquad X_8 = X_1 + X_6 \tag{76}$$

Thus, elements of X_1 give the deflections of slab points when the center span is uniformly loaded; X_2, the deflections when two end spans are uniformly loaded; and X_4, the deflections when all the spans are uniformly loaded. When left end and center spans are loaded, deflections in the left half of the slabs are given by X_7 and the ones in the right half by X_8 (Figs. 22d to 22h).

For the four different uniform loading systems using the moment equations in Figure 21 and the proper set of uniform loading equations, uniform load moments M_x, M_y and M_{xy} can be calculated. For this purpose all the moment equations are expressed in one master equation

$$M = -K_1 \left[K_2(w_{11} - 2w_{12} + w_{13} - w_{14}) + K_3(w_{15} - 2w_{16} + w_{17} - w_{18}) + K_4(w_{19} - 2w_{20} + w_{21} - w_{22}) + K_5(w_{23} - 2w_{24} + w_{25} - w_{26})\right] \tag{77}$$

in which $w_{11}, w_{12}, \ldots, w_{26}$ are uniform load deflections of the slab points as indicated by each individual moment equation for a given position of a slab point. $K_1, \ldots, K_5$ are the constants appearing in that particular equation. Finally, principal moments and their directions are found using Eqs. 72 and 73.

SYMBOLS

A = a constant in deflection equations ($A = \frac{t}{\Delta_x}$); an arbitrary constant; column vector.

a = width of slab.

B = a constant in deflection equations ($B = \frac{s}{\Delta x}$); an arbitrary constant; column vector.

b = center span length (span length in single-span slabs).

$b' = \frac{b}{\text{Cos } \phi}$.

b_e = end span length.

C = a constant in deflection equations ($C = \frac{\Delta_y^2}{\Delta_x^2} - AB$); an arbitrary constant.

D = flexural rigidity of slab ($D = \frac{EI}{1-\mu^2}$).

E = modulus of elasticity of the slab material.

F = a constant in deflection equations ($F = \frac{\Delta_y^2}{\Delta_x^2}(1 - \mu)$).

h = thickness of slab.

I = moment of inertia.

$K_1, \ldots, K_5$ = constants in the general moment equation.

M = moment; moment of internal force couple C, T.

$\overline{M}$ = total average moment.

M_x = bending moment per unit length in the x-direction.

M_y = bending moment per unit length in the y-direction.

M_{xy} = unit twisting moment.

M_{max}, M_{min} = maximum and minimum principal moments.

MX, MX__, ... = column vectors.

P = intensity of the concentrated load.

p = intensity of the uniformly distributed load.

p_{10} = uniform load intensity at typical slab point 10.

S, S^{-1} = coefficient and inverse coefficient matrices for symmetrical loading.

s = segment of Δ_x

t = segment of Δ_x.

U, U^{-1} = coefficient and inverse coefficient matrices for unsymmetrical loading.

w = deflection of the slab surface.

$w_1, w_2, \ldots$ = deflection of slab at network points 1, 2, ...

$X_1, \ldots, X_6$ = solution for uniform load deflections.

Δ = finite distance between two slab points.

$\Delta_x, \Delta_y, \Delta_s, \Delta_t$ = finite distances along directions indicated by subscripts.

δ = angle between the y- and t-axes.

ϕ = angle of skew.

μ = Poisson's ratio for the slab material ($\mu = 0.15$).

θ = angle between the x-axis and the maximum moment direction.

1, 2, 3, ... = network points on the left symmetrical half of a slab surface.

1′, 2′, 3′, ... = network points on the right symmetrical half of a slab surface corresponding to points 1, 2, 3, ...under a symmetrical loading.

Dynamic Load Distribution in Continuous I-Beam Highway Bridges

D. A. LINGER, Associate Professor of Civil Engineering, University of Arizona, and
C. L. HULSBOS, Research Professor of Civil Engineering, Lehigh University

The load distribution to the longitudinal beams is shown for the outer and inner spans and at the interior supports for two types of continuous four-span highway bridges. The load distribution was determined for static and moving loads and indicates the effect of dynamic loading on lateral load distribution. The effective composite sections were determined experimentally for the negative as well as the positive moment regions.

From the results of the load distribution data, influence lines are presented for the lateral distribution of loads and a comparison is made with the AASHO specifications. The effective composite section of the longitudinal stringers, which was required for the load distribution study, is shown and indicates that the distribution and amount of composite action vary from that allowed by the AASHO specifications.

•THE PROBLEM of load distribution in highway bridges made up of longitudinal stringers acting integrally with a roadway slab has been investigated by many researchers (1, 2, 3, 4, 5, 6, 7, 8). These investigations have added materially to the knowledge of the response of highway bridges to vehicular loading. However, the expanded use of this type of bridge has emphasized the need for a better understanding of the way in which it responds to dynamic vehicular loading. Moreover, it is quite evident that the problem of load distribution is not just a static problem, but a dynamic problem. It is this dynamic problem that has been generally ignored by highway engineers and is becoming increasingly important as larger and faster vehicles are used.

The research presented herein is a summary of a load distribution study conducted by the authors in conjunction with a research project (4, 5). To present and discuss the additional data obtained in the experimental program for the impact study, the following report on static and dynamic load distribution and the effective section of the longitudinal stringers is presented.

The investigation of dynamic load distribution was made by first studying how the static live load is distributed to the stringers by the distribution of the bending moments. After the static load distribution was obtained, the dynamic effect of the moving load was studied for its effect on the whole bridge as well as on the individual stringers. The load distribution studies also indicate that considerable longitudinal load distribution occurs in the type of structures studied. The effective section of the longitudinal stringers was required for these studies, and the results of this experimental data add to the understanding of the complex problem of the amount of composite action in a continuous highway bridge.

OBJECTIVE

The objective of this research was to evaluate the response of full-size continuous I-beam highway bridges to dynamic vehicle loadings. The objective of the portion of

Paper sponsored by Committee on Bridges.

the research presented herein was to analyze the effect of dynamic loads on lateral live-load distribution and to present the influence lines for the lateral live-load distribution for the various longitudinal stringers. An additional objective, which is basic to the design of this type of structure, was to determine the amount of effective composite action between the reinforced concrete slab and the longitudinal stringers.

BRIDGE STRUCTURES

The bridges tested are part of the Interstate Highway System around Des Moines, Iowa. Only two of the four bridges studied in this research program are reported in this paper. The two bridge structures included are a continuous aluminum stringer bridge, and a continuous steel stringer bridge (5). Both bridges carry two lanes of traffic and were designed for an H20-S16 loading.

Continuous Aluminum Stringer Bridge

This structure is a 220-ft continuous four-span bridge with four aluminum stringers which act compositely with a reinforced concrete roadway. It has a 30-ft roadway with a 3-ft safety curb on both sides (Fig. 1). It carries traffic on Clive Road over Interstate 35 northwest of Des Moines.

Continuous Steel Stringer Bridge

This 240-ft continuous four-span structure is very similar to the previous bridge except for the longitudinal stringers. The four steel stringers act compositely with a reinforced concrete roadway which is 28 ft wide with a 3-ft safety curb on both sides (Fig. 2). This structure carries the traffic on Ashworth Road over Interstate 35 west of Des Moines.

VEHICULAR LOADING

The vehicle used in the experimental study is a tandem-axle, International L-190 van type truck (Fig. 3). This truck, which is used to check the Iowa State Highway

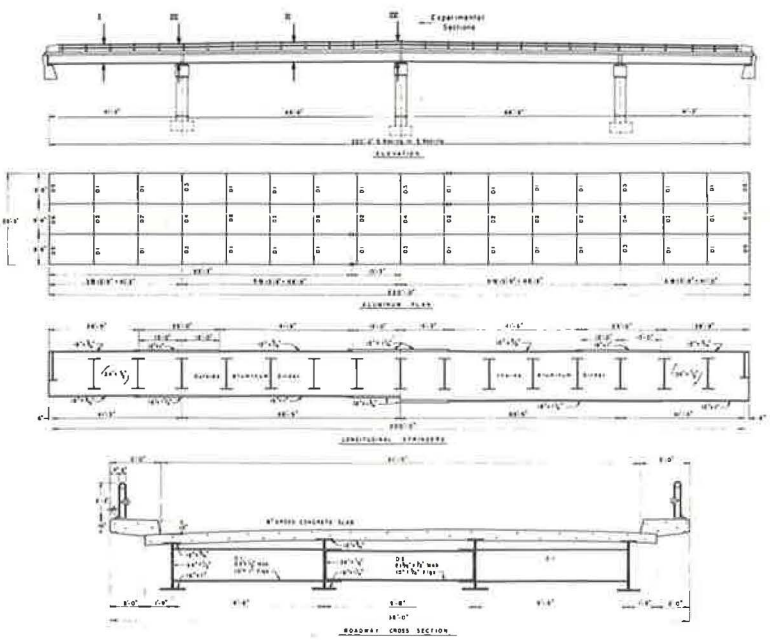

Figure 1. Details of continuous aluminum stringer bridge.

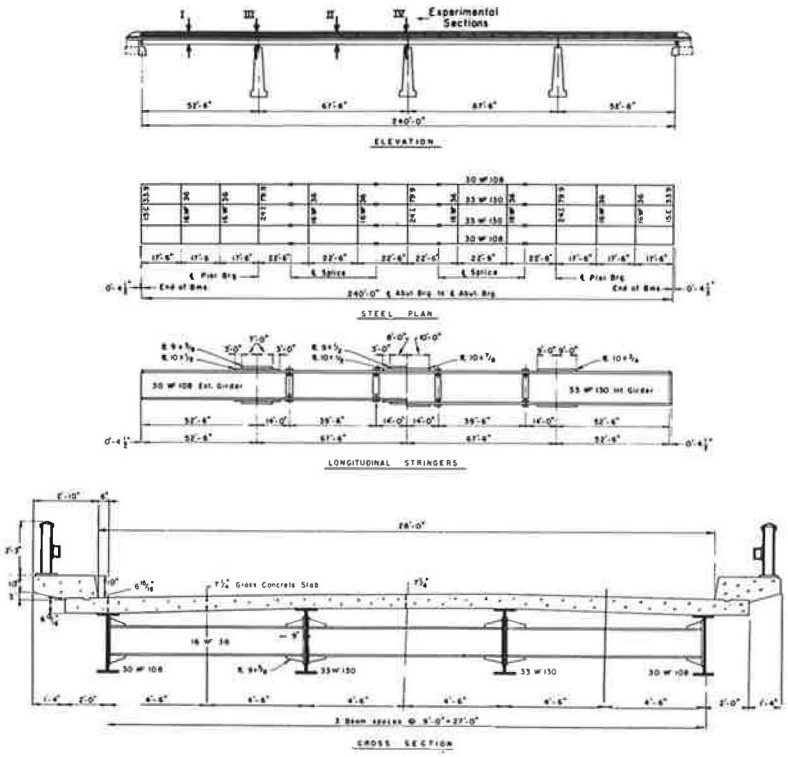

Figure 2. Details of continuous steel WF stringer bridge.

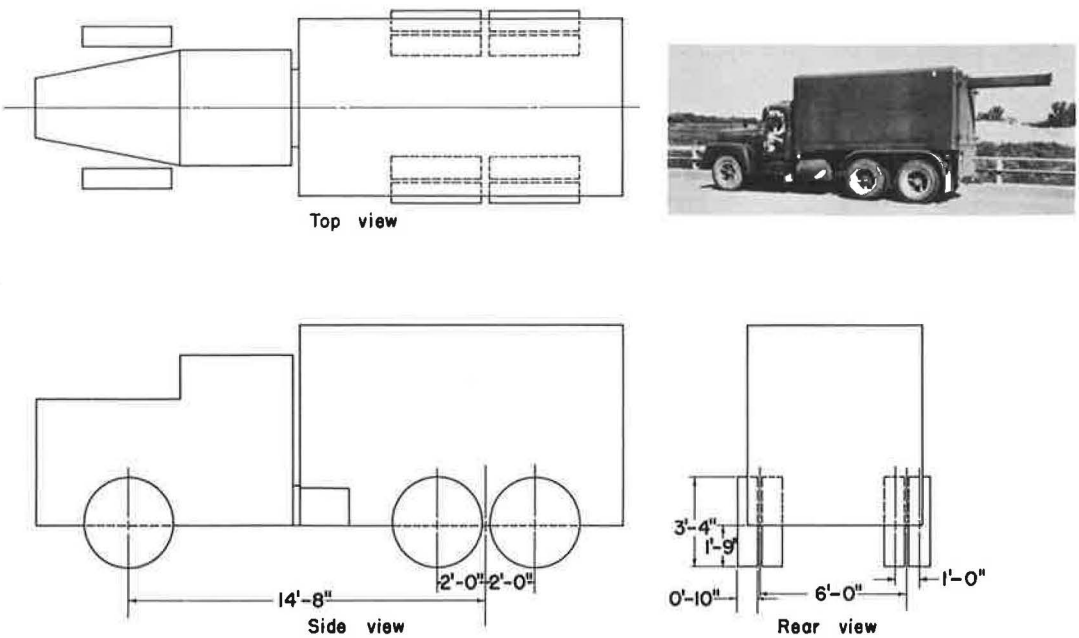

Figure 3. The standard (H-20) loading vehicle.

Commission scales, has a wheel base of 14 ft, 8 in. and a tread of 6 ft. It weighs 40,650 lb with 21,860 lb on the rear axle. This vehicle closely approximates a standard H-20 design load.

The static load distribution was determined by the test vehicle creeping across the bridge with the motor idling. This loading was applied on all the experimental test "lanes" of the bridges (Figs. 4 and 5). Each of the experimental lanes was marked by a painted stripe along which the left front tire of the truck was run. During the speed runs which were used to evaluate the dynamic load distribution, the variation of the position of the vehicle to one side or the other was never more than 1½ in. The dynamic tests were performed along four different lanes on the bridge roadway, two lanes for each direction of travel with one lane corresponding to the highway lane and the other lane at the longitudinal center line of the bridge.

INSTRUMENTATION

Strain Recording Equipment

To determine the dynamic effect of the vehicles, the static and dynamic bridge moments were computed from the strain measured at the extreme bottom fiber of each stringer. To measure the strains, standard SR-4 strain gauges were used.

The strain readings were recorded by a Brush universal amplifier (BL-520) and a Brush direct-writing recorder (BL-274). This equipment produces a continuous record of strain for which the time base can be varied by the speed of the recording paper.

Location of Strain Gauges

The strains were measured in all the stringers in the outer and inner spans and at the interior supports. This allowed the load distribution to be evaluated at all the sections of maximum bending moment for the entire length of the bridge structures. The distribution of live load and the effect of dynamic loading were determined for negative as well as positive moment sections.

Experimental Sections.—The experimental sections instrumented for the evaluation of the bridge moments are described in the following and shown in Figures 1 and 2.

(1) Section 1 is located at a point four-tenths of the outer span from the end support.
(2) Section 2 is located at the middle of the interior span.
(3) Section 3 is located at the first interior support. To eliminate or reduce any effect which the reaction diaphragms might have, section 3 was offset from the center

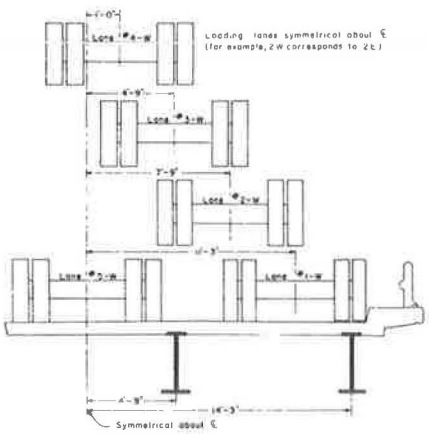

Figure 4. Cross-section showing test "lanes" for the aluminum stringer bridge.

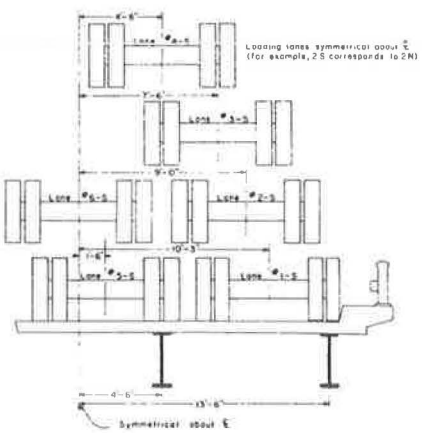

Figure 5. Cross-section showing test "lanes" for the steel stringer bridge.

line of the reaction toward the exterior span. This offset was 1 ft for the aluminum stringer, and 6 in. for the steel stringer bridge.

(4) Section 4 is located at the center interior support. This section is offset from the center line of the reaction a distance equal to the offset of section 3 for each respective bridge structure.

All of the bridges were instrumented at each of the above sections with an SR-4 strain gauge at the center of the bottom flange.

Experimental Neutral Axes.—To obtain the moments required to evaluate the distribution of load, the section moduli of the stringers were required at the sections where the strains were measured. The effective composite section of the longitudinal stringers varies considerably due to cover plates, variable flanges or the proximity of the curb to the outer stringers. These variations in the cross-section result in large changes in the moments of inertia and section moduli from one section to another. The actual section moduli and moments of inertia of the longitudinal stringers were determined experimentally by obtaining the position of the neutral axis of the longitudinal stringers. Five SR-4 strain gauges were positioned at each cross-section of the stringer for which the location of the neutral axis was required. One gauge was located at the center of gravity of the longitudinal stringer, and the other four gauges were at the extreme fibers and the quarter points. The locations of the neutral axes were then determined by plotting to scale the strains obtained from the gauges along each cross-section for various static loadings on the bridge. The neutral axis could then be located very accurately to the nearest $\frac{1}{8}$ in. Once the neutral axes were obtained, the amount of slab necessary to balance the experimentally located neutral axes was determined and the moments of inertia computed. The entire roadway slab thickness was used in these calculations with a modular ratio of 10 for the steel stringer bridge and a ratio of 3.33 for the aluminum stringer bridge. However, once the position of the neutral axis is known, the moment of inertia is independent of the modular ratio used.

TEST RESULTS

The Composite Section

The neutral axes of the stringer cross-sections were determined at the four experimental sections (Figs. 1 and 2) for the aluminum and steel stringer bridges. Only one quadrant of each bridge was instrumented to determine the position of the neutral axes because the bridges are symmetrical about their lateral and longitudinal center lines. The cross-sections of the aluminum and steel stringer bridges at sections 1, 2, 3, and 4 are shown in Figures 6 and 7.

The neutral axes results are not intended for a complete analysis of the variations in cross-section along the entire length of the bridges. They do show that the actual composite cross-section varies greatly at different sections along the bridges as indicated in previous research (3).

Aluminum Stringer Bridge.—The present AASHO specifications would allow 96.0 in. of slab to be used with the interior stringers and 62.25 and 69.0 in. to be used with the exterior stringers in the outer and inner spans, respectively. The experimental results indicate that there is more slab acting compositely than the specifications would allow, except at the interior stringer at section 1. This section of the interior stringer used 3 in. of slab less than that allowed by the specifications. In both positive moment sections, the resulting exterior composite sections are approximately 17 percent less than their corresponding interior composite sections even though the aluminum sections used in the exterior beams were considerably smaller. It is evident from Figure 6 that both the interior and exterior stringers exhibit considerable composite action at sections 3 and 4. This negative moment region would not be allowed composite action according to the specifications.

Steel Stringer Bridge.—The AASHO specifications would allow 87.0 and 67.5 in. of slab to be used with the interior and exterior stringers in all spans. The experimental slab width acting compositely with the interior stringer, is approximately 85 percent of the slab width allowed by the AASHO specifications. Conversely, the experimental

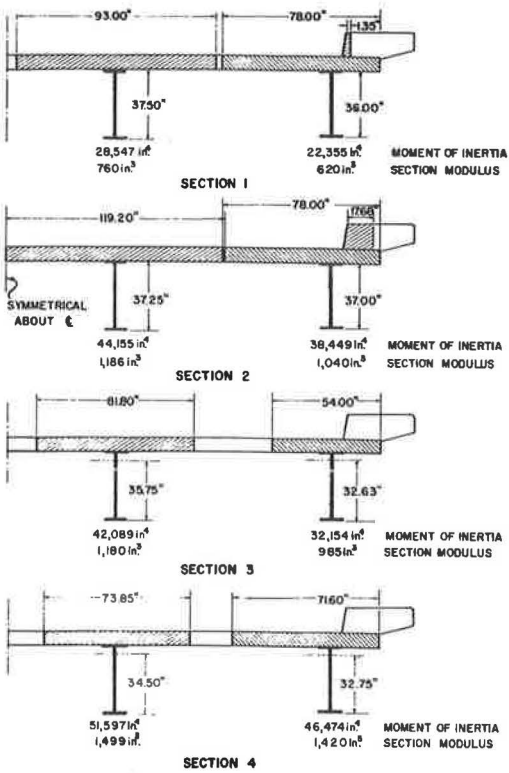

Figure 6. A cross-section of the aluminum stringer bridge at sections 1, 2, 3, and 4 showing the composite moments of inertia, section moduli, and the effective slab.

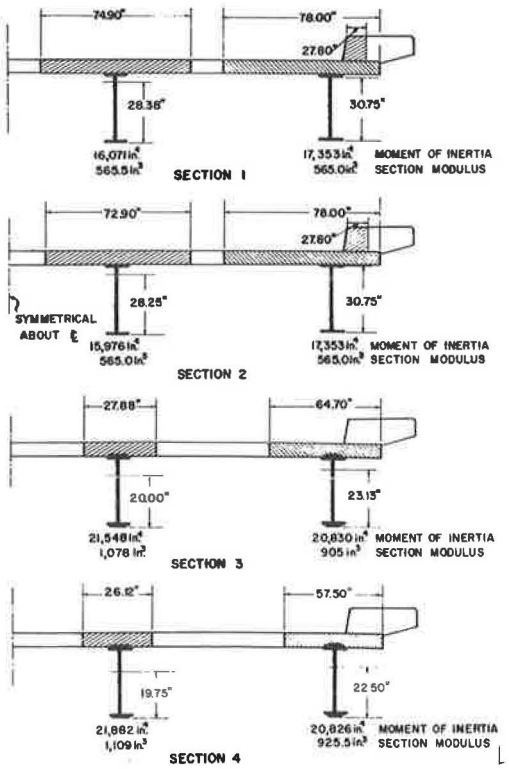

Figure 7. A cross-section of the steel stringer bridge at sections 1, 2, 3, and 4 showing the composite moments of inertia, section moduli, and the effective slab.

slab width acting compositely with the exterior stringer is considerably greater than the amount allowed by the AASHO specifications (Fig. 7). The exact amount of slab is questionable because the sidewalk curb acts integrally with the slab and must be considered in the composite action. It was decided arbitrarily that if more slab was necessary than available, the acting width of slab would be limited to the distance from the slab edge to the mid-point between the stringers, and the remaining amount of concrete necessary to balance the experimental neutral axis would be obtained from the sidewalk curb. This approach was used for both the aluminum and the steel stringer bridges. The reduction in the composite action of the interior stringers over that allowed by the specifications is more than offset by the increase in composite action of the exterior stringers. This increase in composite action at the exterior stringer is more evident in the steel stringer bridge than in the aluminum stringer bridge. The individual composite moments of inertia of the steel stringers are within four percent of their average, whereas the interior and exterior composite sections specified by AASHO are considerably different. The similarity of the actual experimental composite moments of inertia is also evident at experimental sections 3 and 4 which are in negative moment regions. The specifications do not allow any composite action to be used in these regions even though considerable composite action was found.

The composite action occurring in the negative moment regions of the aluminum and steel stringer bridges may be partially due to the way in which the continuous bridges are constructed in Iowa. The roadway slab of this type bridge is placed first in the positive moment sections and then in the negative moment portion of the roadway. As a result, the dead-load tensile stresses in the slab at the supports are minimized.

Also, the shear connectors are extended over the entire length of the stringers, and in some cases, additional reinforcement is placed in the slab over the bridge piers.

Load Distribution

Static Live Load.—The distribution of load in a slab stringer bridge is not readily analyzed by an exact method. Several theoretical methods which offer a convenient means of determining the amount of the live load distributed to each longitudinal stringer have been proposed (1, 2, 6). This report includes only the presentation of data and does not attempt to correlate the data with any theoretical results.

In this experimental study, the load distribution was determined by using the individual moment in each stringer as a percent of the total moment in the bridge cross-section. This procedure gives the percentage of the total live load distributed into each stringer, providing the moment diagrams for all the stringers are identical in shape. This is the assumption used in the design of this type of bridge structure. The live-load moments in the stringers were obtained by multiplying the measured live-load strains by the modulus of elasticity of the stringers and the section moduli for the composite cross-sections. The resulting percentage live-load distribution for the aluminum and steel stringer bridges is shown in Figures 8 through 15. This percentage distribution of load does not take into account the longitudinal load distribution because it is only a percent of the total moment. It has been found in previous studies that the experimental moment is considerably less than the theoretical moment which assumes no longitudinal load distribution (3, p. 34).

The static load distribution diagrams, which show little variation from section to section, have been further analyzed. The resulting influence diagrams are discussed later. The form of the influence line lends itself to a direct discussion and application of these results.

Dynamic Load Distribution.—The dynamic response of the bridges tested was obtained by moving-load tests. These moving-load tests were performed on four test

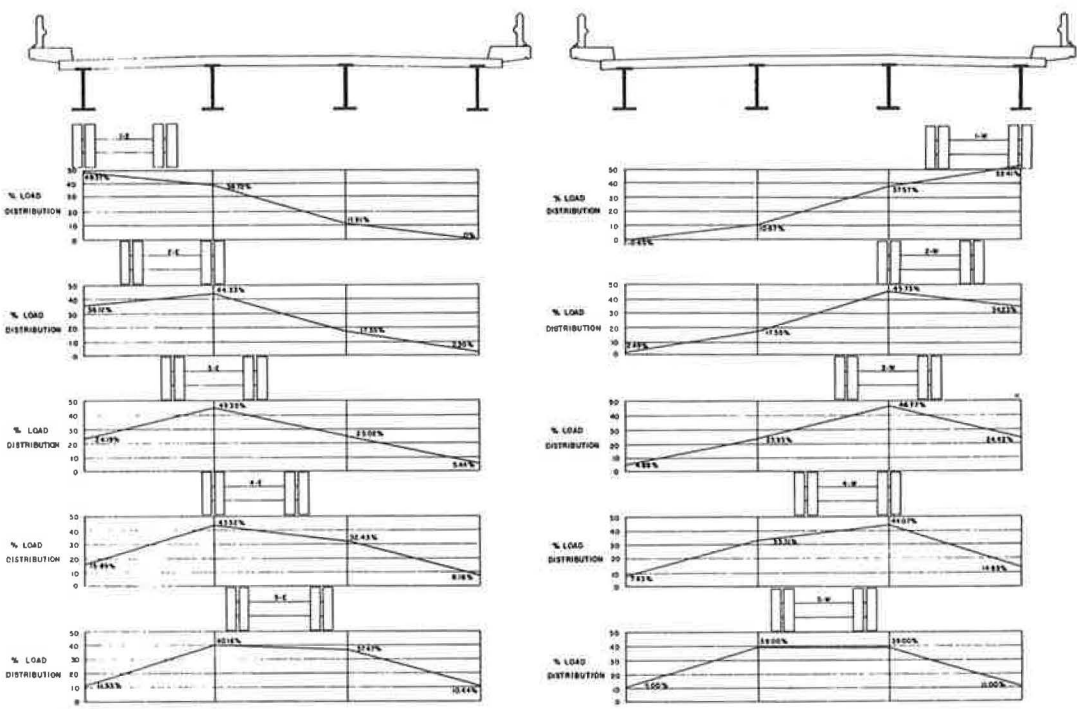

Figure 8. Static load distribution for aluminum stringer bridge at section 1.

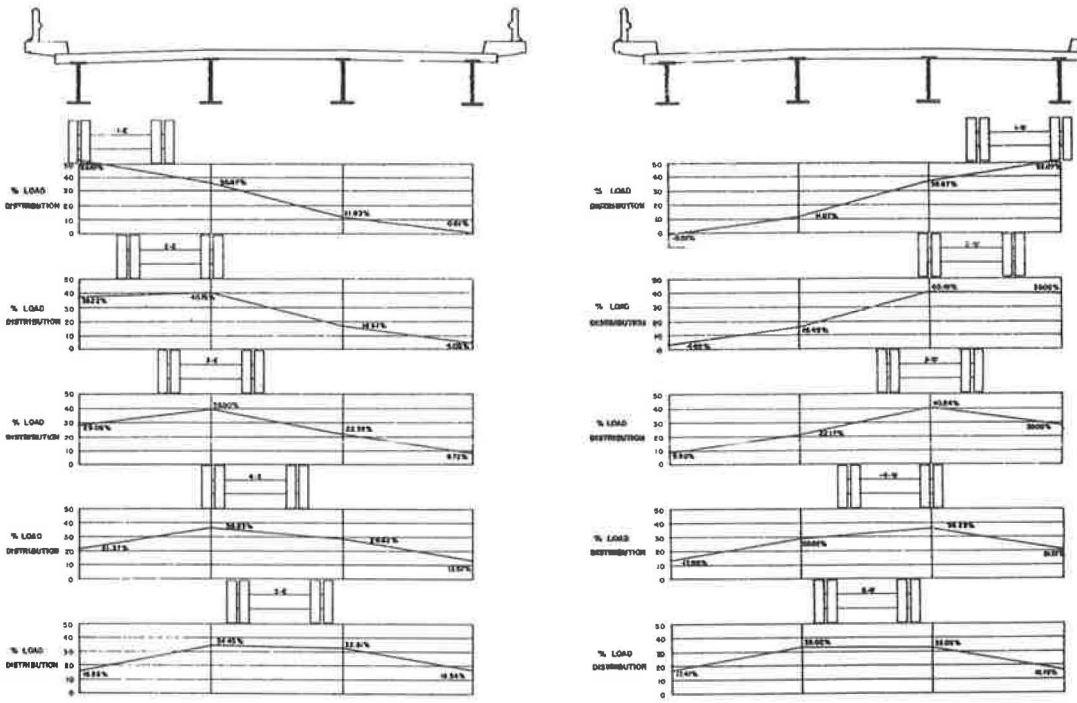

Figure 9. Static load distribution for aluminum stringer bridge at section 2.

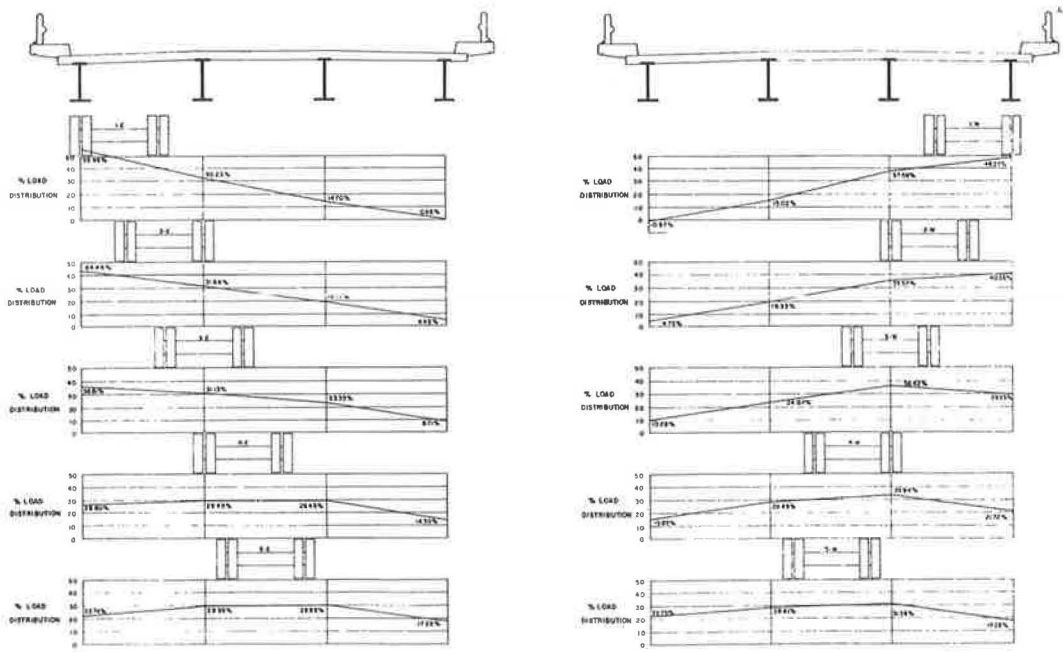

Figure 10. Static load distribution for aluminum stringer bridge at section 3.

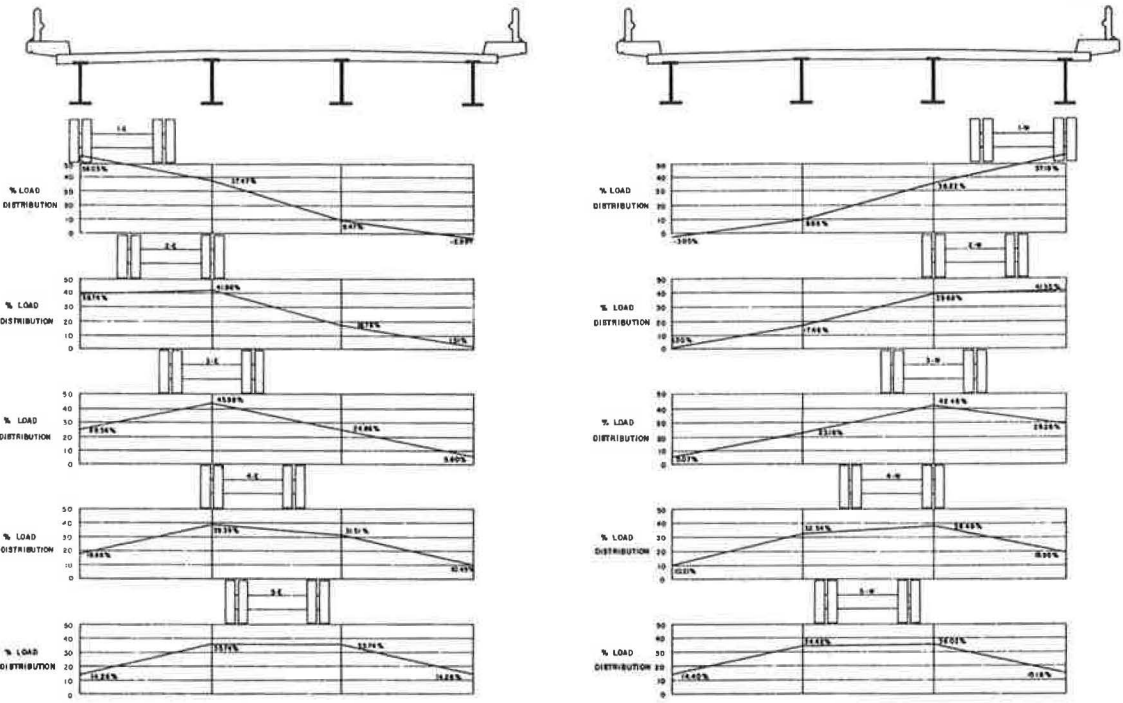

Figure 11. Static load distribution for aluminum stringer bridge at section 4.

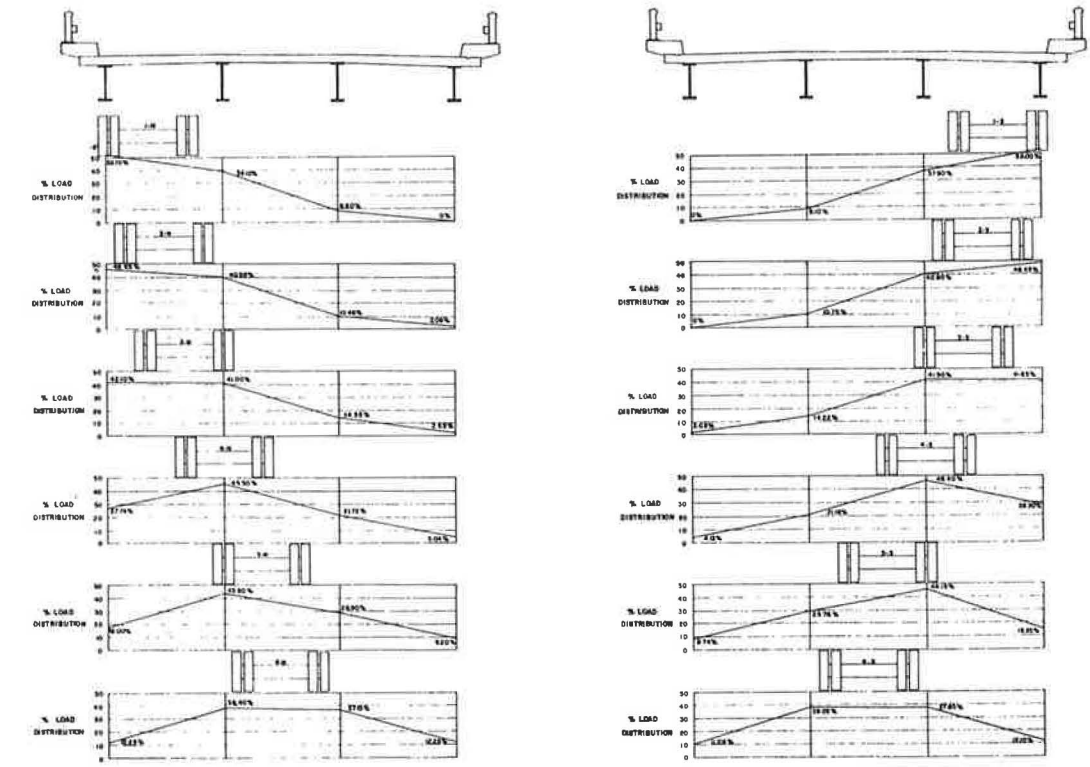

Figure 12. Static load distribution for steel stringer bridge at section 1.

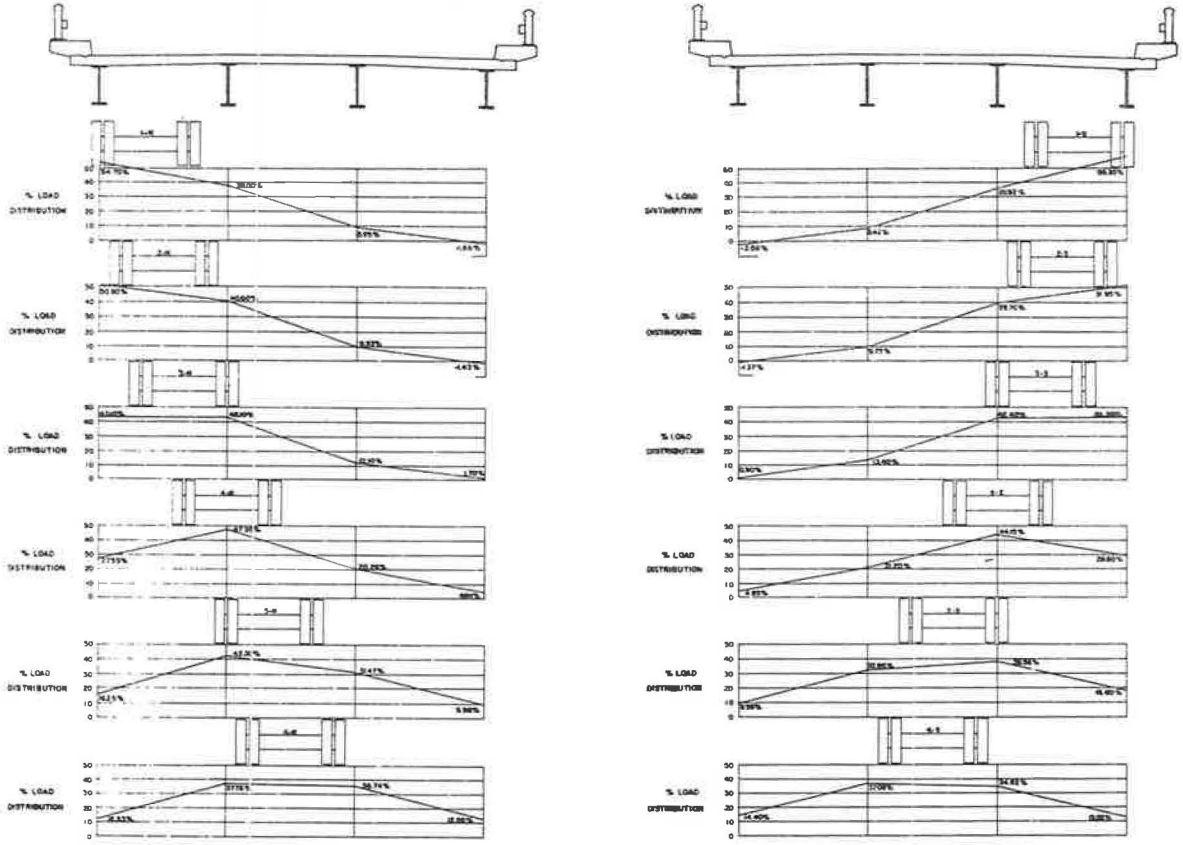

Figure 13. Static load distribution for steel stringer bridge at section 2.

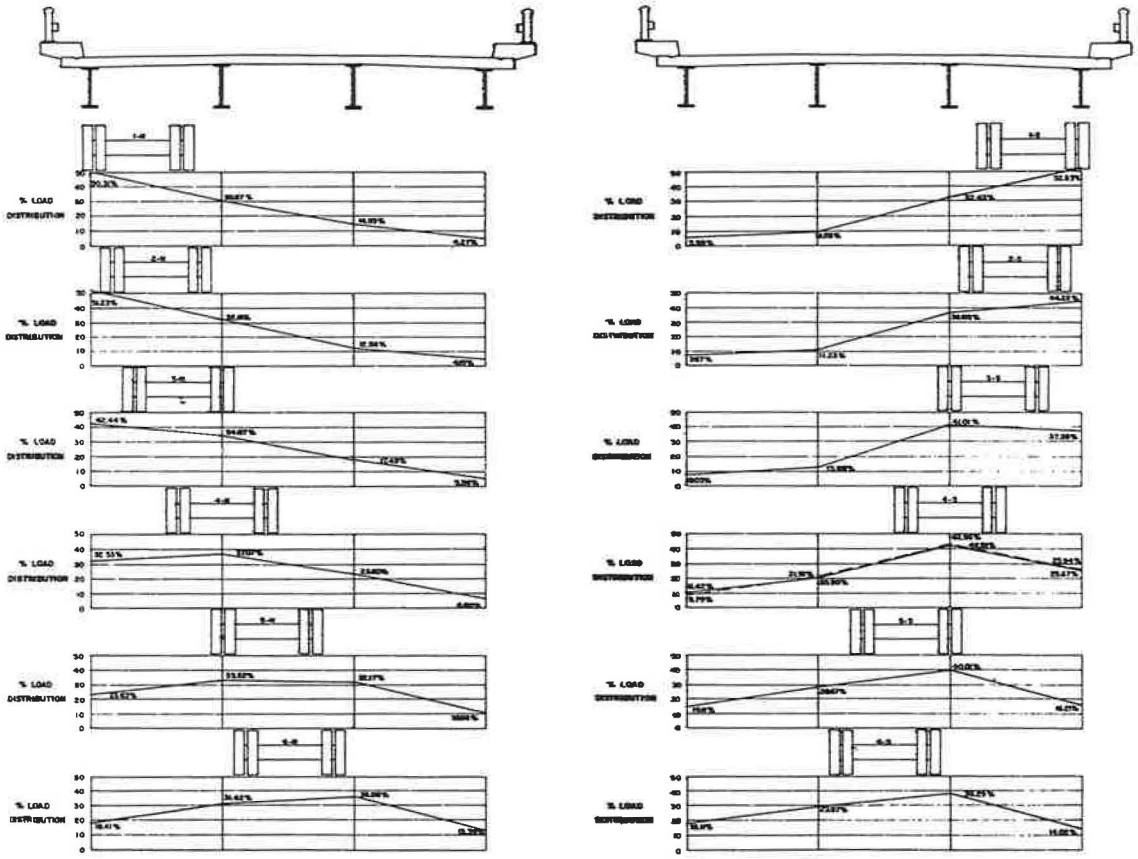

Figure 14. Static load distribution for steel stringer bridge at section 3.

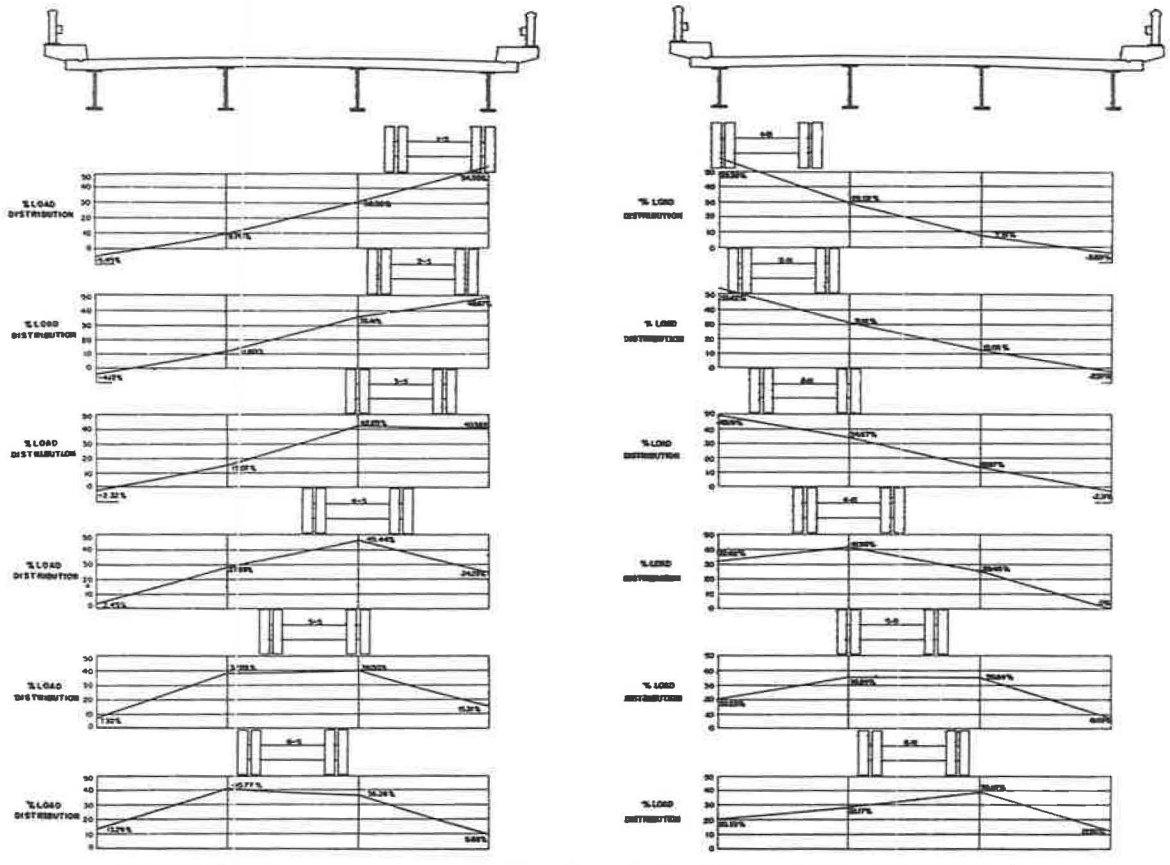

Figure 15. Static load distribution for steel stringer bridge at section 4.

lanes, two for each direction of travel for vehicle speeds beginning at approximately 10 mph and increasing by increments up to the maximum attainable speed. The data from the continuous strain time records were reduced with the vehicle in the same longitudinal position that yielded the maximum static moment.

From these data, the dynamic load distribution to the longitudinal stringers was determined (Figs. 16-23). The dynamic load distribution results indicate a similarity between the static and dynamic load distribution. The largest discrepancies between the static and dynamic load distributions usually occurred at the lower speeds (Figs. 16-23). The largest variation that occurred is eight percent of the load, and the average variation is approximately two and one-half percent of the load. The percentage distribution of moments does not indicate the impact because the percent load distribution is obtained on the basis of the total experimental moment at the section.

The similarity between the static and the dynamic load distribution curves indicates that the vibratory motion of the bridge is superimposed on the static live-load deflection curve for the longitudinal stringers on the other side of the bridge, as well as those under the vehicle. Consequently, the vibration of the bridge did not alter the lateral load distribution to any extent. The largest variation in the lateral load distribution for a dynamic load could have resulted from the lateral "rocking" of the vehicle due to wind and pavement irregularities. However, even this did not materially affect the load distribution. Therefore, the following influence lines for lateral load distribution, although constructed from the static load distribution data, are applicable to dynamic loads as well as static loads.

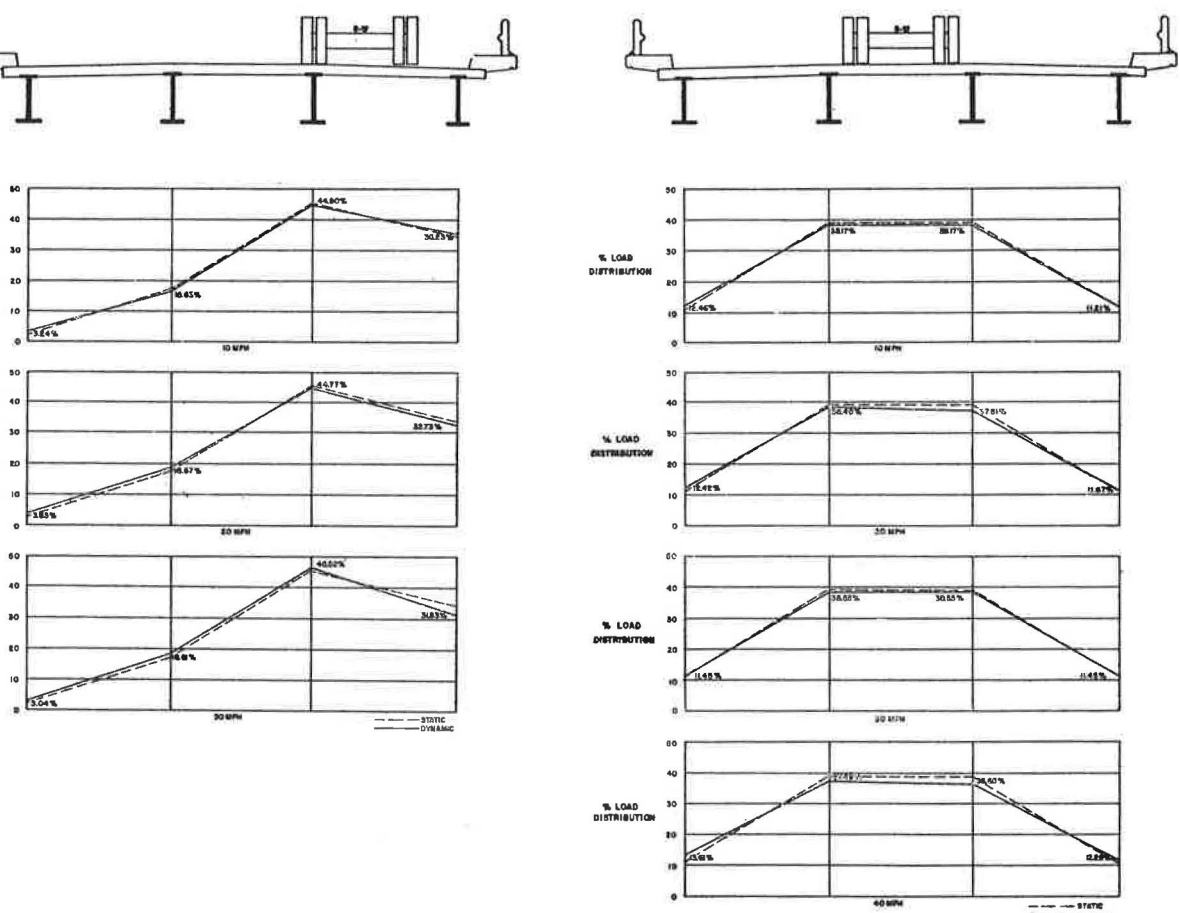

Figure 16. Dynamic load distribution for the aluminum stringer bridge at section 1.

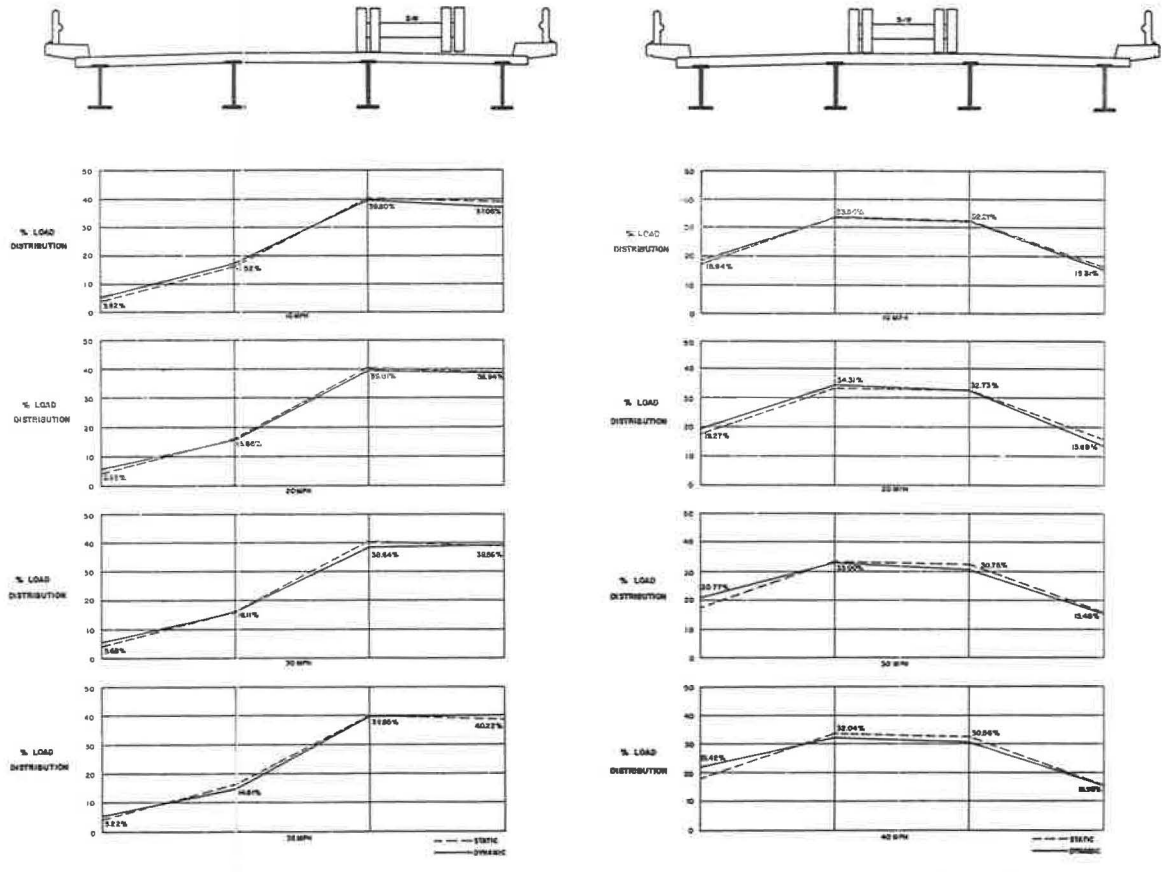

Figure 17. Dynamic load distribution for the aluminum stringer bridge at section 2.

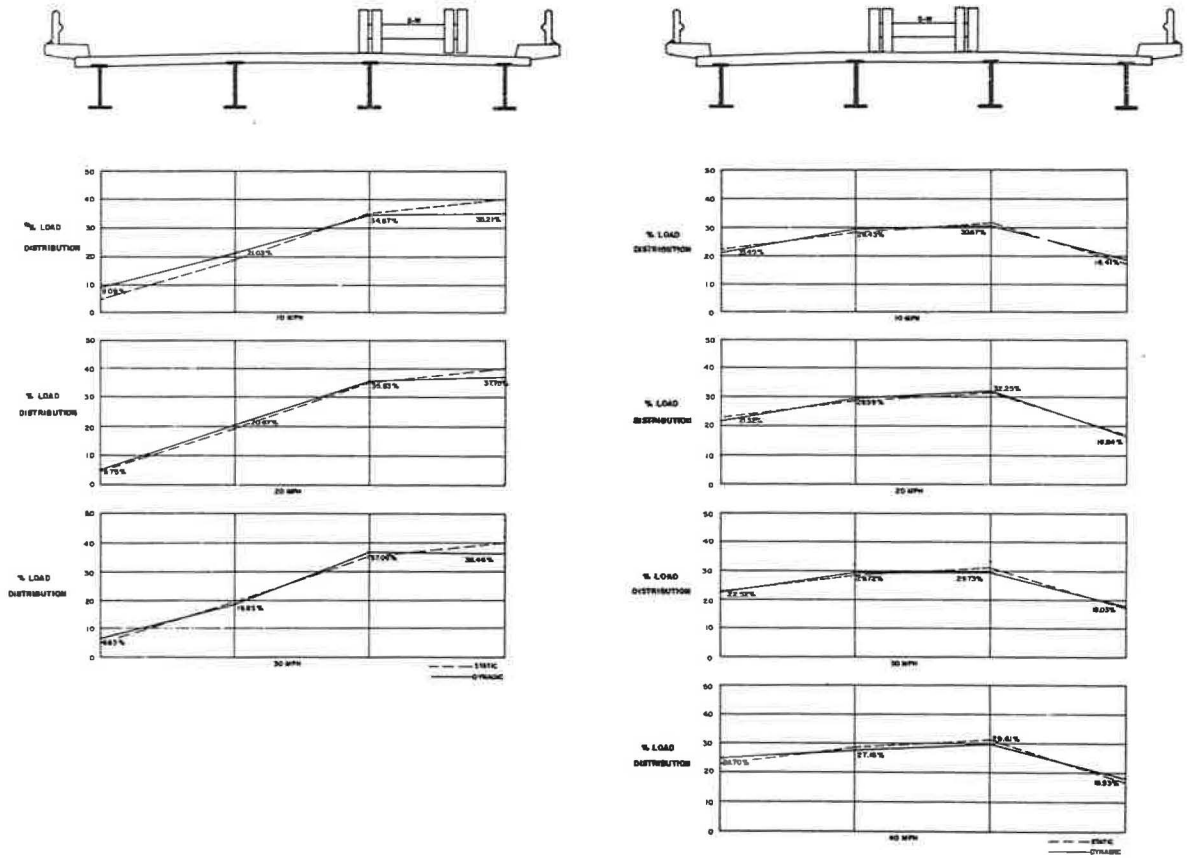

Figure 18. Dynamic load distribution for the aluminum stringer bridge at section 3.

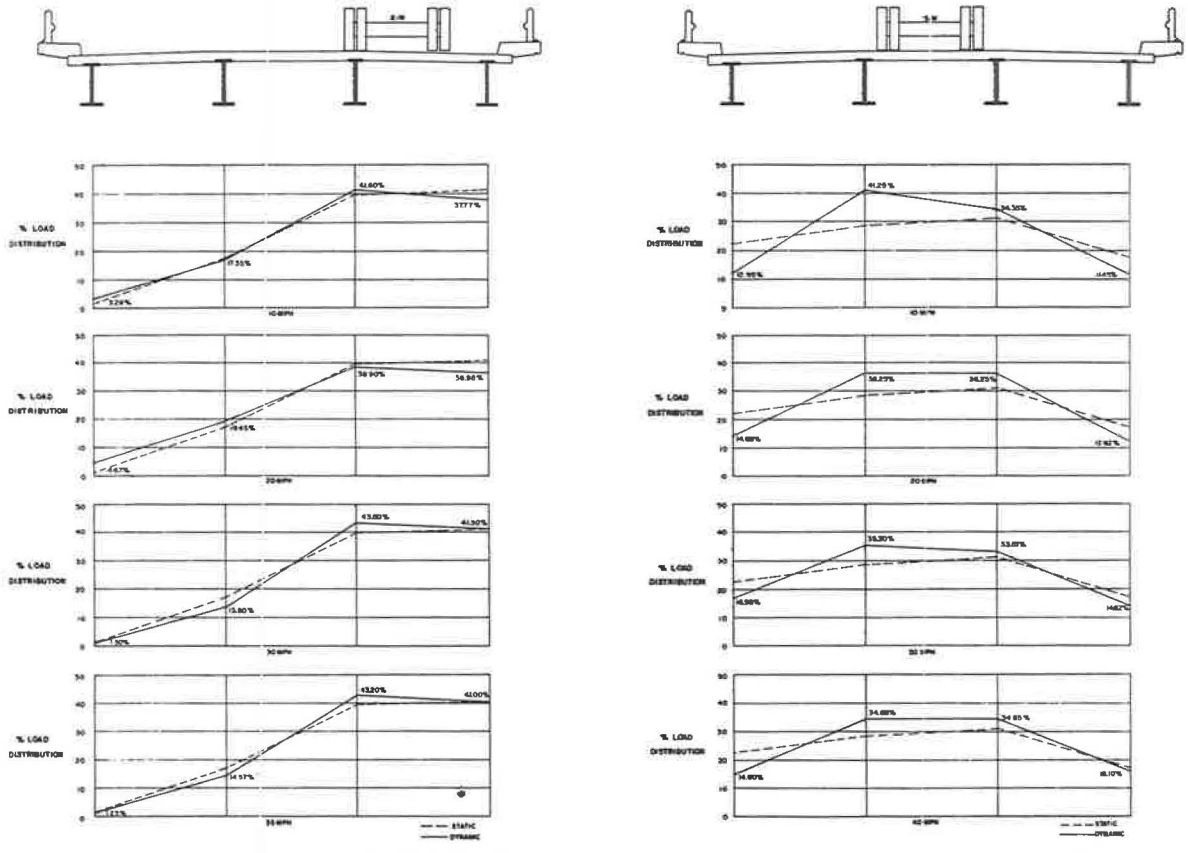

Figure 19. Dynamic load distribution for the aluminum stringer bridge at section 4.

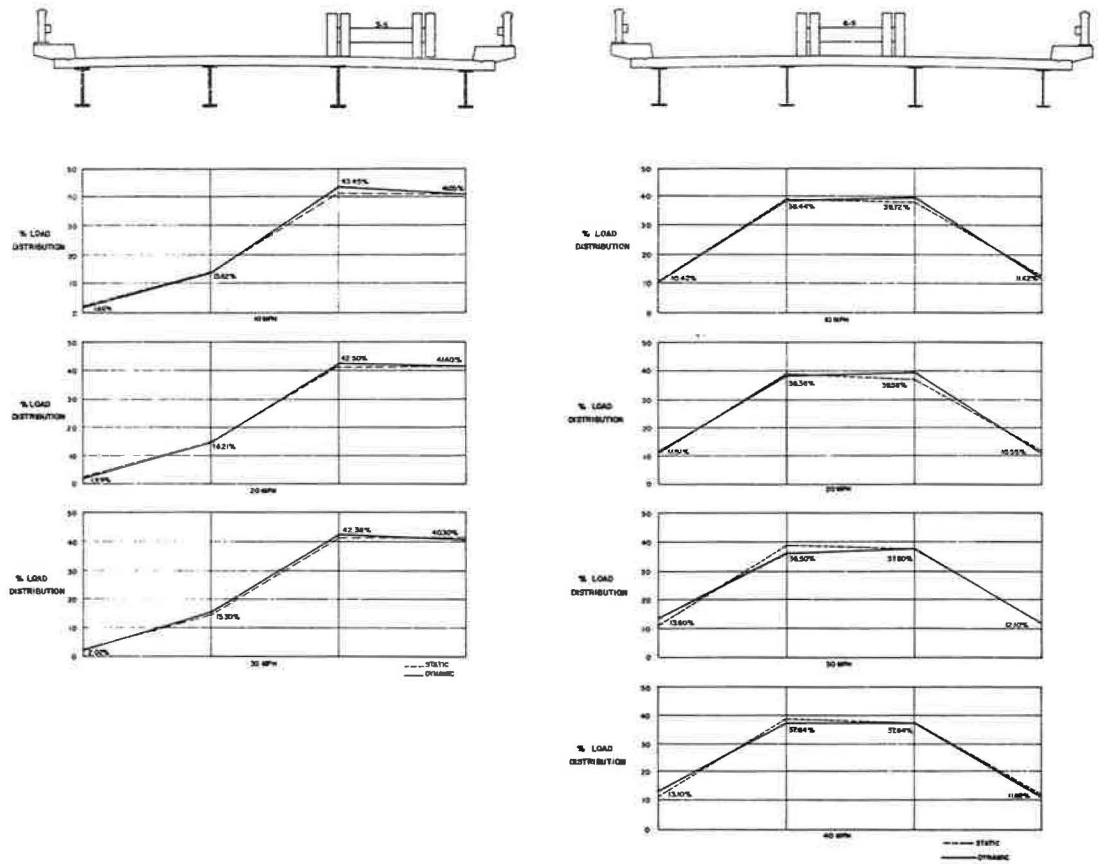

Figure 20. Dynamic load distribution for the steel stringer bridge at section 1.

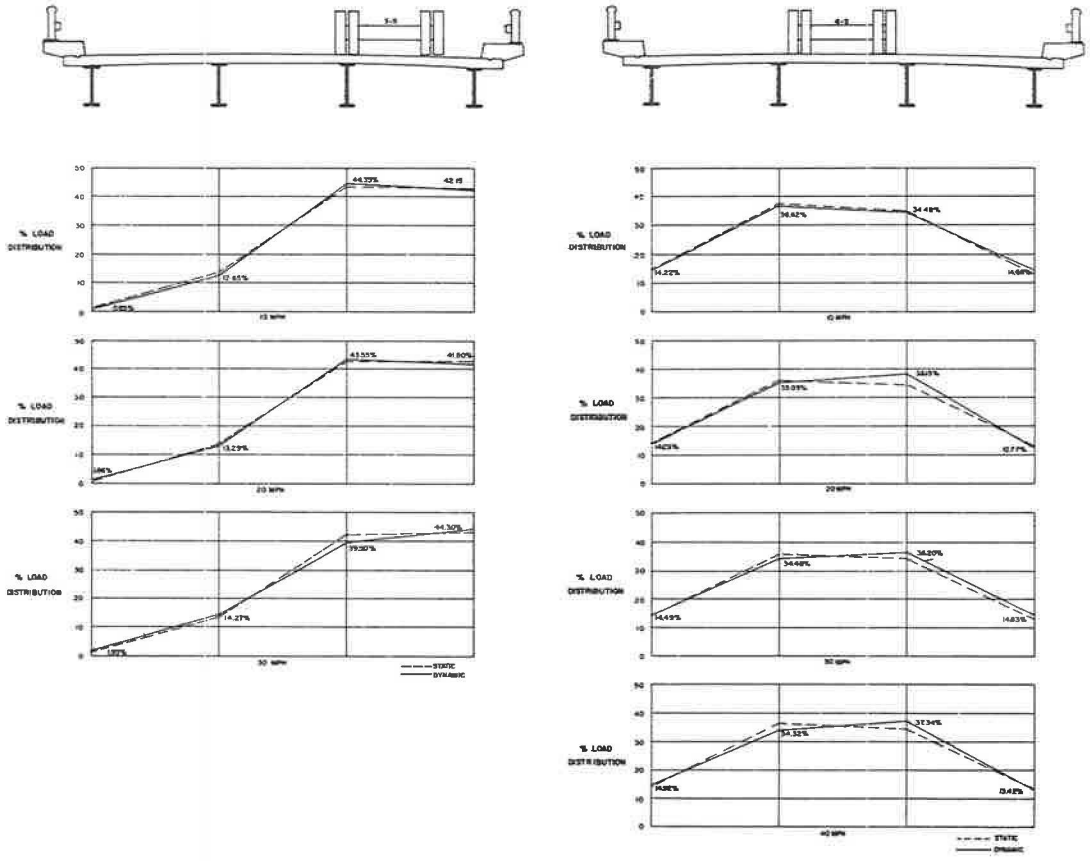

Figure 21. Dynamic load distribution for the steel stringer bridge at section 2.

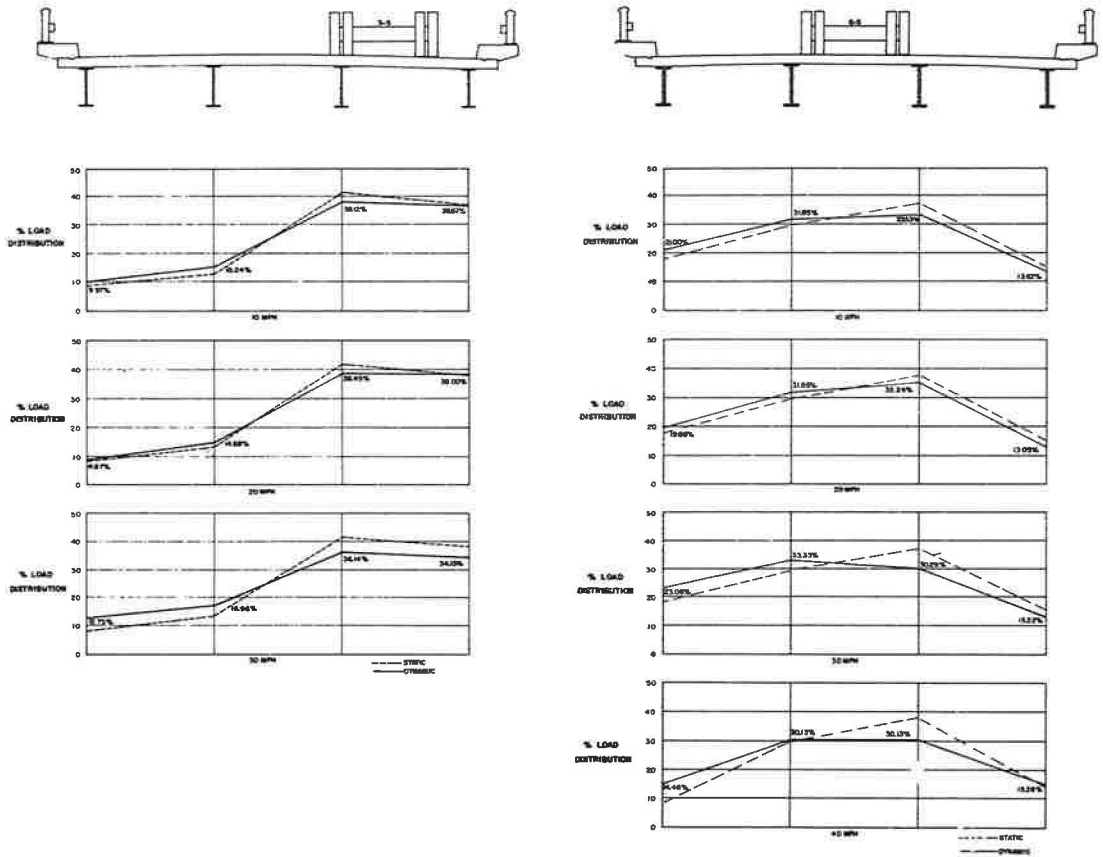

Figure 22. Dynamic load distribution for the steel stringer bridge at section 3.

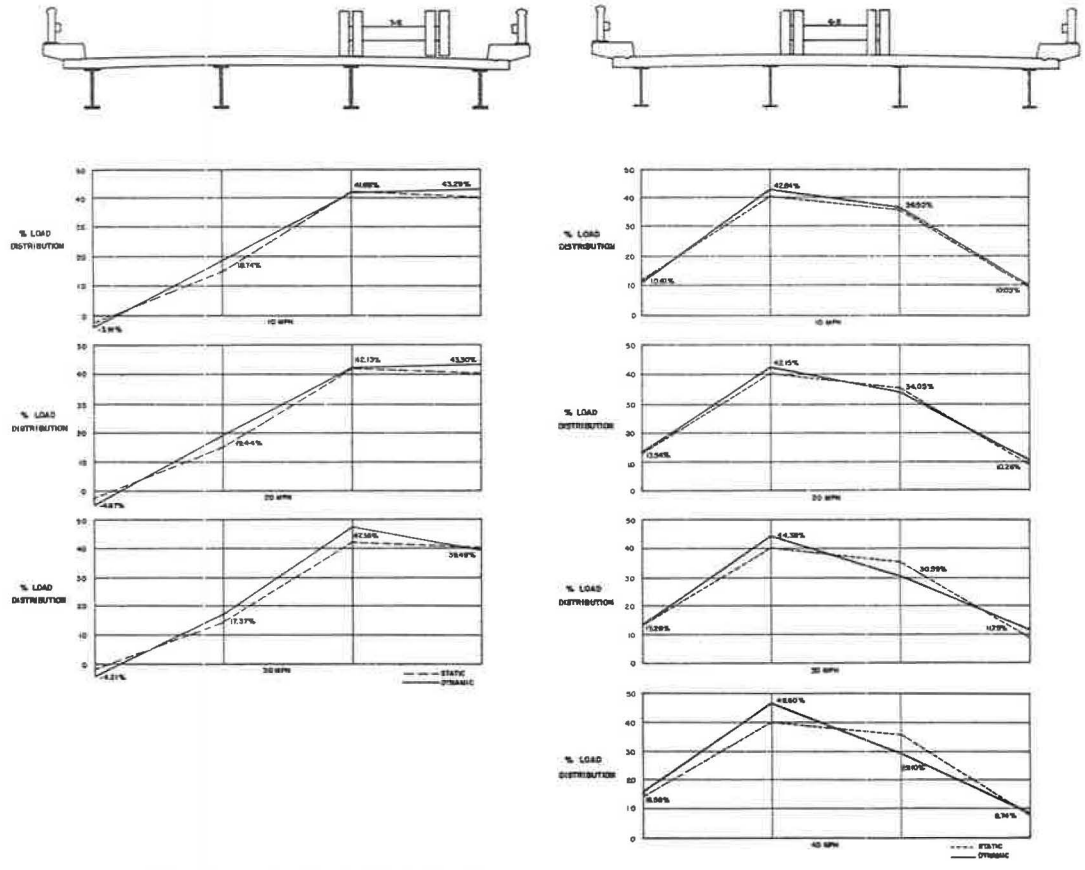

Figure 23. Dynamic load distribution for the steel stringer bridge at section 4.

Influence Lines For The Stringers.—The use of load distribution curves is facilitated by the construction of influence lines for the percentage of a unit vehicle distributed to each stringer. To obtain these influence lines, the static load distribution values were averaged for the symmetrical stringers which correspond with the loading of symmetrical lanes. For example, the value from the one outside stringer with the load in lane 2-S is averaged with the value from the other outside stringer with the load in lane 2-N. These average values were then plotted to correspond with the center line of the vehicle. The resulting influence lines (Figs. 24 and 25) indicate the percentage of a unit vehicle distributed to each respective stringer by the ordinate corresponding to the center line of the vehicle. In order to use these influence lines, it is only necessary to place the desired number of standard vehicles on the bridge cross-section and sum the cumulative influence of each.

Aluminum Bridge Structure.—When two vehicles are placed in their specified lanes and the influence lines in Figure 24 are used, a maximum value of approximately 53 and 57 percent of a vehicle is found to be distributed to an exterior stringer at the positive and negative moment sections, respectively. These percentages of a unit vehicle are equivalent to a wheel-load factor of 1.06 and 1.14, whereas the AASHO specifications yield a wheel-load factor of 1.49 for the exterior stringers in this bridge. Similarly, the maximum percentage of a unit vehicle distributed to an interior stringer at the positive and negative moment sections is approximately 70 and 67 percent, respectively. The equivalent experimental wheel-load factors for these percentages are 1.40 and 1.34, whereas the wheel-load factor given by the AASHO specifications for an interior stringer of this bridge is 1.728. It is interesting to note that the maximum

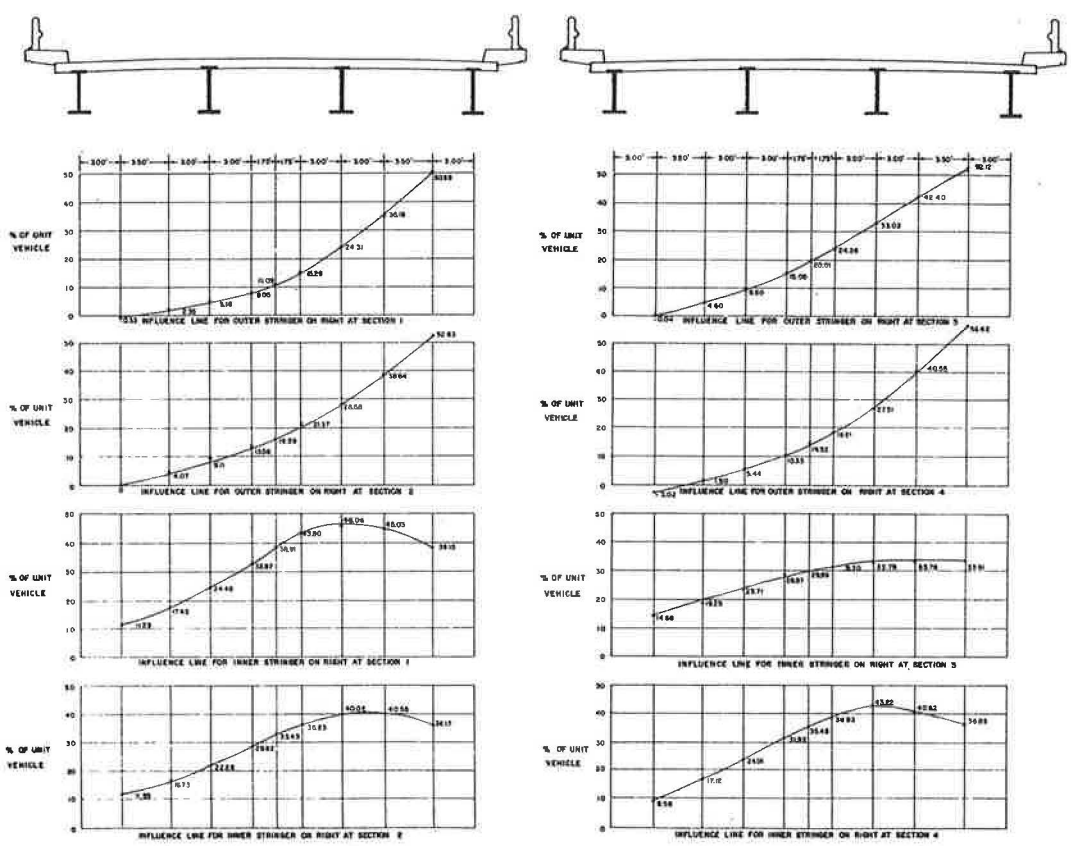

Figure 24. Influence lines for aluminum stringer bridge.

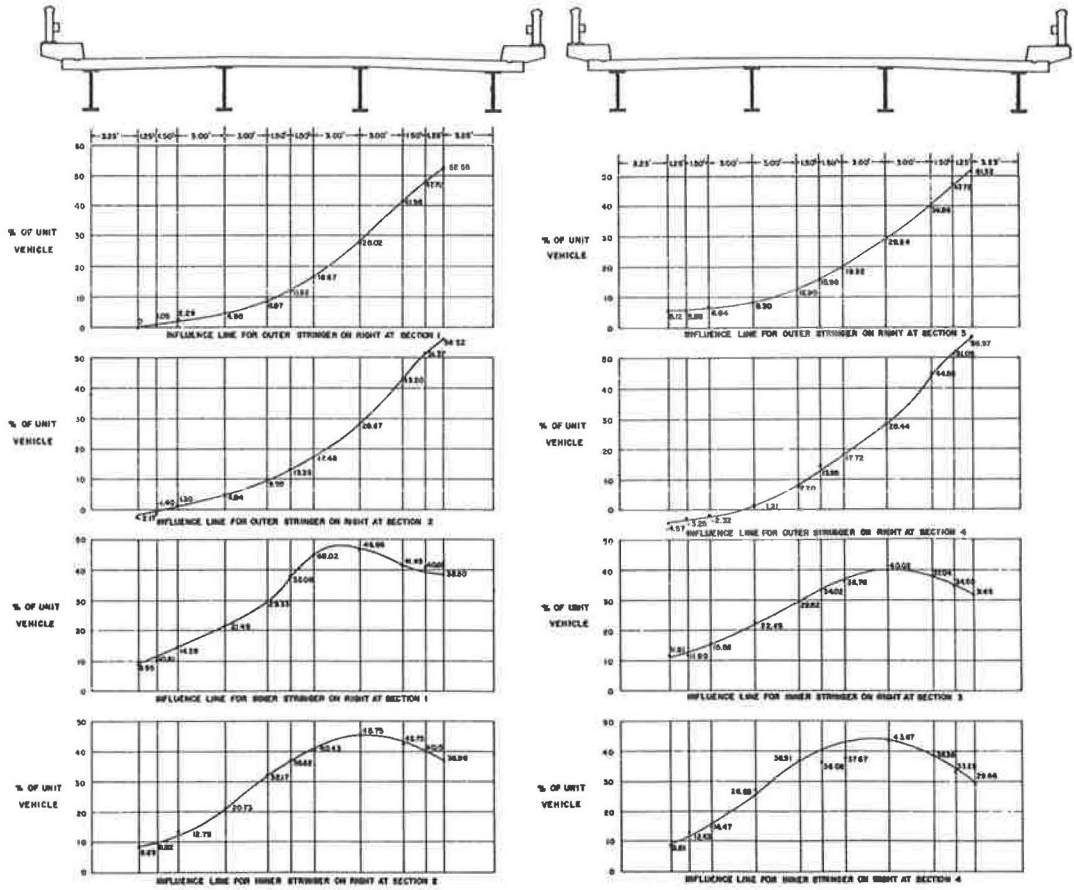

Figure 25. Influence lines for steel stringer bridge.

experimental wheel-load distribution factors occurred at sections 2 and 3 for an exterior stringer and at sections 1 and 4 for interior stringers. The largest wheel-load factors for this bridge are approximately 74 and 79 percent of the wheel-load factors given in the AASHO specifications for an exterior and an interior stringer.

Steel Stringer Bridge.—By placing two vehicles in their respective lanes and by the use of Figure 25, a maximum value of approximately 56 percent of a unit vehicle is found to be distributed to an exterior stringer in both the positive and negative moment sections. This percentage is equivalent to a wheel-load factor of 1.12. The corresponding wheel-load distribution factors for an interior stringer are found to be approximately 1.33 and 1.40 for the positive and negative moment sections. As in the case of the previous bridge, the maximum experimental wheel-load factors are obtained at sections 2 and 3 for the exterior stringers, and at sections 1 and 4 for the interior stringers. These factors are approximately 78 and 83 percent of the values obtained from the AASHO specifications of 1.44 and 1.638 for the exterior and interior stringers.

CONCLUSIONS

Considerable variation was found to exist in the amount of composite action. The exterior stringers had a larger composite section than the specifications would allow, whereas the interior stringers generally had less.

Composite action did occur at the interior supports even though negative live-load moments cause tension in the concrete roadway slab.

The same type of lateral load distribution occurred for both static and dynamic loading conditions.

Influence lines obtained from the experimental load distribution data yield wheel-load factors which are considerably less than the wheel-load factors obtained by the AASHO specifications for the type of structures studied.

ACKNOWLEDGMENTS

Acknowledgement is due to the Iowa Highway Research Board who sponsored this project. Also, the cooperation and assistance of Mark Morris, Steve Roberts, Neil Weldon, and Carl Schach, all of the Iowa Highway Commission, are especially appreciated.

REFERENCES

1. Caughey, R. A., and Senne, J. H., "Distribution of Loads in Beam and Slab Bridge Floors." Final Rpt., Iowa HRB, Iowa Eng. Exp. Sta., Iowa State Univ. (Sept., 1959).
2. Holcomb, R. M., "Distribution of Loads in Beams and Slab Bridges." Iowa HRB Bull. 12, Ames (1959).
3. Hulsbos, C. L., and Linger, D. A., "Dynamic Tests of a Three-Span Continuous I-Beam Highway Bridge." HRB Bull. 279, pp. 18-46 (1960).
4. Linger, D. A., and Hulsbos, C. L., "Dynamics of Highway Bridges." Joint Publication, Iowa Eng. Exp. Sta., Bull. 188, and Iowa HRB Bull. 17, Ames (1960).
5. Linger, D. A., and Hulsbos, C. L., "Forced Vibration of Continuous Highway Bridges." HRB Bull. 339, pp. 1-22 (1962).
6. Newmark, N. M., "Design of I-Beam Bridges." ASCE Proc. (Mar., 1948).
7. Siess, C.P., and Veletsos, A.S., "Distribution of Loads to Girders in Slab-and-Girder Bridges: Theoretical Analyses and Their Relation to Field Tests." HRB Res. Rpt. 14-B, pp. 58-74 (1952).
8. Wise, J.A., "Dynamics of Highway Bridges." HRB Proc., Vol. 32, pp. 180-187 (1953).

Repeated Stresses in Highway Bridges

HENSON K. STEPHENSON, Professor of Civil Engineering, University of Alabama

This report presents an approach to certain problems associated with repeated stresses in highway bridges. This approach includes a proposed method for predicting the frequencies of various levels of stress to which various members of highway bridges may be subjected as a result of individual or vehicle group loads encountered in the various compositions and volumes of traffic for given periods of time or throughout the life of a given structure. For the investigation of varying numbers of repetitions of various intensities of stress and how they may be related to present design criteria for fatigue, it is highly desirable that a reliable method be available for predicting the frequencies of such stresses. It is believed that the method presented accomplishes this objective by providing the means for predicting the frequencies of various levels of stress produced by heavy vehicle loads in any particular part or member of a given bridge corresponding with given traffic conditions. The proposed method takes into account (a) the frequency distribution of heavy truck loads measured in terms of their H-equivalencies on various spans, (b) the lateral placement of vehicles in highway traffic, and (c) the relative frequencies of the stress-producing effects of these loadings at any selected point in a given bridge.

• THIS PAPER presents a suggested procedure for estimating the number of repeated stresses of varying intensities produced by heavy truck loads in highway bridges. The proposed method is made possible by the following facts:

1. Vehicles by type (automobiles, buses, light trucks, heavy trucks, etc.) have been found to occur at random in ordinary highway traffic. This provides the means for estimating the frequencies of specified vehicle groups at a given location, such as at a bridge, mathematically based on the elementary laws of chance.
2. The time and/or distance spacings of vehicles have been found to occur at random in ordinary highway traffic. This randomness makes it possible for traffic engineers and others to apply statistical methods and the theory of probability to traffic problems that could not be solved satisfactorily on the basis of judgment alone (5).
3. The sizes and weights of heavy trucks and their H-equivalencies on various span lengths also have been found to occur at random in ordinary highway traffic. This randomness provides the means for describing the frequency distributions of gross vehicle weights and H-equivalencies for various span lengths on a mathematical basis (1, 5, 6, 9). Once the H-equivalency of a given truck has been determined for a given span, its stress-producing effects may be evaluated mathematically or from charts (see Figs. 7-9).
4. For any simple-span beam bridge of given length, design designation, and type of construction, it has been found that the percent of total design moment per interior beam caused by dead load remains about the same, irrespective of the lateral spacing of beams or stringers (3, 6, 10). Similarly, for a given span the percent of total design moment (or stress) per interior beam caused by live load plus impact also remains

Paper sponsored by Committee on Bridges.

about the same, irrespective of the beam spacings (3, 6, 10). These findings permit the live- and dead-load moments per interior beam or per 10-ft lane to be generalized for the interior beams of simple-span bridges of given construction type and design designation (Fig. 5).

In order to simplify the presentation of this proposed method, the discussion and illustrative examples are based on maximum bending moments in simple-span beam bridges of H15-44 design consisting of a concrete deck of minimum thickness supported by unencased steel beams. It is also assumed that the steel beams in these bridges are so spaced and the deck is of such rigidity that the maximum live-load bending stress produced in an interior stringer by a single vehicle in one lane only will amount to C = 75 percent of that produced by identical vehicles in each lane simultaneously. A more detailed discussion of this concept is given in Appendix A. The ratio of dead-load stresses to total design stresses for such steel beam bridges is smaller than for any of the heavier types of construction, such as reinforced concrete deck girder bridges. This light type of construction is used as a basis of discussion because conclusions concerning the stress-producing effects of a given truck or trucks will be on the conservative side.

EQUIVALENT H TRUCK LOADINGS

If a given heavy truck produced a maximum live-load moment of 445.6 kip-ft, with no impact, on a 50-ft span, it would be the same as that produced by an H20 truck on that span. On a 50-ft span, therefore, this truck would be converted into or rated as an equivalent H truck load weighing 20 tons, or simply an equivalent H20 truck loading. Similarly, if a given truck would produce as much live-load moment on a given span as an H26.4 truck it would have an H-equivalency of 26.4 tons, or 52.8 kips on that span. A more detailed discussion of equivalent H truck loadings is given in Appendix A, and the relative frequencies of equivalent H truck loadings for various spans, as reported by the national truck weight (loadometer) study of 1954, are given in Table 1.

Once the H-equivalency of a given truck has been determined for a given span, its stress-producing effects can be found by Eq. 3, as explained in Appendix A. The same procedure may be used for each heavy truck reported by a loadometer survey; that is, determine the H-equivalency for each truck for each span length (Table 1).

DESIGN-STRESS RATIOS

Design-stress ratios, Q, define the ratios of total actual stresses to total design stresses at any point in a bridge. For example, if design calculations for a 50-ft steel beam bridge of H15 design show a maximum dead-load stress of 8.28 ksi and a maximum live-load plus impact stress of 9.72 ksi in one of the interior stringers, the total design stress would be 8.28 + 9.72 = 18.00 ksi. If a given heavy truck would produce a maximum live-load plus impact stress of 14.56 ksi, the total actual stress in this stringer would be 8.28 + 14.56 = 22.84 ksi. In this case, the design-stress ratio would be Q = 22.84/18.00 = 1.27. The truck under consideration would produce a total stress of 1.27 times the basic design stress of 18.00 ksi, or an overstress of 27 percent. Design-stress ratios resulting from various H-equivalences on 30-, 50-, and 100-ft spans for one truck in one lane only and one truck in each lane simultaneously with varying allowances for impact are shown in Figures 7-9.

Thus, with any given volume of traffic containing a known percentage of heavy trucks (13 tons or more), whose H-equivalencies had been determined (or estimated) such as those given by Table 1, it would be a simple matter to determine the numbers of stress repetitions of various levels that would result from such traffic — taking the vehicles one at a time and assuming that each one would be so positioned laterally to produce maximum live-load stress. For a traffic volume of 500 vph for 50 years with 5 percent heavy trucks and H-equivalencies as given by Table 1, there would be a total of 11 million heavy trucks equally divided between the two directions. The numbers of design-stress ratio that would result, taking the trucks one at a time, with and without impact on a 50-ft and a 100-ft span, would be as given by Tables 2 and 3, respectively.

TABLE 1

RELATIVE FREQUENCIES OF EQUIVALENT H TRUCK LOADINGS[a] FOR 16,888 HEAVY TRUCKS OF THE SIX MAJOR TYPES (9)

Equivalent H Truck Loadings	Span (ft)								
	10	20	30	40	50	60	80	100	Infinite G. V. W.
5	0.04	—	—	—	—	—	—	—	—
6	0.21	—	—	—	—	—	—	—	—
7	0.75	0.12	0.01	—	—	—	—	—	—
8	2.01	0.15	0.15	0.07	0.01	—	—	—	—
9	2.87	1.55	0.49	0.26	0.16	0.05	—	—	—
10	7.16	4.14	3.32	1.87	0.67	0.14	0.01	0.01	0.01
11	15.02	9.74	5.51	5.19	2.75	1.40	0.82	0.76	0.75
12	27.30	10.92	11.43	8.36	4.90	3.85	2.04	1.74	1.53
13	26.83	11.55	10.51	8.94	7.14	4.24	2.58	1.90	1.19
14	11.03	10.57	9.27	7.40	6.90	6.07	3.22	2.05	1.12
15	3.61	12.59	10.56	9.56	7.59	5.94	4.99	3.36	0.77
16	1.84	19.87	10.51	10.18	8.59	7.52	5.42	4.29	0.60
17	0.69	9.28	18.41	15.81	11.17	6.89	5.90	5.91	1.15
18	0.31	5.90	11.95	14.19	12.99	9.53	6.96	6.09	2.90
19	0.12	2.08	3.60	9.06	14.08	11.23	6.85	7.10	4.00
20	0.06	0.69	2.19	5.03	11.85	11.62	7.08	5.91	5.48
21	0.09	0.52	1.01	1.73	4.97	17.31	10.04	7.40	5.55
22	0.02	0.15	0.55	1.04	3.39	6.45	11.20	8.98	4.51
23	0.02	0.07	0.25	0.63	1.13	3.41	14.16	13.21	4.52
24	0.01	0.02	0.09	0.31	0.72	2.14	8.69	12.01	4.58
25	0.01	0.01	0.04	0.15	0.52	0.92	4.45	9.54	6.18
26	—	0.02	0.04	0.05	0.20	0.60	2.59	3.15	8.72
27	—	0.02	0.03	0.05	0.08	0.30	1.48	2.80	9.77
28	—	0.01	0.01	0.02	0.05	0.16	0.69	1.65	8.71
29	—	—	0.04	0.02	0.03	0.06	0.38	0.92	5.65
30	—	0.01	—	0.02	0.01	0.04	0.20	0.57	4.08
31	—	0.01	—	0.02	0.03	0.02	0.08	0.27	3.10
32	—	0.01	—	0.01	0.02	0.04	0.05	0.18	2.59
33	—	—	0.01	—	0.01	0.01	0.02	0.05	2.91
34	—	—	0.01	—	—	0.01	0.01	0.05	2.79
35	—	—	0.01	0.01	—	0.01	0.04	0.01	2.61
36	—	—	—	0.01	0.02	0.01	0.01	0.03	2.00
37	—	—	—	0.01	0.01	0.01	0.01	0.02	1.05
38	—	—	—	—	—	—	0.01	0.02	0.59
39	—	—	—	—	0.01	0.01	—	—	0.29
40	—	—	—	—	—	0.01	—	—	0.13
41	—	—	—	—	—	—	0.01	0.01	0.07
42	—	—	—	—	—	—	0.01	—	0.02
43	—	—	—	—	—	—	—	—	0.02
44	—	—	—	—	—	—	—	0.01	0.03
45	—	—	—	—	—	—	—	—	0.01
50	—	—	—	—	—	—	—	—	0.01
51	—	—	—	—	—	—	—	—	0.01
Total	100.00	100.00	100.00	100.00	100.00	100.00	100.00	100.00	100.00
Max. H Truck	25	32	35	37	39	40	42	44	51
Avg. H Truck	12.24	14.37	15.16	15.93	17.15	18.41	20.25	21.17	25.60
Min. H Truck	5	7	7	8	8	9	10	10	10
Poisson's Coeff., Z	7.2	7.4	8.2	7.9	9.2	9.4	10.3	11.2	15.6

[a]Equivalent H truck loadings based on moments produced by gross vehicle weights on simple spans.

TABLE 2

NUMBER OF STRESS REPETITIONS[a] IN MOST HIGHLY STRESSED STRINGER IN EACH DIRECTION OF A 50-FT SIMPLE-SPAN BRIDGE OF H15-44 DESIGN[b]

Equivalent H Truck Loading	Poisson Distribution for Z = 9.2	Number of Vehicles	Design-Stress Ratio[c]	
			Full Allowance for Impact[d]	No Allowance for Impact[e]
8	0.000101	556	0.676	0.628
9	0.000930	5,115	0.703	0.649
10	0.004276	23,518	0.730	0.670
11	0.013113	72,122	0.757	0.691
12	0.030160	165,880	0.784	0.712
13	0.055494	305,217	0.811	0.733
14	0.085091	468,001	0.838	0.754
15	0.111834	615,087	0.865	0.775
16	0.128609	707,349	0.892	0.796
17	0.131467	723,069	0.919	0.817
18	0.120950	665,225	0.946	0.838
19	0.100158	556,369	0.973	0.859
20	0.077555	426,553	1.000	0.880
21	0.054885	301,868	1.027	0.901
22	0.036067	198,369	1.054	0.922
23	0.022121	121,666	1.081	0.943
24	0.012720	69,960	1.108	0.964
25	0.006884	37,862	1.135	0.985
26	0.003518	19,349	1.162	1.006
27	0.001704	9,372	1.189	1.027
28	0.000784	4,312	1.216	1.048
29	0.000343	1,887	1.243	1.069
30	0.000144	792	1.270	1.090
31	0.000057	314	1.297	1.111
32	0.000022	121	1.324	1.132
33	0.000008	44	1.351	1.153
34	0.000003	17	1.378	1.174
35	0.000001	6	1.405	1.195
Total	1.000000	5,500,000		

[a] Stress effects based on continuous traffic volume of 500 vph (12,000 per day) containing 5% heavy vehicles (in excess of 13 tons gross weight).
[b] Assumed useful life of 50 years; a total of 11 million heavy vehicles occur on this span one at a time, divided equally between the two directions.
[c] See Figure 8 for design-stress ratio equations.
[d] $Q = 0.0270\ H + 0.460$.
[e] $Q = 0.0210\ H + 0.460$.

TABLE 3

NUMBER OF STRESS REPETITIONS[a] IN MOST HIGHLY STRESSED STRINGER IN EACH DIRECTION OF A 100-FT SIMPLE-SPAN BRIDGE OF H15-44 DESIGN[b]

Equivalent H Truck Loading	Poisson Distribution for Z = 11.2	Number of Vehicles	Design Stress Ratio[c]	
			Full Allowance for Impact[d]	No Allowance for Impact[e]
10	0.000013	71	0.755	0.728
11	0.000153	842	0.770	0.740
12	0.000858	4,719	0.785	0.752
13	0.003202	17,611	0.800	0.765
14	0.008965	49,308	0.815	0.777
15	0.020082	110,452	0.830	0.789
16	0.037487	206,178	0.844	0.801
17	0.059979	329,884	0.859	0.813
18	0.083970	461,835	0.874	0.826
19	0.104496	574,728	0.889	0.838
20	0.117035	643,692	0.904	0.850
21	0.119163	655,396	0.919	0.862
22	0.111220	611,710	0.934	0.874
23	0.095820	527,010	0.949	0.887
24	0.076656	421,608	0.964	0.899
25	0.057236	314,798	0.979	0.911
26	0.040065	223,058	0.993	0.923
27	0.026396	145,178	1.008	0.935
28	0.016424	90,332	1.023	0.948
29	0.009682	53,251	1.038	0.960
30	0.005422	29,821	1.053	0.972
31	0.002892	15,906	1.068	0.984
32	0.001472	8,096	1.083	0.996
33	0.000717	3,944	1.098	1.009
34	0.000335	1,842	1.113	1.021
35	0.000150	825	1.128	1.033
36	0.000065	358	1.142	1.045
37	0.000027	148	1.157	1.057
38	0.000011	60	1.172	1.070
39	0.000004	22	1.187	1.082
40	0.000002	11	1.202	1.094
41	0.000001	6	1.217	1.106
Total	1.000000	5,500,000		

[a] Stress effects based on continuous traffic volume of 500 vph (12,000 per day) containing 5% heavy vehicles (in excess of 13 tons gross weight)

[b] Assumed life of 50 years; a total of 11 million heavy vehicles occur on this span one at a time, divided equally between the two directions.

[c] See Figure 9 for design-stress ratio equations.

[d] $Q = 0.0149\ H + 0.606$.

[e] $Q = 0.0122\ H + 0.606$.

FREQUENCIES OF SPECIFIED VEHICLE GROUPS

In a previous report (5) it was shown that Poisson's frequency distributions (12) could be used to determine how often two or more specified vehicles, such as two or more heavy trucks, could be expected to occur within a given length of bridge or a specified distance near the midspan of a bridge. The results of this study are summarized for 250 and 500 vph containing 5 percent heavy trucks in Figures 1 and 2, respectively.

It has also been found that Poisson's Law provided a good estimate for the frequency distribution of gross vehicle weights and H-equivalencies on various spans (Table 1). Here the Poisson equation is

$$P(n) = Z^n e^{-Z}/n! \qquad (1)$$

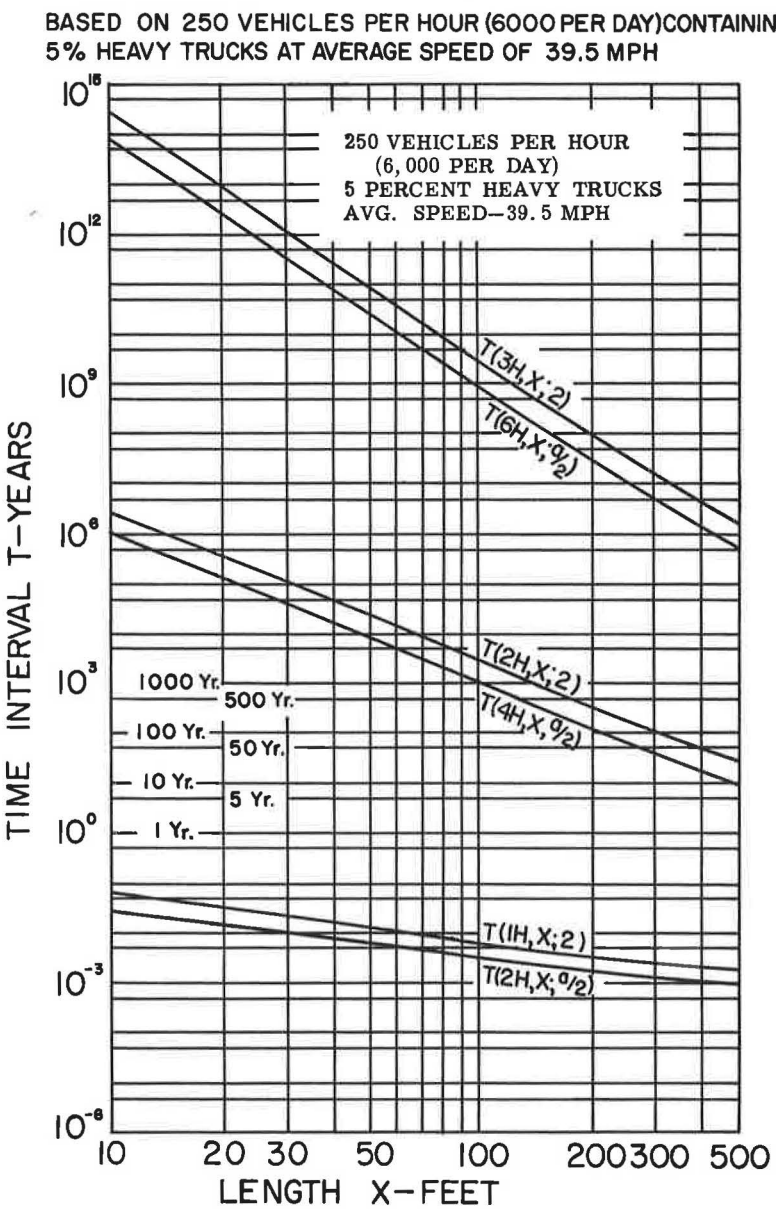

Figure 1. Time interval for typical specified vehicle groups occurring within specified lengths.

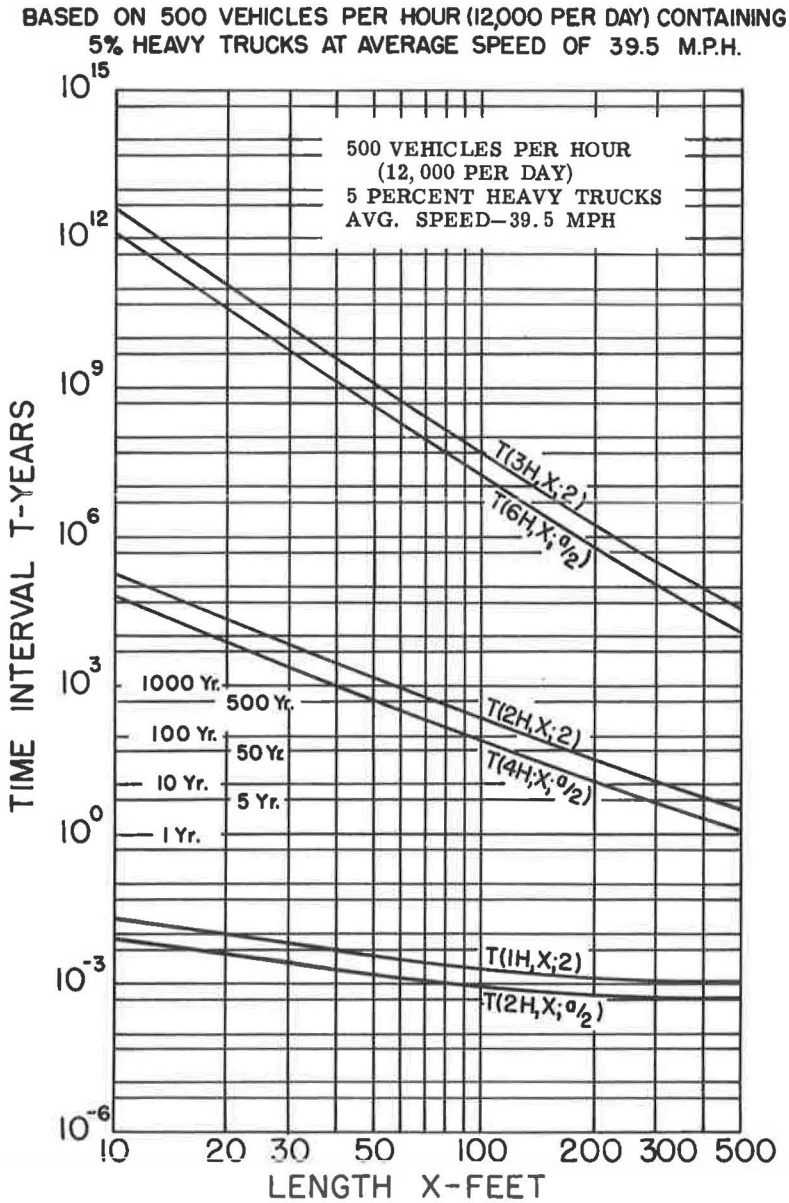

Figure 2. Time interval for typical specified vehicle groups occurring within specified lengths.

Each vehicle constitutes a sample whose H-equivalency is measured in tons. On a 60-ft span, for example, if the H-equivalency fell between 18.60 and 19.49 tons, it would be classified as an equivalent H19-ton truck loading. Table 1 gives the observed frequencies of equivalent H truck loadings, on various spans, for 16,888 heavy trucks reported by the 1954 truck weight survey. For the 50-ft span, the minimum H-equivalency is 8 tons and the average is 17.15 (or 17.2), and the Poisson coefficient is 9.2. This means that the average is 9.2 tons removed from the minimum, or the expected average is 9.2 cells removed from the zero cell. Eq. 1, therefore, would be read: the probability that the H-equivalency of a given vehicle will be n-cells (or in this case n-tons) larger than the smallest or zero cell, when the average is Z cells greater than the zero cell, is equal to $Z^n e^{-Z}/n!$

TABLE 4

NUMBER OF STRESS REPETITIONS[a] IN MOST HIGHLY STRESSED STRINGER IN EACH DIRECTION OF A 50-FT SIMPLE-SPAN BRIDGE OF H15-44 DESIGN[b]

Equivalent H Truck Loadings	Poisson Distribution for Z = 18.0	Number of Occurrences	Design-Stress Ratio[c]	
			Full Allowance for Impact[d]	No Allowance for Impact
8	0.000	—	—	—
9	0.000	—	—	—
10	0.001	2	0.820	0.740
11	0.003	6	0.856	0.768
12	0.012	24	0.892	0.796
13	0.039	78	0.928	0.824
14	0.088	176	0.964	0.852
15	0.144	288	1.000	0.880
16	0.182	364	1.036	0.908
17	0.183	366	1.072	0.936
18	0.148	296	1.108	0.964
19	0.099	198	1.144	0.992
20	0.056	112	1.180	1.020
21	0.027	54	1.216	1.048
22	0.011	22	1.252	1.076
23	0.004	8	1.288	1.104
24	0.002	4	1.324	1.132
25	0.001	2	1.360	1.160
Total	1.000	2,000		

[a] Stress effects based on continuous traffic volume of 500 vph (12,000 per day) containing 5% heavy vehicles (in excess of 13 tons gross weight).
[b] Assumed life of 50 years, resulting from 2,000 occurrences in each direction of one heavy truck in each of two adjacent lanes simultaneously.
[c] See Figure 8 for design-stress ratio equations.
[d] Q = 0.0360 H + 0.460.
[e] Q = 0.0280 H + 0.460.

TABLE 5

NUMBER OF STRESS REPETITIONS[a] IN MOST HIGHLY STRESSED STRINGER IN EACH DIRECTION OF A 100-FT SIMPLE-SPAN BRIDGE OF H15-44 DESIGN

Equivalent H Truck Loadings	Poisson Distribution for Z = 22.0	Number of Occurrences	Design-Stress Ratio[c]	
			Full Allowance for Impact[d]	No Allowance for Impact[e]
14	0.001	3	0.883	0.833
15	0.006	18	0.903	0.849
16	0.019	57	0.923	0.855
17	0.049	147	0.943	0.881
18	0.092	276	0.962	0.898
19	0.134	402	0.982	0.914
20	0.166	498	1.002	0.930
21	0.167	501	1.022	0.946
22	0.141	423	1.042	0.962
23	0.100	300	1.061	0.979
24	0.062	186	1.081	0.995
25	0.034	102	1.101	1.011
26	0.016	48	1.121	1.027
27	0.007	21	1.141	1.043
28	0.003	9	1.160	1.060
29	0.002	6	1.180	1.076
30	0.001	3	1.200	1.092
Total	1.000	3,000		

[a] Stress effects based on continuous traffic volume of 500 vph (12,000 per day) containing 5% heavy vehicles (in excess of 13 tons gross weight).
[b] Assumed life of 50 years, resulting from 3,000 occurrences in each direction of one heavy truck in each of two adjacent lanes simultaneously.
[c] See Figure 9 for design-stress ratio equations.
[d] Q = 0.0198 H + 0.606.
[e] Q = 0.0162 H + 0.606.

The distribution in Table 2 for the 50-ft span where Z = 9.2 was taken from Molina's tables for the Poisson equation (12). For example, in such a population of vehicles, about 101 out of each million would be expected to fall in the 8-ton H-equivalency cell. The other frequencies would be interpreted similarly. Tables 1 and 2 give the numbers of repetitions of various levels of stress with and without impact that would result from 11 million heavy trucks in 50 years taken (one at a time) on 50- and 100-ft spans, respectively.

Table 2 gives 8 tons for the smallest H-equivalency on a 50-ft span. If these vehicles are taken two at a time, one in each direction simultaneously, the smallest total H-equivalency would be 2 × 8 = 16 tons. Likewise, the average for all pairs would be twice the average or 2 × 17.2 = 34.4. In this case, the value of Poisson's coefficient Z = 34.4 - 16.0 = 18.4. The distribution in Table 4, however, is based on Z = 18.0 beause this is the nearest value given in Molina's tables (12). Table 5 gives the distribution for Z = 22.0 for the 100-ft span and is interpreted similarly.

LATERAL PLACEMENT OF VEHICLES IN TRAFFIC

If each of the trucks referred to in Tables 2 and 3 were to pass over the 50- and 100-ft spans and were so positioned laterally to produce maximum stress in an interior stringer, the numbers of repetitions of various levels of stress would be as given in these tables.

If, however, these vehicles are assumed to be positioned laterally according to some logical pattern, then the numbers of repetitions of various intensities of stress would be altered accordingly.

ESTIMATED NUMBERS OF VARIOUS INTENSITIES OF STRESS IN SIMPLE-SPAN BEAM BRIDGES

Table 2 indicates that for the truck population given by the 1954 truck weight survey (Table 1), about one truck in each million heavy trucks would be expected to produce a design-stress ratio of Q = 1.405 with impact or Q = 1.195 without impact. In other words, on a 50-ft steel stringer bridge of H15-44 design, about one truck in a million would produce an overstress of 40.5 percent with impact and 19.5 percent overstress without impact.

Table 4 gives the numbers of repeated stresses in 50 years resulting from one heavy truck in each lane simultaneously on this 50-ft span. The numbers of repeated stresses resulting from a truck in each lane are quite small; the largest overstress given is 36.0 percent with impact and 16.0 percent without impact. The heavier individual trucks will produce higher overstresses than those that would ordinarily occur on the span at the same time.

The combined numbers of repeated stresses indicated by Tables 2 and 4 for the 50-ft span (no lateral placement) are shown in Figures 3 a and b. In these figures the numbers of repeated stresses given by Table 4 (one in each direction simultaneously) do not change the appearance of these histograms.

For this same 50-ft span, if it is assumed that the lateral placement of trucks is such that $\frac{1}{3}$ of them produce maximum live-load stress, $\frac{1}{3}$ produce 90 percent, and the remaining $\frac{1}{3}$ produce 80 percent, the resulting numbers of repetitions would be as shown in Figure 3 c and 3 d.

In a similar manner, the histograms in Figure 4 for the 100-ft span show the numbers of repeated stresses without and with lateral placement of the trucks and without and with impact.

For the 50-ft span of H15-44 design, Figure 3 shows that very heavy traffic with a high percent of heavy trucks would rarely result in overstresses in excess of about 25 percent. For the 100-ft span of H15-44 design, Figure 4 shows that similar heavy traffic would rarely result in overstresses of about 20 percent.

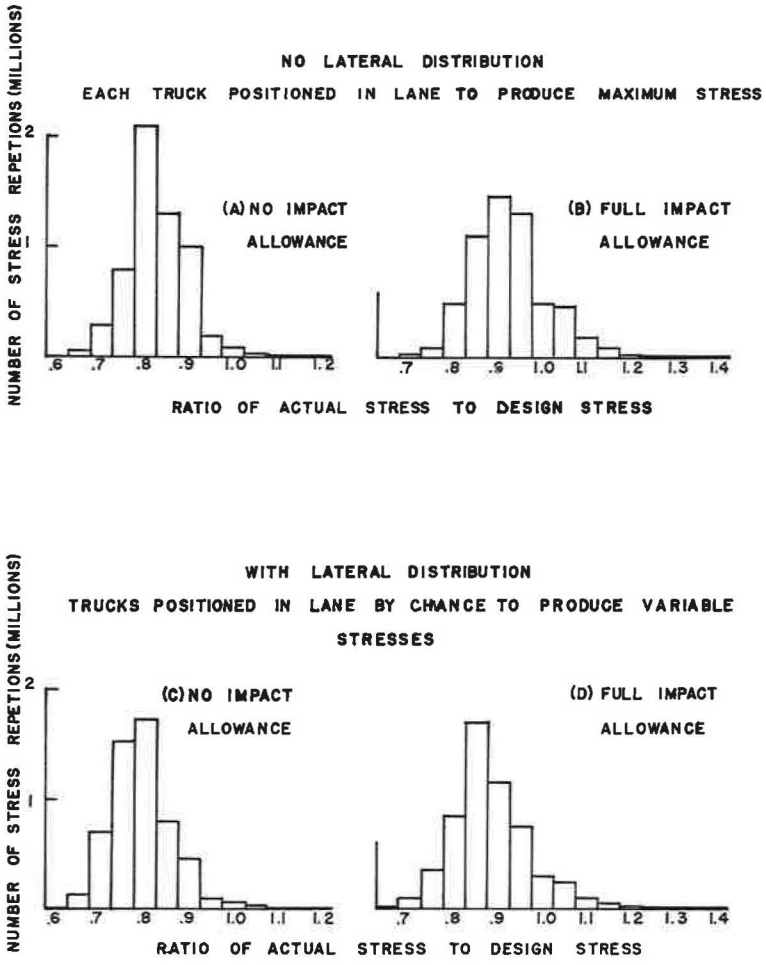

Figure 3. Number of repeated stresses produced in a 50-ft simple-span bridge of H15-44 design during an assumed useful life of 50 years (design-stress ratios based on continuous traffic volume of 500 vph containing five percent heavy trucks weighing 13 tons or more).

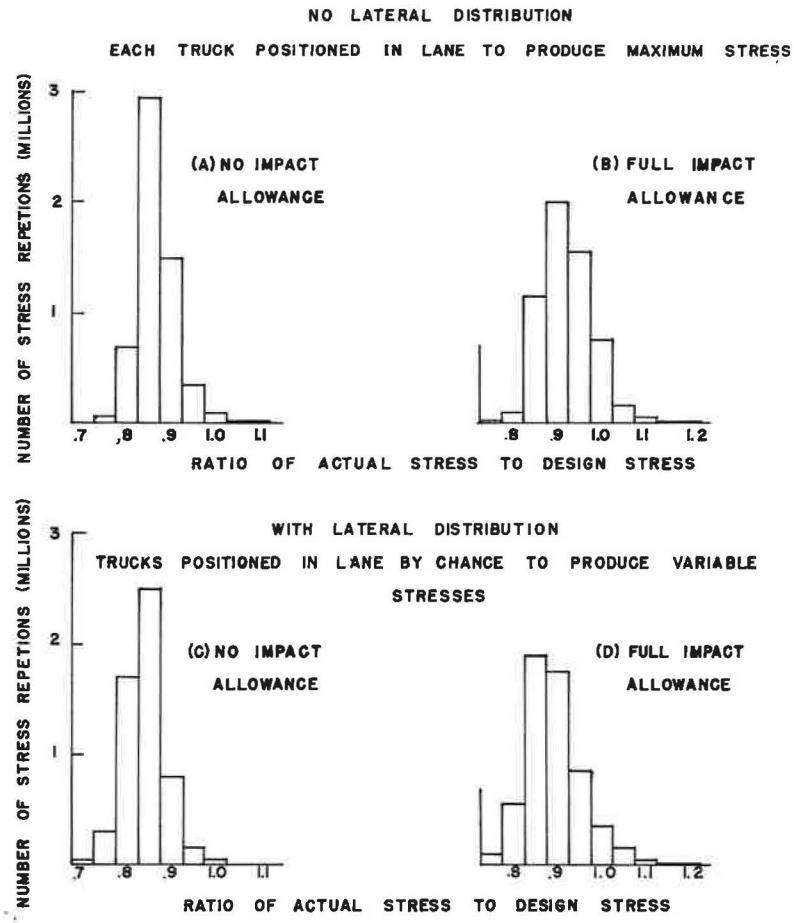

Figure 4. Number of repeated stresses produced in a 100-ft simple-span bridge of H15-44 design during an assumed useful life of 50 years (design-stress ratios based on continuous traffic volume of 500 vph containing five percent heavy trucks weighing 13 tons or more).

Appendix A

MAXIMUM BENDING STRESSES IN SIMPLE-SPAN BEAM BRIDGES

Appendix A presents a brief review of a method for estimating maximum combined bending stresses in simple-span beam bridges produced by dead load, live load, and impact. The maximum live-load and impact stresses are those resulting from any heavy vehicle type or loading found on the highway.

The procedure for estimating the total maximum stress in simple-span bridges of given construction type and design designation is accomplished in two simple steps: (a) convert any particular vehicle under consideration into its equivalent H truck loading on any span by use of the conversion coefficients given in Table 6; and (b) determine the stress-producing effects from charts similar to those in Figures 7 to 9 inclusive depending on the span and loading conditions (1, 3, 4, 6, 7).

The method for estimating the maximum combined bending stresses produced by dead load, vehicle loads and impact in simple-span beam bridges results from three simple observations.

1. It has been shown that any heavy vehicle may be converted into an equivalent H truck loading that will produce the same maximum bending moment on a given span as the particular vehicle under consideration (1, 3, 4, 6). Equivalent H truck loadings, therefore, provide a convenient means for describing or evaluating the stress-producing effects of any particular vehicle on a given span. Heavy vehicles may also be converted into any other equivalent design loading on the basis of moments, shears or any other stress function desired (1, 2).

2. It has been found, for any simple-span beam bridge of given length, that the percent of total design moment per beam caused by dead load remains about the same, irrespective of the lateral spacing of the beams (3, 6). Similarly for a given span, the percent of total design moment per beam caused by live load plus impact also remains

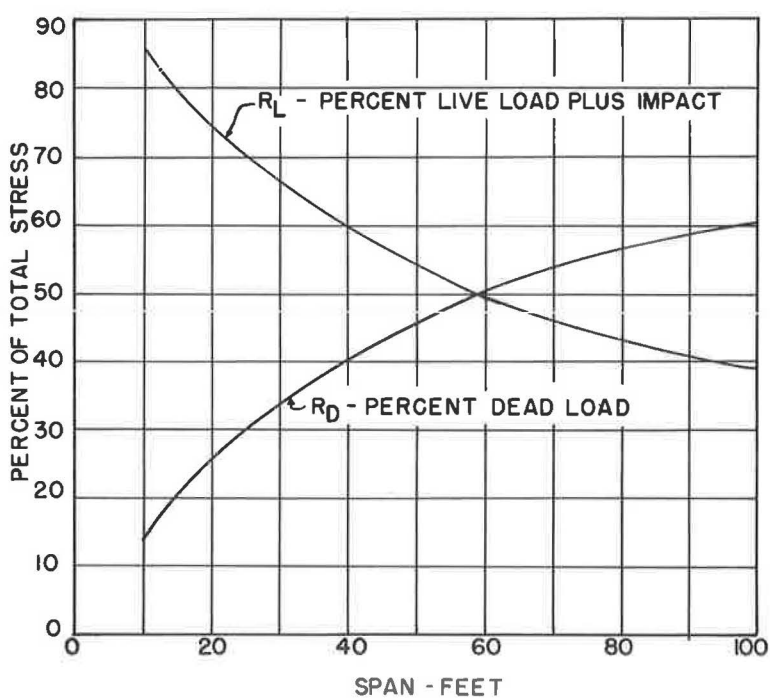

Figure 5. Estimated percent of total design stresses represented by live-load plus impact and dead-load stresses for simple-span beam bridges of H15 design.

about the same, irrespective of the beam spacing (3, 6). For a given span, therefore, it follows that the percent of total design moment caused by live and dead loads, respectively, is about the same per foot width of bridge or per 10-ft lane as it is per beam, irrespective of the beam spacing. These findings permit the live- and dead-load design moments per beam or per 10-ft lane to be generalized for simple-span beam bridges of given construction type and design designation (Fig. 5).

3. For a given bridge, the maximum dead-load stress is a fixed and definite percent of the total design stress. Also, the maximum live-load plus impact stress caused by a given vehicle will vary directly with the weight or H-equivalency of that particular vehicle. From these and preceding observations it has been shown that the total maximum stress caused by dead load, vehicle load, and impact in a given bridge may be expressed by a simple straight-line equation in which the total maximum stress is a function of the H-equivalency of the vehicle under consideration (3, 6). It is usually more convenient, though, to convert this total maximum stress into the ratio that it bears to the allowable stress for which the bridge was designed. This ratio is referred to herein as the design-stress ratio (Figs. 7 to 9).

Method for Estimating Maximum Bending Stresses

The bridges are of H15 design and consist of a non-composite deck of minimum thickness supported by unencased steel beams. It is also assumed that the supporting steel beams are so spaced that the maximum live-load bending stress produced in an interior stringer by a single vehicle in one lane only will amount to C = 75 percent of that produced by identical vehicles in each lane simultaneously. This means that if the given bridge were loaded with vehicles having identical H-equivalencies, one in each lane, the maximum live-load stress produced in a typical interior stringer would be 133 percent of that produced by only one of these vehicles in one lane only.

The reason for selecting this light type of construction is that the ratio of dead-load stresses to total design stresses is smaller than would be the case for any of the heavier types of construction, such as reinforced concrete deck girder spans. Consequently, any conclusions concerning the stress-producing effect of a given vehicle or vehicles on any particular bridge are on the conservative side. Although the discussion and examples are confined to bending moments and bending stresses in simple-span steel beam bridges of H15 design, the method is equally applicable to bridges of other construction types and design designation.

Once the percent of total design stresses caused by live load plus impact and dead load have been determined for bridges of a given type and design designation similar to those shown in Figure 5, it is convenient to consider the method for estimating total maximum bending stress in a given bridge in two parts.

1. Determination of equivalent H truck loadings.
2. Evaluation of total maximum stress caused by a given equivalent H truck loading on a given span corresponding with specified loading conditions.

Equivalent H Truck Loadings

Any heavy vehicle may be converted into an equivalent H truck loading that will produce the same maximum bending moment on a given span as the particular vehicle under consideration. Heavy vehicles also may be converted into any other equivalent design loading on the basis of moments, shears or other stress functions on various span lengths as may be desired (1, 2, 10).

The H-equivalency of a given vehicle on a given span may be determined on an exact basis by finding the maximum moment caused by this particular vehicle on the given span and selecting the standard H truck designation in tons that would produce the same maximum moment. The procedure for any other stress function would be similar.

However, it has been found from numerous investigations of actual vehicles irrespective of the number of spacing of axles, that any normal distribution of load among the axles of a given vehicle will produce slightly less moment on a given span than the same load would produce if it were uniformly distributed over a length L equal to the

wheel base length of the vehicle under consideration (4, 6). This means that the maximum moment caused by any given vehicle on a given span can be estimated quite easily and accurately, but a little on the safe side, by the moment formula resulting from the uniform load of length L and weight W on a span S (Fig. 6). This loading results in the following formula:

$$M = \frac{W}{4} (S - \frac{L}{2}) \quad (2)$$

Eq. 2 provided the basis for calculating the coefficients given in Table 6 for converting heavy vehicles of given weight and wheel base length into equivalent H truck loadings on various span lengths.

The determination and use of the coefficients given in Table 6 can be illustrated by comparing the maximum moment caused by a heavy vehicle weighing 20 tons and having a total wheel base length of 28 ft with that caused by an H 20 truck on a 50-ft simple span. According to Eq. 2, the moment caused by the heavy vehicle would be 360.0 kip-ft. This compares with a moment of 445.6 kip-ft caused by an H 20 truck on a 50-ft span. Therefore, the 20-ton heavy vehicle with 28-ft wheel base causes 80.79 percent as much moment as the H 20 truck on this 50-ft span.

This means that a vehicle, with a 28-ft wheel base, will cause 0.8079 times as much moment on a 50-ft span as a standard H truck of equal weight. It also means that a vehicle of given weight with a 28-ft wheel base will cause as much moment on a 50-ft span as a standard H truck weighing 80.79 percent as much. Therefore, this 20-ton vehicle, with a 28-ft wheel base on a 50-ft span would have an H-equivalency of $20.0 \times 0.8079 = 16.16$ tons or correspond with an equivalent H 16.16 truck on that span.

Design-Stress Relationships

As stated previously, for any simple-span beam bridge of given length, the percent of total design stress (or moment) per beam caused by dead load remains about the same, irrespective of the lateral spacing of the beams (3, 6). Similarly, for a given span the percent of total design stress per beam caused by live load plus impact also remains about the same, irrespective of the beam spacing. Therefore, for a given span it follows that the percent of total design stress caused by live and dead loads, respectively, is about the same per foot width of bridge or per 10-ft lane as it is per beam, irrespective of beam spacing. These findings permit the live- and dead-load design stresses per beam or per 10-ft lane to be generalized for simple-span bridges, or given construction type and design designation similar to those in Figure 5.

With design-stress information for simple-span bridges of given construction type and design designation, similar to that in Figure 5, it has been shown that the total maximum stresses caused by dead load, vehicle load and impact for a given bridge may be expressed by a simple straight-line equation in which the total maximum stress or design-stress ratio is a function of the H-equivalency of the vehicle under consideration (3, 6). Design-stress ratio for a given member is defined as the ratio of actual total maximum stress caused by dead load, vehicle load and impact in the member, to the total stress used for the design of that member.

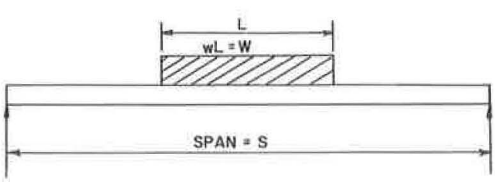

Figure 6. Maximum moment caused by a gross weight of W uniformly distributed over a length L on a span length of S.

The straight-line equation (3, 6) for determining the total maximum bending stress or design-stress ratio produced by trucks of given H-equivalency on a given span for various loading conditions is

$$Q = R_D + R_L \left[\frac{HCK'M_{H(1)}}{KM_L} \right] \quad (3)$$

The dead- and live-load ratios, R_D and

TABLE 6

COEFFICIENTS FOR CONVERTING HEAVY VEHICLE OF GIVEN WEIGHT AND WHEEL BASE LENGTH INTO EQUIVALENT H TRUCK LOADINGS ON SIMPLE SPANS

Wheel Base (ft)	Span (ft)								
	20	30	40	50	60	70	80	90	100
4	1.1250	1.1354	1.0984	1.0636	1.0541	1.0541	1.0470	1.0416	1.0373
6	1.0625	1.0948	1.0695	1.0548	1.0453	1.0386	1.0336	1.0297	1.0277
8	1.0000	1.0543	1.0406	1.0324	1.0269	1.0231	1.0202	1.0179	1.0161
10	0.9375	1.0137	1.0117	1.0099	1.0086	1.0076	1.0067	1.0061	1.0055
12	0.8750	0.9732	0.9828	0.9875	0.9903	0.9921	0.9933	0.9942	0.9949
14	0.8125	0.9326	0.9539	0.9651	0.9719	0.9766	0.9799	0.9824	0.9844
16	0.7500	0.8921	0.9250	0.9426	0.9536	0.9611	0.9665	0.9706	0.9738
18	0.6875	0.8515	0.8960	0.9202	0.9352	0.9456	0.9530	0.9587	0.9632
20	0.6250	0.8110	0.8671	0.8977	0.9169	0.9301	0.9396	0.9469	0.9526
22	—	0.7704	0.8332	0.8753	0.8986	0.9146	0.9262	0.9351	0.9420
24	—	0.7299	0.8093	0.8528	0.8802	0.8991	0.9128	0.9232	0.9314
26	—	0.6893	0.7804	0.8304	0.8619	0.8836	0.8993	0.9114	0.9208
28	—	0.6488	0.7515	0.8079	0.8436	0.8681	0.8859	0.8995	0.9103
30	—	0.8082	0.7226	0.7855	0.8252	0.8526	0.8725	0.8877	0.8997
32	—	—	0.6937	0.7631	0.8069	0.8371	0.8591	0.8759	0.8891
34	—	—	0.6648	0.7406	0.7885	0.8216	0.8456	0.8640	0.8785
36	—	—	0.6359	0.7182	0.7702	0.8061	0.8322	0.8522	0.8679
38	—	—	0.6070	0.6957	0.7519	0.7906	0.8188	0.8404	0.8573
40	—	—	0.5781	0.6733	0.7335	0.7751	0.8054	0.8285	0.8468
42	—	—	—	0.6508	0.7152	0.7596	0.7919	0.8167	0.8362
44	—	—	—	0.6284	0.6969	0.7441	0.7785	0.8049	0.8526
46	—	—	—	0.6059	0.6785	0.7286	0.7651	0.7930	0.8150
48	—	—	—	0.5835	0.6602	0.7131	0.7517	0.7812	0.8044
50	—	—	—	0.5611	0.6418	0.6976	0.7383	0.7694	0.7938
52	—	—	—	—	0.6235	0.6821	0.7248	0.7575	0.7833
54	—	—	—	—	0.6052	0.6666	0.7114	0.7457	0.7727
56	—	—	—	—	0.5868	0.6511	0.6980	0.7338	0.7621
58	—	—	—	—	0.5685	0.6356	0.6846	0.7220	0.7515
60	—	—	—	—	0.5503	0.6201	0.6711	0.7102	0.7409

NOTE: The H-equivalency of any vehicle of given weight and wheel base length on a given span, is equal to the weight of the vehicle times the conversion coefficient for that span corresponding to the given vehicle's wheel base length. For example, a 20-ton vehicle with a 28-ft wheel base on a 50-ft span would have an H-equivalency of 20.0 x 0.8079 = 16.16 tons or correspond with an equivalent H 16.16 truck loading.

R_L, respectively, are given by charts similar to Figure 5. For any particular span, design-stress ratios for a given situation are equal to the dead-load ratio plus some straight-line function of the live-load ratio. The numerator of the fraction in the bracket represents the actual moment plus impact (if any) produced by the vehicle under consideration, and the denominator represents the live-load plus impact moment used for design. If the actual moment for a given situation is greater than the design moment, then the design-stress ratio Q will be greater than 1.000. Conversely, if it is less, then Q will be less than 1.000.

Incidentally, the equations for Q at the bottom of Figures 7 to 9 are based on substituting values of R_D and RR_L from Figure 5 into Eq. 3.

To find the H-equivalency required for a given situation to produce a specified value of Q,

$$H = \frac{KM_L(Q-R_D)}{CK'M_{H(1)}R_L} \qquad (4)$$

Estimating Maximum Bending Stresses Caused by Equivalent H Trucks

In Eq. 3, the design-stress ratio Q is a linear equation. For any given member of a bridge the change in Q varies directly with the values of H, C, and K' in Eq. 3 (Figs. 7 to 9).

On a 50-ft span, for example, Figure 8 shows that one equivalent H30 truck in each lane simultaneously (C = 1.00) with full allowance for impact would result in a maximum design-stress ratio, Q = 1.50. The maximum stress produced in one of the

C = .75 or 1.00 K' = Varies Span Length = 30'

One vehicle in one lane (C = .75) with varying allowance for impact ——
One vehicle in each lane (C = 1.00) with varying allowance for impact ---

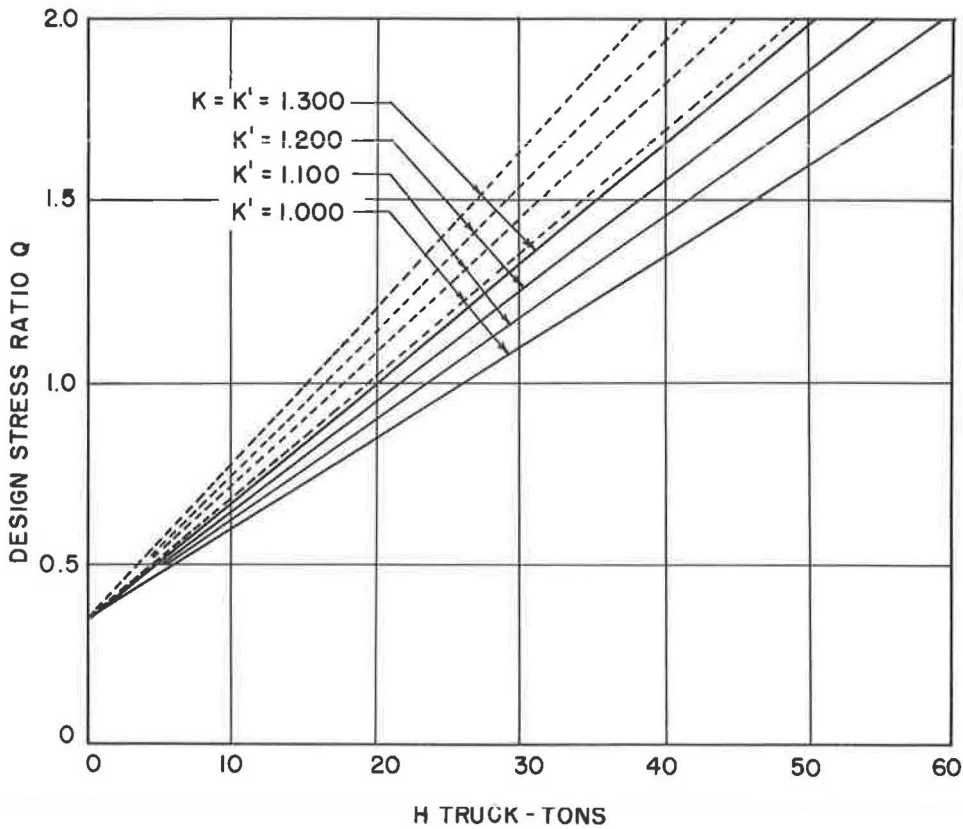

Design Stress Equations for C = 0.75
K = K' = 1.300; Q = .0329H + .340
K' = 1.200; Q = .0305H + .340
K' = 1.100; Q = .0279H + .340
K' = 1.000; Q = .0254H + .340

Design Stress Equations for C = 1.00
K = K' = 1.300; Q = .0439H + .340
K' = 1.200; Q = .0406H + .340
K' = 1.100; Q = .0372H + .340
K' = 1.000; Q = .0338H + .340

NOTE: K = 1.00 + Impact Allowance Required by AASHO Specs.
K' = 1.00 + Impact As Specified (Actual)

Figure 7. Design-stress ratio produced by equivalent H trucks on simple-span bridges of H15 design consisting of non-composite concrete deck supported by steel stringers.

C = .75 or 1.00 K' = Varies Span Length = 50'

One vehicle in one lane (C = .75) with varying allowance for impact ——
One vehicle in each lane (C = 1.00) with varying allowance for impact - -

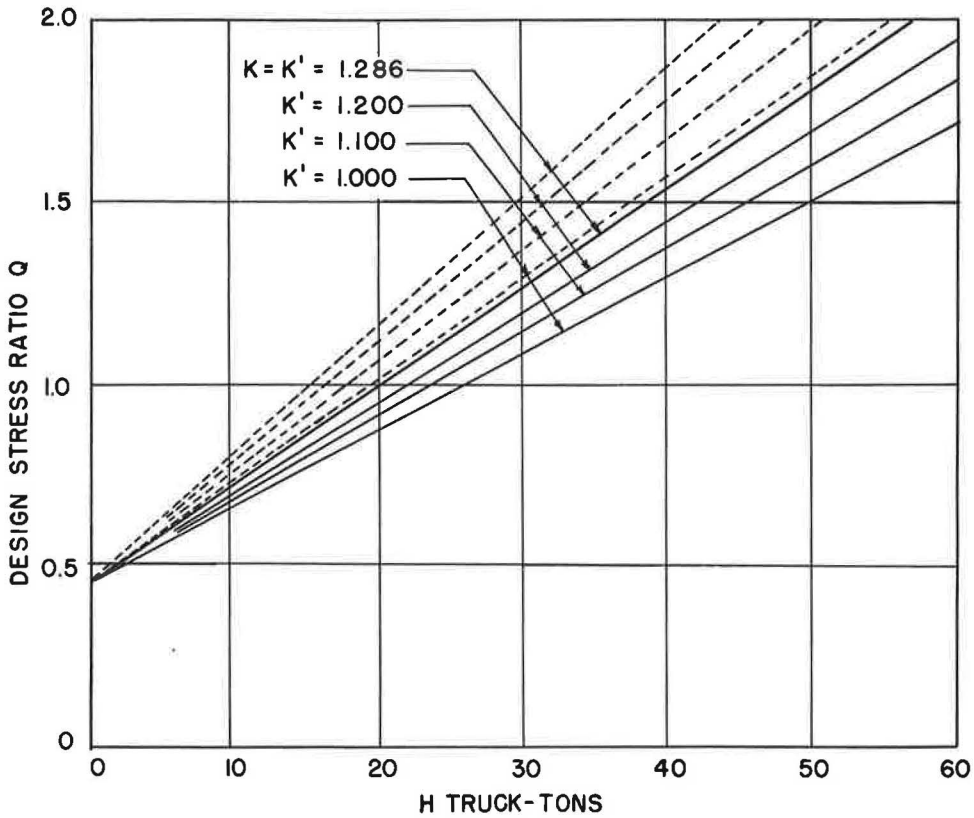

Design Stress Equations for C = 0.75
K = K' = 1.206; Q = .0270H + .460
K' = 1.200; Q = .0252H + .460
K' = 1.100; Q = .0231H + .460
K' = 1.000; Q = .0210H + .460

Design Stress Equations for C = 1.00
K = K' = 1.286; Q = .0360H + .460
K' = 1.200; Q = .0336H + .460
K' = 1.100; Q = .0308H + .460
K' = 1.000; Q = .0280H + .460

NOTE: K = 1.00 + Impact allowance required by AASHO Specs.
K' = 1.00 + Impact as specified (actual)

Figure 8. Design-stress ratio produced by equivalent H trucks on simple-span bridges of H15 design consisting of non-composite concrete deck supported by steel stringers.

C = .75 or 1.00 K' = Varies Span length = 100'

One vehicle in one lane (C = .75) with varying allowance for impact ——
One vehicle in each lane (C = 1.00) with varying allowance for impact ---

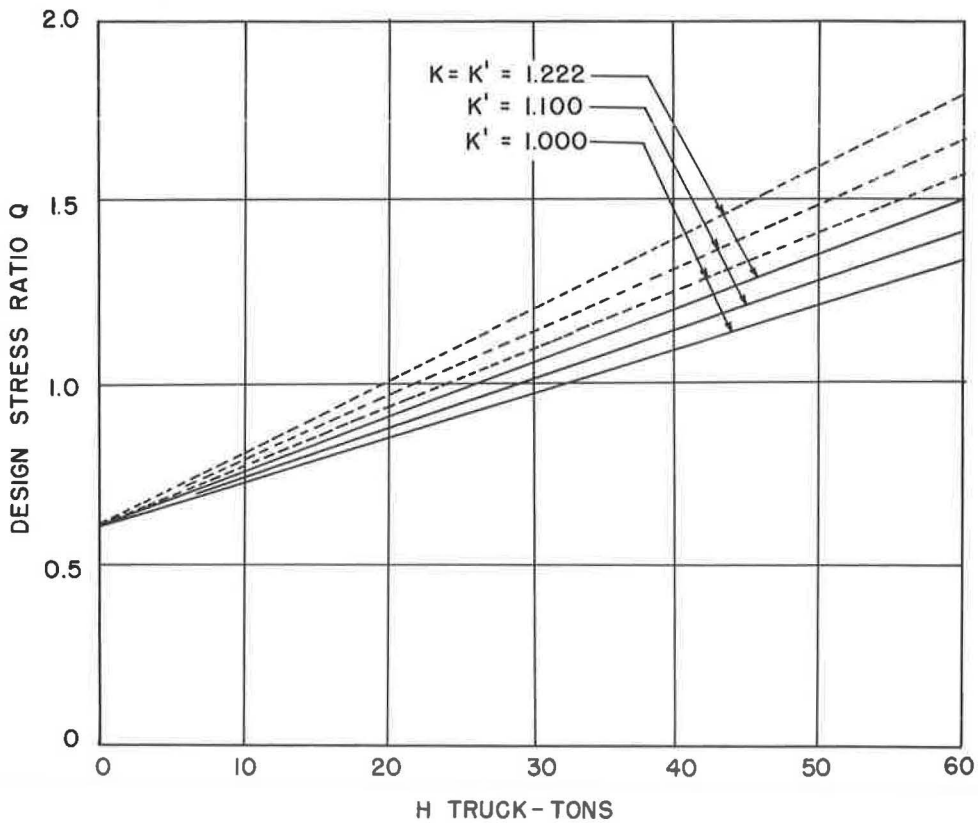

Design Stress Equations for C = 0.75

K = K' = 1.222; Q = .0149H + .606
K' = 1.200; Q = .0146H + .606
K' = 1.100; Q = .0134H + .606
K' = 1.000; Q = .0122H + .606

Design Stress Equation for C = 1.00

K = K' = 1.222; Q = .0198H + .606
K' = 1.200; Q = .0194H + .606
K' = 1.100; Q = .0178H + .606
K' = 1.000; Q = .0162H + .606

NOTE: K = 1.00 + Impact allowance required by AASHO Specs.
K' = 1.00 + Impact as specified (actual).

Figure 9. Design-stress ratio produced by equivalent H trucks on simple-span bridges on H15 design consisting of non-composite concrete deck supported by steel stringers.

interior steel stringers by such a loading would be 150 percent of the basic allowable design stress, or an overstress of 50 percent. However, if the speed of these equivalent H30 trucks were reduced to about 5 mph, which would result in little or no impact, the maximum amount of overstress in an interior stringer would be reduced to about 27 percent.

Similarly, on a 50-ft span, Figure 8 shows that one equivalent H30 truck in one lane only (C = 0.75) with full allowance for impact would result in a maximum design-stress ratio, Q = 1.28, or an overstress of about 28 percent. However, if the speed of this equivalent H30 truck were reduced so as to result in little or no impact, the maximum amount of overstress in an interior stringer would amount to less than 8 percent.

Summary

The preceding discussion shows that the maximum combined bending stresses (design-stress ratios) caused by dead load, live load and impact in simple-span beam bridges may be estimated rather quickly in two simple steps.

1. Convert the heavy vehicle (or axle group load within the vehicle) into its equivalent H truck loading on a given span by use of the appropriate coefficient in Table 6.
2. With the H-equivalency found in the first step, an estimate of the bend stresses caused by it on the given span (steel stringer bridges of H15-44 design) may be read directly from the appropriate chart (Figs. 7 to 9) depending on the span length and loading conditions.

Appendix B

NOTATION

A = average number of vehicles per hour in any one designated direction, or total traffic in both directions, as specified.

C = coefficient representing the fractional part of the total live-load stress in a given member produced by one or more lanes loaded. C = 1.00 if a stringer bridge is loaded with identical vehicles, one in each lane and so placed as to produce maximum stress. For a steel stringer bridge, if one vehicle in one lane only would produce 75 percent as much stress in an interior stringer as identical vehicles in each lane, it would mean that C = 0.75.

D = average speed of traffic in designated direction.

E = number of events or trials between occurrences of vehicle groups as defined.

G = group of vehicles as defined.

H = equivalent H truck in tons. For example, if a given vehicle produces the same maximum moment (or other stress function) in a given member as a standard H truck weighing 23.6 tons, it would be rated as an equivalent H 23.6 truck loading, in which case H = 23.6 tons. H also represents one heavy freight vehicle.

I = impact fraction (maximum 0.30 or 30%) as determined by the AASHO Formula I = 50/(S + 125) in which S = length in feet of the portion of the span which is loaded to produce the maximum stress in the member.

I' = impact fraction assumed in connection with the determination of the stress-producing effects of any given vehicle under consideration. For example, if the speed of a given vehicle were limited to 5 mph, this impact fraction might be considered so small as to be negligible, in which case I' might be assumed equal to zero. Depending on traffic

and conditions, therefore, the impact fraction could be assumed at any reasonable value between zero and the full impact allowance, I, as defined by the AASHO design specifications.

K = $(1.00 + I)$ = coefficient by which the design live-load moment (shear, or other stress function) is multiplied to obtain the live-load plus impact moment (shear, or other stress function) used for design. Thus, $K M_L$ would be equal to the live-load plus impact moment used for design. Similarly, $K V_L$ would be equal to the live-load plus impact shear used for design.

K' = $(1.00 + I')$ = coefficient by which the live-load moment (shear, or other stress function) produced by a given vehicle is multiplied to obtain the live-load plus impact moment (shear, or other stress function) produced on a given span or in a given member by the vehicle under consideration. Thus, $K'M_H$ would be equal to the live-load plus impact moment produced on a given span by any particular vehicle having an H-equivalency of H tons.

M_D = dead-load moment as included in total design moment.

M_L = live-load moment as included in total design moment.

M_T = moment used for design or total design moment.

M_H = moment in an interior stringer (or other member) resulting from equivalent H trucks weighing H tons each. Likewise, M_H represents the moment for one lane produced by equivalent H truck weighing H tons.

$M_{H(1)}$ = moment for lane produced by a standard H truck weighing 1 ton.

P = general term indicating probability that an event will occur as specified.

Q = design-stress ratio — ratio of total actual stress to total design stress in any particular member or part of a given highway bridge.

R_D = (M_D/M_T) = ratio of dead-load moment M_D (shear, or other stress function) to total moment M_T used for design. In terms of shear this ratio would be $R_D = (V_D/V_T)$, and for other stress functions it would be similar.

R_L = $(K M_L/M_T)$ = ratio of live-load plus impact moment, $K M_L$ (shear, or other stress function), used for design to the total design moment, M_T, or total moment (shear, or other stress function) used for design. In terms of shear, this ratio would be $R_L = (K V_L/V_T)$, and for other stress functions it would be similar.

S = span length or that portion of span which is loaded to produce maximum stress in the member under consideration in feet.

T = time interval between occurrences of certain specified events.

V = vehicle interval between occurrences of certain specified events. V may also be used to describe shear as a stress function.

X = length of section or distance along highway (distance interval), in feet, within which the grouping of vehicles is to occur.

Z = average number of vehicles expected within a specified length of X feet or a specified time of t seconds, based on total traffic in both directions. For a specified length of X feet, $Z = AX/5280D$; for a specified time of t seconds, $Z = At/3600$.

$P(2H, X;2)$ = probability of the group, 2H, occurring within X feet in each of the two directions.

$P(G, X;a/2)$ = probability of the group, G, occurring within X feet in any manner in either or both directions.

$E(n, X;2)$ = number of events between occurrences of n vehicles in each of two directions within X feet.

$V(G, X;a/2)$ = vehicle interval between occurrences of the group, G, in any manner in either or both directions within X feet.

$T(G, X;a/2)$ = time interval between occurrences of the group, G, within X feet in either or both directions.

e = exponential base, 2.718, 281....

f = unit stress in psi or as may be defined. f_D = unit stress resulting from dead load; f_L = unit stress resulting from live load; f_T = maximum total design stress; and f_H = stress resulting from vehicle or vehicles weighing H tons each.

n = number of vehicles in a group or sequence but unassigned as to class or type.

t = time interval in seconds within which the grouping of vehicles is to occur.

z = average number of vehicles expected within a length of X feet or a time of t seconds in one designated lane, based on the number of vehicles per hour, (R_1), and average speed of vehicles, D, in that lane.

REFERENCES

1. Stephenson, H. K., and Cloninger, K., Jr., "Method of Converting Heavy Motor Vehicle Loads into Equivalent Design Loads on the Basis of Maximum Bending Moments." Bull. 127, Texas Eng. Exp. Sta. (1952).
2. Stephenson, H. K., and Cloninger, K., Jr., "Method of Converting Heavy Motor Vehicle Loads into Equivalent Design Loads on the Basis of Maximum Shears." Bull. 131, Texas Eng. Exp. Sta. (1953).
3. Stephenson, H. K., and Cloninger, K., Jr., " Stress Producing Effects of Equivalent Design Loads on Modern Highway Bridges." Bull. 132, Texas Eng. Exp. Sta. (1953).
4. Stephenson H. K., "Determination Permissible Vehicle Weights on Bridges of H Loading Design." AASHO Proc., 145-148 (1949).
5. Stephenson, H. K., "Highway Bridge Live Loads Based on Laws of Chance." Paper 1314, Jour. Structural Division, ASCE, Vol. 83, No. ST4 (July 1957).
6. Stephenson, H. K., "Frequencies of Various Levels of Stress in Highway Bridges." HRB Proc., 38: 113-148 (1959).
7. Stephenson, H. K., "Rapid Method for Estimating Maximum Bending Stress in Simple-Span Highway Bridges." HRB Bull. 279, 47-62 (1960).
8. Stephenson, H. K., "How to Figure Steel Weight in Bridges." Engineering News-Record (Feb. 16, 1961).
9. Stephenson, H. K., Noel, J. S., and Mayfield, A. D., "Truck Weight Trends Related to Highway Structures." Bull. 19, Texas Transportation Institute, A & M College of Texas (1962).
10. Stephenson, H. K., "Heavy Truck Loads Related to Overstress in Simple Span Highway Bridges." Texas Transportation Institute, Texas A & M (1963).
11. Greenshields, B. D., and Weida, F. M., "Statistics with Applications to Highway Traffic Analyses." Eno Foundation (1962).
12. Molina, E. C., "Poisson's Exponential Binomial Limit." Van Nostrand (1943).

Load-Deformation Characteristics of Elastomeric Bridge Bearing Pads

EARL V. CLARK, Enjay Laboratories, Linden, N. J., and
KENDALL MOULTROP, Associate Professor of Civil Engineering, University of Rhode Island

In 1958, a tentative specification for elastomeric pads as expansion bearings was adopted by AASHO. This specification was based largely on the results of a cooperative program undertaken by the Rhode Island Department of Public Works and the engineering firm of Charles A. Maguire and Associates. Their work was based on the load-bearing properties of neoprene measured at room temperature. The adequacy of neoprene as a bearing material has been proved by the success of elastomeric bearing pads. Other elastomers are equally suited, however. A cooperative program by the Enjay Laboratories and the University of Rhode Island was undertaken to extend the work to two such materials, butyl rubber and chlorinated butyl rubber (chlorobutyl), and as a further extension of the previous work, to investigate the effects of accelerated aging and load-bearing properties at low temperatures. The results of these evaluations demonstrated that butyl, chlorobutyl, and neoprene bearing pads were equivalent in compressive and shear load-deformation properties when evaluated at room temperature. Furthermore, these materials displayed excellent resistance to the effects of accelerated aging. All three bearings displayed the same dynamic and static creep properties.

The one significant difference observed was in low-temperature load-bearing properties. The butyl and chlorobutyl bearing pads were two to three times more flexible than the neoprene pad and retained their low-temperature flexibility advantage even after accelerated aging conditions.

•IN RECENT YEARS, elastomeric pads have been widely used as bridge bearings because of their low cost, freedom from maintenance, and effectiveness under compressive and shear loads. The pads take very little space compared to steel rollers or rocker arms, distribute the load evenly at all times, and compensate for mechanical and thermal stress in all directions. In Great Britain and France, elastomeric pads have been used as bearings for railroad bridges. In the United States, California, Florida, North Dakota, Rhode Island, and Texas have used these bearings for highway bridges.

In 1958, the Rhode Island Department of Public Works, Division of Roads and Bridges, in cooperation with the engineering firm of Charles A. Maguire and Associates of Providence, conducted an evaluation of the load-deformation characteristics of elastomeric bearings (1, 2). This work served as the basis for a tentative specification for expansion bearings adopted in 1958 by the Operating Committee on Bridges and Structures of the American Association of State Highway Officials (Appendix A).

Paper sponsored by Committee on Bridges.

Available information on elastomeric bearings is confined to the load-deformation properties of neoprene measured at room temperature. In 1959, a cooperative program was undertaken by the Enjay Laboratories of Linden, N. J., and the University of Rhode Island to extend this work to other selected elastomers and to investigate the effects of simulated aging and load deformation at low temperatures. Because elastomeric properties can be markedly affected by temperature, this information should be particularly useful to design engineers in specifying elastomeric bearings for applications where low temperatures persist during winter months. The main problem that might be encountered at low temperatures is excessive slippage caused by an increase in stiffness of the pads. Elastomeric materials characteristically become stiffer as temperature is lowered.

The elastomer used in bearings should possess mechanical stability under compressive and shear loads and should be resistant to atmospheric aging. The adequacy of neoprene in this respect is one of the reasons for its choice as a bearing material. However, other elastomeric materials are equally suited. Two such materials are covered in this study—a copolymer of isobutylene and isoprene called butyl rubber, and a chlorinated modification of this basic structure called chlorobutyl. Chlorination improves the heat-aging characteristics and low-temperature properties of the basic butyl polymer. Both polymers are characterized by low chemical unsaturation and hence are inherently resistant to degradation by aging (combination of heat, oxygen, ozone) and most chemicals. Also, butyl's unique molecular structure is responsible for high hysteresis (mechanical damping), impermeability to gases and liquids, and excellent low-temperature flexibility. Therefore, butyl polymers should be admirably suited to serve the primary function of elastomeric-bearing pads, particularly in those areas where low temperatures are experienced.

This report describes the load-deformation studies conducted by the University of Rhode Island and the Enjay Laboratories on bearing pads made from neoprene, butyl, and chlorinated butyl rubber. The studies are similar to those of Maguire and Associates (1, 2), except provisions were made to conduct tests at low temperatures (-45 F).

MATERIALS

The materials selected for testing consisted of 6- × 12- × 1-in. molded pads of butyl, chlorobutyl, and neoprene. The neoprene was a commercially produced bearing pad. Pads of this size have a shape factor of 2, which is well above the minimum of 1.25 specified by AASHO. Shape factor indicates the relative compressive stiffness of a pad and is the ratio of loaded area to the total area free to bulge. The formula for computing shape factor is given in Appendix A. When pads having the same compression area and same hardness are subjected to the same load, the pad having the greatest free bulging area, hence lowest shape factor, will have the greatest vertical deformation.

Pads of both hardness levels listed in the AASHO tentative specification were tested (60 ± 5 and 70 ± 5 Shore "A" hardness). The properties of the pads are compared to the specification in Appendix B. The butyl and neoprene pads were well within the specification limits. The chlorobutyl pad was below the tensile strength specification, but it gave load-bearing properties equivalent to the higher tensile strength butyl and neoprene pads. The inadequacy of tensile strength in predicting the general performance of elastomeric materials is well known (1).

TEST EQUIPMENT

The equipment used at the University of Rhode Island simulated a typical bridge beam pier interface. Compressive loads simulating bridge loads were applied by means of a 300,000-lb Tinius-Olsen universal testing machine. Shear loads simulating expansion and contraction effects were applied by means of a 40,000-lb hydraulic jack.

The apparatus consisted of two concrete blocks cast between two pairs of structural steel angles. Vertical loads were applied through the concrete blocks to the bearing

assembly. The steel angles formed a frame which allowed horizontal loads to be applied to the bearing unit without subjecting the test apparatus to external lateral stresses. The pads were placed two at a time between the concrete blocks, and a steel plate was then placed between them (Figs. 1 and 2).

Compressive loads were applied vertically by means of the testing machine, and shearing loads were applied horizontally by the hydraulic jack. Two dial indicators, one on each side and calibrated in 0.001-in. graduations, were used to measure vertical deformation. One dial, centrally located, was used to measure horizontal deformation.

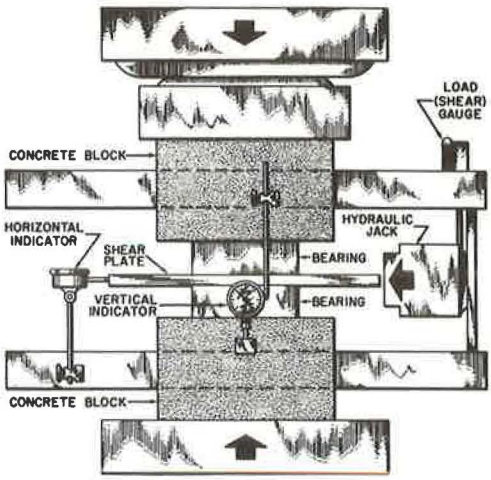

Figure 1. Testing apparatus.

Low temperatures were obtained by pumping methylene chloride, cooled by dry ice, through copper tubes to cylinders embedded in the concrete compression blocks. The steel plate placed between the pads was also cooled by the methylene chloride. The temperature was measured by means of thermocouples placed between the pad and the concrete blocks, and between the steel plate and one of the pads. The detailed test procedures are described in Appendix C.

RESULTS

The following information was obtained on butyl, chlorobutyl, and neoprene bearing pads of 60 ± 5 and 70 ± 5 Shore "A" hardness:

1. Compression and shear load deformation at room temperature (75 ± 5 F) and at low temperature (-45 ± 5 F);

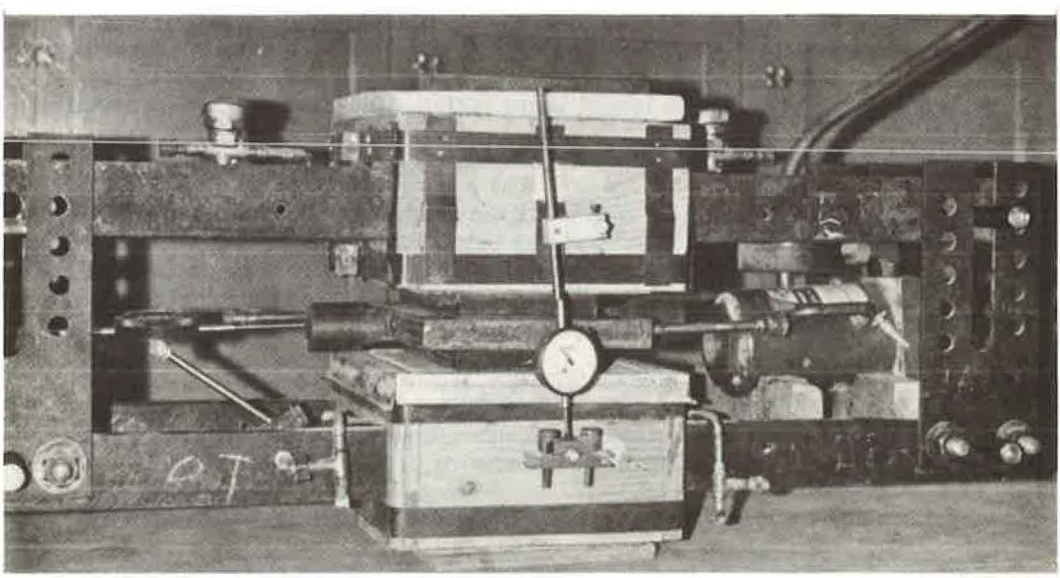

Figure 2. Testing apparatus.

2. Compression and shear load deformation at the previous conditions after accelerated aging at 250 F for 5 days and after additional 5-day aging of the same pads (referred to in the text as 5- + 5-day aging);

3. Simulated fatigue at room temperature by cyclic horizontal deformation under compressive load;

4. Compression set at room temperature and under conditions of outdoor exposure; and

5. Water absorption measured by volume increase of the bearing pads at room temperature.

Information was obtained on both 60 and 70 Shore "A" hardness pads. The data on the 70 hardness pads will be discussed in detail, but that obtained on the 60 hardness pads will only be summarized. All data are included for reference.

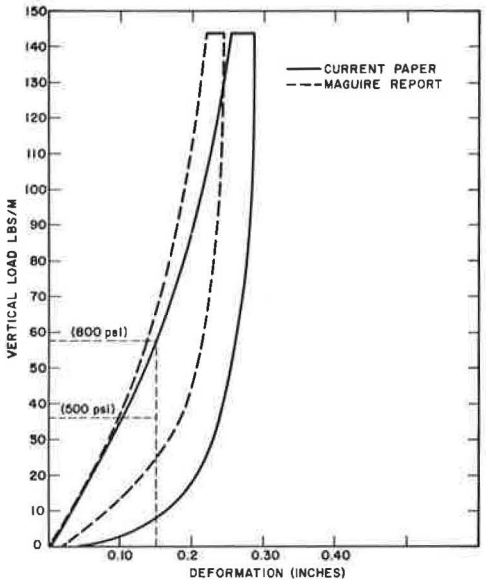

Figure 3. Vertical tests of commercial neoprene bearing pads at room temperature, Shore A 70 ± 5.

Before discussing the results of this investigation, a comparison with the earlier data reported by Maguire and Associates seems worthwhile. Compressive load-deformation data in this study on the neoprene pad are shown in Figure 3 in comparison to similar data reported by Maguire and Associates (1). The agreement between these two sets of data is excellent, indicating good reproducibility of the test in spite of the normal variations expected in rubber compounding. A similar comparison of shear loading data is shown in Figure 4. Again, the agreement between the two sets of data is quite good. In this study the maximum horizontal and vertical loads

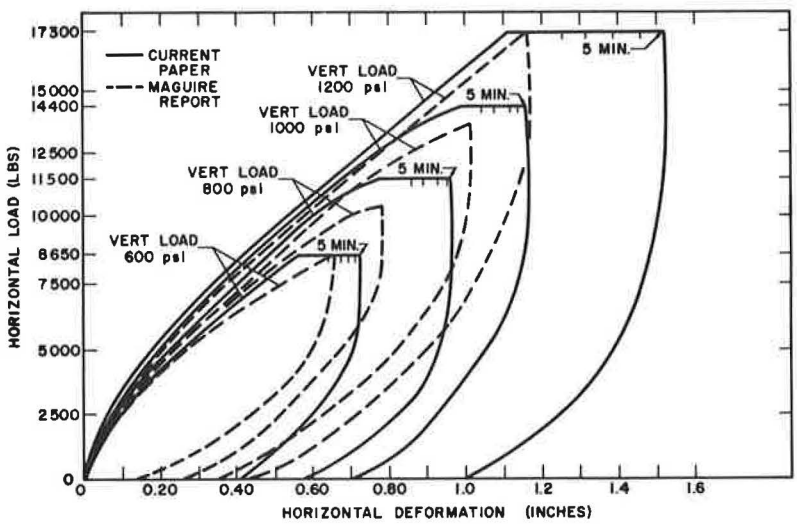

Figure 4. Horizontal tests of commercial neoprene bearing pads at room temperature, Shore A 70 ± 5.

were maintained for 5 minutes resulting in an increase in horizontal deformation. However, in the Maguire work on these particular tests, the load was released immediately after the maximum values were obtained. Hence, no increase in horizontal deformation was reported. The excellent agreement between these two sets of data is gratifying and lends considerable substance to the comparison of the elastomeric materials.

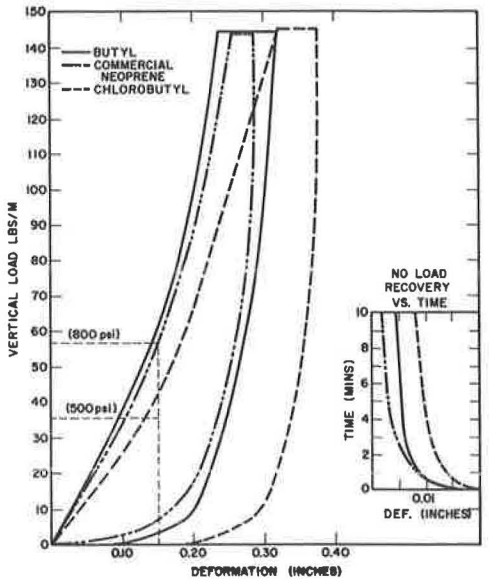

Figure 5. Vertical tests at room temperature, Shore A 70 ± 5.

Room Temperature Evaluations

The compressive load-deformation characteristics of the butyl and neoprene bearing pads were found to be identical (Fig. 5). The chlorobutyl pad showed greater deflection under the same load conditions. However, this pad was seven Shore "A" points softer than the butyl or neoprene pad (Appendix B) and hence would be expected to give slightly greater deflection. The pad could also be made stiffer by an increase in shape factor (1, 3). After the load was removed, the pads showed equal recovery for all practical purposes.

During the time the vertical load was held constant, both butyl bearings showed a slightly larger increase in deformation than the neoprene bearing (Fig. 5). This phenomenon of increased deflection with time is termed creep. Although the difference between the butyl and the neoprene pads is small, it was observed consistently throughout this work during the 5-min constant load conditions. However, it will be subsequently shown that the long-term creep properties of butyl and chlorobutyl are not substantially different from neoprene.

The shear load-deformation (combined horizontal and vertical load) characteristics of the butyl, chlorobutyl, and neoprene bearings are shown in Figures 6, 7, and 8, respectively. For each polymer, the data are plotted for vertical loads up to 1,200 psi. For convenience, the polymers are compared at 600- and 800-psi vertical loads in Figure 9. As was the case with compressive load, the butyl and neoprene pads are nearly identical in load deflection, but the softer chlorobutyl bearing showed greater deflection. The no-load recovery and creep properties of the polymers were similar in shear as in compression.

Low-Temperature Evaluation (-45 F)

Elastomeric materials will all tend to stiffen as the temperature is decreased. Stiffening can be controlled to some extent by the choice of compounding ingredients, for example, plasticizer and filler type. However, the inherent temperature sensitivity of the polymer itself is by far the most important variable. The differences in compressive deformation among the three pads are shown in Figure 10. At the same hardness level, the butyl bearing was over twice as flexible as the neoprene bearing as measured by percent deformation at 800-psi vertical load. As would be expected, the softer chlorobutyl pad was approximately $1\frac{1}{2}$ times more flexible than the butyl and over 3 times more flexible than the neoprene bearings. The no-load recovery was a further demonstration of the good low-temperature flexibility of the two butyl materials. The rate of recovery was almost identical to that at room temperature.

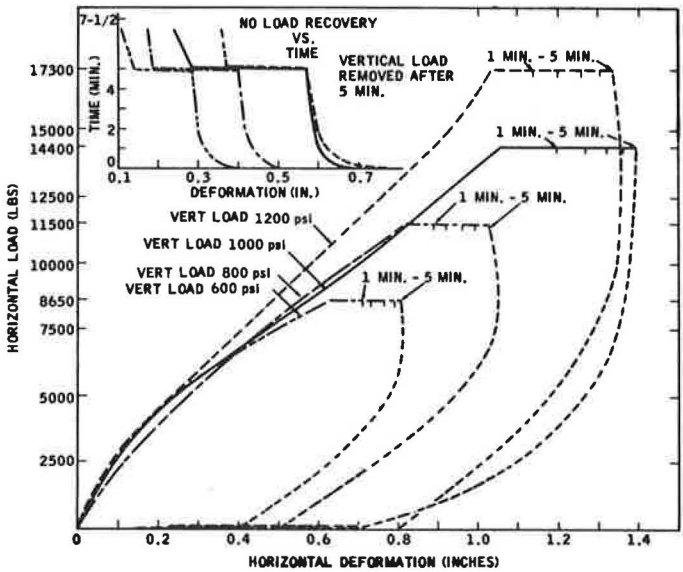

Figure 6. Horizontal test of butyl at room temperature, Shore A 70 ± 5.

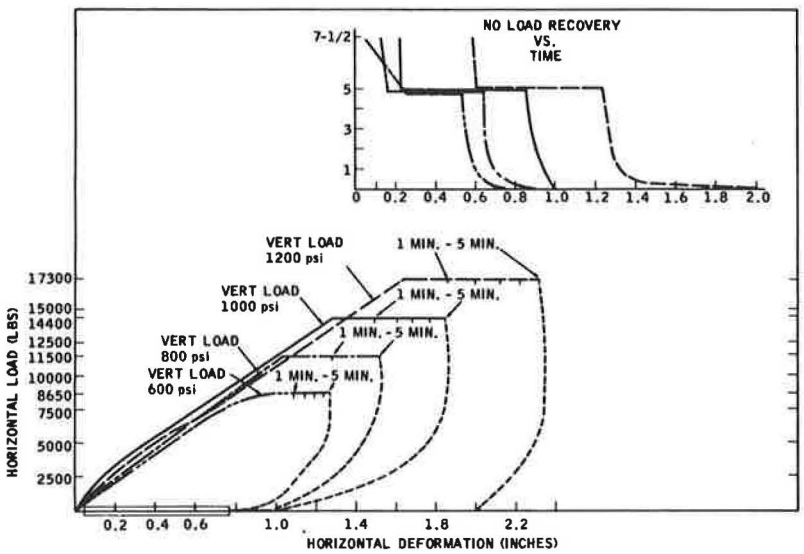

Figure 7. Horizontal test of chlorobutyl at room temperature, Shore A 70 ± 5.

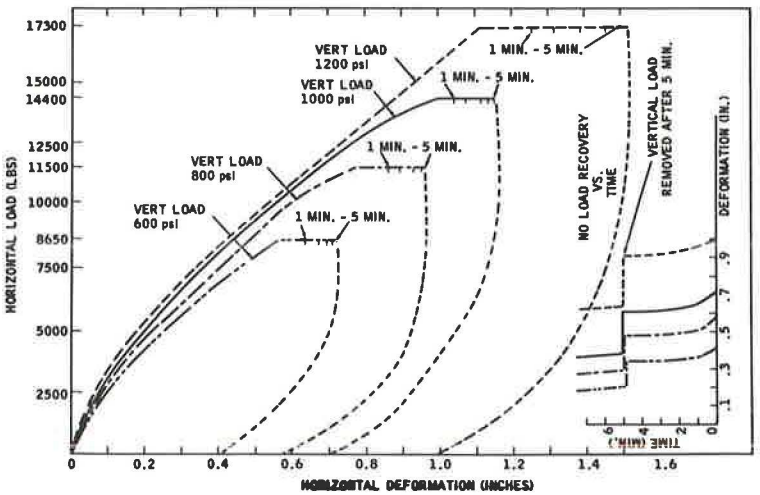

Figure 8. Horizontal test of commercial neoprene at room temperature, Shore A 70 ± 5.

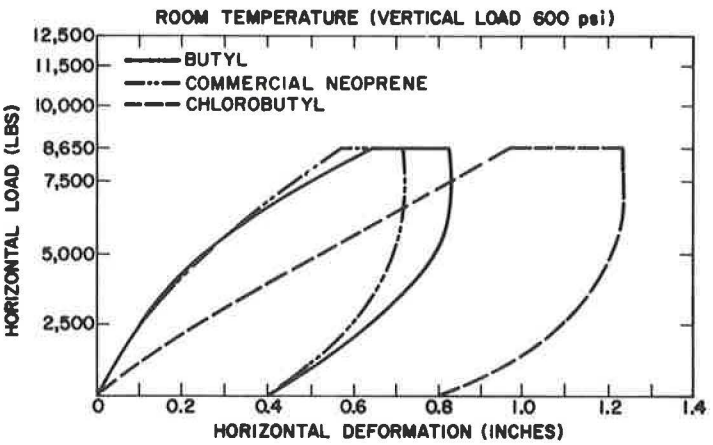

LS-62-11328

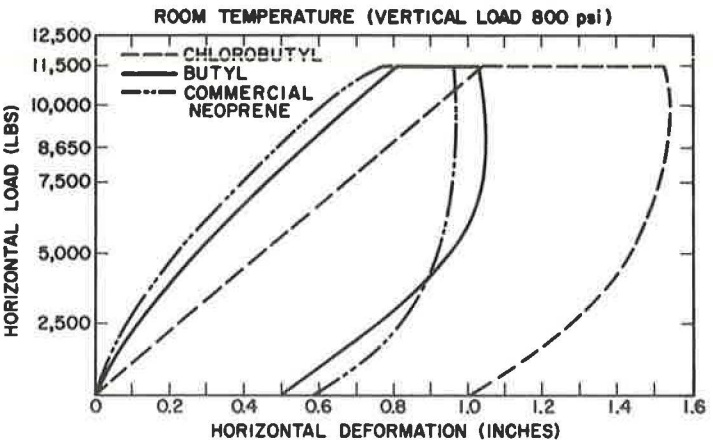

LS-62-11327

Figure 9. Horizontal tests, Shore A 70 ± 5.

Under shear loading conditions (combined horizontal and vertical load) the difference between the two butyls and the neoprene pads was even greater. The shear deformation properties of the three bearings are shown in Figures 11, 12, and 13. The rate of no-load recovery was again an indication of the good low-temperature flexibility of the two butyl pads. For convenience, a comparison of the three bearings at 600- and 800-psi vertical load is shown in Figure 14. The difference in flexibility between the elastomeric materials is further demonstrated in Table 1.

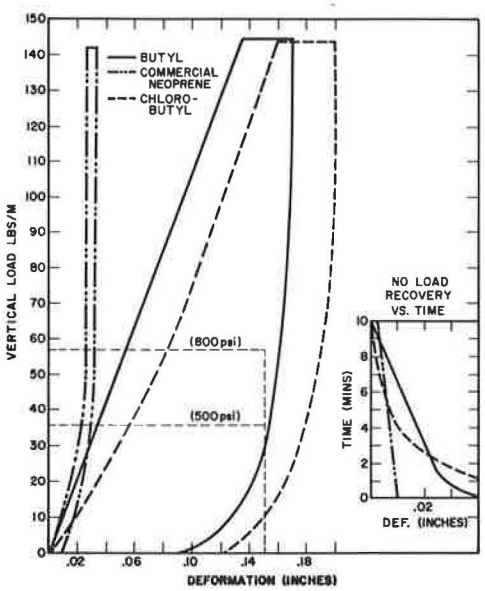

Figure 10. Vertical tests at -45 F, Shore A 70 ± 5.

A temperature of -40 to -45 F is commonly used when testing elastomeric materials. In fact, the AASHO tentative specification for bearing pads requires a Young's modulus determination at -40 F. Although the load-deformation studies were conducted only at -45 F, similar results would be expected over a range of temperatures as indicated by the hardness data shown in Table 2.

It must be recognized that hardness is only a rough measure of stiffness. However, it is well known that hardness correlates with compressive modulus (3). Hence, the differences shown are a reasonable indication of the relative load-deformation properties of the bearings at the various temperatures indicated. It is clear that over the entire temperature range shown, neoprene was substantially stiffer than the two butyl bearings.

Accelerated Aging Evaluations

When subjected to the effects of atmospheric aging, elastomeric materials will slowly undergo changes in physical properties. Neoprene characteristically becomes

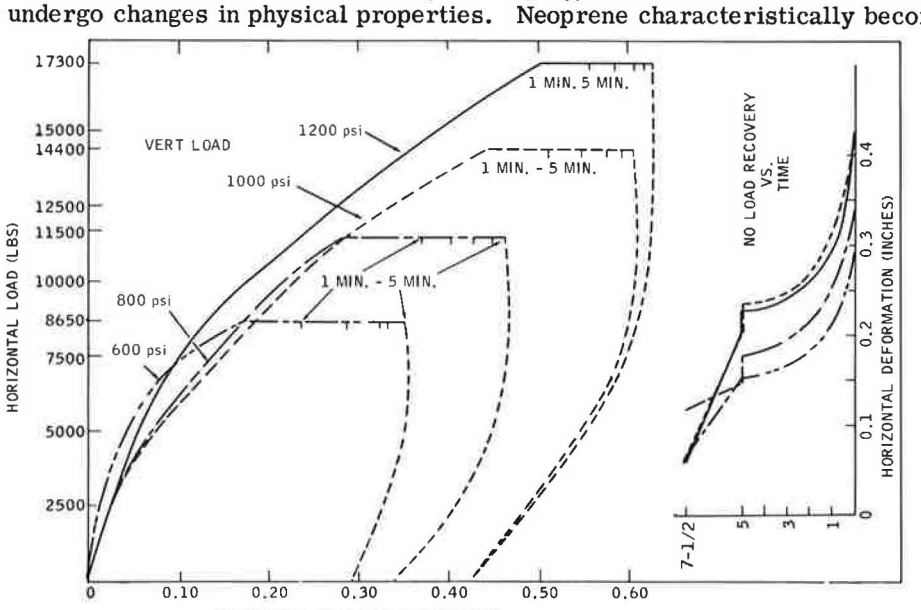

Figure 11. Horizontal test of butyl at -45 F, Shore A 70 ± 5.

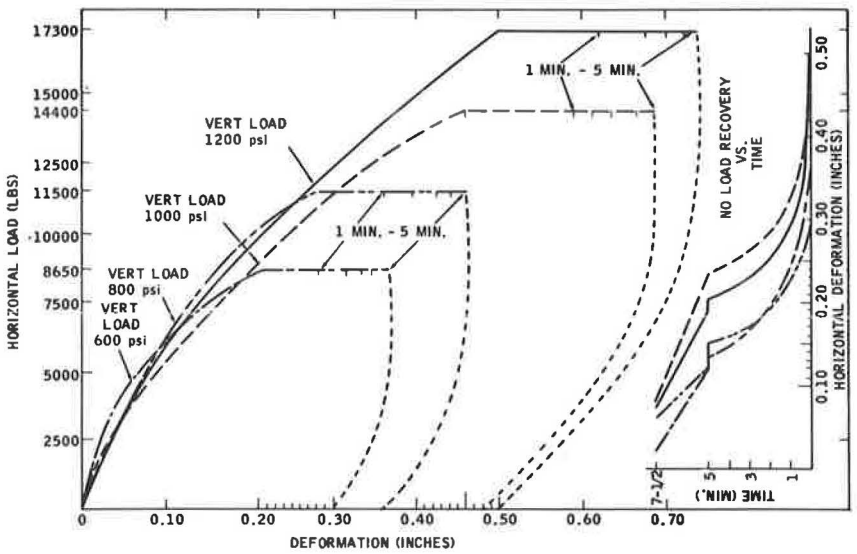

Figure 12. Horizontal test of chlorobutyl at −45 F, Shore A 70 ± 5.

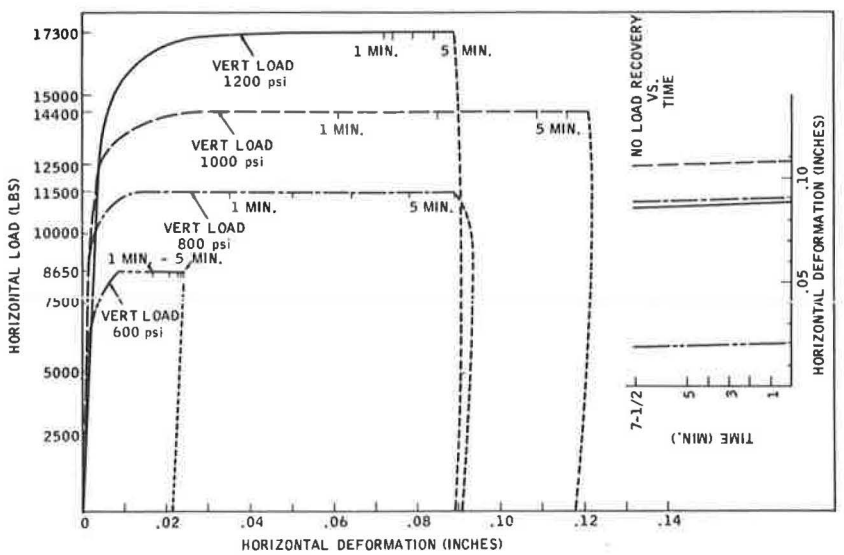

Figure 13. Horizontal tests of commercial neoprene at −45 F, Shore A 70 ± 5.

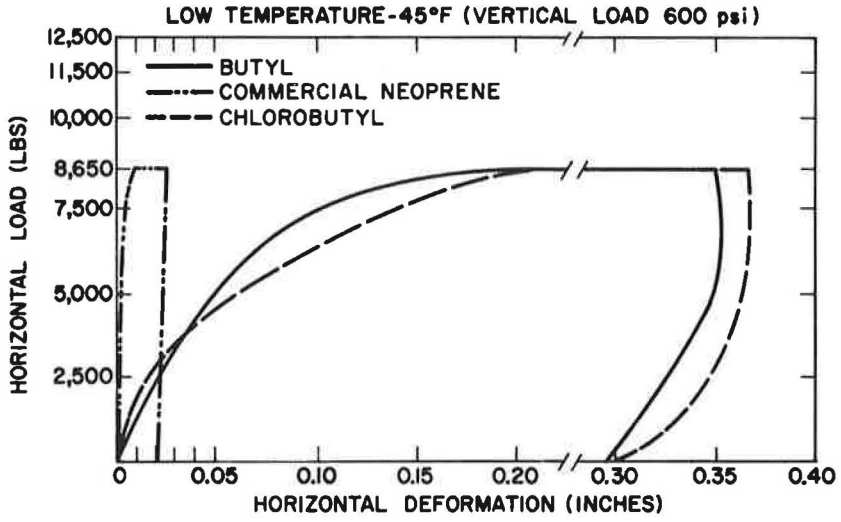

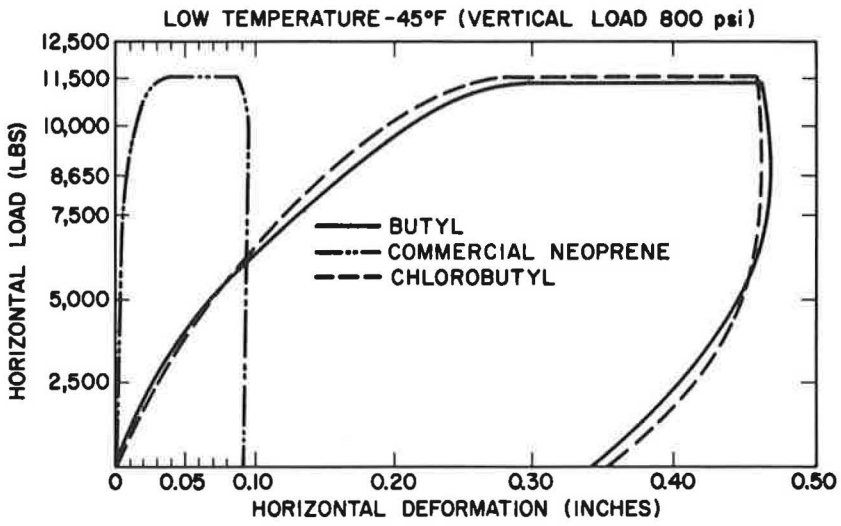

Figure 14. Horizontal tests, Shore A 70 ± 5.

TABLE 1

SHEAR DEFORMATION AT ROOM TEMPERATURE AND AT -45°F		
VERTICAL LOAD: 800 PSI HORIZONTAL LOAD: 11,500 POUNDS		
BASE ELASTOMER	HORIZONTAL DEFLECTION, INCHES	
	75°F	-45°F
BUTYL	0.82	0.28
CHLOROBUTYL	1.04	0.28
NEOPRENE	0.77	0.01

TABLE 2

POINT INCREASE IN SHORE "A" HARDNESS COMPARED TO R.T.*				
BASE ELASTOMER	0°F	-10°F	-20°F	-40°F
BUTYL	6	6	6	10
CHLOROBUTYL	4	4	5	8
NEOPRENE	11	11	15	19
*70 SHORE "A" HARDNESS PADS STORED 48 HOURS AT TEMPERATURE INDICATED.				

hard and brittle, but butyl tends to become more flexible. However, when properly compounded, both polymers are exceptionally resistant to atmospheric degradation. In fact, retention of physical properties after 15 to 20 years of atmospheric exposure can be demonstrated for both polymers in certain types of applications. These properties were substantiated in this study by subjecting the bearing pads, after testing at room temperature and -45 F, to accelerated aging under severe conditions of 5 days at 250 F, retesting, and again aging for 5 days at 250 F (5- + 5-day aging). These conditions would be comparable to many years of normal temperature exposure.

Table 3 summarizes the compressive deflection data taken from Figures 5, 15, and 16, and shows the characteristic effect of aging on the butyl, chlorobutyl, and neoprene bearings. Although there was a slight increase in compressive deflection at room temperature with the butyl pads and a slight stiffening with the neoprene pad, all three materials displayed excellent stability under the severe conditions chosen.

Similar effects were noted when the aged pads were subjected to shear loading at room temperature. This is given in Table 4 which summarizes the data in Figures 6 to 8 and 17 to 22.

Accelerated aging did not greatly affect the low-temperature compressive-load-bearing properties of the three bearings. This is demonstrated by data from Figures 10, 23, 24, and Table 4. Shear loading studies at -45 F after aging also showed that butyl pads retain their

TABLE 3

COMPRESSIVE LOAD-DEFORMATION AT ROOM TEMPERATURE			
BASE ELASTOMER	% DEFLECTION AT 800 PSI		
	ORIGINAL	AGED 5 DAYS AT 250°F	AGED 5 + 5 DAYS AT 250°F
BUTYL	14	14	17
CHLOROBUTYL	18	18	20
NEOPRENE	15	13	12

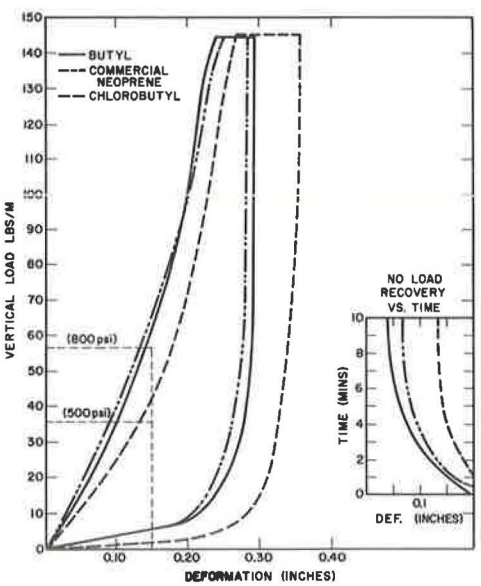

Figure 15. Vertical tests at room temperature (aged 5 days at 250 F), Shore A 70 ± 5.

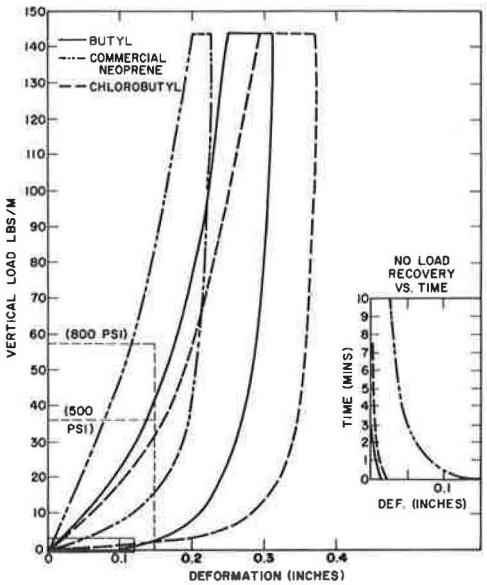

Figure 16. Vertical tests at room temperature (aged 5 + 5 days at 250 F), Shore A 70 ± 5.

TABLE 4

SHEAR LOAD-DEFORMATION AT ROOM TEMPERATURE				
BASE ELASTOMER	VERT. LOAD, PSI	HORIZONTAL DEFLECTION, INCHES		
		ORIG.	AGED 5 DAYS AT 250°F	AGED 5 + 5 DAYS AT 250°F
BUTYL	600	0.63	0.65	0.75
	800	0.82	0.79	0.91
CHLOROBUTYL	600	0.92	0.86	0.94
	800	1.04	1.00	1.20
NEOPRENE	600	0.56	0.50	0.43
	800	0.77	0.60	0.57

COMPRESSIVE LOAD-DEFORMATION AT -45°F			
BASE ELASTOMER	% DEFORMATION AT 800 PSI		
	ORIGINAL	AGED 5 DAYS AT 250°F	AGED 5 + 5 DAYS AT 250°F
BUTYL	5.5	6.5	7.0
CHLOROBUTYL	8.0	8.0	7.0
NEOPRENE	2.5	3.5	2.0

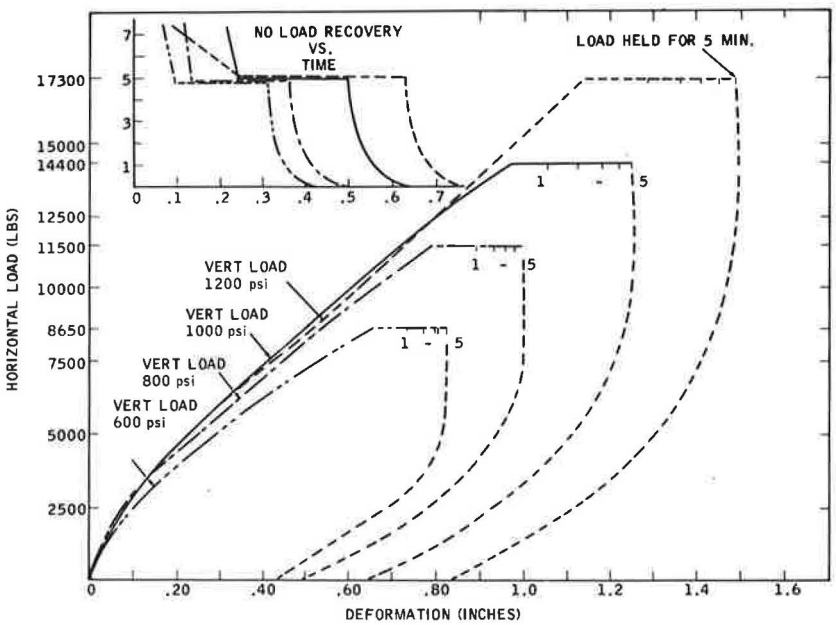

Figure 17. Horizontal test of butyl (aged 5 days at 250 F), Shore A 70 ± 5.

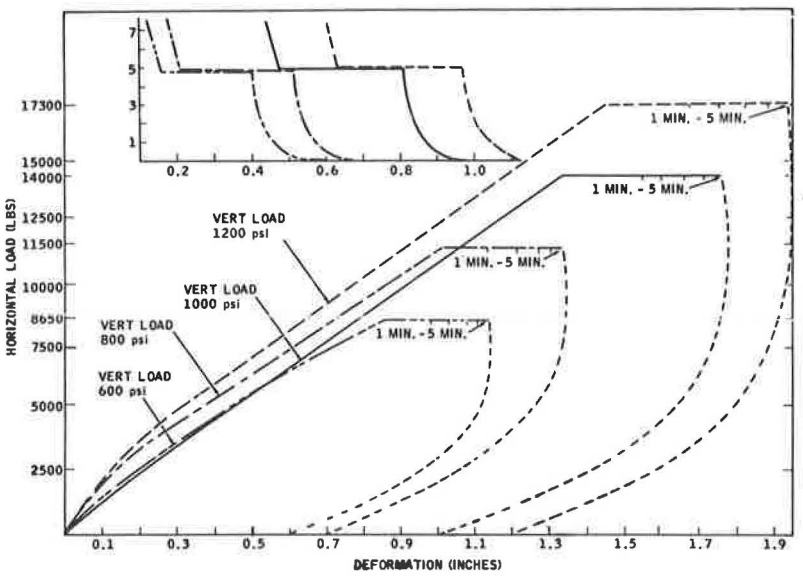

Figure 18. Horizontal test of chlorobutyl (aged 5 days at 250 F), Shore A 70 ± 5.

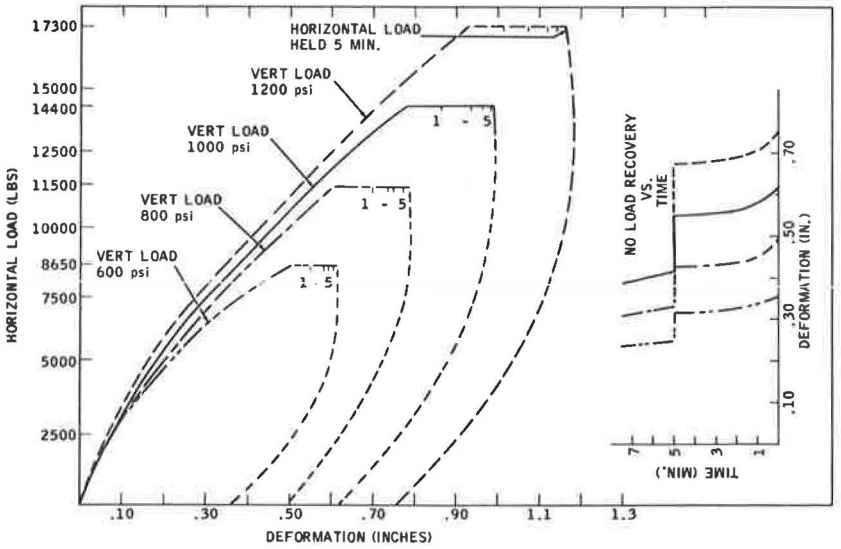

Figure 19. Horizontal test of commercial neoprene(aged 5 days at 250 F),Shore A 70 ± 5.

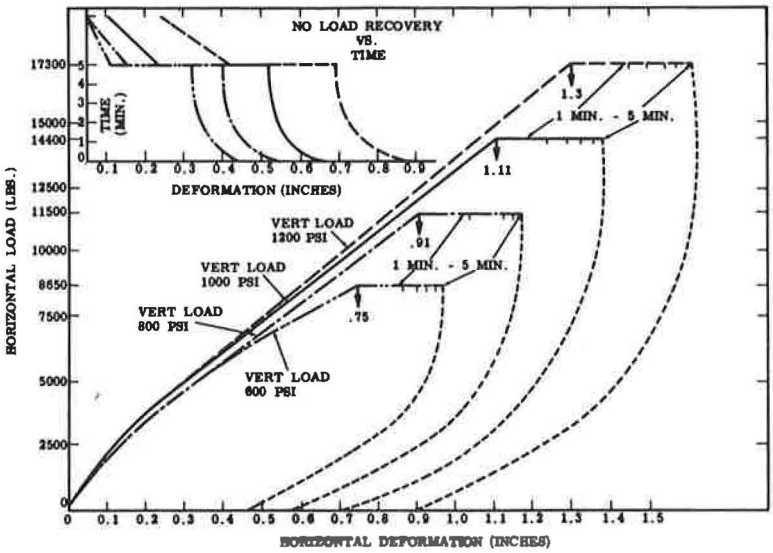

Figure 20. Horizontal test of butyl at room temperature (aged 5 + 5 days at 250 F), Shore A 70 ± 5.

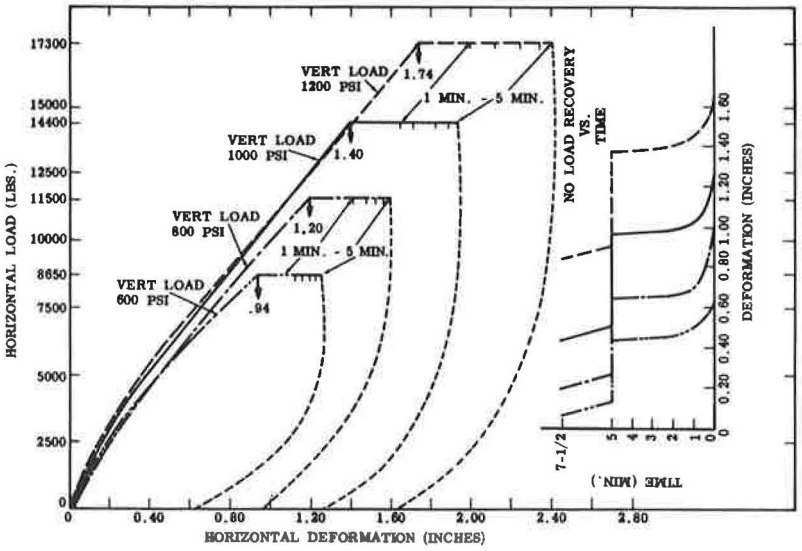

Figure 21. Horizontal test of chlorobutyl at room temperature (aged 5 + 5 days at 250 F), Shore A 70 ± 5.

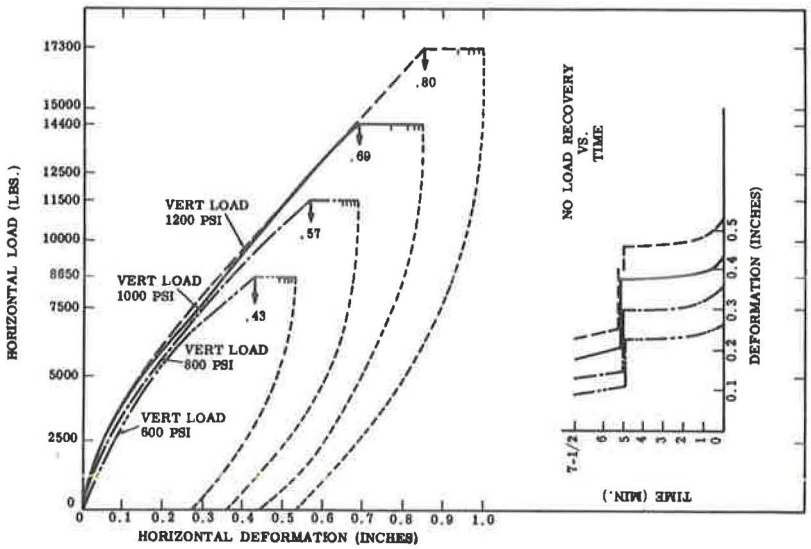

Figure 22. Horizontal test of commercial neoprene at room temperature (aged 5 + 5 days at 250 F), Shore A 70 ± 5.

good low-temperature flexibility. Interestingly, it was not possible to obtain accurate horizontal deformation on the neoprene pad until a vertical load of 1,200 psi was achieved. At the lower vertical loads the pad consistently slipped, hence the data recorded are not a true measure of horizontal deflection. It might be interpreted from these observations that slippage could be a problem if the bearing pads become too stiff. The low-temperature shear loading data are summarized in Table 5 from data taken from Figures 11 to 13 and 25 to 30. One notable point is the effect that the test

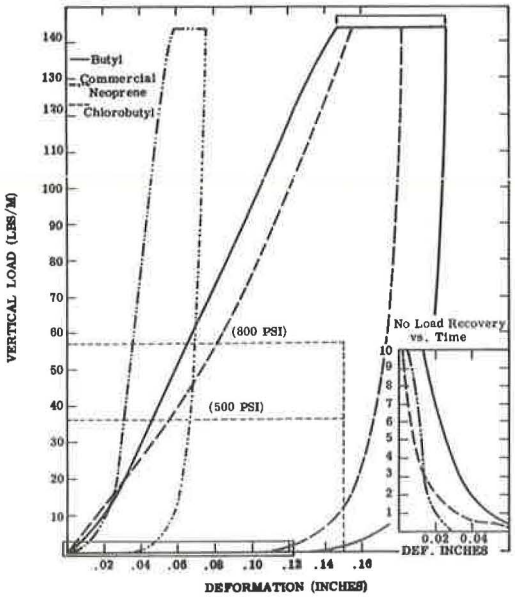

Figure 23. Vertical tests at -45 F (aged 5 days at 250 F), Shore A 70 ± 5.

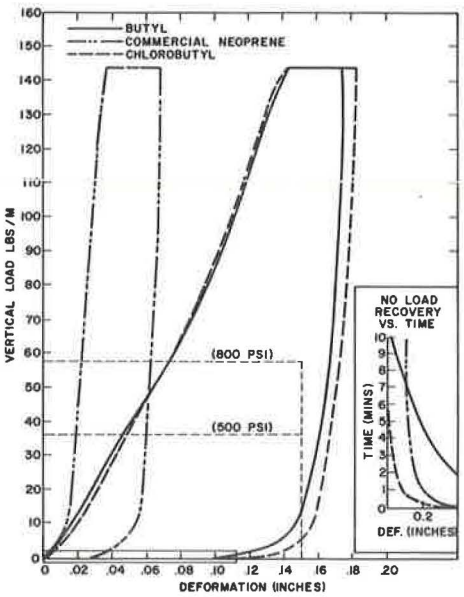

Figure 24. Vertical tests at -45 F (aged 5 + 5 days at 250 F), Shore A 70 ± 5.

condition used for aging has on the properties of butyl and neoprene compounds. The compressive and shear load data on pads aged at 250 F showed a tendency toward neoprene's stiffening and butyl's softening. This is consistent with the known properties of these polymers on aging. However, at less severe conditions, for example 70 hours at 212 F as required in the AASHO specification, butyl polymer will show no change or a slight stiffening (Appendix B). As the test time is prolonged or the temperature raised, most butyl compounds will show the characteristic softening. Actually, the exact opposite will occur with neoprene, initial softening followed by stiffening, if the appropriate test conditions are chosen (4). The main point, however, is that both polymer types are extremely resistant to aging.

TABLE 5

SHEAR LOAD-DEFORMATION AT -45°F				
BASE ELASTOMER	VERT. LOAD, PSI	HORIZONTAL DEFLECTION, INCHES		
		ORIG.	AGED 5 DAYS AT 250°F	AGED 5 + 5 DAYS AT 250°F
BUTYL	600	0.17	0.17	0.23
	800	0.28	0.29	0.27
CHLOROBUTYL	600	0.21	0.35	0.26
	800	0.28	0.38	0.29
NEOPRENE	600	0.008	0.035*	0.016*
	800	0.012	0.040*	0.038*
*PAD SLIPPED				

Fatigue Tests

Maguire and Associates (1) point out that bearing pads are subjected to dynamic loading under actual service conditions and the resulting deflections result in dynamic creep. To determine whether the three elastomeric bearing pads would show any gross differences in dynamic creep, similar tests were performed; that is, alternating horizontal loadings over a 3-hr period. Table 6 compares the horizontal deflections obtained on the three pads.

Although the butyl and chlorobutyl bearings were slightly more flexible than neoprene and showed greater horizontal deflection, the change in deflection during the test period was virtually the same for all three pads. Comparison of the data obtained on the neoprene pad with those reported by Maguire showed approximately the same horizontal deflection.

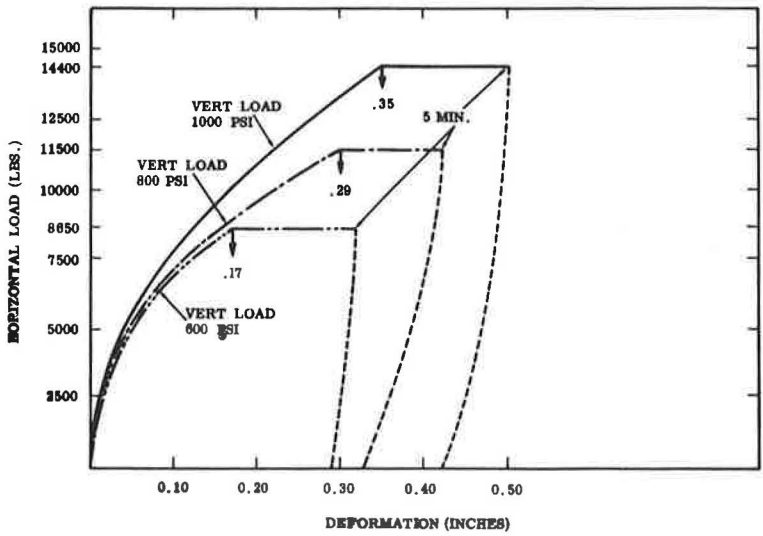

Figure 25. Horizontal test of butyl at -45 F (aged 5 days at 250 F), Shore A 70 ± 5.

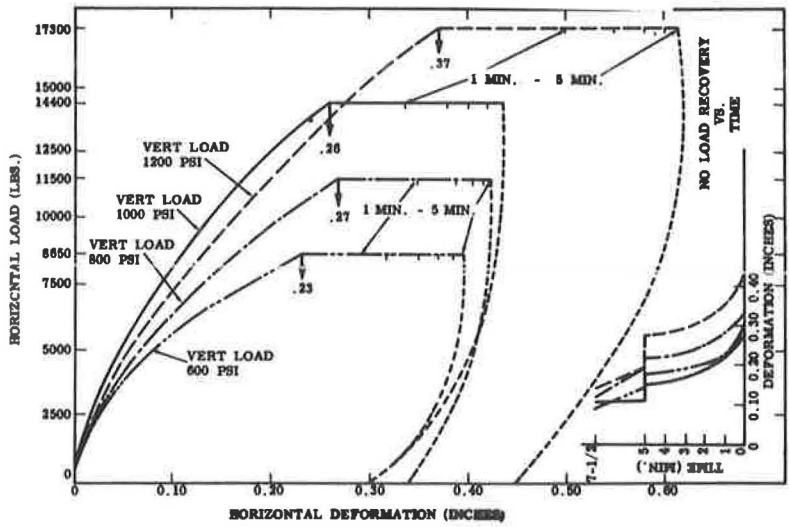

Figure 26. Horizontal test of butyl at −45 F(aged 5 + 5 days at 250 F), Shore A 70 ± 5.

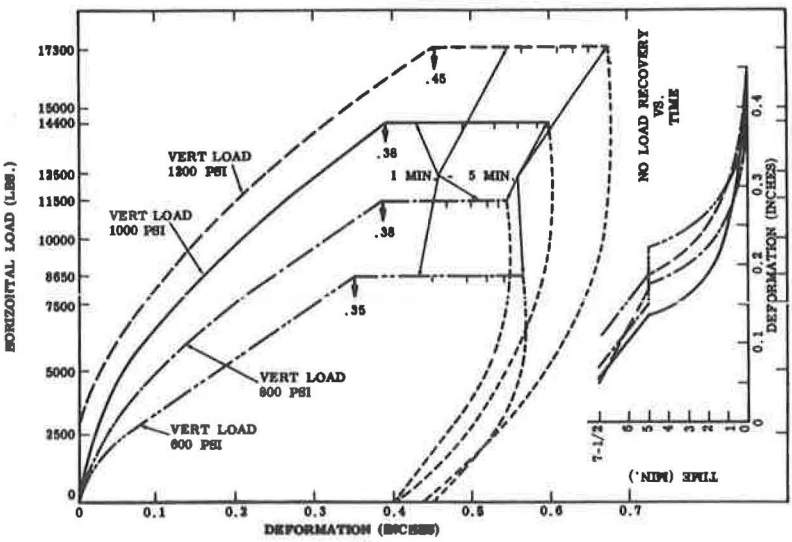

Figure 27. Horizontal test of chlorobutyl at −45 F(aged 5 days at 250 F),Shore A 70 ± 5.

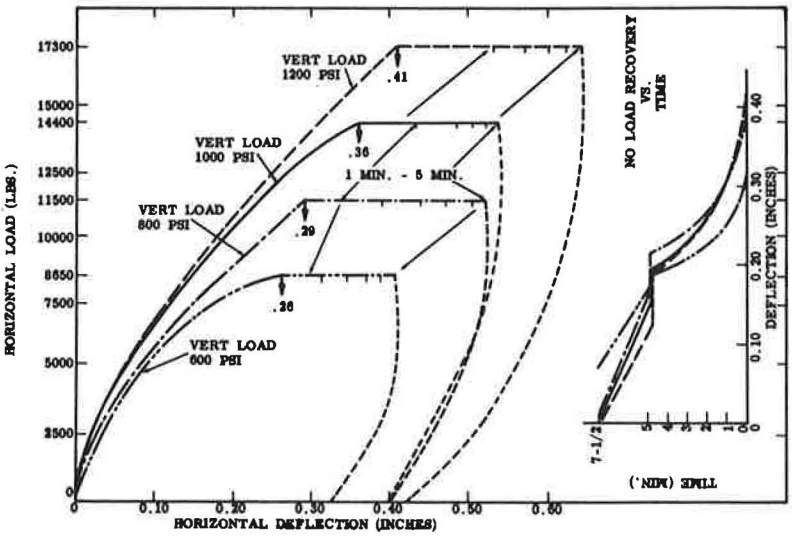

Figure 28. Horizontal test of chlorobutyl at -45 F (aged 5 + 5 days at 250 F), Shore A 70 ± 5.

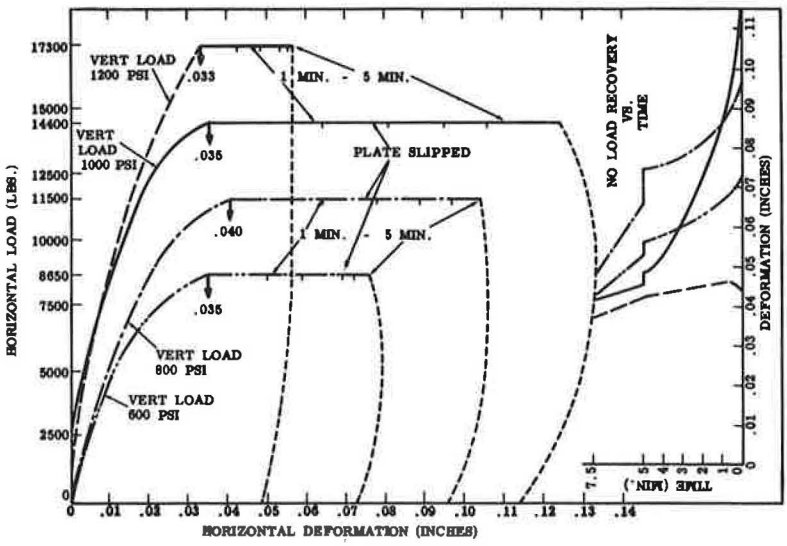

Figure 29. Horizontal test of commercial neoprene at -45 F (aged 5 days at 250 F), Shore A 70 ± 5.

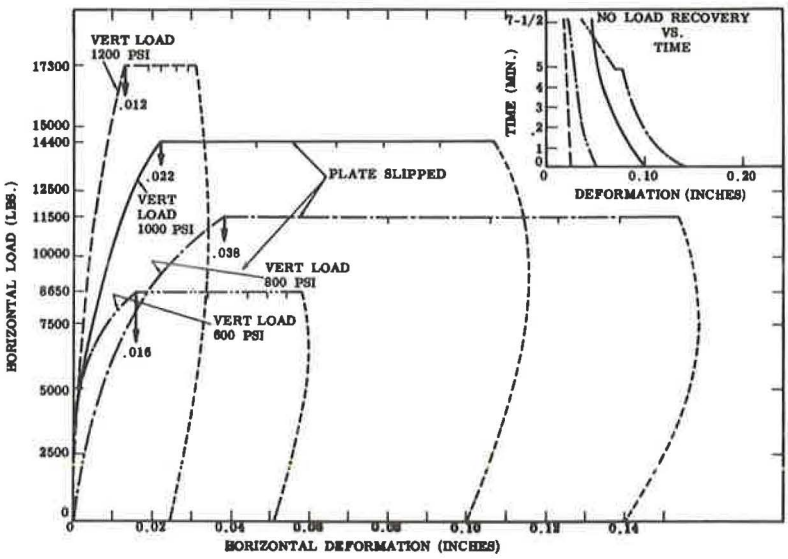

Figure 30. Horizontal test of commercial neoprene at -45 F (aged 5 + 5 days at 250 F), Shore A 70 ± 5.

Creep, as measured by the change in vertical deformation with time, is shown in Figures 31, 32, and 33 for the three polymers. Although the butyl pads showed slightly greater initial vertical deformation as compared to neoprene, the increase in deformation (creep) was essentially the same for all three bearings (Table 7). A true measure of dynamic creep would require much longer term testing (1).

Compression Set

Compression set, run at constant deflection and constant load, is defined in ASTM D-395 as a measure of the resistance of an elastomeric material to long-term deformation under load. Although not an absolute measure, materials that show high set when run at constant deflection would probably be poor in load-bearing applications. Again, although not absolute, materials that show the same compression set at constant deflection might be expected to give reasonably equivalent long-term compressive and shear load-bearing properties. When run under constant load conditions, compression set gives a rough measure of creep. High compression set at constant load would be indicative of poor creep properties. Also, similar constant load set properties of different materials would be an indication of similar creep properties.

Compression set at constant deflection was run on samples of the three polymers using the procedure outlined in Appendix C. The evaluation was carried out over a 14-month period with the samples

TABLE 6

CYCLES	MAXIMUM DEFLECTION (INCHES)					
	BUTYL		CHLOROBUTYL		NEOPRENE	
	LEFT	RIGHT	LEFT	RIGHT	LEFT	RIGHT
1		1.20		1.18		1.08
2	.96		.89		.79	
3		1.00		1.09		.96
4	.90		.88		.70	
5		.92		1.06		.92
6	.88		.88		.66	
7		.91		1.03		.86
8	.88		.88		.68	
9		.88		1.00		.84
10	.86		.88		.62	
11		.84		1.00		.84
12	.86		.88		.62	
13		.84		.96		.82
14	.85		.88		.64	
15		.84		.96		.80
16	.84		.84		.63	
17		.84		.96		.79
18	.84		.84		.62	
ΔCYCLE 1-18	0.12	0.36	0.05	0.22	0.17	0.29

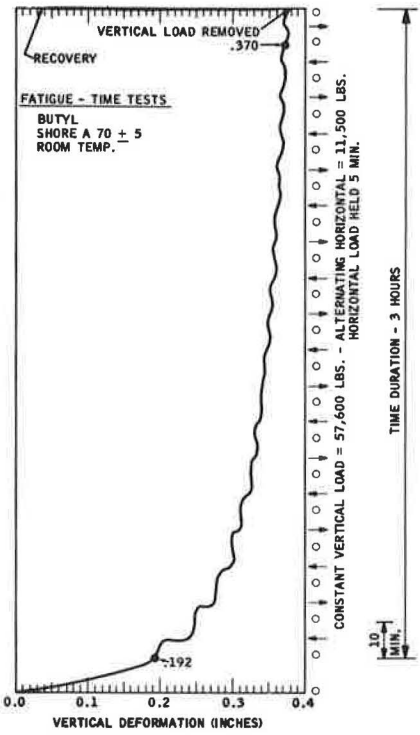

Figure 31.

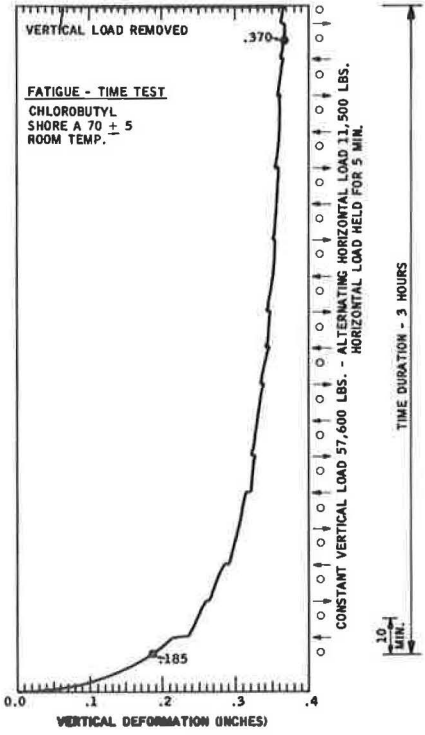

Figure 32.

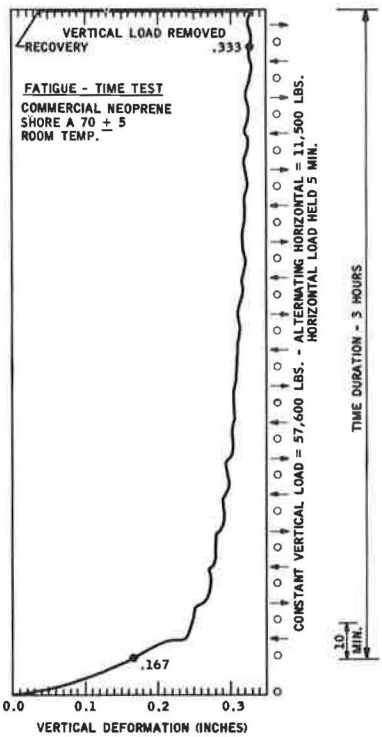

Figure 33.

TABLE 7

DYNAMIC CREEP			
VERTICAL LOAD: 800 PSI HORIZONTAL LOAD: 11,500 POUNDS			
BASE ELASTOMER	% VERT. DEFORMATION		% CREEP*
	ORIGINAL	FINAL	
BUTYL	19.2	37.0	93
CHLOROBUTYL	18.5	37.0	100
NEOPRENE	16.7	33.3	100
* % CREEP = FINAL DEFLECTION MINUS INITIAL DEFLECTION DIVIDED BY INITIAL DEFLECTION x 100.			

TABLE 8

COMPRESSION SET AT CONSTANT DEFLECTION					
BASE ELASTOMER	% SET AT MONTHS INDICATED				
	4	6	8	10	14
BUTYL	14.2	21.0	25.4	26.6	26.6
CHLOROBUTYL	15.1	21.1	26.4	28.1	28.4
NEOPRENE	14.3	19.1	25.8	26.3	26.6

exposed to ambient conditions beginning January 9, 1961, in New Jersey. The three polymers are equivalent in set at constant deflection (Table 8).

As mentioned previously, compression set at constant load is a rough indication of the creep properties of an elastomeric material. Tests run for 6 months at room temperature, according to the procedure outlined in Appendix C, showed that a butyl, chlorobutyl, and neoprene pad are identical in this respect (Table 9).

Water Absorption

Bridge-bearing pads will be subjected to water contact from rain and water runoff from the deck span. Depending on the location of the pad and the construction of the bridge, they may be in contact with water for reasonably long periods of time. The water absorption properties of the butyl, chlorobutyl, and neoprene bearing pads were evaluated by immersing the materials in water at room temperature for one year. Figure 34 shows that all three polymers are excellent with respect to water absorption. The butyl shows virtually no increase in volume, the chlorobutyl only $1\frac{1}{2}$ percent, and the neoprene pad approximately $4\frac{1}{2}$ percent.

The most important aspect of water absorption (not evaluated in this study) is the effect it might have on the load-bearing properties of the polymers. This might be particularly important at subfreezing temperatures. Generally speaking, however, at normal temperatures the properties of elastomeric materials are little affected by water.

Evaluation of 60 ± 5 Shore "A" Hardness Bearing Pads

A similar series of evaluations was made with neoprene, butyl, and chlorobutyl bearings in the 60 ± 5 hardness range. Data from room temperature tests follow the

TABLE 9

COMPRESSION SET AT CONSTANT LOAD			
BASE ELASTOMER	% SET AT DAYS INDICATED		
	14	60	180
BUTYL	5.2	7.0	8.2
CHLOROBUTYL	5.4	7.1	8.3
NEOPRENE	5.1	7.5	8.9

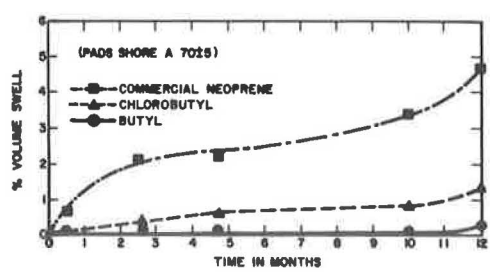

Figure 34. Water immersion at room temperature.

same trends as those noted with 70 hard pads, i.e., all three bearing pads are about equivalent in compressive and shear load-bearing properties both before and after accelerated aging. Although the differences are slight, the characteristic increase in flexibility with butyl and chlorobutyl and stiffening with neoprene was observed on aging.

Generally, the low-temperature data on pads at the two hardness levels agree fairly well. This was particularly true with chlorobutyl. The data on the pads aged 5 days were all somewhat inconsistent with the 70 Shore "A" data and with the 5 + 5 day aged 60 Shore "A" pads. No logical explanation is apparent unless temperature control was poor or bearing slippage occurred.

REFERENCES

1. Maguire, Charles A., and Associates, "Elastomeric Bridge Bearing Pads—Report of Tests and Design Procedures." (1958).
2. Pare, R. L., and Keiner, E. P., "Elastomeric Bridge Bearings." HRB Bull. 242, 1-19 (1960).
3. Cardillo, R. M., and Kruse, D. F., "Load Bearing Characteristics of Butyl Rubber." Paper (61-WA-335) ASME (1961).
4. Morton, M., "Rubber Technology." Reinhold (1959).

Appendix A

T.1 (59) Art. 1.6.47, Expansion Bearings. Tentative Specification
T.2 (58), Expansion Bearings, is repealed and the following substituted:

Amend this article by adding the following:

In lieu of the above requirements elastomeric bearing pads may be used for spans of 80 feet or less, subject to the following:

(a) The relationship between the loaded face and the side areas expressed as a "Shape Factor." For rectangular-shaped bearings with parallel (not over approximately 5° slope) loading surfaces

$$S = \frac{ab}{2t\,(a + b)}$$

where
S = shape factor;
a and b = length and width; and
t = thickness.

(b) The total of the positive and negative movements caused by anticipated temperature change shall not exceed one-half the thickness of the pad.

(c) Unit pressure on elastomeric bearing pads shall not exceed 500 psi under dead load nor 800 psi under a combination of dead load plus live load plus impact. The initial deflection under dead, live, and impact loads shall not exceed 15 percent of the thickness of the pad. Elastomeric bearing pads shall be cast in a single integral layer except that multiple-layer pads, separated by nonelastic sheets to restrain deformation in thick pads, may be permitted. The variation in thickness in the longitudinal direction (taper) shall not exceed five percent of the length of the pad. The least horizontal dimension of the pad shall not be less than five times the thickness (shape factor 1.25 minimum).

(d) The physical properties of the pads shall conform to the following specifications:

The pads shall be of the compound known as Neoprene, shall be cast in molds under pressure and heat. Compositions

for pads shall meet the requirements listed. Test specimens shall be in accordance with ASTM Method D 15, Part B.

TABLE 10

Physical Properties	Grade (Durometer)	
	60	70
Original Physical Properties		
Hardness ASTM D 676	60 ± 5	70 ± 5
Tensile Strength, Minimum psi, ASTM D-412	2,500	2,500
Elongation at Break, Minimum Per Cent	350	300
Accelerated Tests to Determine Long-Term Aging Characteristics		
Oven Aged, 70 Hours/212°F., ASTM D-573		
Hardness, Points Change, Maximum	0 to +15	0 to +15
Tensile Strength, % Change, Maximum	±15	±15
Elongation at Break, % Change, Maximum	−40	−40
Ozone, 1 ppm in Air by Volume, 20% Strain, 100 + 2°F., ASTM D-1149*		
100 Hours	No Cracks	No Cracks
Compression Set, 22 Hours/158°F., ASTM D-395, Method "B"		
% Maximum	25	25
Low Temperature Stiffness, ASTM D-797		
At −40°F., Young's Modulus, Maximum psi	10,000	10,000
Tear Test, ASTM D-624, Die "C"		
Pounds/lin. in., Minimum	250	250

*Samples to be solvent wiped before test to remove any traces of surface impurities.

Appendix B

TABLE 11

ELASTOMERIC BEARING PADS

	60 Durometer				70 Durometer			
	AASHO Spec	Commercial Neoprene[1]	Butyl	Chlorobutyl	AASHO Spec	Commercial Neoprene[1]	Butyl	Chlorobutyl
Original Physical Properties								
Tensile Strength, psi	2500 min	2650	2710	2330	2500 min	2900	2650	2200
Elongation, %	350 min	575	680	530	300 min	340	480	430
Hardness, Shore "A"	60 ± 5	60	64	61	70 ± 5	75	75	68
Oven Aged 70 Hours at 212°F								
Tensile Change, %	± 15 max	− 10	− 8	− 14	± 15 max	+ 5	− 8	− 9
Elongation Change, %	− 40 max	− 27	− 23	− 15	− 40 max	− 25	− 27	− 9
Hardness Change, Pts	0 to + 15	+ 7	+ 1	+ 6	0 to + 15	+ 5	+ 6	+ 4
Ozone Resistance, After 100 Hours at 1 ppm								
100°F, 20% Strain	No Cracks	No Cracks	No Cracks	No Cracks	No Cracks	No Cracks	No Cracks	No Cracks
Tear Strength ASTM D-624, Die "C"								
Pounds Per Linear Inch	250 min	270	290	275	225 min	270	305	275
Low Temperature Stiffness, Young's Modulus, psi								
At −40°C (−40°F)	10,000 max	8500	5000	7800	10,000 max	7600	9200	5400
Compression Set, Method B, %								
22 Hours at 158°F	25 max	18	21	19	25 max	12	22	19

[1] Information obtained from Supplier

Appendix C

TEST PROCEDURE

Compressive Load Tests

The pads, two at a time with the steel plate between them, were subjected to the full vertical compressive load of 144,000 lb (2,000 psi on 6- × 12-in. area) to "set" the pads. This load was removed immediately after application. The full load was then applied again with vertical deformation recorded every 10,000 lb. The full load was then held for 10 minutes with vertical deformation being recorded after 5, 6, 7, 8, 9, and 10 minutes. The load was applied at such a rate that the full load was applied in approximately 4 minutes. The load was then released with deformation readings being made every 10,000 lb. After the load was removed, deformation readings were made every minute for 10 minutes to indicate "recovery."

Shear Load Tests

The pads, two at a time with the steel plate between them, were subjected to a vertical compressive load of 43,200 lb (600 psi). The plate was then pushed horizontally with increasing horizontal loads to a maximum of 40 percent of the vertical load; in this case the maximum was 17,280 lb. The horizontal movement of the plate was recorded every 5,000 lb. The maximum horizontal load was maintained for 5 minutes with horizontal deformation readings recorded every minute. The corresponding

vertical deformations were recorded. As the horizontal load was released, both horizontal and vertical deformation readings were made every 5,000 lb. After the horizontal load was removed, deformation readings were made every minute for 5 minutes to indicate recovery. The vertical load was then released and horizontal and vertical deformations recorded. Additional readings were made of vertical and horizontal deformation after $2\frac{1}{2}$ minutes. This procedure was repeated for vertical loads equivalent to 800 psi, 1,000 psi, and 1,200 psi. By removing the vertical load as well as the horizontal, it was possible to determine the indicated movement of the plate beyond the pads. If necessary, the pads were recentered on the steel plate between horizontal tests.

Fatigue Tests

The fatigue tests were a repetition of the horizontal tests. Two 6- × 12- × 1-in. pads with a steel plate between them were placed in the test apparatus and subjected to a sustained vertical load of 57,600 lb (800 psi). A horizontal force of 23,000 lb (assumed to be divided 11,500 on each pad) was alternately applied against the opposite 6-in. faces. The horizontal movement of the steel plate was recorded every 5,000 lb. The maximum horizontal load was maintained for 5 minutes and then released. The jack was then moved to the opposite side and the procedure repeated in the opposite direction. This reversal was repeated 9 times (9 forward and 9 back) and took place in a total elapsed time of approximately 3 hours. The vertical load was maintained throughout the test with vertical deformation being recorded.

Constant Deflection Tests

The sample specimen, 2 × 2 × 1 in., was compressed between steel plates with spacer bars on each side of it. The spacer bars were 0.75 ± 0.001 in. thick so that a 25 percent deflection resulted when the plates were drawn together in contact with the spacers. Duplicate 70 Shore "A" hardness samples were evaluated.

All test samples were cut from 9- × 12- × 1-in. bridge pads, placed in the test device and exposed to outdoor weathering beginning January 9, 1961. All data are the result of gaging the samples after they had remained at room temperature for 2 hours.

Constant Load Tests

The sample specimen, 1 × 1 × 0.5 in., was placed between the plates of a calibrated spring loading device (Method A ASTM D-395) under a 400-lb load (the limit of the apparatus). The duplicate samples evaluated were cut from the same bridge pads as used in the constant deflection tests. Testing conditions were indoors at room temperature. Observations were recorded at 14, 60, and 180 days.

Discussion

S. W. SCHMITT, Elastomers Laboratory, E. I. du Pont de Nemours and Co.—The University of Rhode Island Report, carried out in cooperation with the Enjay Laboratories, is an excellent effort and the authors are to be complimented. A number of test conditions do not simulate actual use, however, and any conclusions which are drawn should be interpreted with a few additional thoughts in mind. These specific comments are offered:

1. Low-temperature load-deformation tests, to be meaningful, should be run to simulate the actual bridge conditions when ambient temperatures change. A bridge span will contract slowly and an elastomeric pad will gradually stiffen as the temperature goes down. The deflection tests in this report were carried out on pads that were

conditioned at a temperature of -45 F. The forces were applied and deflections measured entirely at this temperature. The actual load deflection curve for a bridge pad should be obtained by varying the two factors of temperature and deflection in small increments. A variation over the entire seasonal temperature range should be run.

2. Appendix B gives data on the pads tested to determine conformance to AASHO specification. Data on the neoprene pads were obtained from the supplier of the pads, but the others were presumably tested at the Enjay Laboratory. For comparability it would have been preferable for one laboratory to obtain all the data.

3. It is interesting to note that both butyl and chlorobutyl pads soften and lose load-bearing capacity as a result of aging at 250 F, but neoprene pads increase in load-bearing capacity.

4. Dynamic creep is shown as percentage creep rather than as actual increase in deformation. When this increase is shown in mils, neoprene is 166 as compared with 178 for butyl and 185 for chlorobutyl for the 70 hardness pads. More important, the creep values for the 60 hardness pads were 100 mils for neoprene, 167 for butyl and 190 for chlorobutyl (appended data). This data would indicate that neoprene compares most favorably even for the short test period involved. Longer test evaluations of ten years by the Elastomers Laboratory indicate that neoprene vulcanizates can be designed with creep-resistant properties equal to or superior to those of natural rubber, which has excellent creep-resistant properties.

5. Water absorption is largely controlled by the ratio of surface exposure to volume. Obviously, in a bridge pad installation, the edge surface only would be exposed and the pads would absorb negligible amounts of water.

6. The methods used for testing compression set are not very clear. The attempt to correlate compression set with creep and load-bearing performance is believed to be speculative.

EARL V. CLARK and KENDALL MOULTROP, Closure—The authors wish to thank their friends from DuPont for their comments. In reviewing these, however, it is feared that Mr. Schmitt has interpreted the presentation of these data as unjustly favoring one product compared to another. This was not intended. The authors have tried to present the results of an extensive study comparing three elastomers as bridge-bearing pads. It is only by such continued exploration in this relatively new application for rubber that the ultimate utility of elastomeric bridge-bearing pads will be defined. Continued work will uncover advantages that were not realized when elastomeric bearings were first introduced to the bridge engineer. Evidence of this can be found in work published by Zuk, HRB Bull. 315, 27-34 (1962), showing that elastomeric bearings reduce impact stresses, hence could lead to structural economy and/or improved fatigue life. This could be a significant advantage for elastomers, particularly the high hysteresis type which display high mechanical damping.

Of course, research invariably suggests areas for further work. For example, the need for information at low temperatures was emphasized by Fairbanks, Jour. of Structural Division Proceedings, ASCE, 73-85 (Dec. 1961). Reservations in this same area have also been expressed in private communications with bridge engineers from state highway departments and private enterprise.

In view of this, data at low temperatures seemed to be a needed and significant contribution to the growing information on elastomeric bearing pads. Similarly, data demonstrating the longevity of these materials might alleviate reservations in this area and contribute to the expanded use of elastomeric bearings. Finally, a variety of elastomers can be compounded to meet the basic specifications for bridge-bearing pads, although at present only neoprene can be used. Data are needed to demonstrate the load-bearing properties of other elastomers and thus assist the bridge engineer in selecting and designing an elastomeric bearing that will best suit the service condition to be encountered.

With this as background, it is hoped that the following will answer Mr. Schmitt's specific comments:

1. Although Mr. Schmitt's suggested test procedure perhaps more closely simulates actual service conditions, it is felt that the results could not be easily interpreted and would be very difficult to reproduce. To obtain reliable engineering data, it is essential that rubber specimens be tested at some equilibrium temperature. This insures that the temperature recorded is indeed the temperature of the specimen under test. Preconditioning is a common and necessary technique to insure temperature equilibrium. Moreover, it is seriously doubted that the performance of the elastomers tested would have been very different using the suggested technique. Of course, the reporting of additional data in this area would be most useful to bridge engineers.

2. The commercial neoprene pads were available only from the rubber manufacturer, a reputable organization where ability to run the standard ASTM tests was not questioned.

3. The authors indeed agree and stated that the neoprene pad showed a slight stiffening, while the other pads tested showed a slight increase in compressive deflection. However, the basic contention is that the very severe aging conditions chosen demonstrate that all three bearing pads will display excellent retention of load-bearing properties with age. Stiffening under load, however, does not indicate superior load-bearing properties. Stiffening under load usually contributes to increased creep.

4. Although creep is normally expressed as percentage, the authors take no exception to recording the actual increase in deformation, provided the original deflection is also noted. The comment regarding creep with the 60 Shore "A" hardness pads is well taken. However, in expressing creep in conventional terms, namely percent, one observes the 60 hard neoprene pad showed only half the creep of the 70 hard pad. Although creep generally increases with hardness, this magnitude of difference is totally unexpected. The data on the other two polymers tested were consistent with experience. No ready explanation for this can be offered.

5. Water absorption tests were run according to the standard ASTM methods. The results are completely relative, and it was stated that all three elastomers were excellent in this respect.

6. The compression set method used was ASTM D-395, which was modified as explained in Appendix C. No attempt was made to directly correlate compression set with creep or load-bearing properties. The reader is referred to the section on test equipment.

Suggestions for Reducing Costs in Prestressed Concrete Bridges

NORMAN L. SCOTT, Executive Secretary, Prestressed Concrete Institute, Chicago, Ill.

The objective of this report is to offer a number of ideas for decreasing the cost of prestressed concrete bridges. With the exception of the proposal for increased tensile stresses, all of the ways can be incorporated within the existing 1961 AASHO Standard Specifications for Highway Bridges or the 1961 Interim Specifications. The primary theme here is "keep it simple." About one-half of the suggestions must be incorporated during the initial conception of the bridge design, but the other one-half deals with details. Several of the schemes advanced are especially worthwhile where headroom is critical. If headroom is not critical, a design using large sections with wide spacing is suggested.

• PRESTRESSED CONCRETE has now been established as economical and practical for bridges ranging from 40 to 100 ft in all parts of the country. With the exception of a half dozen states, prestressed concrete is almost always considered at some phase of the planning for bridges in the medium-span range.

Bridge engineers are generally not considering prestressed concrete for short-span bridges (below 40 ft) and long spans (120 to 500 ft). Bridge engineers might also investigate the material for these span ranges because experience both here and abroad indicates that prestressed concrete is often competitive. With the existing AASHO-PCI standards, prestressed concrete is not generally competitive with reinforced concrete on spans below 30 ft. However, the solid and cored flat slabs have often been an economical solution for spans of 30 to 40 ft (Fig. 1). The slabs can be designed with either a composite concrete topping left exposed with grouted joints or covered with an asphaltic wearing surface.

Prestressed concrete should also be seriously considered for long-span bridges. There are numerous examples of long-span structures designed within alternate materials that have resulted in awards to prestressed concrete. An outstanding example is the Lake Maracaibo Bridge in Venezuela (Fig. 2) with five 771-ft spans of stayed girder construction that are 148 ft above the shipping channels; reinforced concrete towers 300 ft high; 620-ft post-tensioned cantilever girders for the long span; a prestressed drop-in span 151 ft connecting the cantilevers; and staying elements for the cantilever girders also of prestressed concrete. Another example is the Medway Bridge in England (Fig. 3) which will have a 500-ft center span and 312-ft side spans when completed. The approach spans are of precast post-tensioned I-girders; the center span consists of two 200-ft box-section cantilevers with a 100-ft drop-in span; and the bridge is approximately 144 ft wide and about 107 ft above high water.

The United States has the materials and the design and construction know-how, but is lagging far behind European countries in this area. So much for short- and long-span bridges. Because the main objective of this report is to suggest ways for saving money on medium-span bridges, the following will apply to designs in this range.

Paper sponsored by Committee on Construction Practices — Structures.

Figure 1. Prestressed flat slab bridge at Eureka, Calif. Spans are 30 ft except for navigation span which is 105 ft composed of post-tensioned I-girders. The piers are of 20-in. square pretensioned square piles.

Figure 2. Lake Maracaibo Bridge.

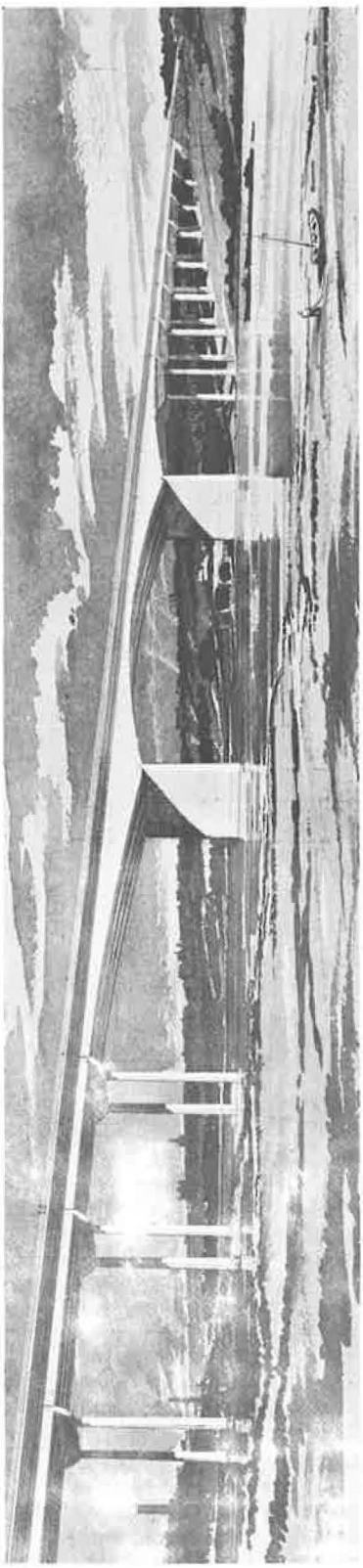

Figure 3. Medway Bridge.

Suggestions one through seven deal with ideas that would usually be considered in the initial planning of the bridge. Suggestions eight through sixteen pertain to schemes for simplifying details to cut production and construction costs. Almost all of the suggestions proposed herein have one common principle: the design should be so made that production and construction operations will be as simple as possible.

1. Use standard sections. —The use of standard bridge sections has become such a common practice that this suggestion is hardly worth mentioning. But departments that do not now have a set of practical and economical standards for prestressed concrete girders would be well advised to settle on the proven AASHO-PCI standards rather than trying non-standard sections. Single purpose steel forms are the only acceptable answer for casting prestressed concrete beams. These forms are expensive, and in order to reduce write-off costs they should be used over and over. States that have used standard sections for a period of years are now paying almost nothing for form write-off. For example, Florida has been using standard AASHO-PCI sections since 1957. Former Assistant State Highway Engineer William E. Dean told a Purdue University Conference that bid prices on type II beams came down four percent, type III beams more than six percent, and type IV beams almost ten percent between 1959 and 1961. This drop in prices occurred even though Florida was buying fewer beams in 1961 than in 1959.

2. Wherever practical make parts in bridge identical. —Naturally it is not often possible to make a bridge composed of identical spans and girder sizes with the same pier design, etc., but this should still be considered as the most desirable solution. If the principle of repetition is held to be of utmost importance, it is often possible to rework the design in such a way that many aspects of the bridge design are identical. For example, on overpass structures it is often possible to use the same girder section throughout by expanding the spacing on the short spans (Fig. 4). Prestressed concrete manufacturers and bridge contractors offer better bids on work that allows repetitive operations. Labor costs are always much higher during the early stages of an operation involving repetitive work than after the team gets coordinated and into a routine. Experience has shown that producers and contractors attach a great deal of importance to this consideration and for good reason.

3. Use as few girders as possible in each span. — This means that if there is a choice of using four type IV girders or six type III girders, choose the four-girder design. This, of course, assumes that headroom is not a problem. The wider spacing of girders may require a thicker or

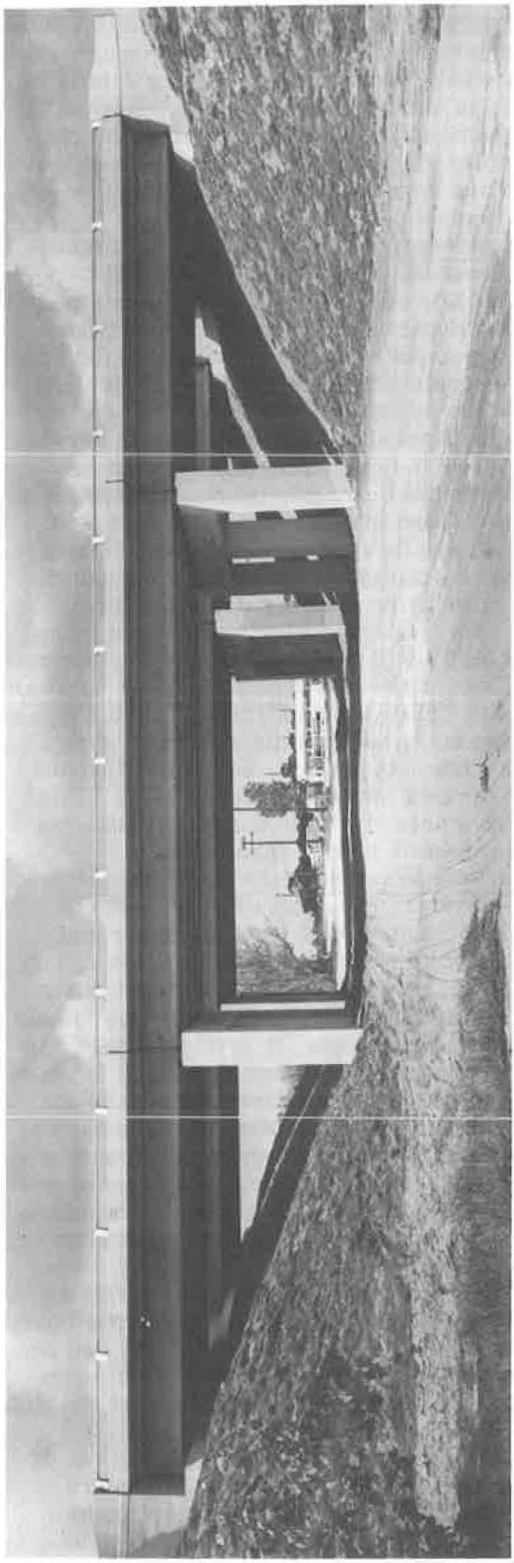

Figure 4. Typical overpass on Sunshine State Parkway, Florida. Structure is a fine example of design simplicity which is a key factor in low-cost prestressed bridges.

a more heavily reinforced deck slab, but the savings in girder costs will usually more than offset higher slab costs. It is also often possible to use fewer girders per span without going to larger sections by prestressing them higher (Figs. 6 and 7).

4. Prestress sections higher. — The AASHO-PCI standards can be prestressed to the upper limits allowed by the AASHO specifications without ill effects. A review of present practice shows that many States could prestress their sections considerably higher and either get longer spans or reduce the number of girders in each span. An AASHO-PCI type III girder will span up to 80 ft with a 5-ft spacing (H 20-S16-44 loading), and a type IV girder will span 100 ft on 6-ft centers. To aid the designer in choosing the most economical beam size and spacing, it is often helpful to prepare a set of beam-spacing charts for standard sections. This task is made easier with the use of a computer. Figure 8 shows a simplified version of a design chart prepared for this purpose by the Office of Bridge Engineer, State Highway Commission of Wisconsin.

5. Consider possibility of specifying higher release strength to prestress sections higher. — The AASHO specifications allow a net prestress of 60 percent of the strength of the concrete at release. Almost all States are now releasing at a concrete strength of 4, 000 psi. This means that the maximum permissible prestress in the bottom of the girder is 2, 400 psi. If the release strength was set at 5, 000 psi, one could precompress the same section to 3, 000 psi. With 6, 000-psi release, the prestress could be increased to 3, 600 psi. Figure 8 shows the influence of release strength on the girder design.

Higher release strengths may require (or at least induce) higher 28-day strengths, but concrete technology has now advanced to the point where 7, 000-8, 000 psi concretes are practical for routine production in many areas. This idea is especially useful where headroom is critical, because it may allow the use of a smaller section. The approach could also save

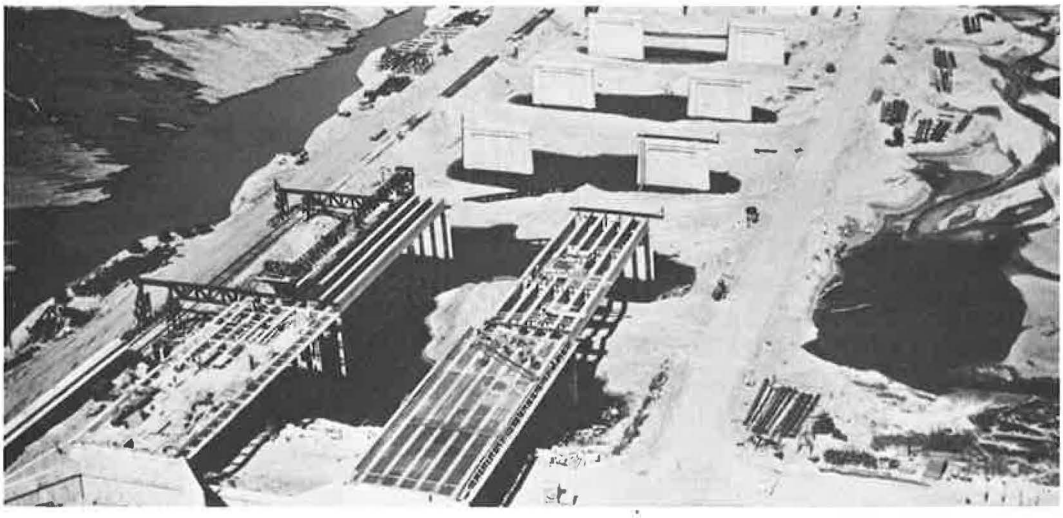

Figure 5. On larger bridges it is easier to get good repetition. This bridge over the Platte River near Ashland, Nebr., used 168 identical beams 110 ft long. The pilings for the piers were also of one size (14-in. octagonal) although the lengths necessarily varied (65 to 95 ft).

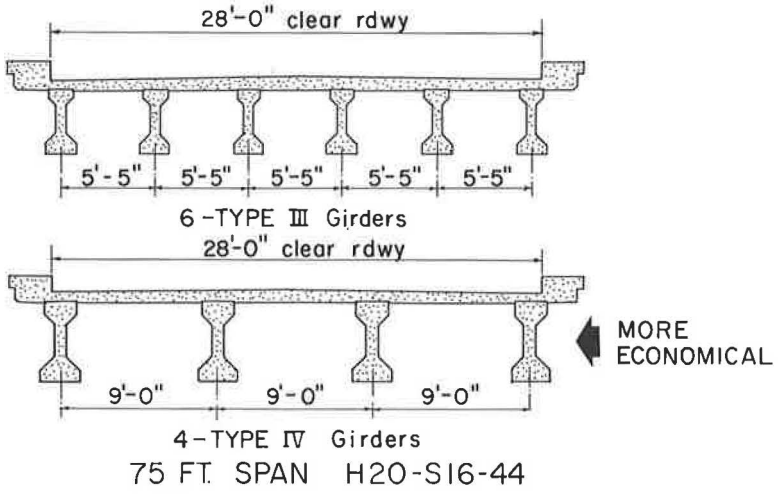

Figure 6.

money even when headroom is not critical if the increase in prestress would allow stepping down to a smaller standard. For example, if a design calls for four type III girders per span but they are only lightly prestressed, it may be possible to put more prestress into a type II girder by calling for a higher concrete release strength and thus save money on each girder.

The bridge for the elevated roadway at Chicago's O'Hare Field was designed with a very low depth-to-span ratio by using pretensioned I-sections released at strengths as high as 6,600 psi. The 28-day strength for the concrete exceeded 8,000 psi (Fig. 9). The prestressed concrete fabricator carefully prepared for these requirements and was completely satisfied with the project.

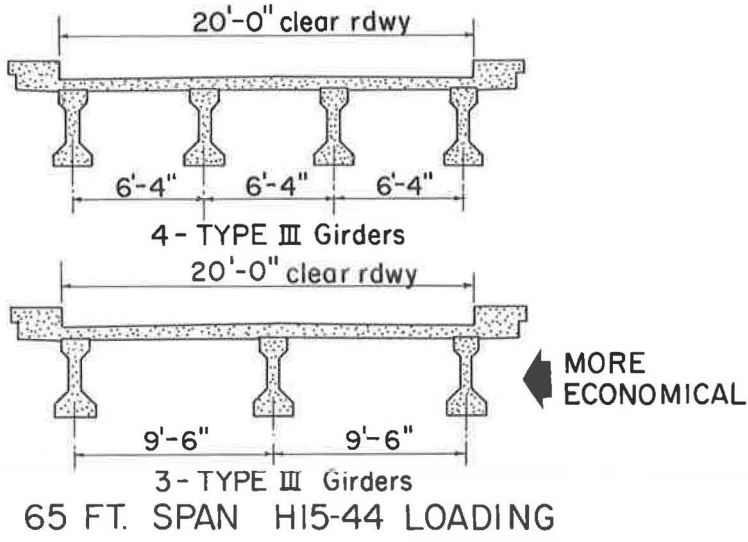

Figure 7.

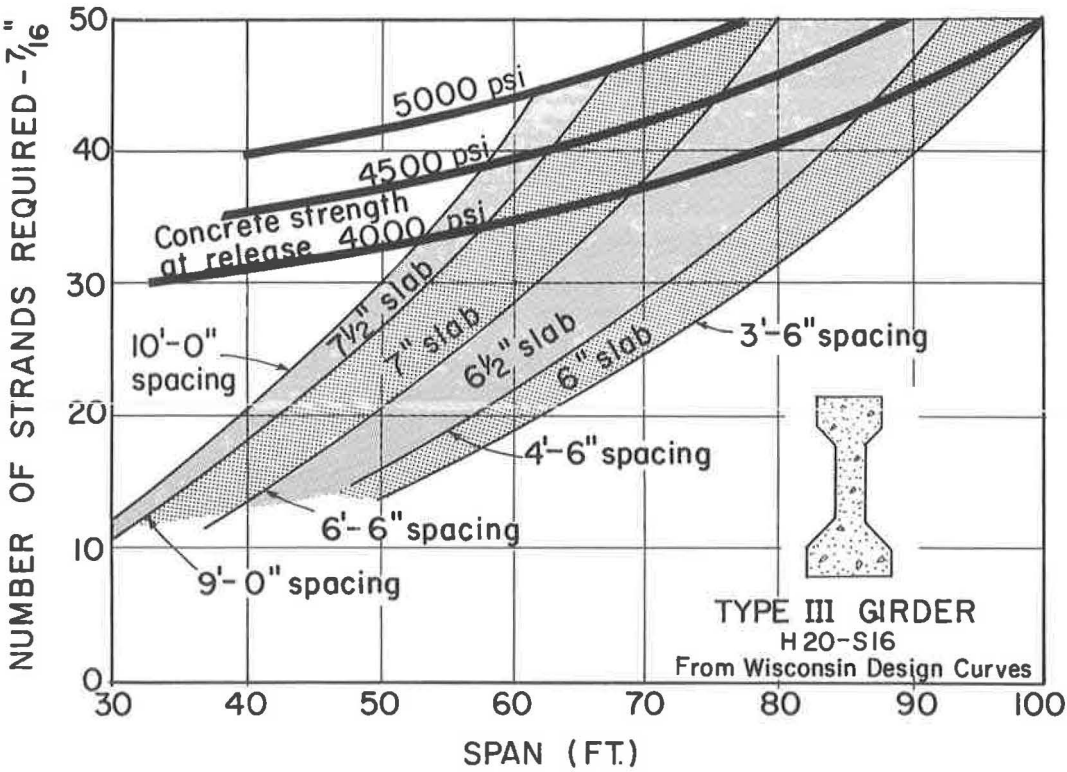

Figure 8. Typical simple design chart for prestressed bridge girders.

Figure 9. Elevated roadway structure at Chicago's O'Hare Field.

6. Use mild steel continuity in composite deck. —Due to the many considerations in continuous design, it is not possible to say that mild steel continuity will always make a more economical design than simple spans. But the idea is worth investigating, because aside from the possible immediate savings, continuity offers several fringe benefits. Perhaps one of the best benefits is the elimination of the costly and troublesome joints in a bridge. Continuity also improves the appearance of overpass structures by closing the gaps between the girder ends. Mild steel will also increase the rigidity and ultimate strength capacity of the bridge, although under the existing specifications there is certainly no need for this. The Portland Cement Association conducted some rather extensive research on this type of bridge (1) (Fig. 10).

Prestressed concrete box beams and cored slabs which have a low depth-to-span ratio to start with can be designed for even longer spans with the use of continuity. In urban interchange structures where headroom is important, this could be an economical solution.

7. Use prestressed piles to double as foundations and piers. —If the L/D ratio is not greater than 25, it is entirely practical to use prestressed piles to double as columns for the piers. This can be considerably more economical than using a separate foundation and pier (Figs. 1 and 11). When more than four square prestressed piles are required for each pier, the structure may not present the most pleasing appearance from below; however, this is not an important factor in many river crossings. Cylindrical prestressed piles can even solve the appearance problem, making an acceptable design for urban and freeway structures.

Washington has had good success with the pretensioned cylindrical pile pier (Fig. 12). Bridge Engineer Winfred T. Robertson told the Seattle ACI fall convention that its bridges built with prestressed pile piers average about $11 psf, whereas structures resting on piles, conventional footings, and piers cost between $15 and $18 psf. He also reported that for stream and lake crossings, the cost difference between bridges supported by pile piers and those of more conventional design equals or exceeds the cost of cofferdams, seals and footings.

The details in a prestressed bridge can also make the difference between an expensive design and an economical one. Following are some ideas for paring costs in the bridge details.

8. Eliminate end blocks in pretensioned girders. —The 1961 Interim Specifications now allow use of pretensioned I-girders without end blocks. Laboratory research and field tests have proven that they are not necessary. The end block has always been a problem for prestressed concrete producers. End block forms cost more money than straight forms but the big cost has been in production setup time. Side forms for every

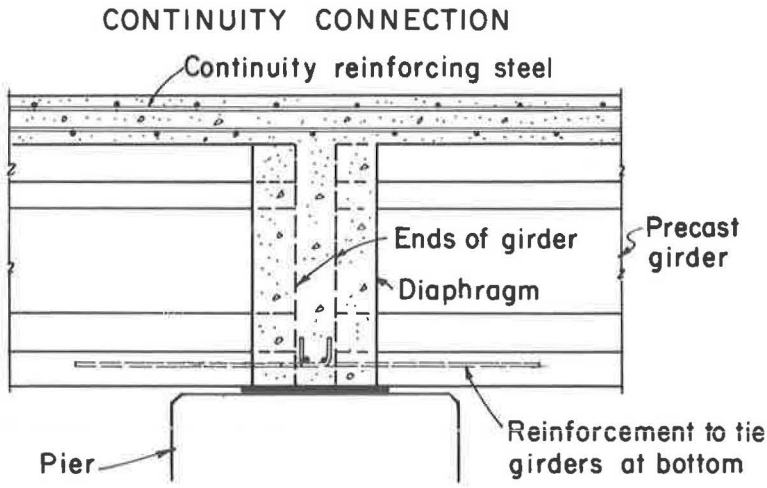

Figure 10. Typical section at pier of precast prestressed concrete bridge made continuous by use of mild steel in deck.

Figure 11. Four 24-in. square prestressed piles extend to provide pier columns for typical Florida crossing.

Figure 12. Driving pretensioned cylinder piles for a bridge in Tacoma, Wash.; 48-in. piles driven plumb to act as columns for piers.

end block type girder have to be individually assembled. Without end blocks the forms can be assembled into one continuous line with end bulkheads set in where required (Fig. 13). States making the change to girders without end blocks will notice a decrease in prices reflecting the reduction of labor costs for assembling and dismantling forms.

9. Eliminate projections from sides of girders whenever possible. —When steel bearing plates must project beyond the sides of the girder, it is better to add this plate after the girder is cast by welding or other fastening methods. Projecting plates and bars that are to be cast in the beams require that the side forms be cut to receive the projecting items. Of course, the location of these holes changes with each different girder. These cutting and plugging operations are not only time-consuming, but they ruin the forms prematurely (Fig. 14).

10. Eliminate shear keys. —Depending on how they are designed, shear keys can be a nuisance at best or a significant cost item at worst. In any event they do not contribute to improving composite action as has been shown by laboratory and full-scale

tests. This is just one more cost item that can be eliminated without sacrificing structural behavior. Portland Cement Association Bulletin D35 reports on horizontal shear research and includes references to several other studies.

11. Hold down amount of mild steel in prestressed girders. —There are many bridge offices designing prestressed girders on a "don't skimp on the reinforcing" policy. Although this sounds commendable, such practice can easily lead to uneconomical designs. The extra steel usually serves a very limited purpose and simply makes an important contribution to high costs. Shear reinforcing should be computed as recommended in the AASHO specifications. The amount of steel required at the quarter point is carried back to the end. End zone steel should be designed according to provision 19 in the 1961 Interim Specifications. When mild steel in a girder starts to exceed 8 lb/ft for a type II, 10 lb for a type III, or 12 lb for a type IV, the designer should take a careful look at each piece to see if it is really necessary.

Figure 13. A line of finished girders with end blocks (left), and a line of forms for similar girders (right). Due to presence of end block, each beam must be formed up individually. Without end blocks forms are set up in one continuous line with sections permanently assembled in easily handled lengths.

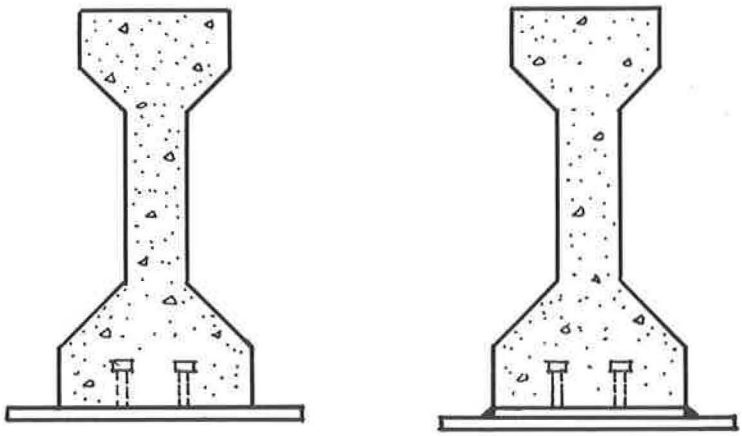

Figure 14.

12. Design stirrups so that fabrication is simple. —It is very helpful to the producer if the stirrups are detailed in such a way that he can make prefabricated cages of the reinforcement. If the stirrups cannot be made into cages, then they should be designed so that they can be easily tied into place after the strands are tensioned. It is not necessary to have the stirrups surround the strands, and such a procedure greatly increases fabrication costs. If the designer feels that he must have stirrups surrounding the strands, he should place just a few at close intervals at the ends of the beam. An even simpler practice is to use metal strapping (Fig. 15). Beyond the bond transfer zone of the strand (about 50 strand diameters) there are no significant lateral stresses in the beam, and wrap-around stirrups or metal straps serve no useful purpose. Notice that the second beam line from the right in Figure 13 shows the strands tensioned and the end bulkheads set, but the mild steel reinforcing has not yet been placed. This is the normal sequence of operations. It can be seen here that surrounding stirrups would either have to be bent in place or threaded on the strands prior to tensioning and then spaced out. Either way the operation is expensive and time-consuming. Of course, metal strapping can be placed on the strands after tensioning with no difficulty. Notice that a prefabricated cage similar to that in Figure 16 C can be placed over the tensioned strands whether they be straight or deflected. The AASHO specifications require a transverse bar in the bottom of pretensioned girders. This can be easily handled by tying in a small straight bar. An alternate to the prefabricated cage is a design employing two bars (Fig. 16 B). This bar provides a tie for the composite slab, vertical shear reinforcement and the bottom transverse tie all in one piece.

13. Use largest and strongest strand available. —Use of large diameter strand and strand with higher ultimate strength will reduce costs. The material cost is lower in the first place, but labor costs are reduced also. As an example, consider a beam designed with 65 strands ($\frac{3}{8}$-in. diameter) with an ultimate strength of 250, 000 psi. The same net prestressing force can be provided by 31 strands ($\frac{1}{2}$-in. diameter) with an ultimate strength of 270, 000 psi, but the material cost will be 14 percent lower. The larger diameter strand will often provide an added bonus because of the opportunity to increase the eccentricity of the smaller strand pattern.

14. Use elastomeric pads instead of metal bearing assemblies. —Laboratory tests and field experiences indicate that synthetic rubber pads are perfectly satisfactory for bridge bearings. The use of these pads in place of metal bearing assemblies can mean large savings in the cost of prestressed bridges. Metal bearing assemblies often represent a sizeable proportion of the cost of a bridge superstructure. Elastomers can reduce bearing costs as much as 95 percent and may even do a better job.

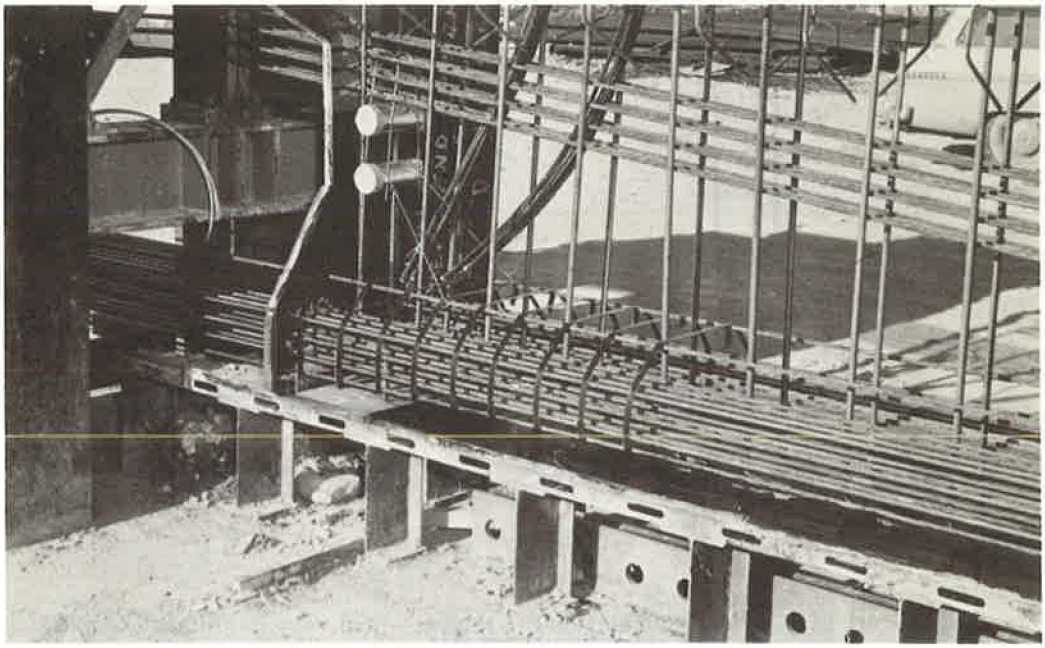

Figure 15. Use of metal strapping.

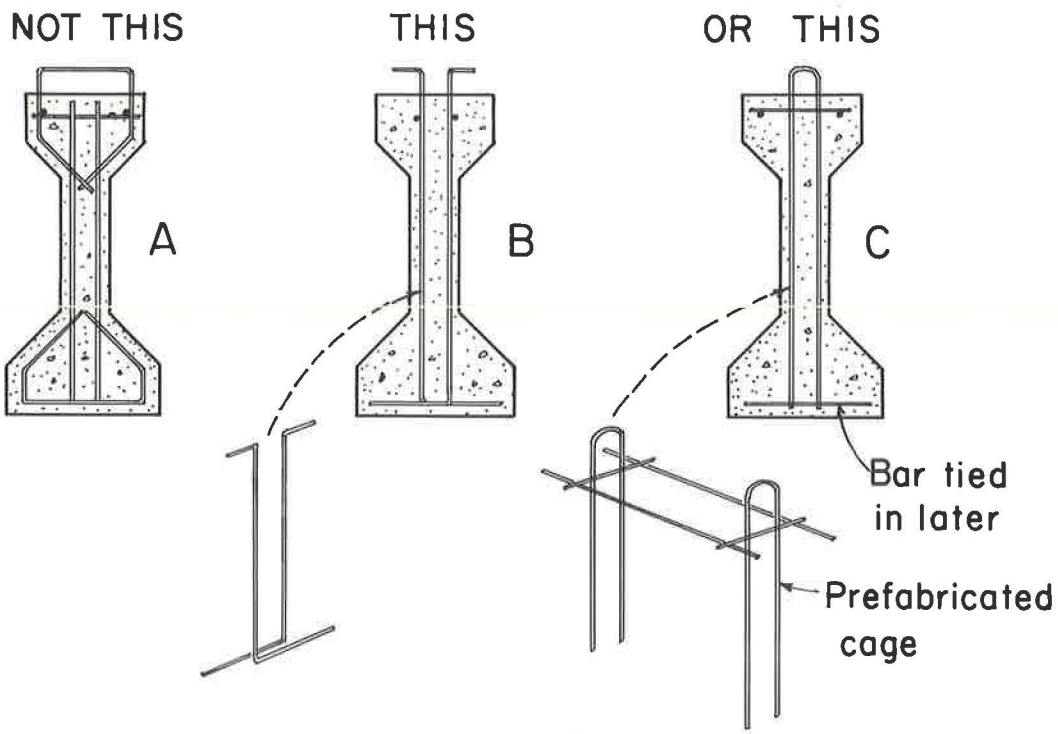

Figure 16.

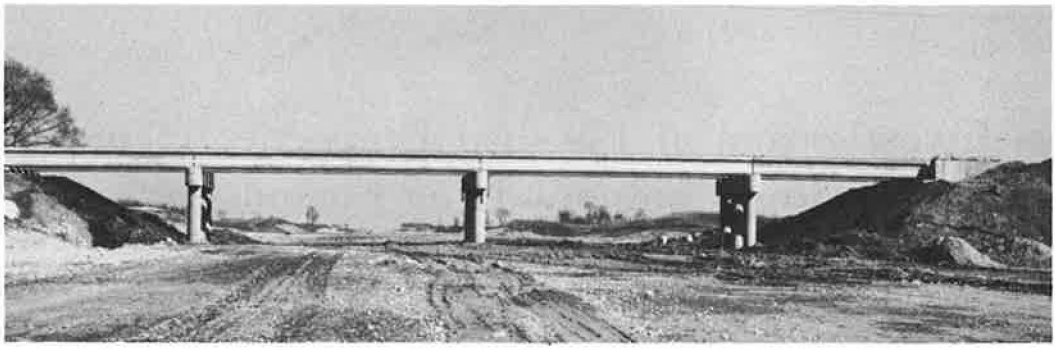

Figure 17. Typical structure on Illinois Toll Highway incorporated many of the cost-saving ideas listed herein.

15. Eliminate steel base plates for elastomeric pads. —This may not be practical if the bridge is on a skew or on a superelevated curve because there must be some positive method of keeping the bearings in place. But for a straight bridge, the steel base plates can be safely eliminated. When the plate is eliminated the bottom of the girder must be true and smooth in the bearing area.

16. Eliminate or reduce diaphragms. —Casting concrete diaphragms on prestressed bridges is a costly problem for bridge contractors. If the diaphragms are cast prior to casting the deck, the contractor must make elaborate preparations for a very small amount of concrete. If they are cast with the deck, his formwork is complicated considerably over a straight deck-forming job. From a design standpoint, the deck will provide at least as much distribution as assumed in the 1961 AASHO Interim Specifications. (S/5.5 for I-girders.) The diaphragms add little or nothing to the distribution of live loads depending on how they are designed. The often used design which consists of a concrete rib with a tie bolt running through the middle adds almost nothing to the distribution of live loads because of its inadequate ability to transmit transverse bending moment (2).

All of the previous suggestions for reducing costs have been tried in actual field experience and have proven satisfactory. As a point in fact, suggestions 1, 2, 6, 7, 8, 9, 10, 12, 14, 15 and 16 were incorporated in prestressed concrete structures on the Illinois Tollroad, completed in 1958 (Fig. 17). As a result of these measures, the Northern Illinois Toll Highway Commission was able to get an unusual value for its money in these structures which have performed almost flawlessly. George Jackson, Chief Engineer of the Commission, says that in these four years they have had no maintenance expense for the prestressed girders.

The proposals suggested in this paper are all possible within the existing AASHO Specifications for Highway Bridges. Another design procedure that would greatly reduce the cost of prestressed bridges is to allow tensile stresses in the bottom of the beams under full live load. The AASHO test road has shown that with 300-psi tension under design load, a prestressed bridge will perform perfectly even under 1½ million loading repetitions. For a fully prestressed section (i.e., maximum precompression) the allowance of 300-psi tension would reduce strand requirements 15 percent. For sections not prestressed so heavily the reduction would be even greater. It is understood that the HRB Bridge Advisory Committee has recommended that tensile stresses be allowed in pretensioned beams. Bridge engineers may wish to note this future specification change so that they may take advantage of it as soon as it goes into effect.

REFERENCES

1. PCA Development Department Bull. D34, D35, D43, D45, D46, and D51.
2. Janney, Jack, and Eney, W. J., "Full Scale Test of Bridge on Northern Illinois Toll Highway." World Conference on Prestressed Concrete Proc. (See also PCA Dev. Dept. Bull. D51.)

An Investigation of Physical Properties of an Epoxy Bonding Compound for Composite Beam Bridge Construction

H. A. MIKLOFSKY and M. J. GONSIOR, Respectively, Professor of Civil Engineering, University of South Carolina; and Graduate Research Assistant in Civil Engineering, Rensselaer Polytechnic Institute

This paper presents information on the basic properties of an epoxy resin bonding compound which is being studied for use as a structural connection for highway construction, including composite beam bridges. Several important physical properties of this resin have been determined, such as the tensile, compressive, shear, flexural fatigue, and torsional fatigue strength of the resin as a plastic, and also its modulus of elasticity and coefficient of expansion. Additional tests on the resin as an adhesive included the single shear strength and tensile strength between steel and concrete, effect of freeze-thaw cycling, effect of concrete curing on adhesive bond, consistency of adhesive, strength development of adhesive, storage life of adhesive, working life of liquid adhesive, and other related properties.

The results show that an epoxy resin formulation satisfying the strength demands of a composite beam bridge can be achieved, subject to the restrictions imposed by the testing program. However, further studies of performance and characteristics are necessary before the selected epoxy resin formulation can be approved for use as a connector; such as creep, fatigue on glued joints, impact, strength gain under various temperature conditions, and durability.

•THE WIDESPREAD industrial and commercial applications of epoxy bonding compounds have demonstrated that these materials are extremely durable and possess such properties as hardness and an ability for adhering to metal and other materials. Although these same properties would appear to qualify epoxy resins as a means of effecting structural connections, this field of application has remained relatively unexplored. The subject of this report is concerned with the investigation of physical properties of an epoxy resin bonding compound for use as a connection device for highway construction, including composite beam bridges. The work was performed at Rensselaer Polytechnic Institute for the Bureau of Physical Research, Department of Public Works, State of New York, in cooperation with the U. S. Department of Commerce, Bureau of Public Roads.

Because a large number of compounds can be formulated using the epoxy resins in combination with different catalysts, curing agents, fillers, flexibilizers, etc., the first problem was the selection of a suitable formulation for detailed study. This was accomplished by requesting recommendations in consultation with representatives of several producers of epoxy resins. With the recommended formulations as a starting point, a series of physical tests was conducted to classify the various formulations on a comparative basis, and also as a means for revising the formulations to serve the intended applications best. Several basic tests were conducted.

Paper sponsored by Materials and Construction Department and Committee on Bridges.

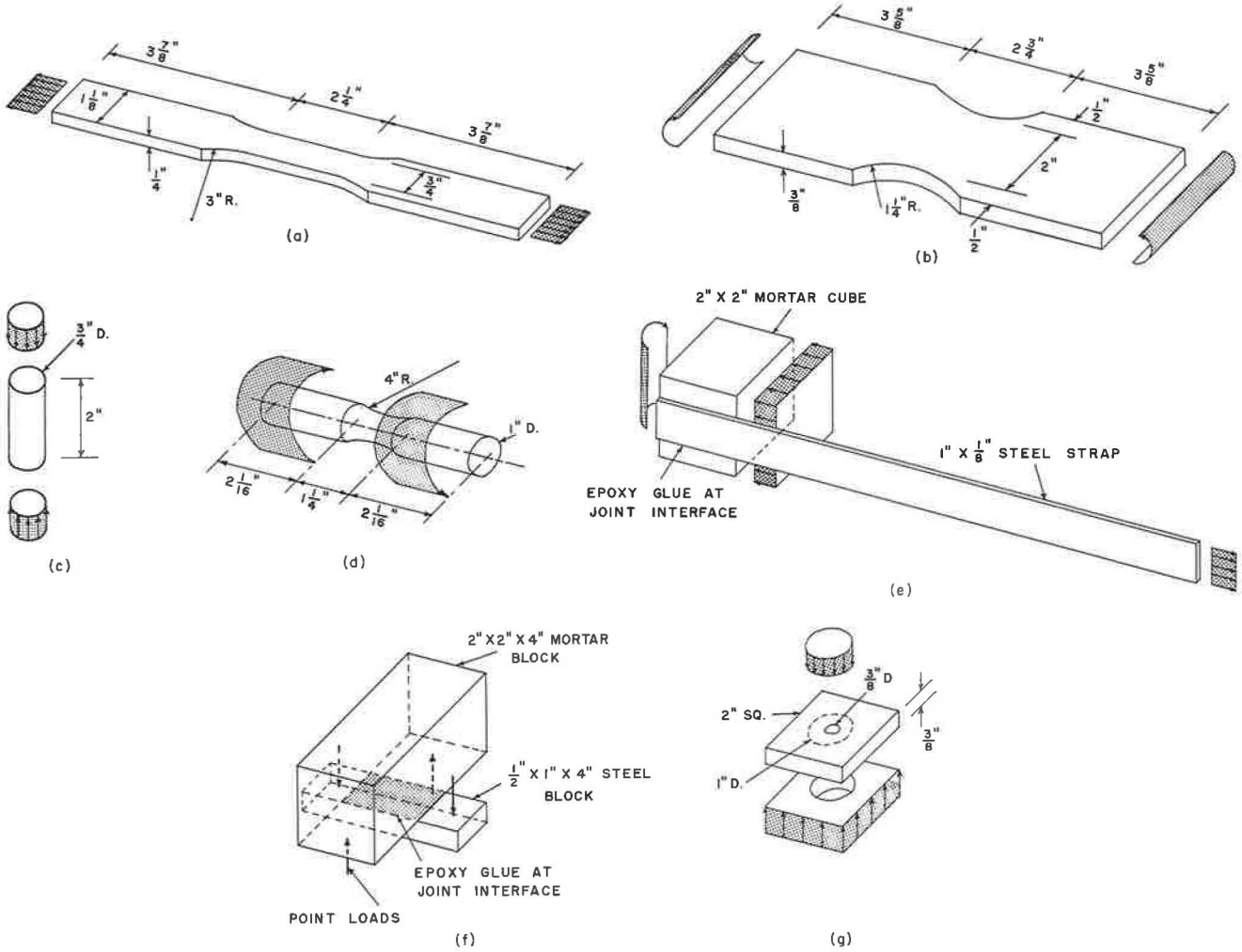

Figure 1. Specimen dimensions: (a) tension, (b) bending fatigue, (c) compression, (d) torsion fatigue, (e) single shear adhesion, (f) tension adhesion, (g) shear.

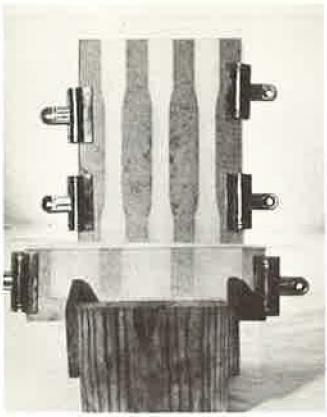

(a)

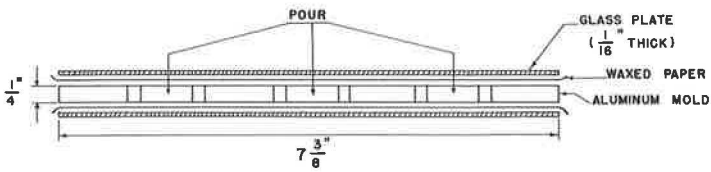

(b)

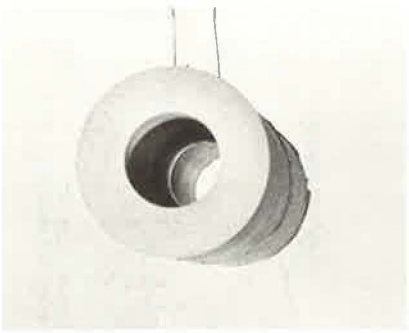

(c)

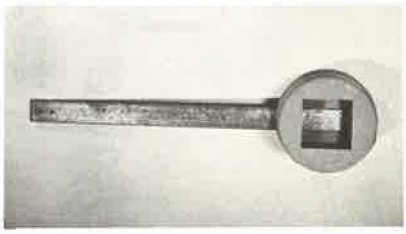

(d)

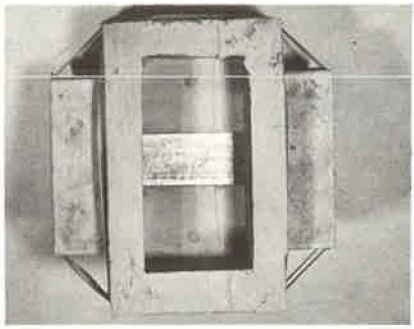

(e)

Figure 2. Mold types for casting specimens: (a) molds for tension and shear plastic specimens, (b) open-end view of tension specimen mold assembly, (c) silicone rubber mold for torsion specimen, (d) steel strap inserted in silicone rubber mold before casting single shear adhesion specimen, (e) steel bar inserted in silicone rubber mold before casting tension adhesion specimen.

TEST SPECIMENS

Figure 1 shows seven types of test specimens, their dimensions, and the manner of loading. The method of testing was similar in detail to the 1961 Standards of the American Society for Testing Materials, as identified in Table 1, but were modified or extended whenever necessary or convenient to do so (1). These tests were essentially intended to provide a means of classifying the various compounds, as well as to serve as a basis for control and comparison with other research results.

The tension, bending fatigue, and shear specimens were cast in aluminum molds which were coated with a thin film of silicone rubber; the silicone rubber acted as a release agent for the epoxy resin (Fig. 2a). Each mold was prepared by sandwiching the sheet of aluminum (with a cut-out the shape of the specimen) between two sheets of glass. On assembly of the mold, the inside surfaces of the glass were lined with heavy waxed paper to prevent the epoxy sticking to the glass. After the poured epoxy specimen had cured for approximately 24 hr, the molds were disassembled and the specimens were removed and placed in conditioning according to the schedule shown in Table 1. Table 1 gives the combinations of conditioning times and conditioning temperatures studied.

The compression and torsion fatigue specimens were cast in silicone rubber molds (Fig. 2c). Before testing, the ends of the compression specimen were machined square with the specimen axis.

To simulate the single shear condition in adhesive bond which would exist in a composite beam, mortar blocks glued to steel straps were tested in single shear. These specimens were cast in silicone rubber molds (Fig. 2d). Each mold consisted of two pieces which could be disassembled, one of which previously had been sandblasted. After the steel strap was inserted into the mold, the surface was coated with a thin layer of epoxy using a small paint brush. The thickness of the layer was approximately 0.015 in. The two pieces of the mold were held together by means of rubber bands. A 2-in. mortar cube was then cast on top of the epoxy in three layers, each of which was densified by tamping with fingers. The top of the mortar cube was struck off even with the top of the mold, and a sheet of waxed paper and a sheet of glass placed on top to prevent evaporation of the mortar moisture.

TABLE 1

CONDITIONING SCHEDULE FOR SEVEN TYPES OF TEST SPECIMENS

Test	Equivalent ASTM	Conditioning Time of[a]				Conditioning Temperature of				
		3 Days	7 Days	21 Days	90 Days	-40 F	20 F	77 F	120 F	180 F
Tension	D 638-60T	x	x	x	x	x	x	x	x	x
Flexural fatigue	D 671-51T		x					x		
Compression	D 695-54	x	x	x	x	x	x	x	x	x
Shear	D 732-46	x	x	x	x	x	x	x	x	x
Torsional fatigue	D 671-51T			x				x		
Single shear adhesion[b]	---	x	x	x	x	x	x	x	x	x
Tension adhesion[b]	C 321-57	x	x	x	x[c]	x	x	x	x	x

[a] Add two days at room temperature: one before conditioning, one after conditioning.
[b] Cured three days in water at room temperature before conditioning.
[c] 90-day tests not conducted for -40 and 20 F.

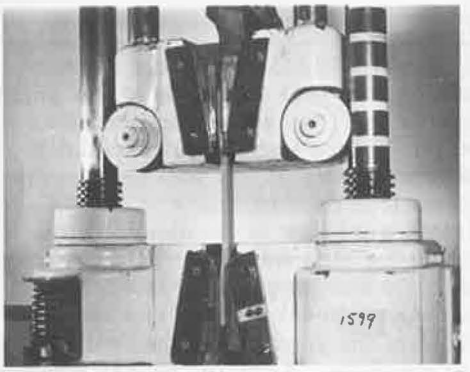

(a)

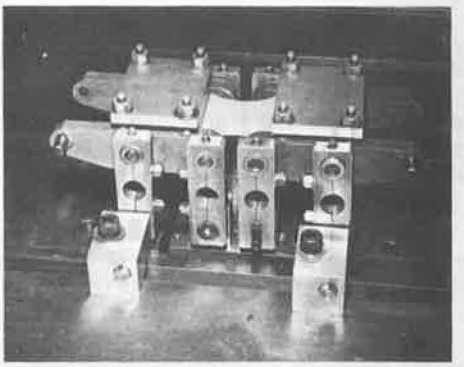

(b)

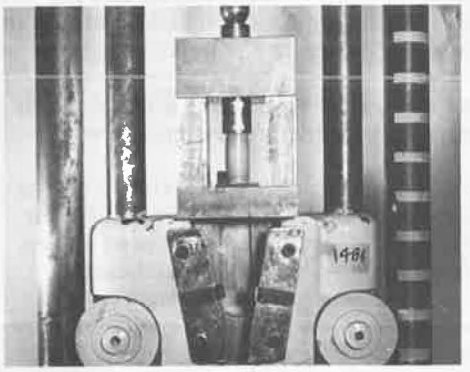

(c)

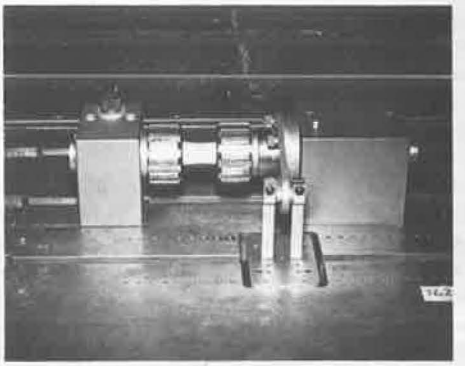

(d)

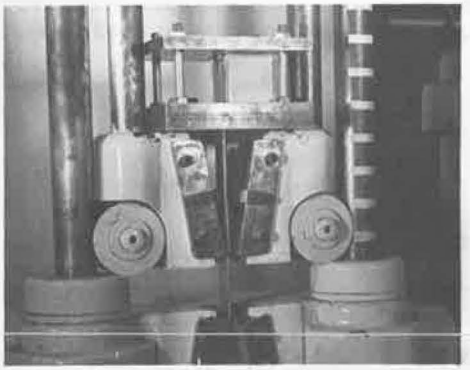

(e)

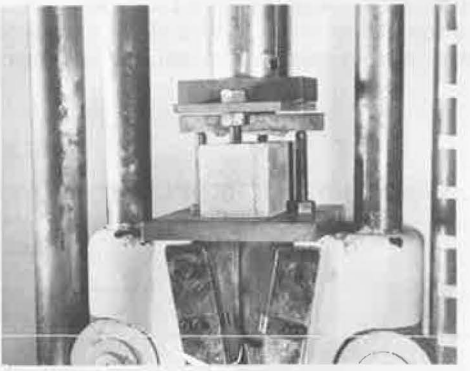

(f)

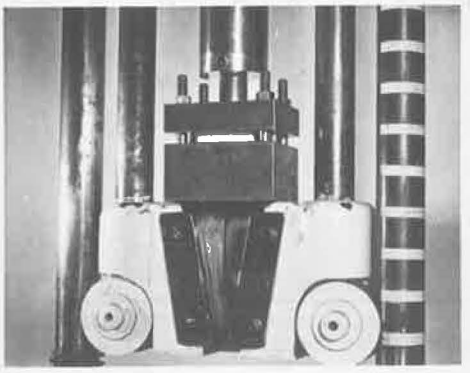

(g)

Figure 3. Specimens in testing machines: (a) tension test, (b) bending fatigue test, (c) compression test, (d) torsion fatigue test, (e) single shear adhesion test, (f) tension adhesion test, (g) shear test.

The single shear specimens were allowed to cure in their molds for one day; after which the molds were disassembled, and the specimens placed in a water tank for three days to insure adequate mortar curing. The specimens were then placed in conditioning according to Table 1.

The tension adhesion specimens were prepared in the same manner as the single shear adhesion specimens. Figure 2e shows the type of silicone rubber mold used for casting.

Figure 3 shows the various specimens being tested. A Riehle Model P-3 precision hydraulic universal testing machine was used for static tests, with a deformation rate of 0.05 in. per min. Sonntag universal testing machines were used for conducting the fatigue tests, operating at a rate of 1,800 cycles per minute.

The following criteria for failure were established:

Test	Criterion
Tension	Fracture load
Bending fatigue	Number of cycles for fracture
Compression	Maximum load or load at 25 percent deformation
Torsion fatigue	Number of cycles for fracture
Single shear adhesion	Fracture load
Shear	Maximum load
Tension adhesion	Fracture load

In the cases of the compression test, single shear adhesion test, shear test, and tension adhesion test different modes of failure were noted (Figs. 4, 5 and 6). Tension adhesion failures were similar to Figure 6.

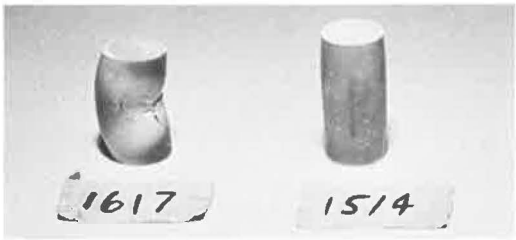

Figure 4. Compression failures by buckling (left) and bulging (right).

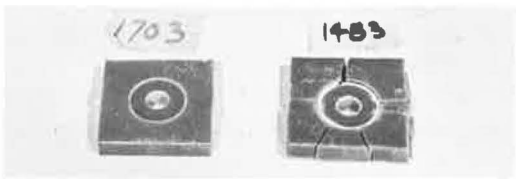

Figure 5. Shear failures by punching shear (left) and brittle shattering (right).

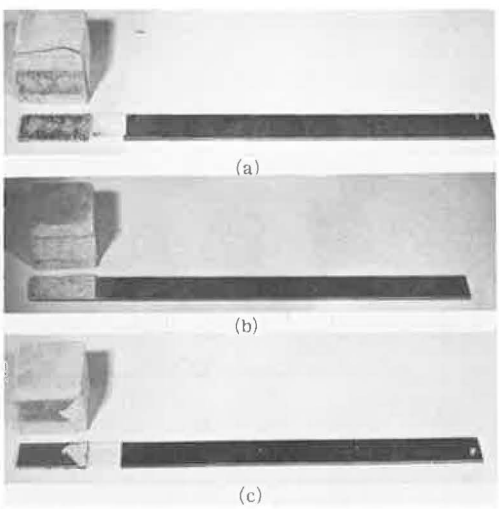

Figure 6. Single shear adhesion failures at (a) bond, (b) mortar, (c) bond and mortar.

FORMULATION

The preceding series of tests was conducted on most of the recommended formulations, and the formulations were revised as experience and test results indicated the necessity to do so. The results of the strength tests alone were not the critical factor in determining formulation revision. Other pertinent properties were viscosity, sprayability, brittleness, and flexibility. After a series of tests and observations had been made on all the recommended formulations and their revisions, enough information was accumulated to select a single formulation for detailed study. It is this formulation that is herein reported.

This formulation is given in Table 2.

Once this formulation had been selected, a production series of testing was carried out to determine the physical properties of this formulation both as a plastic and as an adhesive. In accordance with ASTM recommendations, a sufficient number of speci-

TABLE 2

STUDY FORMULATION

Component	Parts by Weight
A:	
Resin[a]	100
Silica flour No. 219	12.5
B:	
Liquid polymer, LP-3	50
Silica flour No. 219	47.3
DMP-10	6.25
DMP-30	3.75
Bentone 38	2.5
Anti-foam 24[b]	2.5

[a]Equivalent epoxide weight 175-200, viscosity 10,000-15,000 cps.
[b]General Electric product or equivalent.

mens for each conditioning time and temperature and type of test were made so that the results would represent adequate sampling. In general, between three and five specimens undergoing the same test were made from different batches so that the variation in mixing from batch to batch would be included in arriving at an average test result for each conditioning situtation. About 1,200 specimens were involved.

Figure 7 shows the strength of the tension specimens vs the ages of the specimens at the time of testing for 180 F conditioning, with scattering of test data. A large number of specimens were rejected for one reason or another: warpage, air holes, fractures at other than the critical section, damage during handling, conditioning time

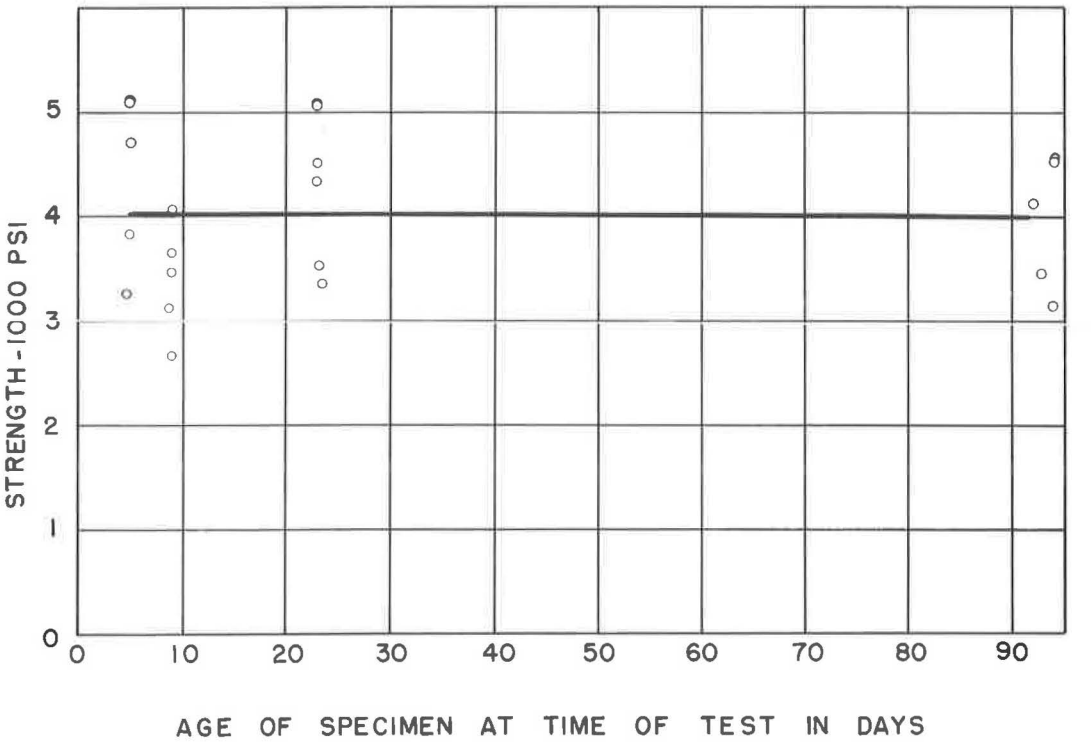

Figure 7. Strength of tension specimen vs specimen age for 180 F.

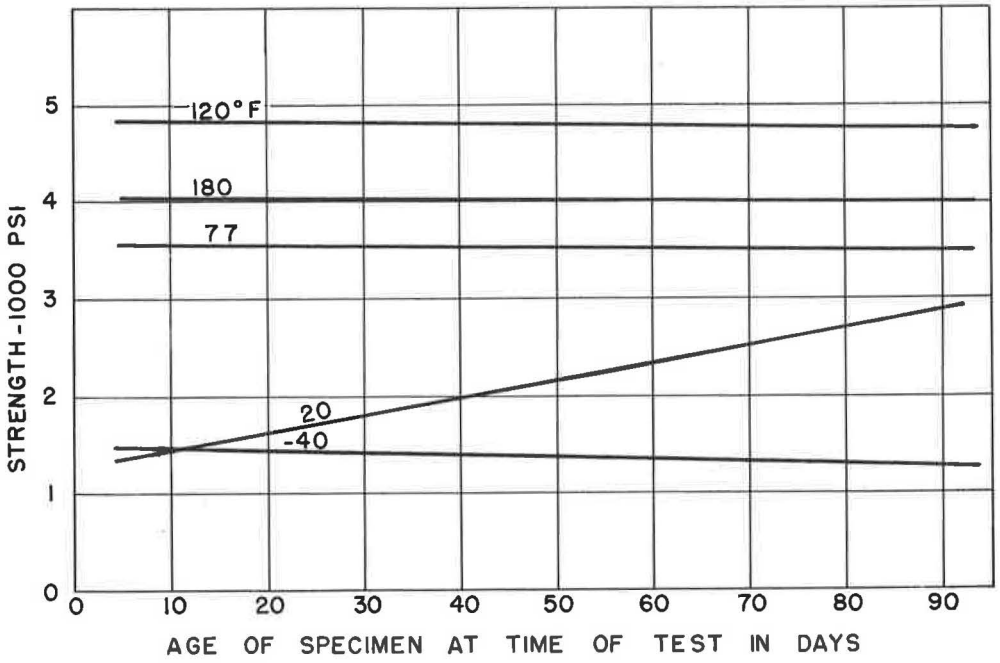

Figure 8. Strength of tension specimen vs specimen age for all conditioning temperatures.

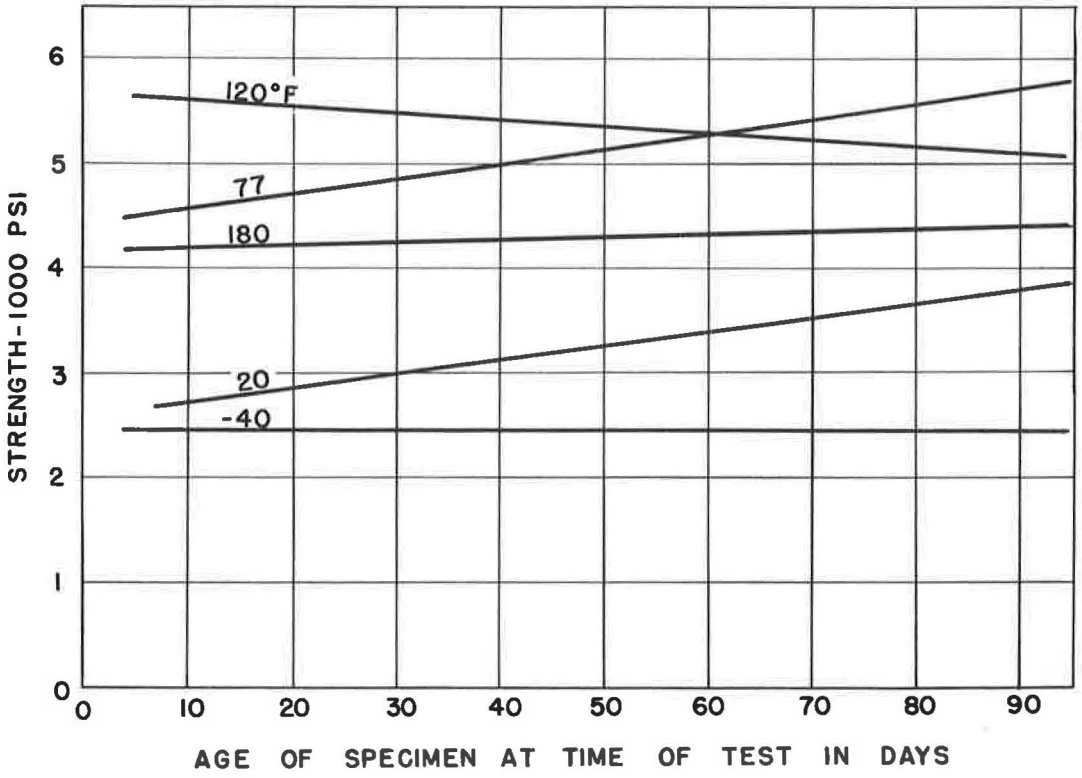

Figure 9. Strength of shear specimen vs specimen age for all conditioning temperatures.

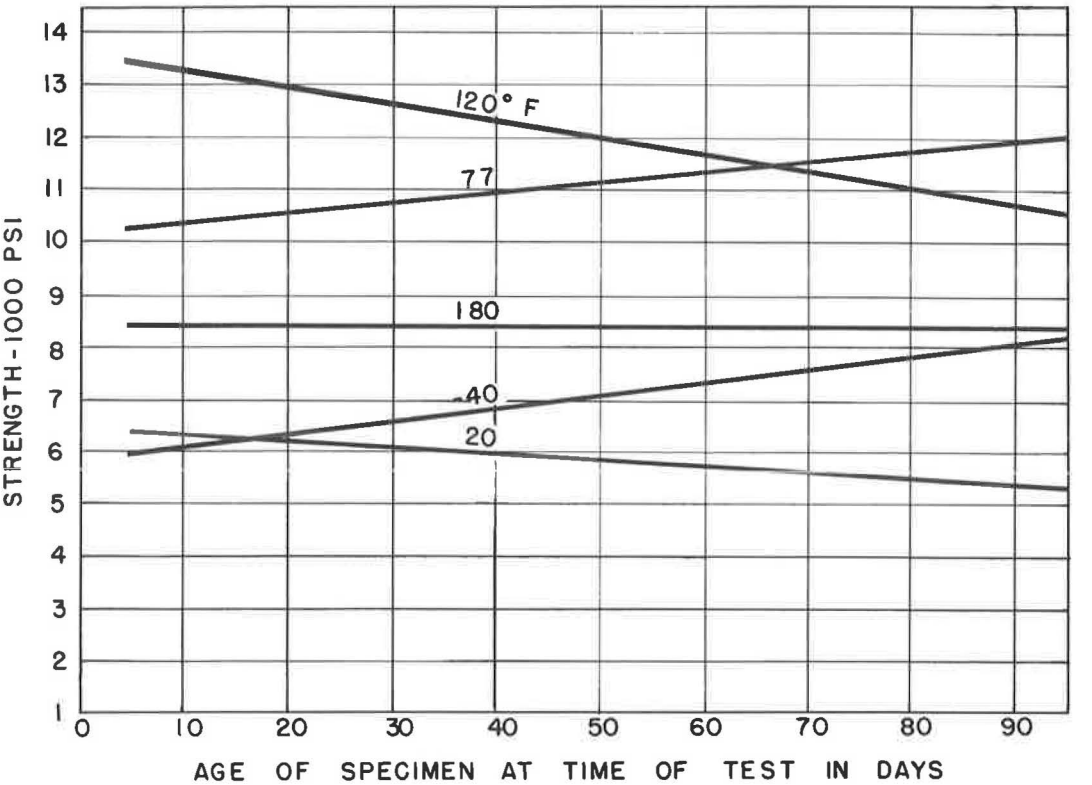

Figure 10. Strength of compression specimen vs specimen age for all conditioning temperatures.

not within an arbitrary 5 percent tolerance, or Chauvenet's criteria (2). After the test results were plotted on the graph, a least squares adjustment was made to determine a straightline relationship between strength and age of specimen. A least squares adjustment was also made using a second-order (parabolic) curve on some of the data, but the differences between straightline and parabola curves were insignificant; hence the straight line was chosen. Figures 8 through 12 show these linear relationships for the various types of tests represented by the conditioning combinations of Table 1.

A study of these figures, which are the over-all compilations for each test, shows no intelligible correlation between the types of tests; except that of the five curing temperatures used, 120 F appears consistently to be the most favorable curing temperature for the epoxy resin as a plastic in the early phases of curing. It is concluded, therefore, that each formulation must be evaluated by experiment for each test type in order to obtain reliable information. Further, tension adhesion and single shear adhesion specimens failed primarily in the mortar; therefore, these test results reflect the mortar strength only.

Figures 13 and 14 give the fatigue data for the bending fatigue and torsion fatigue specimens, respectively, in the form of S-N plots. Because numerous specimens were involved, and the process was time consuming, arbitrarily the bending fatigue S-N data was obtained for seven days conditioning at 77 F and the torsion fatigue data was obtained for 21 days conditioning at 77 F. Circles with arrows on the graphs indicate non-failure of specimen, and discontinuance of the test at the number of cycles plotted. The investigators feel that the plotted points indicate the general trend and are reluctant to define the limits of the scatter-band accurately or to write the equation of the S-N curve from the available information.

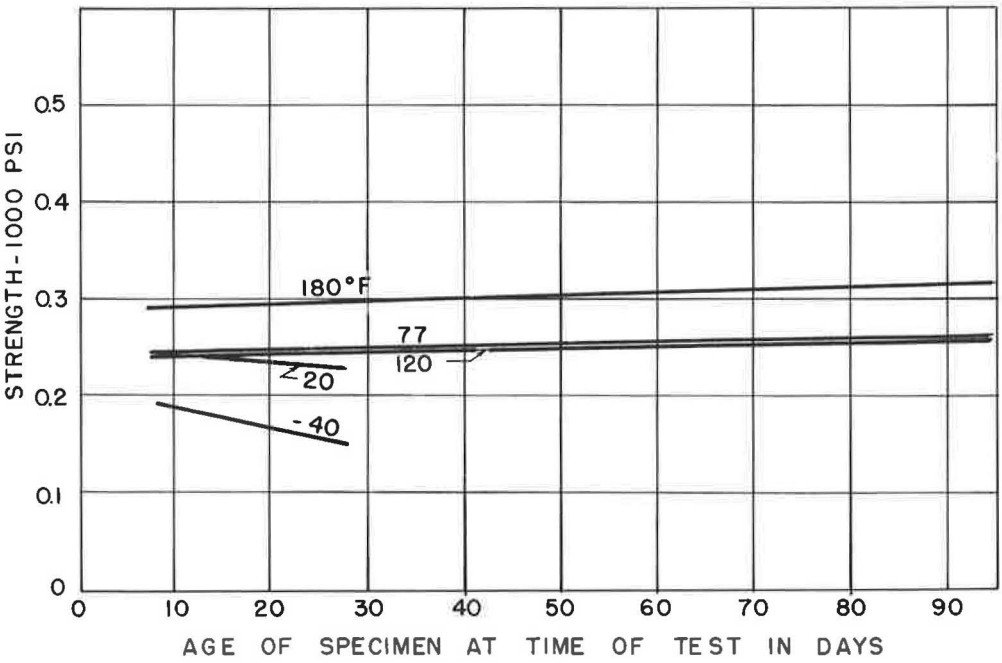

Figure 11. Strength of tension adhesion specimen vs specimen age for all conditioning temperatures.

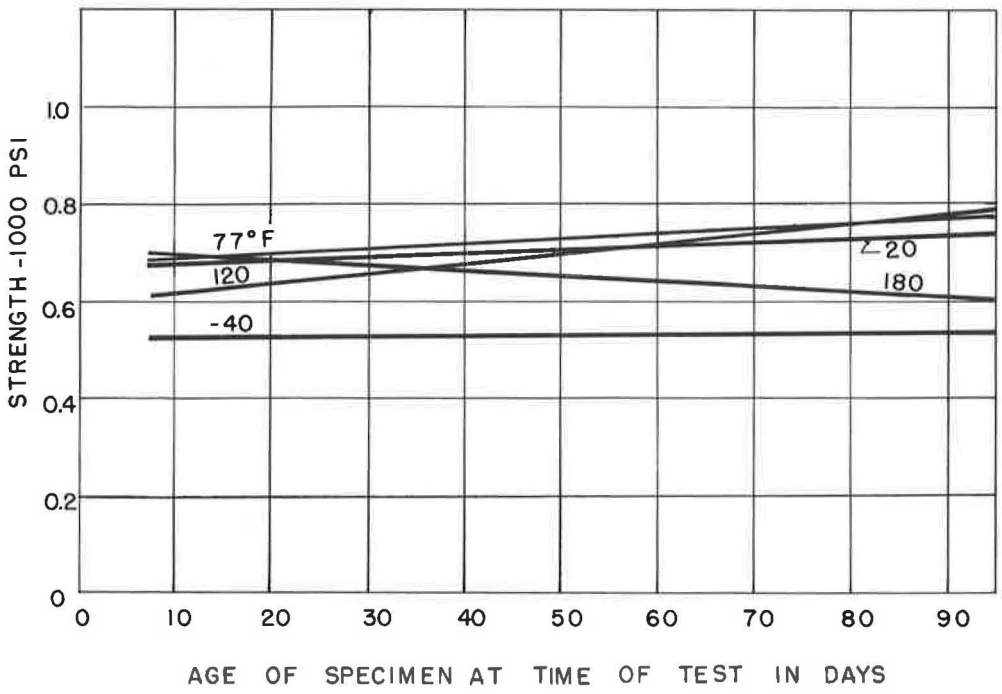

Figure 12. Strength of single shear adhesion specimen vs specimen age for all conditioning temperatures.

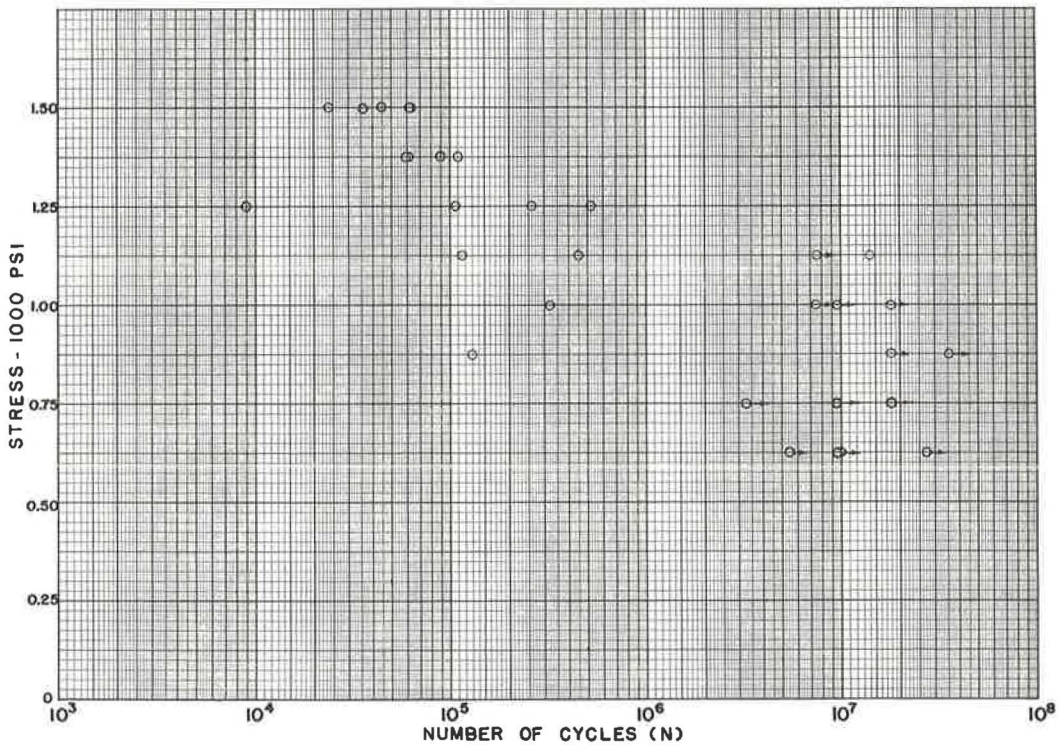

Figure 13. S-N data for bending fatigue tests.

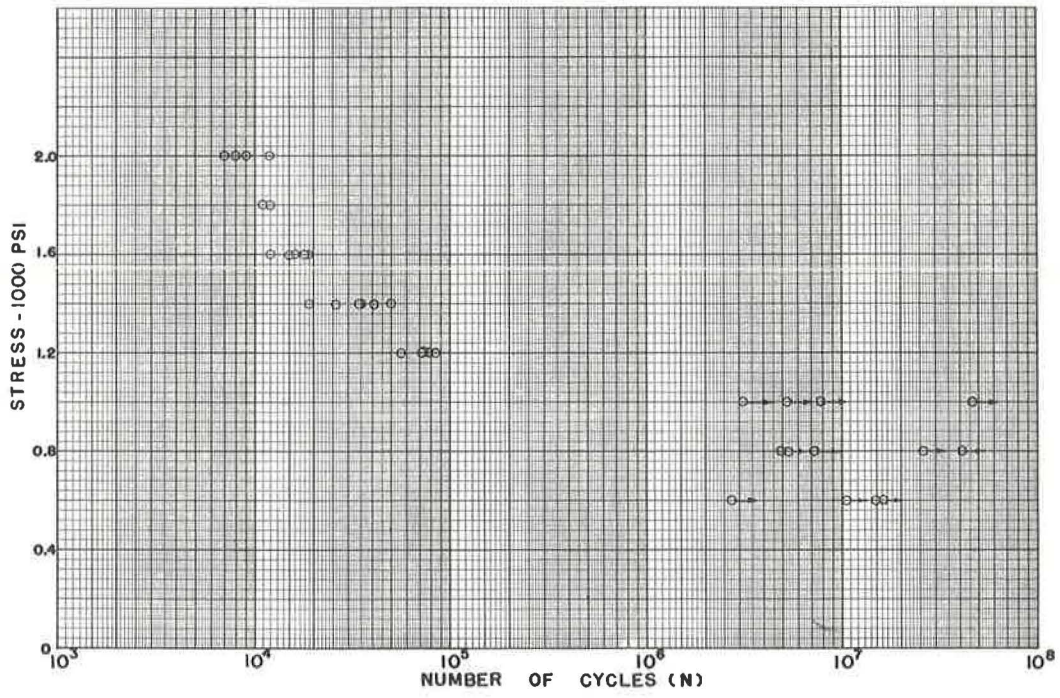

Figure 14. S-N data for torsion fatigue tests.

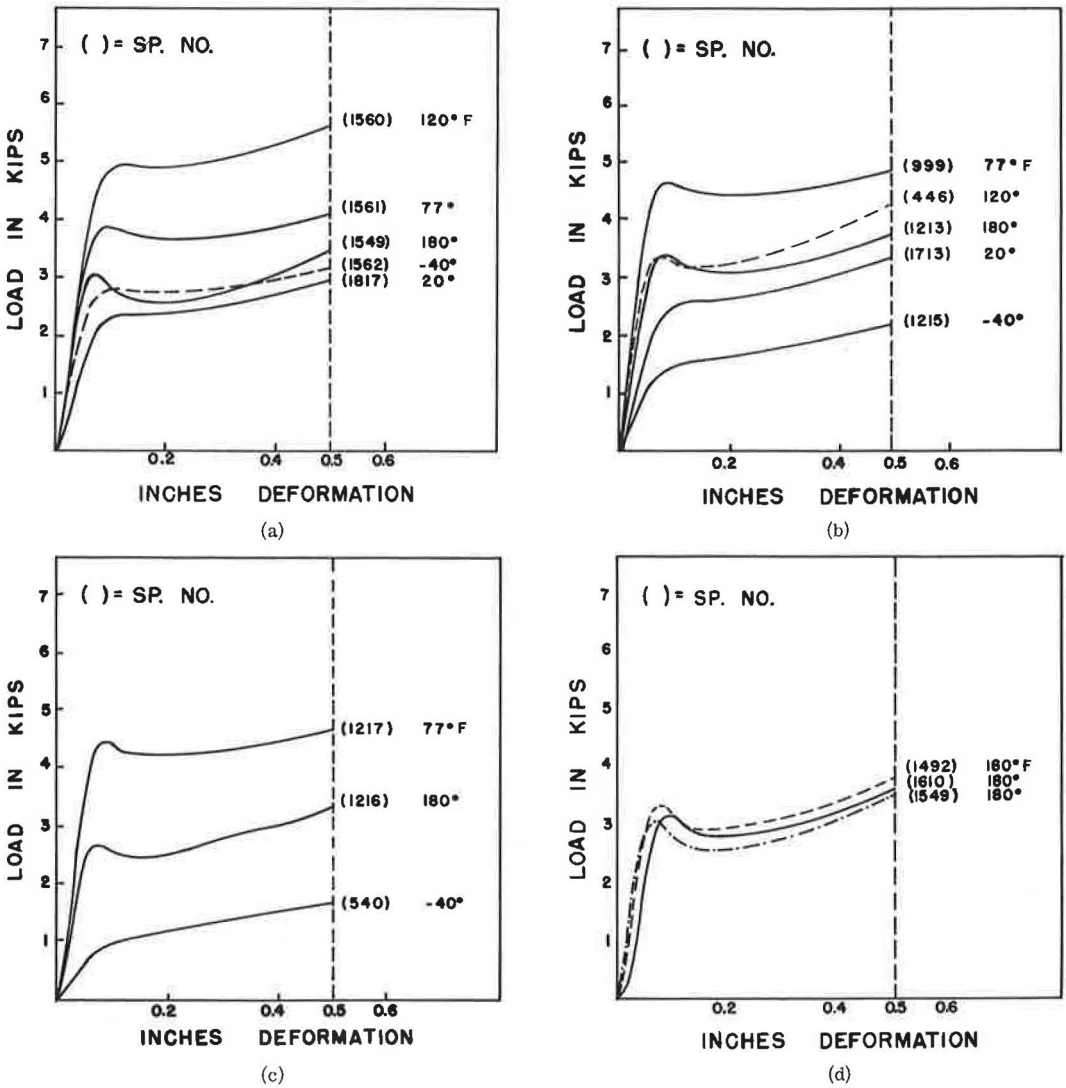

Figure 15. Compression load-deflection curves for (a) 3 days at 5 temperatures, (b) 3 mo at 5 temperatures, (c) 7 mo at 3 temperatures, (d) 3 days at 180 F.

TABLE 3

INITIAL TANGENT MODULUS OF ELASTICITY

Conditioning Temperature (°F)	Tangent Modulus of Elasticity		
	3-Day Conditioning	3-Month Conditioning	7-Month Conditioning
180	360,000		341,000
120	540,000	456,000	
77	442,000		490,000
20	323,000	315,000	
-40	357,000		262,000

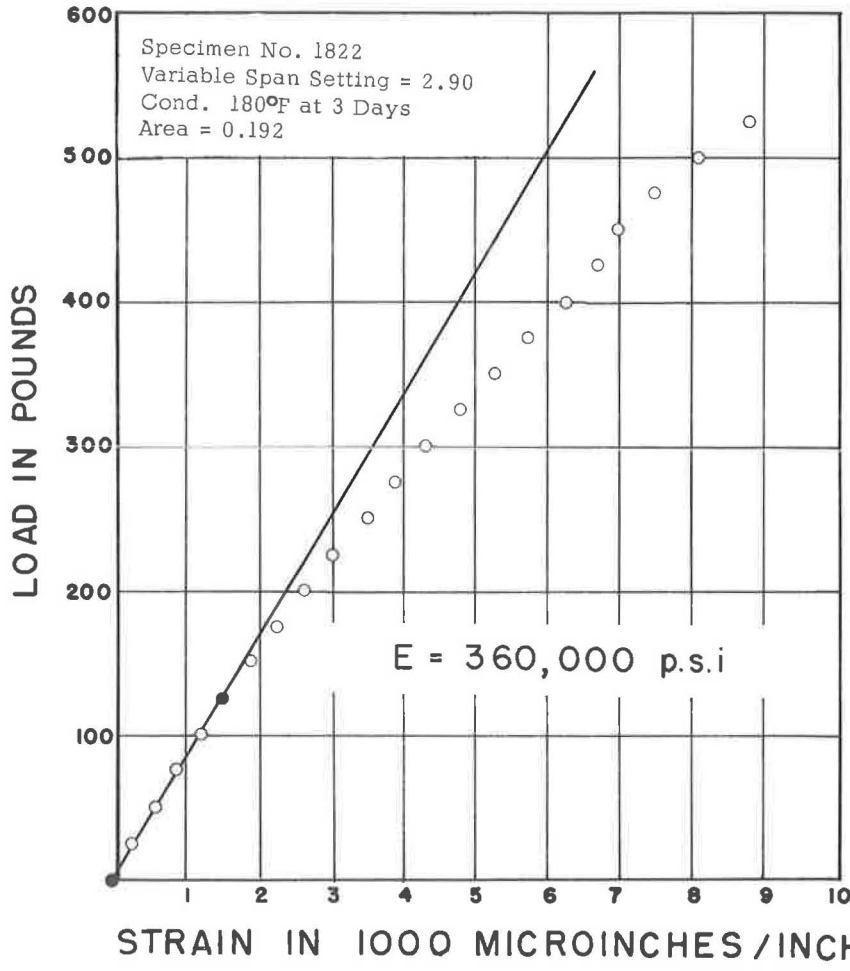

(a)

Sample Calculation—Specimen No. 1822

Indicated Gage Factor for Variable Span Setting of 2.90 = 2.41
Indicated Gage Factor for Variable Span Setting of 2.18 = 2.07
Actual Gage Factor = 2.09

$$\text{Actual Strain} = \text{Indicated Strain} \times \frac{\text{Indicated Gage Factor}}{\text{Actual Gage Factor}}$$

$$= (1490 + 80)\,\frac{2.41}{2.09} = 1810$$

$$E = \frac{P}{A\,e} = \frac{125\,(10^6)}{0.192\,(1810)} = 360,000 \text{ p.s.i.}$$

(b)

Figure 16. Initial tangent modulus of elasticity for tension specimen: (a) load strain data for 3 days conditioning at 180 F, (b) sample calculation for modulus of elasticity for Fig. 16a.

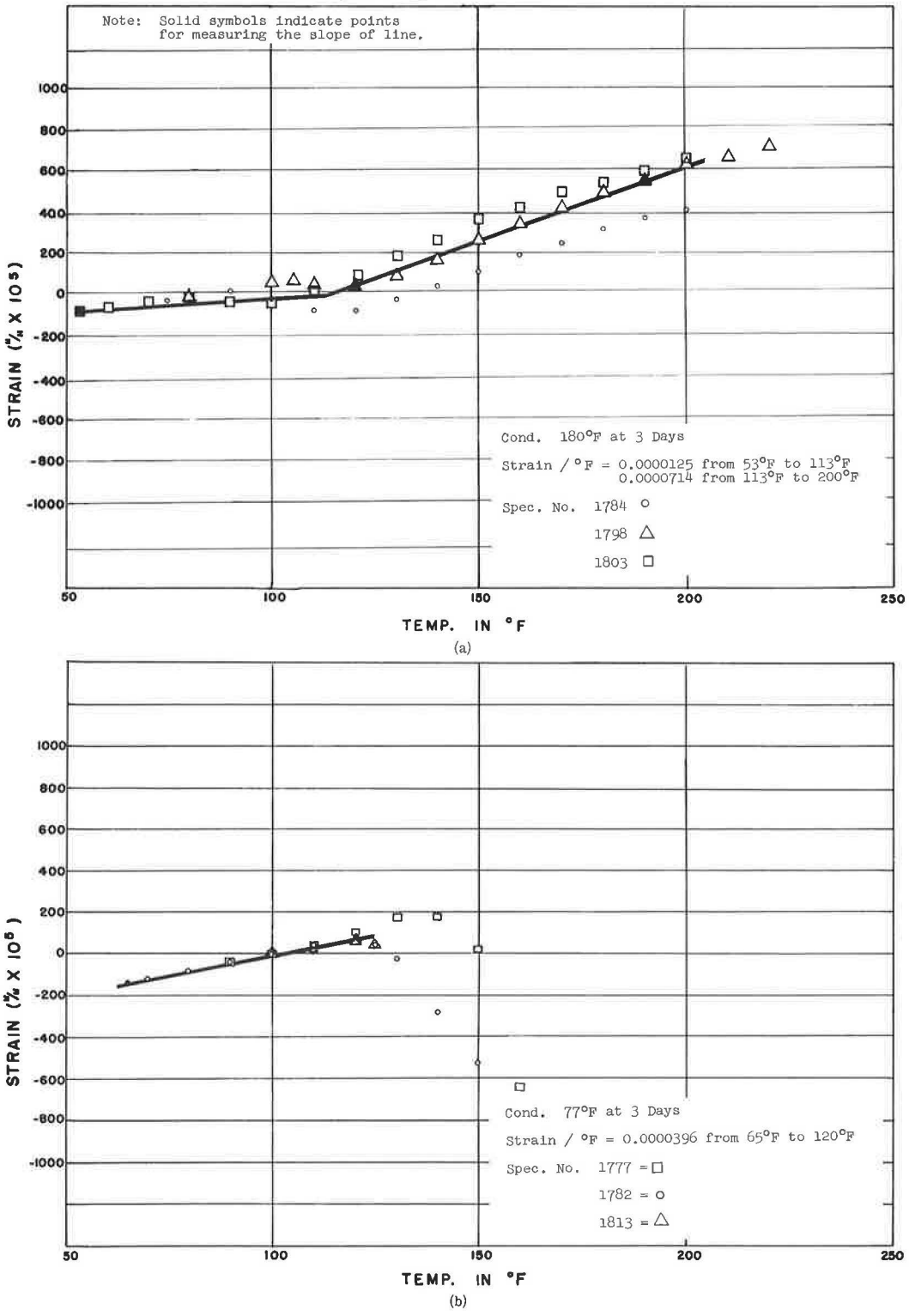

Figure 17. Coefficient of expansion data for 3 days conditioning (a) at 180 F, (b) at 77 F.

Figures 15a through 15c show load-deflection diagrams for compression specimens conditioned for three days, three months, and seven months, respectively. Only a single selected load-deflection diagram is shown for each conditioning temperature. These diagrams are merely indicated to show the general shape of the load-deflection curve, and were traced from the load-deflection indicator graph on the testing machine. These graphs show the relative displacement between the heads of the testing machine, and thereby indicate the deformation of the 2-in. long specimen for various loads. Figure 15d shows a set of load-deflection curves for compression specimens conditioned for three days at 180 F.

Modulus of elasticity tests were performed on a limited number of tension specimens, using SR-4 strain gages. Figure 16a shows the load-strain data for a tension specimen conditioned for three days at 180 F. The calculation of the initial tangent modulus of elasticity from these data is shown in Figure 16b. Table 3 summarizes the modulus of elasticity results for several conditioning situations. The purpose of these tests was only to obtain an approximate scale on the stiffness of the material and to develop the general shape of the stress-strain diagrams.

Tests for the coefficient of expansion of the epoxy resin were also conducted. In these tests, a quartz tube dilatometer, as described in ASTM D 696-44, was used to measure the elongation of 3/8-in. diameter by 3-in. long epoxy resin specimens, as they were heated in a Marshall testing furnace. A thermocouple attached to the specimen was used to measure the temperature.

Figures 17a and 17b show the coefficient of expansion data for specimens cured for three days at 180 and 77 F, respectively. Because the ambient temperature of the room could not be lowered at various times of the day, it became necessary in plotting the data to relate all strains to an arbitrary zero-strain reference temperature, which was the highest initial temperature of any set of specimens plotted on one graph. This is the reason negative initial strains appear on these graphs.

In testing, direct elongation readings for the 3-in. long specimens were recorded. These readings were converted to strains, prorated by comparison to a steel specimen of the same dimensions which was tested in the same way, and reduced to the zero reading at the base temperature before plotting on the graphs.

For each specimen tested, a transition point was observed. That is, the coefficient of linear thermal expansion changed when a certain temperature was reached. For those specimens cured at 180 F, two coefficients were calculated for the ranges of temperature indicated, both before and after the transition point. Also, for most specimens cured at temperatures below 180 F, this transition point manifested itself by complete softening of the material. On each graph a straight line is drawn over a range of temperatures which can conveniently represent an average of the data presented. This straight line has been used to compute the coefficient of thermal expan-

TABLE 4

COEFFICIENTS OF EXPANSION FOR TEMPERATURE RANGES INDICATED

Conditioning Temperature (°F)	3-Day Conditioning		7-Day Conditioning	
	Coeff. of Expansion (in./in./°F)	Temp. Range (°F)	Coeff. of Expansion (in./in./°F)	Temp. Range (°F)
180	0.0000125	53-113	0.0000114	70-120
	0.0000714	113-200	0.0000750	120-200
120	0.0000438	70-150	0.0000388	60-150
77	0.0000396	65-120	0.00004	65-140
20	0.0000225	70-110	0.0000213	60-100
-40	0.00004	60-100	0.000035	60-100

TABLE 5

EFFECT OF STORAGE LIFE OF COMPONENTS ON CONSISTENCY

Batch No.	Time Tested	Storage Time[a]	Room Humidity (%)	Room Temp. (°F)	Viscosity (cps) Comp. 1	Viscosity (cps) Comp. 2
73	At mixing	1 mo	39	73	23,250	20,000
	After storage		34	77	14,950	17,750
84	At mixing	3 mo	58	73	18,350	28,450
	After storage		42	72	4,000	22,750
95	After storage	19 days	33	75	12,400	25,050
98	After storage	33 days	—	78	17,500	24,500
100	After storage	61 days	32	75	14,600	22,750

[a]At 77 F, 50 percent relative humidity.

sion, which is applicable only within the range of temperatures indicated. Table 4 gives additional data for other curing schedules.

ADDITIONAL TEST DATA

In addition to the previous series of physical tests, several other tests were conducted which were considered pertinent to the problem of bonding composite concrete-to-steel beams. Some of these included the following:

1. Test for determining proper steel surface preparation. In this test, using single shear adhesion specimens, different methods for preparing the steel surface were investigated. Several solvents were tried for cleaning the steel surfaces. These were ineffective because it was found that the steel also had to be roughened in addition to being clean in order to insure adequate bonding. From the standpoint of field construction feasibility, one of the best surface preparations yielding consistent results was sandblasting.
2. Test for effect of freeze-thaw cycling on adhesive bond. Single shear specimens were prepared in the usual manner, wet cured for three days and conditioned for seven days at 77 F. They were then subjected to 53 cycles of freezing in air and thawing in water at a rate of 8 cycles per day in a Conrad machine. From the results of these tests it was concluded that freeze-thaw cycling had an adverse effect on the failure strength of the specimens. However, because all failures were mortar failures, these tests indicated the deterioration of strength occurring in the mortar, and it has not been proven whether the epoxy resin is affected by freeze-thaw cycling.
3. Effect of storage life of components on consistency. Table 5 gives information concerning the effect of storage life of formulation components on consistency. Batches 73 and 84 were hand-mixed using small wooden tongue-blades. After a one-month storage period of each component, it was discovered that much of the silica flour filler material had settled out of each component, and could not be satisfactorily remixed into the components by means of hand mixing. This phenomenon was even more pronounced in the case of a three-month storage after initial mixing. In this case, even the liquid ingredients in the components tended to separate because of differences in their specific gravities. This separation of components during storage, and resulting difficulty in remixing after storage, caused a large drop in viscosity, which once again was due mainly to the settling of the silica flour.

Batches 95, 98, and 100 were made from components mixed with an electric drill. The viscosities of the components of these batches did not vary widely after their respective storage times. This indicates that, when properly mixed, neither component undergoes a serious change in viscosity over a lengthy storage period. Visual observation also demonstrated that there was much less tendency for the filler to settle out after machine mixing, because this mix looked fairly homogeneous throughout. This was not the case with hand mixing.

TABLE 6

EFFECT OF STORAGE LIFE OF FORMULATION COMPONENTS ON STRENGTH OF CURED SPECIMENS

Batch No.	Spec. No.	Type	Stress (psi)	No. of Cycles (x 1,000)	Conditioning Time[a] (days)	Average Strength (or cycles to failure)
68[b]	842	TE	3,380		7	
	843	TE	3,440		7	3,530
	844	TE	3,770		7	
	845	BE	1,237	133	7	
	846	BE	1,250	63	7	106,000
	847	BE	1,250	122	7	
	848	S	5,230		21	
	849	S	4,810		21	5,027
	850	S	5,040		21	
	851	SS-A	773		7	
	852	SS-A	734		7	745
	853	SS-A	728		7	
	854	T	1,200	93	21	
	855	T	1,200	75	21	84,000
	856	T	1,200	84	21	
	808	C	11,200		21	
	816	C	11,310		21	11,317
	817	C	11,440		21	
73[c]	925	TE	3,780		7	
	926	TE	3,490		7	3,580
	927	TE	3,470		7	
	928	BE	1,125	171	7	
	929	BE	1,125	131	7	732,000
	930	BE	1,125	1,894	7	
	931	S	3,340		7	
	932	S	4,320		7	3,970
	933	S	4,250		7	
	934	SS-A	596		7	
	935	SS-A	721		7	655
	936	SS-A	648		7	
	937	T	1,200	90	21	
	938	T	1,200	110	21	100,000
	939	T	1,200	—[d]	21	
	940	C	9,900		7	
	941	C	10,900		7	10,427
	942	C	10,480		7	
84[e]	1,163	TE	3,190		7	
	1,164	TE	N.G.		7	3,190
	1,165	TE	N.G.		7	
	1,166	BE	1,250	10	7	
	1,167	BE	1,250	12	7	15,000
	1,168	BE	1,250	23	7	
	1,169	S	5,750		7	
	1,170	S	5,725		7	5,508
	1,171	S	5,050		7	
	1,172	SS-A	848		7	
	1,173	SS-A	833		7	845
	1,174	SS-A	853		7	
	1,175	T	1,200	51	21	
	1,176	T	1,200	93	21	72,000
	1,178	C	14,250		7	
	1,179	C	10,510		7	12,380

[a] At conditioning temperature of 77F.
[b] Stored 7 days at 77F, 50 percent relative humidity.
[c] Stored 1 mo at 77F, 50 percent relative humidity.
[d] Deflection failure.
[e] Stored 3 mo at 77F, 50 percent relative humidity.

TABLE 7

TEST RESULTS OF SINGLE SHEAR ADHESION SPECIMENS FOR VARIOUS TIME LAPSES BETWEEN APPLICATION OF EPOXY AND MORTAR[a]

Batch No.	Spec. No.	Time Lapse (min)	Strength (psi)
56	630	10	644
	631	20	687
	632	30	--[b]
	633	40	665
	634	50	718
	635	60	600
62	809	50	768
	810	60	630
	811	70	660
	812	80	680
	813	90	460
	814	100	653
73	1,790	90	640
	1,791	120	615
	1,792	150	648
	1,793	180	562
	1,794	210	716
	1,795	240	805
	934	5-15	596
	935	5-15	721
	936	5-15	648

[a]For conditioning of 7 days at 77F. All specimens suffered mortar failure.

[b]Broke in handling.

4. Effect of storage life of formulation components on strength of cured specimens. Table 6 shows the effect of storage life of the formulation components on the strength of cured specimens. A comparison of these test results with the over-all series of test results given in Figures 7 through 12 shows that the storage life of the components has no significant effect on the strength of the cured system.

5. Test for interchangeability of different brands of epoxy resins in the same formulation. A series of specimens was cast from batches of this formulation using different brands of epoxy resin. These test results, when compared with the general series of test results of Figures 7 through 12, show that there is no significant difference between different brands of epoxy resin as long as they meet the specifications of an equivalent epoxide weight 175 to 200, and viscosity between 10,000 and 15,000 cps.

6. Working life of epoxy resin formulation. Table 7 shows the results of tests that were conducted to determine the effect of a time lag between the application of epoxy to a steel strap, and the further application of mortar on top of the epoxy. These strengths are comparable with those in Figure 12, and all failures occurred in the mortar, indicating adequate bonding. Thus it can be concluded that time lapses of up to four hours, and possibly more, may safely be allowed between the application of epoxy to the steel and the further application of mortar to the epoxy.

7. Tests of single shear adhesion specimens without epoxy shear connectors. In these tests the steel was sandblasted only, and the mortar was placed wet on top of the sandblasted area. In all cases the shear strengths of these specimens were less than one-fourth the values given by Figure 12, and bond failures were observed. These tests proved the definite increase in shear strength due to the epoxy resin.

CONCLUSIONS

Several important conclusions have been drawn from the results of this investigation.

General (Applying to All Epoxy Formulations)

1. Several factors other than strength alone govern the choice of a suitable formulation. Examples are sprayability, viscosity, brittleness, ability to set in the presence of water, pot life, and resilience. A single epoxy formulation has been developed as described in this report, which satisfies all of these considerations for the applications investigated.
2. A non-standard shear test (the Single Shear Adhesion Test) has been developed which is considered reliable for predicting the shear strength of a metal-to-concrete adhesive system.
3. A viscosity of 20,000 centipoises for each component of a two-component epoxy formulation will allow for proper spraying applications. To facilitate spraying, heating the components as part of the spraying operation is desirable.
4. There appears to be no definite correlation between the different types of physical tests; therefore, each formulation should be evaluated in all types of tests for each specific application.
5. Power mixing is superior to hand mixing for preparation of the components and for mixing the components together. The use of power mixing for preparing the components provides for a longer storage life without settling of filler materials.
6. Silica flour filler is abrasive with spray equipment; nevertheless, some equipment manufacturers make allowance for this with easily replaceable parts.
7. Sandblasting is the most satisfactory method for preparing a steel surface, and is recommended for composite beam construction in the field.

Specific (Applying Primarily to Particular Epoxy Formulation Studied and Presented Herein)

1. In properly prepared adhesion specimens of steel-to-mortar, with an epoxy adhesive, the mortar is the weakest component of the cured system.
2. Epoxy resins from different manufacturers are interchangeable in the formulation described in this report, provided that they are within the limits of epoxide equivalent weight and viscosity specifications.
3. The epoxy formulation described in this report does not hinder proper concrete curing and vice versa.
4. In using the recommended formulation, the concrete should be applied within four hours after application of epoxy to the steel.
5. Freeze-thaw cycling of steel-to-mortar adhesion specimens did not noticeably affect the epoxy, but did cause considerable mortar strength loss.

Culminating this study a series of quarter-scale composite beams, using the epoxy resin as a shear connector, were statically loaded to failure and their behavior studied by means of strain gages and other deformation indicators. The performance of these beams was compared with that of monolithic concrete T-beams and stud shear connected concrete to steel composite beams which were loaded to failure under identical conditions. The results of these tests are reported elsewhere (3).

The results of this investigation show that an epoxy resin formulation satisfying the strength demands of a composite beam bridge can be achieved, subject to the restrictions imposed by the testing program. However, further studies of performance and characteristics are necessary before the selected epoxy resin formulation can be approved for use as a connector; such as creep, fatigue on glued joints, impact, strength gain under various temperature conditions, and durability. These studies are now being made in an extension to the research project.

ACKNOWLEDGMENTS

This paper is based on the experimental investigation presented elsewhere (3). The research was sponsored by the Bureau of Physical Research, New York State Depart-

ment of Public Works in cooperation with the U.S. Department of Commerce, Bureau of Public Roads. Personnel of the Bureau of Physical Research collaborated in the planning of the project, assisted in certain phases of the laboratory studies, and acted as technical advisors.

REFERENCES

1. "ASTM Standards on Plastics." American Society for Testing, 12 ed. (March 1961).
2. Hetenyi, N., "Handbook of Experimental Stress Analysis." Wiley (1950).
3. Miklofsky, H.A., Brown, M.R., Jr., and Gonsior, M.J., "Epoxy Bonding Compounds as Shear Connectors in Composite Beams." Interim Report, Physical Research Project No. 13, Engineering Research Series RR 62-2, N.Y. State Department of Public Works, Bureau of Physical Research (Oct. 1962).